University College London
Department of Chemistry

Theoretical Investigations of Two-Dimensional Magnets

Andrea Taroni

September 2007

A Thesis
submitted for the degree of Doctor of Philosophy
at the University of London

ProQuest LLC
789 East Eisenhower Parkway
P.O. Box 1346
Ann Arbor, MI 48106-1346

Ai Miei

perché ci sono, sempre.

Abstract

This Thesis addresses the thermodynamic behaviour of two-dimensional magnets. The objective is to evaluate the role played by external perturbations in these systems by use of analytical and computational techniques. To this end, extensive Monte Carlo simulations have been performed on Ising, XY and Heisenberg spin models in the presence of symmetry breaking crystal fields, external magnetic fields and long range dipolar interactions.

The effects of four-fold symmetry are examined in detail, since this is common in nature. In the 2dXY model, such a crystal field acts as a marginal perturbation which drives the system to non-universal critical behaviour only upon rescaling to exponentially large length scales. This has the implication that real, finite systems are unexpectedly robust to their presence. On the other hand, the four-state clock model is recovered in the limit of extremely strong fields, which exhibits Ising critical behaviour. The nature of this crossover from XY to Ising behaviour is studied in detail, using numerical and analytical methods.

The picture that emerges from this analysis is that there are two principal categories of two-dimensional magnets: those belonging to the so-called Ising universality class and those belonging to the XY class. A detailed survey of the experimental literature confirms this classification. However, a considerable number of experimental systems also exhibit behaviour which is intermediate between these two regimes. It is argued these materials are susceptible to the crossover mechanism induced by the presence of four-fold fields.

Contents

Acknowledgements 12

Symbols and Abbreviations 14

Introduction 16

I Theoretical Background 19

1 Magnetism: An Overview 20

1.1 Free Magnetic Moments 20

1.1.1 Ground State of Free Magnetic Ions 22

1.1.2 Spin-Orbit Coupling 22

1.2 Interactions 23

1.2.1 Dipolar Interaction 24

1.2.2 Exchange Interaction 24

1.3 Spin Hamiltonians 29

1.3.1 Transition Metal Ions 29

1.3.2 Rare Earth Ions 31

1.4 Model Magnetism 31

1.4.1 Ising Model 32

1.4.2 Weiss Molecular Field Model 38

1.4.3 Continuous Models 39

1.5 Historical Development 40

1.6 Concluding Remarks 41

2 Phase Transitions and Critical Phenomena **42**

2.1 Phase Transitions 43

2.1.1 Basic Considerations 43

2.1.2 Thermodynamic Considerations 45

2.1.3 Landau's Mean Field Theory 49

2.2 Critical Phenomena 51

2.2.1 Critical Exponents, Power Laws and Scale Invariance 51

2.2.2 Statistical Mechanics 55

2.2.3 Universality 62

2.2.4 Finite Size Scaling 63

2.2.5 Renormalization Group Theory 66

2.3 Monte Carlo Method 70

2.3.1 Metropolis Algorithm 70

2.3.2 Cluster Algorithms 72

2.3.3 Practical Issues 73

2.4 2dXY Model 76

2.4.1 Kosterlitz-Thouless Transition 80

2.4.2 2dXY Model on a Finite Lattice 85

II Investigations of Critical Phenomena in Two-Dimensional Systems **89**

3 Aims and Objectives of the Present Work **90**

4 Survey and Classification of Experimental Data **92**

4.1 Universality in Two-Dimensional Magnetic Systems 92

4.1.1 Layered Magnets 94

4.1.2 2dXY Layered Magnets 114

4.1.3 Ultrathin Film Magnets 119

4.1.4 Other Two-Dimensional Magnetic Systems 128

4.1.5 Further Remarks 129

4.2 Universality in Two-Dimensional Non-Magnetic Systems 131

4.2.1 Structural Transitions 131
4.2.2 Melting at Surfaces 134
4.2.3 Quantum Systems 136
4.3 Conclusions 137

5 Long Range Order in Two-Dimensional Systems 139
5.1 Two-Dimensional Heisenberg Model 140
5.1.1 Crossover Due to Single Ion Anisotropy I. Simple Case . . . 145
5.1.2 Crossover Due to Single Ion Anisotropy II. Complex Case . . 147
5.2 Influence of Symmetry Breaking Fields on the 2dXY Model 149
5.2.1 Numerical Results 151
5.2.2 Clock Models and Extended Universality 159
5.2.3 RG Analysis of the Villain Model 164
5.2.4 Critical Isotherms 170
5.3 Re-evaluation of Experimental Situation 172
5.3.1 Layered Magnets 172
5.3.2 Ultrathin Magnets 176
5.3.3 Structural Transitions at Surfaces 177
5.4 Discussion 178

6 Competing Long and Short Range Interactions 180
6.1 Long Range Interactions 181
6.1.1 Discrete Systems 182
6.1.2 Continuous Systems 185
6.1.3 Problems in Simulation 186
6.2 Competing Length Scales in the Ising Model 186
6.2.1 Equivalent Neighbour Model 187
6.2.2 Dipolar Coupling I. Isotropic 190
6.2.3 Dipolar Coupling II. Anisotropic 192
6.3 Competing Length Scales in Continuous Spin Systems 192
6.3.1 Dipolar XY Model 193
6.4 Heisenberg Model in the Presence of Shape Anisotropy 194
6.4.1 Influence of Shape Anisotropy 195

6.5 Discussion 198

7 Conclusions and Perspectives **200**

7.1 Experimental Classification 200

7.2 Theoretical Results 201

7.2.1 Symmetry Breaking Anisotropies 201

7.2.2 Long Range Interactions 202

7.3 Future Work 203

A Spin Wave Analysis of the Classical Heisenberg Model **205**

A.1 Heisenberg Ferromagnet 205

A.1.1 Expression for the Magnetisation 208

A.1.2 Influence of Anisotropies 209

A.2 Heisenberg Antiferromagnet 210

A.2.1 Influence of Anisotropies 212

A.3 Concluding Remarks 214

B Conventions for Describing Ordered Surface Structures **215**

B.1 Wood's Notation 215

B.2 Matrix Notation 216

C Some Notes on Mean Field Theory **218**

Bibliography **221**

List of Figures

1.1 An electron in a circular orbit 21
1.2 Addition of angular momenta 23
1.3 Schematic representation of molecular hydrogen. 26
1.4 Bonding diagram for the hydrogen molecule 27
1.5 Ising lattice 33
1.6 Magnetisation as a function of temperature for the Ising model . . . 35
1.7 Inverse susceptibility as a function of temperature for para-, ferro- and antiferromagnetic systems 37
1.8 A spin wave. 40

2.1 Density-temperature phase diagram for a fluid 44
2.2 Phase diagram for a simple ferromagnet 45
2.3 Projections of a thermodynamic surface onto different planes 48
2.4 Landau free energy 49
2.5 Power laws resulting from different critical exponents 52
2.6 Ising model at the critical point 54
2.7 Probability density functions of the magnetisation for the Ising model 58
2.8 Critical opalescence in a binary fluid 60
2.9 Effects of finite size on a phase transition 64
2.10 Correlation function for a critical 2d Ising system of finite size . . . 65
2.11 Finite size scaling data collapse for the 2d Ising model 66
2.12 Block Spins 67
2.13 Spin coordinates. 72
2.14 Evolution of the magnetisation in Monte Carlo time 74
2.15 Effects of finite size on the 2d Ising model 75

2.16 A vortex anti-vortex pair 80
2.17 XY model lattice configurations 81
2.18 RG trajectories for the 2dXY model 84
2.19 Monte Carlo magnetisation data for the 2dXY model 87
2.20 Monte Carlo magnetisation data for the HXY model 88

4.1 Histograms of β values in two-dimensional magnets. 93
4.2 Illustration of a layered magnet 94
4.3 Temperature dependence of the order parameter of $BaNi_2(PO_4)_2$ . . 96
4.4 Crystal structure of K_2NiF_4 99
4.5 Critical behaviour of the order parameter of K_2CoF_4 100
4.6 Field-dependent critical behaviour of Rb_2MnCl_4 102
4.7 Magnetisation as a function of temperature for K_2CuF_4 106
4.8 Temperature dependence of the inverse correlation length of Rb_2CrCl_4 109
4.9 Temperature dependence of the correlation length of $MnPS_3$ 111
4.10 Critical behaviour of tanol suberate 113
4.11 Metamagnetic transitions in CSDAB and CSEN 114
4.12 Temperature dependence of the susceptibility of Rb_2CrCl_4 116
4.13 Field dependence of the magnetisation of Rb_2CrCl_4 117
4.14 Chirality associated with XY spins antiferromagnetically coupled on a triangular lattice 119
4.15 Critical behaviour of Fe(100) on V(100) and Ni on Cu(100) 124
4.16 Decrease in T_c with the number of layers in ultrathin films 125
4.17 Magnetisation and susceptibility plots of Fe(100) on W(100) 127
4.18 β as a function of d_{Fe} for Pd layers δ-doped with Fe 128
4.19 Histograms of β values in two-dimensional magnets 130
4.20 Critical behaviour in the order-disorder phase transition of sulfur chemisorbed on ruthenium 132
4.21 Histogram of β values for non-magnetic two-dimensional systems . . 134
4.22 Critical behaviour of xenon physisorbed on graphite 135
4.23 Histogram of β values for all two-dimensional systems 137

5.1 Heisenberg model lattice configurations 142

5.2 Magnetisation and susceptibility data or the 2d Heisenberg model . 144
5.3 Susceptibility and correlation length behaviour in the 2d Heisenberg model 145
5.4 Phase diagram for the Heisenberg model in the presence of single ion anisotropy. 146
5.5 Monte Carlo magnetisation curves for the Heisenberg model in the presence of single ion anisotropy 147
5.6 Log-log plot of magnetisation data for the Heisenberg model in the presence of single ion anisotropy 148
5.7 Monte Carlo magnetisation curves for the Heisenberg model in the presence of single ion anisotropy and in plane four-fold field 150
5.8 Temperature-field phase diagram for the XY model in the presence of four-fold and six-fold crystal fields 151
5.9 Magnetisation data for the XYh_2 and XYh_3 models 152
5.10 Magnetisation data for the XYh_6 model 153
5.11 Magnetisation data for the XYh_4 model 154
5.12 Fourth order cumulant U_L plotted against temperature for the XYh_4 model 155
5.13 Fourth order cumulant U_{32} plotted against U_{32} for different values of h_4. 156
5.14 Comparison of p-state clock models for $p = 4$, 6 and 8 160
5.15 Comparison of the four-state clock model and the Ising model . . . 162
5.16 Comparison of the Potts and clock model energy profiles 163
5.17 Comparison of the $p = 4$ Potts and clock models 164
5.18 Comparison between the XY and HXY (Villain) models in the $h_4 \rightarrow \infty$ limit. 167
5.19 Magnetisation-field data for a 2dXY system 171
5.20 Spin wave energy dispersion in K_2FeF_4 and Rb_2CrCl_4 176
5.21 Ising lattice with nearest and next-nearest neighbour interactions . 178

6.1 Symmetry breaking between the in-plane and out-of-plane orientation of the spins in the two-dimensional Ising model 182
6.2 Effects of the increasing range of interaction in the 2d Ising model . 184

6.3 Influence of long range interactions in the Ising model 188
6.4 Binder cumulants for the equivalent neighbour Ising model 189
6.5 Typical spin configurations for the dipolar uniaxial model on a square lattice 191
6.6 Monte Carlo magnetisation of SA Heisenberg models 195
6.7 Shape anisotropic Heisenberg model lattice configurations 196
6.8 Comparison of the pure and SA Heisenberg models 197

A.1 Bravais lattices for the square antiferromagnet. 211
A.2 Dispersion relation (A.32) for a one-dimensional antiferromagnet. . 212

B.1 Adsorbed monolayer on an fcc(100) surface 216

List of Tables

2.1 Thermodynamic potentials for a magnetic system. 46
2.2 Definitions of the principal critical exponents 53
2.3 Critical exponent values for selected universality classes 55
2.4 Presence of long range order according to spin and lattice dimensionality 63

4.1 List of 2d critical exponents for layered magnets 96
4.2 List of 2d critical exponents for ultrathin magnets 122
4.3 Classification of non-magnetic systems 133

5.1 Critical exponents for the XYh_4 model determined from numerical simulations. 157
5.2 Properties of K_2FeF_4 and Rb_2CrCl_4 174

Acknowledgements

I thank my supervisor, Steven Bramwell, for giving me the opportunity to work with him on a project I have enjoyed tremendously. His insight and enthusiasm were invaluable in keeping me going, and I am grateful for having been allowed to work with a great degree of freedom and independence. I also thank Peter Holdsworth, whom I have come to think of as my second supervisor, for his considerable help and ongoing interest in my work. Peter and Steve form a great double act, and not just on a scientific level. I feel privileged to have been the recipient of their generosity of time and of spirit.

I thank the past and present members of office g19 in UCL Chemistry, particularly Luke and Kieran, for the countless conversations I had with them, some of them even constructive. Actually, Luke provided me with technical assistance on many occasions, without which I would have been lost. Simon Banks helped me considerably, especially in my first year, and kindly read through a first draft of the thesis. Andrew Wills deserves a special mention for having got me into the world of spin systems in the first place. Thanks also to Tom Fennell, Christian Rüegg, and the other regular attendees of the spin meetings across the road in the LCN, to Andrea Sella and Stephen Price for lending me the kit to perform the critical opalescence experiments, and to Dickon Champion for declaring me his protégé.

I enjoyed six wonderful months at the Laboratoire de Physique of the ENS in Lyon. I thank the members of Laboratory for providing me with a stimulating and fun environment in which to work in. In particular, I thank Jean-Yves Delannoy for his kind hospitality, Maxime Clusel for his patience in the face of my naive questions, and Seb Paulin for the coffee breaks. I will also remember with fondness my brief visits to the Ångströmlaboratoriet in Uppsala. Björgvin Hjörvarsson and his research group continually reminded me of experimental reality, and I enjoyed my conversations with Martin Pärnaste, my experimental counterpart.

I am grateful to the EPSRC for a studentship, and to the ESF, CECAM, and UCL graduate school for travel bursaries.

Of course much of the help I received was on a human level. My parents and family have always been there, and words don't do justice to the importance of that. My friends, both in London and further afield, have always reminded me that it's the people that surround you that matter most. The Queensbridge Irregulars have for a number of years given me a great game of football to look forward to on Monday nights. Finally, I thank Silvia for lots of little things which as a whole add up to rather more than the sum of the parts.

Symbols and Abbreviations

Variables

$\langle x \rangle$	mean average of a quantity x
$\langle i, j \rangle$	used in sums to denote the set of all variables with $i \neq j$
β	indicates either the inverse temperature or the order parameter critical exponent
d	dimensionality of the system
$\mathbf{H}$	magnetic field vector
h	scalar value of the magnetic field
H	Enthalpy
$\mathcal{H}$	Hamiltonian or total energy operator of a system
J	exchange coupling
L	'linear' size of a discrete system. In a hypercubic lattice this represents the length of one side of the hypercube
n	dimensionality of the order parameter
N	system size. For a hypercubic lattice $N = L^d$
$\mathbf{r}$	spatial vector joining two nuclei
T	temperature, defined in units of J unless stated otherwise
ϕ	polar angle with respect to the z-axis
θ	azimuthal angle with respect to the x-axis

Physical Constants

h	Planck constant, $6.626\,176 \times 10^{-34}$ Js
$\hbar$	$\hbar = h/2\pi$
k_B	Boltzmann constant, $1.380\,662 \times 10^{-23}$ JK^{-1}
e	elementary charge, $1.602\,176 \times 10^{-19}$ C
m_e	electron mass, $9.109\,383 \times 10^{-27}$ kg

Acronyms

AFM	Antiferromagnet
BH	Bramwell and Holdsworth
ESR	Electron Spin Resonance
FM	Ferromagnet
FSS	Finite Size Scaling
JKKN	José, Kadanoff, Kirkpatrick and Nelson
KT	Kosterlitz and Thouless
MC	Monte Carlo
MOKE	Magneto-Optic Kerr Effect
PND	Powder Neutron Diffraction
RG	Renormalization Group
SCND	Single Crystal Neutron Diffraction

Introduction

Two-dimensional magnets have been a topic of considerable interest in recent years due to remarkable developments in film deposition and patterning techniques. These allow the creation of magnetic thin films with monolayer precision, which are considered to be of large technological potential. Less fashionable *quasi* two-dimensional magnets also exist in the form of three-dimensional layered materials with weak intralayer interactions. From a theoretical perspective two-dimensional magnets are highly attractive, since they represent experimental realisations of Hamiltonians in which the perturbations are very well defined. This allows fundamental questions concerning finite size and dimensionality aspects of magnetism to be addressed.

Low dimensional magnetism is profoundly affected by many body correlations and strong fluctuations. In order to capture these characteristics theoretically, statistical mechanical 'model magnets' are devised, which although simple to define mathematically, are strikingly meaningful physically. As a result, one can make predictions of the thermodynamic behaviour of real systems and anticipate, for instance, the evolution of the magnetisation as a function of temperature. Of particular interest is the manner in which the transition from the ferromagnetic to the paramagnetic state (or *vice versa*) is undergone.

A model which plays a prominent role in this work is the 2dXY model, since it exhibits a particularly rich phenomenology. Although the onset of spontaneous long range order is precluded by the Mermin-Wagner theorem [1], it may be induced through perturbations such as single-ion anisotropies arising from spin orbit coupling, long range dipolar interactions, or the finite size of a system. Much of the work in this Thesis explores the interplay between these perturbations and how

'2dXY behaviour' is modified, or indeed why it may be retained, in their presence.

A cornerstone in the study of phase transitions is the concept of universality. Entire families of systems behave identically in the neighbourhood of a critical point, such as the liquid-gas critical point in a fluid or the Curie point in a ferromagnet, at which two phases become indistinguishable. Near the critical point, thermodynamic observables do not depend on the details of the intermolecular interactions and so the critical exponents, which quantify how observables go to zero or infinity at the transition, depend only on the range of interaction, symmetries of the Hamiltonian, and spatial dimensionality of the system. Universality arises as the system develops fluctuations of all sizes near the critical point, which wash out the details of interaction and render the system scale invariant. Thus, although mostly concerned with magnetism, the results presented in this work apply to two-dimensional many-body systems in general.

The Thesis is organised as follows.

The first part describes some theoretical background. In particular, Chapter 1 reviews the microscopic origins of magnetism using the Heitler-London theory more commonly encountered in the context of chemical valency. Although by no means the most fundamental approach, this magneto-mechanical parallelism provides a firm basis from which to understand the basic properties of cooperative magnetic phenomena such as ferromagnetism.

The statistical mechanical nature of spin models impinges heavily on the theory of phase transitions and critical phenomena, which is overviewed in Chapter 2. Some important concepts are introduced, such as that of universality, and the Renormalization Group approach is discussed as a powerful tool with which to understand phenomena in the vicinity a critical point. The Monte Carlo method is also discussed, since this has been the main tool adopted for the numerical investigations carried out in this work.

The second part of the Thesis presents work concerning magnetic phenomena in two dimensions. Integral to this is a detailed survey and classification of the experimental literature, which is performed in Chapter 4. The evidence for two-dimensional magnetism is presented, and the main results from the numerous

experimental investigations in the literature are summarised. A quantity which is followed with particular interest is the magnetisation critical exponent β, since it is indicative of the universality class each system belongs to. A similar survey is also performed for non-magnetic two-dimensional systems.

Chapter 5 examines the mechanisms which lead to long range order in two-dimensional continuous spin systems. An important phenomenon encountered in this section is that of crossover between regimes belonging to different universality classes. Establishing the point at which quantities such as the critical exponents change, the nature of their change and what drives this change turns out to be crucial in order to rationalise the behaviour of these systems. A detailed study of the 2dXY model in the presence of symmetry breaking crystal fields is performed, concentrating on the case with four-fold symmetry in particular. The results which arise from this analysis are directly compared to the experimental information collected in Chapter 4.

Finally, Chapter 6 considers the influence of long range interactions, specifically those of the dipolar type, on two-dimensional spin systems. The complex nature of the dipolar interaction presents considerable difficulties in simulation, consequently an approximative model taking shape anisotropy into account is also considered, which is found to lead to interesting physics in its own right.

Part I

Theoretical Background

Chapter 1

Magnetism: An Overview

This chapter introduces the microscopic origins of magnetism by considering the so-called magneto-mechanical parallelism, whereby magnetic moments are expressed in terms of angular momenta and the main results from quantum chemistry applied. Emphasis is placed on the concept of *exchange*, an entirely quantum mechanical phenomenon with no classical counterpart. This serves to demonstrate that at its root, magnetism is a macroscopic display of quantum effects. Subsequently, it will be shown that once the exchange interaction is assumed, simple magnetic models in which there are interactions between many magnetic moments can be constructed. Finally, the chapter ends on a historical note, in which some of the milestones in twentieth century physics which have been pivotal in the understanding of ferromagnetism are outlined.

1.1 Free Magnetic Moments

The magnetism of materials originates from the motion of electrons, which may be either itinerant or localised. In this chapter the emphasis is on localised systems, and scant attention will be paid to itinerant ones. A single electron of charge $-e$ undergoing a circular orbit of radius r with an angular frequency ω gives rise to a current I and hence a magnetic moment $\boldsymbol{\mu}$, as depicted in Figure 1.1. Given that the angular momentum $\mathbf{l}$ is a vector parallel to $\boldsymbol{\mu}$ with a magnitude $l = m_e v r$, where v is the linear velocity, it is straightforward to show that the magnetic moment is

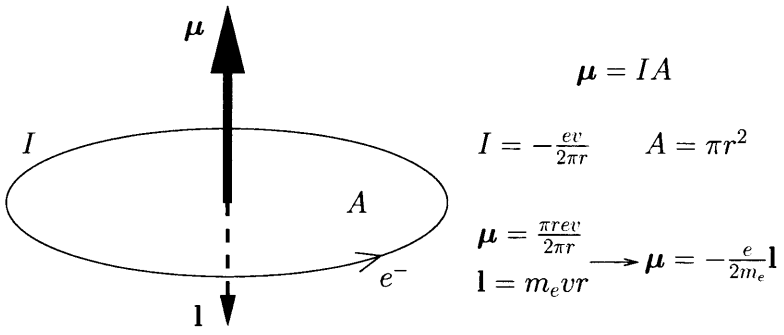

Figure 1.1: An electron $-e$ in a a circular orbit gives rise to an magnetic moment $\boldsymbol{\mu} = -\frac{e}{2m_e}\mathbf{l}$.

proportional to the angular momentum

$$\boldsymbol{\mu} = -\frac{e}{2m_e}\mathbf{l}. \tag{1.1}$$

The magneto-mechanical parallelism also applies in quantum mechanics and in fact the magnetic moment can be replaced, within a proportionality constant $\frac{e}{2m_e}$, by the angular momentum operator ℓ. The magnitude of the orbital angular momentum is $\hbar\sqrt{\ell(\ell+1)}$, so $\boldsymbol{\mu} = -\frac{\hbar e}{2m_e}\sqrt{\ell(\ell+1)}$. One may combine the fundamental constants to form the Bohr magneton, μ_B, which in SI units has the magnitude

$$\mu_B = \frac{\hbar e}{2m_e} = 9.2732 \cdot 10^{-24}\ \mathrm{A\,m^2}, \tag{1.2}$$

whereupon $\boldsymbol{\mu} = -\mu_B\sqrt{\ell(\ell+1)}$. Although the orbital angular momentum gives the same proportionality constant as the classical argument, the angular momentum associated with an electron's spin degree of freedom, $\mathbf{S}$, has a spin magnetic moment

$$\boldsymbol{\mu}_s = -g\mu_B\frac{\mathbf{S}}{\hbar} \tag{1.3}$$

where g takes the value 2.0023 for free electrons. The spin magnetic moment in (1.3) can be derived from Dirac's relativistic theory of the electron, which predicts a g-factor of 2 [2,3]. The small deviation from 2 arises due to the interaction with the magnetic field, with the correction Δg to first order in α being $\Delta g = \alpha/\pi$, where α is the fine structure constant ($\alpha = e^2/\hbar c \simeq 1/137$).

1.1.1 Ground State of Free Magnetic Ions

Single electron states are characterised by the ket symbol $|n, \ell, m_\ell, m_s\rangle$, where n, ℓ, m_ℓ and m_s are the four principal quantum numbers. For atoms having more than one electron, the total orbital and spin angular momenta $\mathbf{L}$ and $\mathbf{S}$ are defined as the vector sums of $\boldsymbol{\ell}_i$ and $\boldsymbol{s}_i$, respectively. Their components along the axes of quantisation are given by $M_L = \sum_i m_i$ and $M_S = \sum_i m_{si}$. The atomic states (terms), obtained by the Coulomb interactions between the electrons, are designated by the symbol ${}^{2S+1}L$, where $2S+1$ denotes the spin multiplicity. These states are $(2L+1)(2S+1)$-fold degenerate, and applying the famous Hund rules allows the identification of the ground state. For example, the Cr^{2+} ion, which has the d^4 configuration, has the ground state

$$|L, M_L, S, M_S\rangle = |2, M_L, 2, M_S\rangle, \tag{1.4}$$

which is denoted by the term symbol ${}^5D$.

1.1.2 Spin-Orbit Coupling

In free atoms, ions in chemical complexes or localised electron states like the $4f$ electrons in rare earth elements, the spin and orbital angular momenta couple and only the total angular momentum $\mathbf{J} = \mathbf{L} + \mathbf{S}$ is conserved. Therefore the states have the form $|J, M_J, L, S\rangle$ and are denoted as ${}^{2S+1}L_J$.

Since $\mathbf{J}$ is a constant of motion, one may think of its direction as being fixed and that $\mathbf{L}$ and $\mathbf{S}$ precess about $\mathbf{J}$ maintaining the triangular relation depicted in Figure 1.2. Consequently the magnetic moment (for constant $\mathbf{J}$) is given by the component of $2\mathbf{S} + \mathbf{L}$ parallel to $\mathbf{J}$

$$\boldsymbol{\mu}_J = -g\frac{\mu_B}{\hbar}(\mathbf{L} + 2\mathbf{S}). \tag{1.5}$$

Since the states are characterised by the eigenvalues of $\mathbf{J}$, this is rewritten as

$$\boldsymbol{\mu}_J = -g_J\frac{\mu_B}{\hbar}\mathbf{J}, \tag{1.6}$$

where

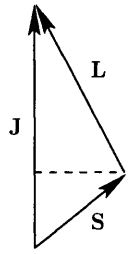

Figure 1.2: Addition of **L** and **S** angular momenta.

$$g_J = 1 + \frac{J(J+1) + S(S+1) - L(L+1)}{2J(J+1)} \tag{1.7}$$

is known as the Landé g-factor, which depending on the relative contributions of the spin and orbit angular momenta may take different values. Thus, in an external magnetic field **H**, the state $|J, M_J\rangle$ is split into $2J+1$ equally spaced states with a separation $g_J \mu_B H$, a phenomenon known as the Zeeman effect.

If magnetic ions are placed in a crystal, they are subject to the crystal electric field produced by the surrounding ionic charges. In transition metal ions this effect is larger than the LS coupling and therefore their electronic states cannot be specified by the value of **J**. On the other hand, in rare earth ions the effect of the crystal field is smaller than the LS coupling and the ionic state may be regarded as the lowest energy state among energy levels split by the LS coupling. This difference between the transition metal and rare earth ions is discussed further in Section 1.3.

1.2 Interactions

In this section the different types of magnetic interaction are considered. These allow the magnetic moments in a solid to communicate with each other and cooperate to potentially produce long range order.

1.2.1 Dipolar Interaction

When considering magnetic systems one thinks first about the interaction between two magnetic moments, and undoubtedly the dipolar interaction plays an important role in magnetism. Two magnetic dipoles $\boldsymbol{\mu}_1$ and $\boldsymbol{\mu}_2$ separated by a distance $\mathbf{r}$ have an energy equal to

$$E_{\text{dip}} = \frac{\mu_0}{4\pi r^3}\left[\boldsymbol{\mu}_1 \cdot \boldsymbol{\mu}_2 - \frac{3}{r^2}\left(\boldsymbol{\mu}_1 \cdot \mathbf{r}\right)\left(\boldsymbol{\mu}_2 \cdot \mathbf{r}\right)\right], \tag{1.8}$$

where μ_0 is the permeability of free space. The interaction depends on the separation and the degree of mutual alignment of the magnetic moments, and it will become clear in this Thesis that these complex characteristics provide quite a challenge when considering this effect in many body systems. Typically, the order of magnitude of the interaction for two moments of $\mu \sim 1\mu_B$ separated by $r \sim 1$ Å is approximately $\mu/4\pi r^3 \sim 10^{-23}$ J, which is equivalent to about 1 K in temperature. As many materials order at much higher temperatures (up to 1043 K in Fe, for example), the dipolar interaction is too weak to account for their ordering. It is, however, manifest on a macroscopic scale through domain formation and demagnetising effects. There are also materials which order at lower temperatures, in some cases even at millikelvin temperatures, where the dipolar interaction does dictate the characteristics of the ordered phase. A notable example is the 'dipolar spin ice' pyrochlore material holmium titanate [4].

1.2.2 Exchange Interaction

The exchange interaction is fundamentally electrostatic in nature, originating from a quantum exchange term in the Coulomb interaction between electrons on neighbouring ions. It arises because the Pauli exclusion principle requires that the wavefunctions of two electrons be antisymmetric with respect to particle interchanges. Consequently, the relative directions of two interacting spins cannot be changed without changing the spatial distribution of the charge. The resulting changes in the electrostatic energy of the whole system act as if there were a direct coupling between the directions of the spins involved. The idea of such an exchange coupling between the spins of two or more atoms first appeared clearly in the work of Heitler

and London [5] on chemical bonding.

Heitler-London Theory for Molecular Hydrogen

Consider two hydrogen atoms a and b, and denote the atomic orbitals of the isolated atoms $\phi_a(\mathbf{r}_1)$ and $\phi_b(\mathbf{r}_1)$ respectively. The wavefunction of the joint state can be approximated as a product of the single electron states $\phi_a(\mathbf{r}_1)\phi_b(\mathbf{r}_2)$. However, this product state does not obey exchange symmetry, as swapping the two electrons around gives $\phi_a(\mathbf{r}_2)\phi_b(\mathbf{r}_1)$, which is not a multiple of the starting configuration. Heitler-London theory assumes the linear combination of the orbital wavefunctions for the isolated atoms

$$\Psi_{\pm}(\mathbf{r}_1, \mathbf{r}_2) = \frac{1}{\sqrt{2(1 \pm S)}} \left[\phi_a(\mathbf{r}_1)\phi_b(\mathbf{r}_2) \pm \phi_a(\mathbf{r}_2)\phi_b(\mathbf{r}_1)\right], \tag{1.9}$$

where the prefactor is a normalisation factor in which S is the overlap integral between $\phi_a(\mathbf{r}_1)$ and $\phi_b(\mathbf{r}_2)$

$$S = \langle a|b\rangle = \int \phi_a^*(\mathbf{r}_1)\phi_b(\mathbf{r}_2)d\tau. \tag{1.10}$$

The Hamiltonian $\hat{\mathcal{H}} = \mathcal{H}_0 + \Delta\mathcal{H}$ of the hydrogen molecule is given by the sum of two H_2^+ ions:

$$\mathcal{H}_0 = -\frac{\hbar^2}{2m}\nabla_1^2 - \frac{\hbar^2}{2m}\nabla_2^2 - \frac{e^2}{4\pi\epsilon_0}\left(\frac{1}{r_{a1}} + \frac{1}{r_{b2}} + \frac{1}{r_{a2}} + \frac{1}{r_{b1}}\right), \tag{1.11}$$

and an electron repulsion term

$$\Delta\mathcal{H} = \frac{e^2}{4\pi\epsilon_0}\left(\frac{1}{r_{12}}\right). \tag{1.12}$$

The expectation values of the Hamiltonian with respect to the symmetric and antisymmetric functions may be calculated as

$$E_{\pm} = \frac{H_{ii} \pm H_{ij}}{1 \pm S^2}, \tag{1.13}$$

in which H_{ii} and H_{ij} are usually referred to as the Coulomb and exchange integrals, defined as

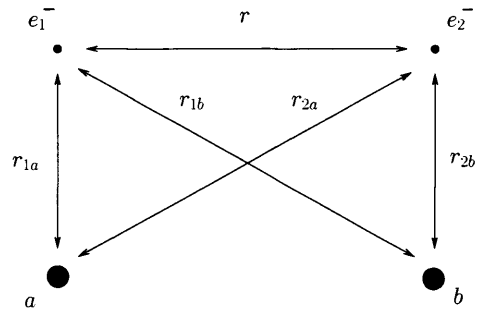

Figure 1.3: Schematic representation of molecular hydrogen.

$$H_{ii} = \langle ab|\hat{\mathcal{H}}|ab\rangle = \iint \phi_a(\mathbf{r}_1)\phi_b(\mathbf{r}_2)\hat{\mathcal{H}}\phi_a(\mathbf{r}_1)\phi_b(\mathbf{r}_2)d\tau_1 d\tau_2 \tag{1.14a}$$

$$H_{ij} = \langle ab|\hat{\mathcal{H}}|ba\rangle = \iint \phi_a(\mathbf{r}_1)\phi_b(\mathbf{r}_2)\hat{\mathcal{H}}\phi_a(\mathbf{r}_2)\phi_b(\mathbf{r}_1)d\tau_1 d\tau_2. \tag{1.14b}$$

So far the spin part of the wavefunction has been ignored, and only the spatial part considered. For an electron the Pauli principle restricts the *overall* wavefunction to being antisymmetric, which demands knowledge of the parity of the spin function. It turns out that the space symmetric (+) solution calls for the spin antisymmetric 'singlet' function, and conversely, the space antisymmetric (−) function calls for any one of the three symmetric 'triplet' functions. The energy separation between the singlet and triplet states is

$$\Delta E = E_- - E_+ = E_t - E_s = 2\frac{H_{ij} - H_{ii}S^2}{1 - S^4}. \tag{1.15}$$

Heisenberg [6], Dirac [7] and Van Vleck [8] independently showed that it is possible to parameterise the energy difference between the singlet and triplet states using $\mathbf{S}_1 \cdot \mathbf{S}_2$ in the effective Hamiltonian

$$\mathcal{H}_{\text{HDV}} = -\frac{J}{2}(1 + 4\mathbf{S}_1 \cdot \mathbf{S}_2), \tag{1.16}$$

where J is called the exchange energy. It is easily shown that this Hamiltonian has eigenvalues $-J$ for the triplet state and $+J$ for the singlet state, so by comparison with (1.15) $\Delta E = 2J$ and J is deduced to be

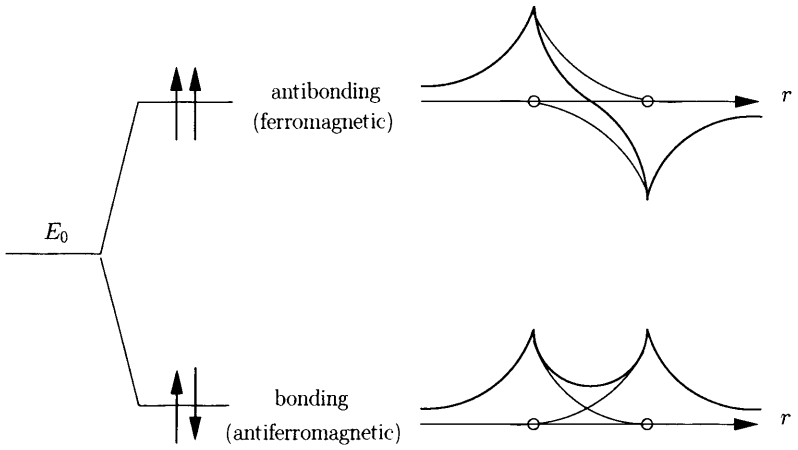

Figure 1.4: Bonding in a hydrogen molecule. The bonding orbital is of lower energy than the antibonding orbital, favouring the singlet ground state in which two electrons fill the bonding state. H_2 has a lower energy than two isolated H atoms (E_0). Heitler and London's theory of chemical valency also provides an embryonic explanation of ferro- and antiferromagnetism.

$$J = \frac{H_{ij} - H_{ii}S^2}{1 - S^4}. \tag{1.17}$$

This equation may be further simplified as the overlap integral S is a small quantity, so S^2 and S^4 may, to a first approximation, be ignored. Thus the exchange energy is roughly equal to the exchange integral, $J \simeq H_{ij}$. In molecular hydrogen the exchange constant is negative, *i.e.* a singlet ground state where the spins are antiparallel (bonding), whereas the triplet state where the spins are parallel (antibonding) has an energy greater than the energy of two unbound atoms. This situation is depicted in Figure 1.4.

Beyond Hydrogen

The theory for the chemical valency in H_2 can be extended to apply to a general coupling between two unpaired electrons associated with neighbouring sites. A negative value of J corresponds to an antiferromagnetic bond, whilst a positive J to a ferromagnetic bond. What the actual sign of J turns out to be depends on the relative magnitudes of the Coulomb, exchange and overlap integrals. It is perhaps unsurprising to find that situations in which $J > 0$ are somewhat less common than those in which $J < 0$.

The constant term in the Heisenberg-Dirac-Van Vleck Hamiltonian (1.16) can be absorbed into other constant energy terms, and so an effective Hamiltonian which consists of a single spin-dependent term can be written as

$$\hat{\mathcal{H}} = -2J\mathbf{S}_1 \cdot \mathbf{S}_2. \tag{1.18}$$

In turn this can be generalised to describe the behaviour of many other magnetic systems with general spin $\mathbf{S}$. By summing it over the pairwise spin-spin interactions in the system one may define the Heisenberg Hamiltonian [9]

$$\begin{aligned} \hat{\mathcal{H}} &= -2J \sum_{i>j} \mathbf{S}_i \cdot \mathbf{S}_j \\ &= -J \sum_{\langle i,j \rangle} \mathbf{S}_i \cdot \mathbf{S}_j \end{aligned} \tag{1.19}$$

where $\langle i, j \rangle$ implies the summation runs over all nearest neighbour spins only. This is an approximation based on the fact that orbital overlap decreases rapidly with distance. Two essential features distinguish the exchange interaction in (1.19) from the dipolar interaction (1.8). The first is that, although it is an electrostatic force, the exchange interaction acts as if there were a very large coupling between spins because of the constraints imposed by the Pauli principle. The second is that exchange is isotropic, which is to say that its strength does not depend on the spatial position of $\mathbf{S}_i$ relative to $\mathbf{S}_j$. Both these facts are consistent with experiment: ferromagnetism is a strong effect, and ferromagnetic media are, to a first approximation, isotropic.

So far only direct exchange has been considered, although this need not necessarily be the case. Neighbouring single electrons may be separated by an intervening ion, whereupon one refers to superexchange. Furthermore, the exchange interaction between magnetic ions can also be mediated by conduction electrons. This is the case in the Ruderman, Kittel, Kasuya and Yosida (RKKY) interaction, also referred to as itinerant exchange, which takes the form of a distance dependent coupling

$$J_{\mathrm{RKKY}}(r) \propto \frac{\cos(2k_{\mathrm{F}}r)}{r^3}, \tag{1.20}$$

at large r (assuming a spherical Fermi surface of radius k_{F}). This interaction is long range and has an oscillatory dependence on the distance of the magnetic moments, and so depending on the separation it may be either ferromagnetic or antiferromagnetic.

1.3 Spin Hamiltonians

The Heisenberg Hamiltonian (1.19) is a good approximation to lowest order in overlap. In practice, however, the Hamiltonians of real systems are considerably more complex, and are subject to important perturbations, most notably crystal fields. In order to explain particular experimental observations, other terms must be added to (1.19). In this section the origins of such phenomenological Hamiltonians are briefly indicated, leaving a more detailed treatment to dedicated textbooks [10, 11]. The present discussion is restricted to insulators.

1.3.1 Transition Metal Ions

The most important feature of the transition metal ions is that the unpaired (*i.e.* magnetic) electrons lie in the incomplete $3d$ shell, which is the outermost in the ion. They are consequently easily influenced by any external fields produced by neighbouring ligands, which is to say that the crystal field is likely to be one of the dominating terms in the Hamiltonian. Consequently one might expect the contributions to the Hamiltonian to be, in order of decreasing strength,

$$\mathcal{H} = \mathcal{H}_{\text{intra-atomic Coulomb}} + \mathcal{H}_{\text{crystal field}} + \mathcal{H}_{\text{spin-orbit}} + \mathcal{H}_{\text{Zeeman}}. \tag{1.21}$$

The intra-atomic Coulomb interaction leads to spectroscopic energy levels, as discussed in Section 1.1.1. It is generally sufficient to consider only the lowest term, since term energies are orders of magnitude smaller than magnetic energies.

The behaviour of a given term in a crystal field is dictated by group theory. Cubic symmetry is the most common symmetry encountered in crystals, and it is possible to predict how a particular term is split in such a case. Furthermore, it is generally found that the crystal field splitting quenches the orbital angular momentum, leaving spin only magnetism.

Introducing the LS coupling partially restores the orbital angular momentum, and leads to g-factors modified from the free electron value. This occurs as follows. Consider the LS coupling and Zeeman terms in (1.21), which are

$$\mathcal{H}_{\text{sp-orb}} = \lambda \mathbf{L} \cdot \mathbf{S}, \tag{1.22}$$

where λ is the spin-orbit coupling parameter, and

$$\mathcal{H}_{\text{Zeeman}} = \mu_B (\mathbf{L} + 2\mathbf{S}) \cdot \mathbf{H}. \tag{1.23}$$

To second order in perturbation theory, the expectation value of $\mathcal{H}_{\text{sp-orb}} + \mathcal{H}_{\text{Zeeman}}$ leads to

$$\mathcal{H}_{\text{eff}} = \sum_{\mu,\nu} \left(\mu_B g_{\mu\nu} H_\mu S_\nu - \lambda^2 \Lambda_{\mu\nu} S_\mu S_\nu - \mu_B^2 \Lambda_{\mu\nu} H_\mu H_\nu \right) \tag{1.24}$$

as the effective Hamiltonian for a non-degenerate ground state split by the crystal field. The first term represents an effective Zeeman energy in which the g-value has been replaced by the g-tensor

$$g_{\mu\nu} = 2 \left(\delta_{\mu\nu} - \lambda \Lambda_{\mu\nu} \right), \tag{1.25}$$

where $\Lambda_{\mu\nu}$ is a coefficient arising from the perturbation calculation. The second term represents the single ion, or magnetocrystalline anisotropy. Since $\Lambda_{\mu\nu}$ reflects the symmetry of the crystal, it follows that the spin Hamiltonian must also reflect this symmetry. For example, for axial symmetry $\Lambda_{xx} = \Lambda_{yy} = \Lambda_\perp$ and $\Lambda_{zz} = \Lambda_\parallel$. Thus, neglecting the last term, the effective axial Hamiltonian is

$$\begin{aligned} \mathcal{H}_{\text{eff}} = {} & g_\parallel \mu_B H_z S_z + g_\perp \mu_B (H_x S_x + H_y S_y) + D \left[S_z^2 - \frac{1}{3} S(S+1) \right] \\ & + \frac{1}{3} S(S+1)(2\Lambda_\perp + \Lambda_\parallel), \end{aligned} \tag{1.26}$$

where $D = \lambda^2(\Lambda_{\|} - \Lambda_{\perp})$. The third term in (1.24) gives rise to the so-called Van Vleck paramagnetism, which is temperature independent.

Although the magnetocrystalline anisotropy is the most significant effect to arise from the influence of crystal fields, other mechanisms affecting the isotropy of (1.19) also exist. For example, it can be shown than an anisotropic exchange term of the form

$$\sum_{i \neq j} (\mathbf{S}_i \cdot \mathbf{D}_{ij} \cdot \mathbf{S}_j + \mathbf{d}_{ij} \cdot \mathbf{S}_i \times \mathbf{S}_j) \tag{1.27}$$

arises from the combined effect of an effective exchange J_{eff} and spin-orbit coupling. $\mathbf{d}_{ij}$ and the traceless asymmetric tensor $\mathbf{D}_{ij}$ result from first and second order spin-orbit coupling, respectively. It can be shown that $\mathbf{d}_{ij} \approx J_{\text{eff}}(\Delta g/g)$ and $\mathbf{D}_{ij} \approx J_{\text{eff}}(\Delta g/g)^2$, where $\Delta g = g - 2$ is the deviation of the g-factor from the free electron value.

1.3.2 Rare Earth Ions

The unpaired electrons of the rare earth ions are shielded by the $5s^2p^6$ shells and are much less affected by crystal fields. Therefore the Hamiltonian is likely to consist of the following terms, in order of descending strength

$$\mathcal{H} = \mathcal{H}_{\text{intra-atomic Coulomb}} + \mathcal{H}_{\text{spin-orbit}} + \mathcal{H}_{\text{crystal field}} + \mathcal{H}_{\text{Zeeman}}, \tag{1.28}$$

i.e. the spin-orbit coupling is a stronger perturbation than the crystal field. This allows the crystal field perturbation to be applied after establishing the value of $\mathbf{J} = \mathbf{L} + \mathbf{S}$. The splitting of the state $|J, M_J\rangle$ is determined by expressing the crystal field in operator equivalents of $\mathbf{J}$.

1.4 Model Magnetism

In many practical cases, the single ion anisotropy is the most influential perturbation to the Heisenberg Hamiltonian (1.19), and other terms such as the anisotropic

exchange and the dipolar interaction may be neglected. Consequently an effective spin Hamiltonian may be written for zero field

$$\hat{\mathcal{H}} = -J\sum_{\langle i,j\rangle} \mathbf{S}_i \cdot \mathbf{S}_j + \sum_i D(S_i^z)^2, \tag{1.29}$$

where negative and positive D correspond to the anisotropy favouring axial alignment (in the z direction) or planar alignment of the spins, thus destroying the rotational invariance of the Heisenberg Hamiltonian. This situation is analogously captured by anisotropic exchange

$$\hat{\mathcal{H}} = -\sum_{\langle i,j\rangle} J_{ij}\left[a(S_i^x S_j^x + S_i^y S_j^y) + b(S_i^z S_j^z)\right]. \tag{1.30}$$

The limiting cases in which $(a,b) = (0,1)$, $(1,0)$ and $(1,1)$ correspond to the Ising, XY and Heisenberg models, which have one, two and three component spins, respectively. Experimentally, it is possible to realise one-, two- and three-dimensional approximations of these models with the appropriate anisotropies.

As will become clear in Chapter 2, spin models are useful in the discussion of critical phenomena. They provide a link between the microscopic picture of magnetism with the macroscopic observation of bulk thermodynamic quantities, such as the magnetisation. To illustrate this as clearly as possible, a highly idealised model which has played a prominent role in the understanding of cooperative phenomena is considered: the Ising model [12].

1.4.1 Ising Model

Consider a square lattice of N sites, on each of which lies a spin taking one of two values, either $+1$ or -1. This can be thought of as an extreme case of uniaxial anisotropy, in which the spins can only be 'up' or 'down'. Each spin interacts with its nearest neighbours through an exchange potential J. The Hamiltonian is

$$\mathcal{H}\{s_i\} = -J\sum_{\langle i,j\rangle} s_i \cdot s_j - h\sum_{i=1}^{N} s_i, \tag{1.31}$$

although in this discussion the second term is set to zero for convenience. A given

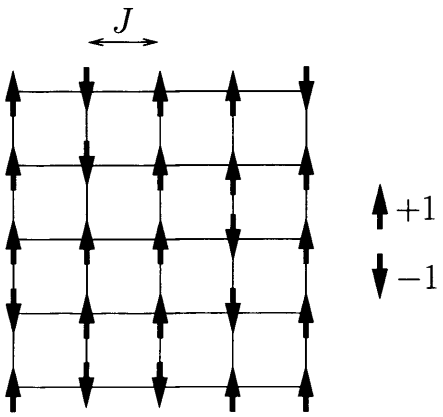

Figure 1.5: A square lattice decorated with Ising spins, which may only take one of two values.

set of numbers $\{s_i\}$ specifies a configuration of the whole system, as shown in Figure 1.5. Assuming equilibrium Boltzmann statistics, the partition function is, in terms of the inverse temperature $\beta = 1/k_B T$,

$$Q(h,\beta) = \sum_{s_1}\sum_{s_2}\cdots\sum_{s_N} e^{-\beta E_i\{s_i\}}, \tag{1.32}$$

where each s_i ranges independently over the values ± 1, giving 2^N terms in the summation. All the thermodynamic functions may be obtained by differentiating the Gibbs free energy

$$G(h,\beta) = -\frac{1}{\beta}\ln Q(h,\beta). \tag{1.33}$$

Thus, the enthalpy H and the specific heat C_h correspond to

$$H(h,\beta) = \frac{\partial}{\partial\beta}\left[\ln Q\,(h,\beta)\right] \tag{1.34}$$

$$C_H(h,\beta) = k\beta^2\frac{\partial^2}{\partial\beta^2}\left[\ln Q\,(h,\beta)\right], \tag{1.35}$$

and the magnetisation M and the magnetic susceptibility χ are given by

$$M(h,\beta) = \frac{1}{\beta}\frac{\partial}{\partial h}\left[\ln Q\left(h,\beta\right)\right] \tag{1.36}$$

$$\chi(h,\beta) = \frac{1}{\beta}\frac{\partial^2}{\partial h^2}\left[\ln Q\left(h,\beta\right)\right]. \tag{1.37}$$

Evaluating the partition function Q is in general a complex task. Before explaining the mathematical details of how this is done, it is perhaps helpful to consider qualitatively three limiting cases in the Hamiltonian (1.31).

1. J > 0 A positive exchange constant favours ferromagnetism such that all the spins are parallel to each other in the ground state[a]. The two-dimensional Ising model is a rare example of a system for which the partition function has been exactly calculated [14]. It displays a continuous phase transition at a critical temperature $T_c = 2J/\ln(1+\sqrt{2}) \simeq 2.269\,J$ [15]. Focusing on the evolution with temperature of the intensive (or 'per spin') magnetisation

$$m = \frac{1}{N}\sum_{i=1}^{N} s_i, \tag{1.38}$$

one notices that it decreases from unity with increasing temperature. At low temperature, J dominates and the system is ordered, but with increasing thermal randomisation the system begins to disorder, and eventually undergoes a phase transition into a paramagnetic phase in which the magnetisation tends to zero, as shown in Figure 1.6. A qualitatively similar behaviour is found in many spin models, and understanding the quantitative details of these phase transitions is a large area of study which will be considered more carefully in the next chapter.

2. J < 0 In the case of a negative exchange constant, it is energetically favourable to align the spins antiparallel to each other to give an antiferromagnetic ground

[a]If one thinks carefully the Ising model has two ground states, one in which all spins point 'north' and the other in which they all point 'south'. The fact that in the thermodynamic limit ($N \to \infty$) only one of these states is 'chosen' is an example of broken symmetry. That is to say the system undergoes a transition to a ground state possessing a symmetry not present in the original Hamiltonian. For a classic layman's account on these ultimately rather profound considerations, see the article by Anderson [13].

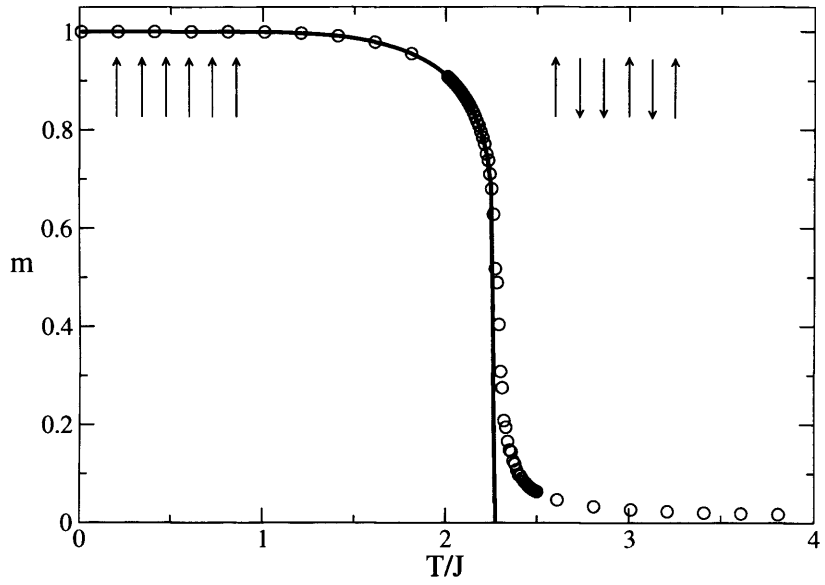

Figure 1.6: Magnetisation as a function of temperature for the Ising model. The circles represent Monte Carlo data for a system consisting of 10 000 spins (see Section 2.3 for a discussion on how data such as this is calculated), the solid line is the exact solution derived by Onsager [14].

state. Measuring the intensive magnetisation is of limited value in this case, as the spins cancel each other out. A more suitable order parameter is the staggered magnetisation, which quantifies the difference between the magnetisations of the two interpenetrating sublattices which together form the crystal lattice of the system. This is defined as

$$m_s = \frac{1}{N}\sqrt{\left(\sum_i \mathrm{sgn}(i)s_i\right)^2}, \tag{1.39}$$

where $\mathrm{sgn}(i)$ is ± 1 depending on which sublattice the site i lies. Antiferromagnets based on triangular lattices are also known to lead to interesting physics. One can easily see that placing Ising spins on a triangular plaquette leads to an ambivalent situation: if spin **a** points up and spin **b** points down, it is not clear where spin **c** ought to point. The fact that the energy of all the pairwise interactions cannot be simultaneously minimised as a result of geometrical constraints leads to unexpected magnetic phenomena, and in recent years there has been a surge of interest in these so-called *frustrated* magnets [16, 17].

3. J = 0 Setting the exchange coupling to zero implies dealing with an uncoupled paramagnetic system. Calculating Q thus becomes trivial, since it factorises into a product of single site terms, each describing a single Ising spin in a magnetic field h. Consequently

$$Q = \left[\exp\left(\frac{h}{k_BT}\right) + \exp\left(-\frac{h}{k_BT}\right)\right]^N = \left[2\cosh\left(\frac{h}{k_BT}\right)\right]^N. \tag{1.40}$$

The magnetisation per spin $m = M/N$ is given by

$$\begin{aligned}\langle m\rangle &= -\frac{1}{N}\frac{\partial G}{\partial h} = \frac{\partial}{\partial h}(k_BT\ln Q) = k_BT\frac{1}{Q}\frac{\partial Q}{\partial h} \\ &= \frac{\exp\left(\frac{h}{k_BT}\right) - \exp\left(-\frac{h}{k_BT}\right)}{\exp\left(\frac{h}{k_BT}\right) + \exp\left(-\frac{h}{k_BT}\right)} = \tanh\left(\frac{h}{k_BT}\right).\end{aligned} \tag{1.41}$$

Hence the susceptibility is

$$\chi = \frac{\partial m}{\partial h} = \frac{1}{k_BT}\frac{1}{\cosh^2\left(\frac{h}{k_BT}\right)}, \tag{1.42}$$

although generally it is simpler to consider the susceptibility in zero field

$$\chi(h \to 0) = \frac{1}{k_BT}. \tag{1.43}$$

The expressions for N uncoupled spins can be derived by simply scaling the results (1.41) and (1.43) by a factor of N. For the susceptibility one has thus derived the famous Curie law

$$\chi(T) = \frac{N}{k_BT}, \tag{1.44}$$

which displays a characteristic $1/T$ divergence, as shown in Figure 1.7.

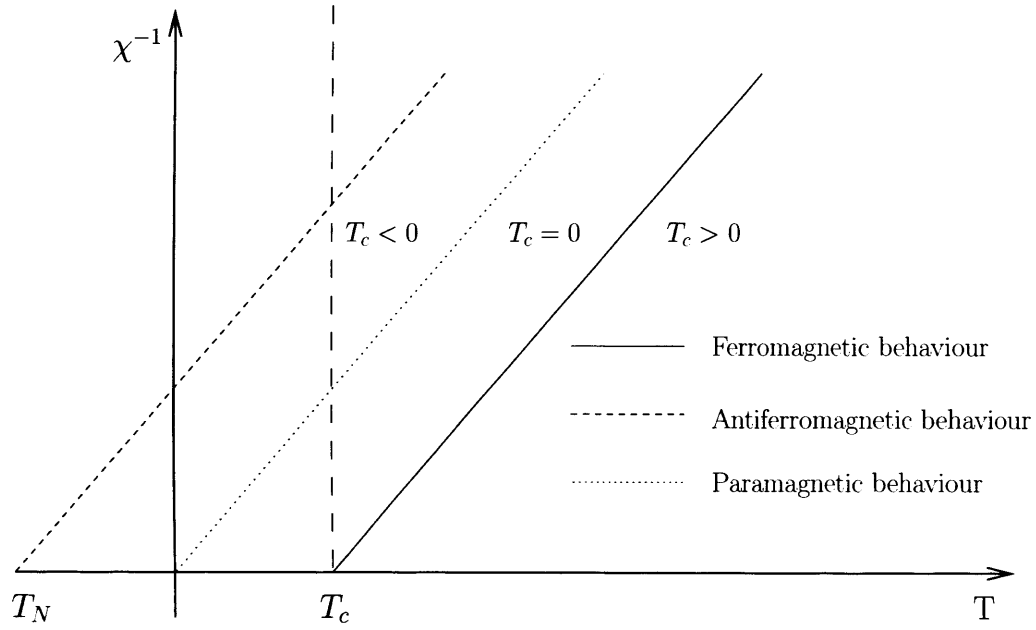

Figure 1.7: Inverse susceptibility as a function of temperature for para-, ferro- and antiferromagnetic systems. The Curie-Weiss law states that $\chi \propto 1/(T - T_c)$ for $T > T_c$. Plotting the inverse susceptibility is common practice with experimental data as the extrapolation of the linear region to low temperature allows one to establish the average coupling present between the spins. A negative intercept with the abscissa implies antiferromagnetism whereas a positive intercept implies ferromagnetism.

1.4.2 Weiss Molecular Field Model

The earliest microscopic theory of ferromagnetism is due to Weiss [18, 19], who in 1907 tried to understand what happens when $J \neq 0$ by postulating that each spin experiences the presence of an effective field h_{eff} due to the magnetic moment of all the other spins. This phenomenological 'molecular field' theory furnishes a remarkable description of the salient experimental facts, and has the merit of great simplicity. The essential step lies in approximating the Hamiltonian (1.31) in a form appropriate to a paramagnetic spin in an effective field h_{eff}

$$\mathcal{H}\{s_i\} = -\sum_i s_i h_{\text{eff}} \tag{1.45}$$

where

$$h_{\text{eff}} = \sum_j J_{ij}\langle s_j\rangle + h. \tag{1.46}$$

Here, the first term is the molecular, or mean field, and the second term is the external field. If the spins reside on a d dimensional lattice, then the coordination number z of each site is $2d$, and

$$h_{\text{eff}} = zJM + h, \tag{1.47}$$

where $M = \langle s_j\rangle$ is the average value of s_j. The magnetisation may be calculated self-consistently from Equation (1.41)

$$M = \tanh\left(\frac{zJM + h}{k_B T}\right). \tag{1.48}$$

Even in the absence of an external magnetic field h, the same idea may be applied to obtain a spontaneous magnetisation. Setting $h = 0$

$$M = \tanh\left(\frac{zJM}{k_B T}\right). \tag{1.49}$$

Approximating $\tanh x$ to $x + \frac{1}{3}x^3$ for small x, and after solving for M, the relation (1.49) reduces to

$$\chi = \frac{\partial M}{\partial h} = \frac{1}{k_B(T - T_c)}, \tag{1.50}$$

where χ denotes the magnetic susceptibility and

$$T_c = \frac{zJ}{k_B}. \tag{1.51}$$

Equation (1.50) has a singularity at $T = T_c$, and this identifies the critical point or 'Curie temperature'. In the case of T_c being negative the system is an antiferromagnet, in which case one refers to the Néel temperature T_N.

There are two successes in particular which make Weiss theory stand out. Firstly, above T_c it correctly predicts the so-called Curie-Weiss law (1.50), *i.e.* the inverse susceptibility as a function of temperature is linear, as shown in Figure 1.7. Secondly, the theory predicts a universal 'critical behaviour' just below T_c, which although quantitatively wrong, is at least qualitatively correct. Understanding why this is the case took many more decades of work, but the answer lies in the evaluation of the partition function (1.32). The molecular field approach approximates the interacting scenario of the Ising model to a simpler non-interacting one, *i.e.* it is a mean field theory. However, the many-body nature of spin systems is such that it is not sufficient to simply average the interactions out. Fluctuations play a crucial role, and must be explicitly included in order to improve the theoretical description.

1.4.3 Continuous Models

In continuous spin systems such as the XY and Heisenberg models, the simplest excited states at low temperature are phased combinations of spin deviations on neighbouring sites, known as spin waves, or when quantised, magnons (Figure 1.8). These excitations arise essentially because it is energetically favourable to 'smear out' spin flips over many ions. In one dimension the magnon energy depends on the wavevector $\mathbf{q}$ as [20]

$$E(\mathbf{q}) = 4JS(1 - \cos(\mathbf{q}\,a)), \tag{1.52}$$

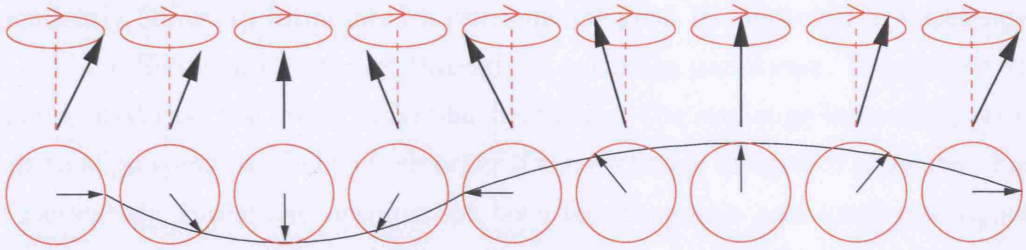

Figure 1.8: A spin wave.

where a is the lattice constant. The equivalent expression for a two-dimensional lattice is derived in a classical calculation in Appendix A.

In two-dimensional systems the influence of spin waves is dramatic, since it prevents the onset of spontaneous long range order. This is a result which is generally referred to as the Mermin-Wagner theorem [1]. In experiment, spontaneous ordering is restored by the presence of perturbations such as those discussed above. This emphasises the fact that capturing the correct form of the Hamiltonian is crucial if one is to explain the experimental data at hand.

1.5 Historical Development

Formulated before the advent of quantum mechanics, the great mystery of Weiss's theory was how to explain the very large molecular fields. For a ferromagnet with $S = \frac{1}{2}$ and $T_c \sim 10^3$ K, it follows from (1.51) that $h_{\text{eff}} = k_B T_c/\mu_B \sim 1500$ T, an enormous magnetic field which quite evidently cannot be explained by the dipolar interaction (1.8). Following the experimental discovery in 1925 by Uhlenbeck and Goudsmit [21, 22] that the electron has an internal degree of freedom, which by analogy with the other angular momenta has become known as the spin[b], a number of notable theoretical developments occurred. In 1927 Heitler and London [5] published their quantum mechanical calculation of the H_2 molecule, showing the importance of the exchange integral. This gave the molecular field of the Weiss model a direct quantum mechanical origin. Prior to this Heisenberg [6], and in-

[b]In fact this analogy is somewhat limited. The actual origin of spin was discovered by Dirac on formulating relativistic quantum mechanics [3, 23, 24].

dependently Dirac [7], formulated a phenomenological Hamiltonian in which spins located on different sites interact through an exchange parameter. Heisenberg also demonstrated that the Weiss molecular field is just the exchange interaction which tends to align spins parallel to each other if the exchange integral is negative. Thus the Heisenberg model can account for both ferromagnetic and antiferromagnetic order, and furthermore allows for the presence of spin waves. By coincidence, 1925 was also the year in which the Ising model was devised [12]. Although highly simplified, this model has the merit of allowing mathematical rigour and has proven to be immensely useful in providing further insight on the nature of phase transitions. Onsager's exact solution of the two-dimensional case [14] is in this respect considered an achievement of pivotal importance. Further information on the history of magnetism, particularly with regards to the main developments prior to the twentieth century, is found in the books by Mattis [25] and Mohn [26].

1.6 Concluding Remarks

This chapter has attempted to justify the form of the Hamiltonians of insulating magnetic materials from microscopic considerations. However, it is clear that in doing so a series of drastic approximations and assumptions have been made. Hence one generally refers to the spin *models*, which are invoked as a hypothesis that is justified in so far as it fits experimental data. Likewise, the exchange (J) and anisotropy (D) energies are usually considered as parameters to be determined from experiment. Despite these caveats, the degree of physical insight spin models give is remarkable, and they are usually taken as the starting point for discussions of ferro-and antiferromagnetism in insulators.

The role of perturbations is crucial in determining the precise behaviour of a particular spin model. For example, it has been shown how the single ion anisotropy gives a mechanism whereby a mainly spin-type magnetic moment is coupled with the directionality of the crystal. In fact, in continuous two-dimensional spin systems long range order can only occur through the presence of perturbations, since it would otherwise be precluded by the Mermin-Wagner theorem. Much of the work in this Thesis is concerned with understanding the influence of such perturbations.

Chapter 2

Phase Transitions and Critical Phenomena

This chapter reviews the main concepts concerning phase transitions and critical phenomena, focusing in particular on magnetic systems. As discussed in the previous chapter, the study of phase transitions has proven to be of particular significance in condensed matter physics as a result of there being good experimental realisations of simple Hamiltonians. These simple idealisations, known as model magnets, provide an excellent starting point for a discussion on many-body systems and their statistical mechanics. In fact, it turns out the statistics of other non-magnetic systems can usually be formulated in terms of effective spin Hamiltonians, such that the 'magnetic language' of spins and exchange couplings has become commonplace when referring to cooperative phenomena.

The study of critical phenomena has brought about some of the most profound theoretical discoveries of twentieth century physics, and as a result there is an enormous literature on the subject [27–31]. With hindsight, it is possible to recognise two paradigm shifts which have been pivotal in leading the way to the current status of understanding. The first one, which is actually rather difficult to place historically, was the realisation that classical thermodynamics fails in the vicinity of a transition point. To gain insight as to why this is the case it is necessary to recognise the cooperative effects inherent to many-body systems by invoking statistical mechanics. The second paradigm shift occurred with the development of

theories based on an expected scale invariance near the critical point, which make it feasible to renormalize the interactions present in many-body systems.

In a sense this chapter will mirror this historical evolution. In the first section, the thermodynamic concepts which underlie the basic theory of phase transitions are presented. Although these provide a rather good description of experiment, they will be shown to break down near the transition points of so-called continuous phase transitions. A fundamentally different approach is required in order to rationalise these critical phenomena, and this is provided by statistical mechanics, discussed in the second section. Subsequently, the so-called scaling and Renormalization Group (RG) theories will be discussed, albeit with a focus on general ideas and results rather than mathematical rigour. The third part of the chapter examines the Monte Carlo methods. These are widely adopted computational techniques which circumvent having to evaluate the partition function exactly, a problem which is generally intractable analytically. The final part of the chapter makes use of these theoretical tools in order to examine the unusual properties of a model which plays an important role in this Thesis: the 2dXY model.

2.1 Phase Transitions

2.1.1 Basic Considerations

Phase transitions are generally associated with a sharp change in the properties of a substance. Everyday examples include the changes of state undergone by water and the transition from the ordered, ferromagnetic state to the disordered, paramagnetic state observable in magnets. Two types of phase transitions can be distinguished, denoted *first order* and *second order*, or *discontinuous* and *continuous*, respectively. The two phases between which the transition occurs are distinguished by an *order parameter* which is zero in the disordered phase and nonzero in the ordered phase. At a first order transition, the order parameter changes discontinuously at the transition, whereas the change at a second order transition is continuous, but not differentiable as a function of an intensive variable, such as the temperature.

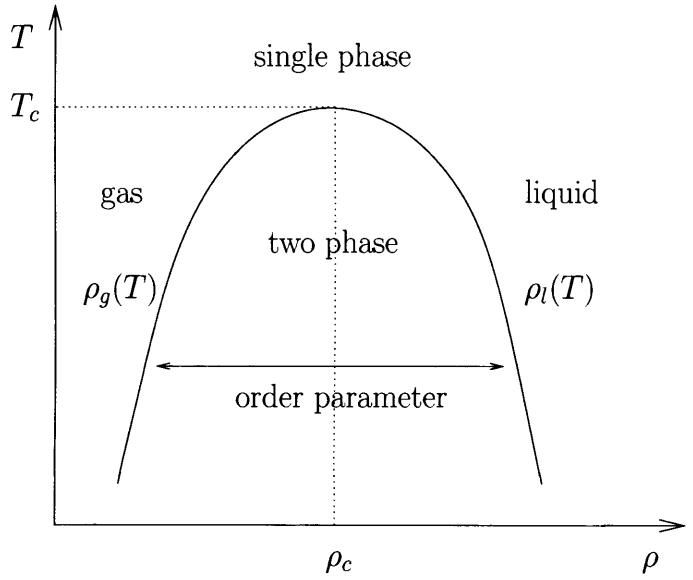

Figure 2.1: Density-Temperature phase diagram for a fluid at fixed pressure. The order parameter for the liquid-gas transition is $|\rho_g(T) - \rho_l(T)|$.

Liquid-Gas Transition

As a practical example, consider the phase diagram of a typical fluid at fixed pressure shown in Figure 2.1. Below a *critical temperature* T_c it is found that as the density is increased at fixed temperature it is not possible to pass from the gaseous phase to the liquid phase without passing through a regime in which the two phases coexist. Crossing this regime involves a discontinuous jump in the system density and a latent heat, and is typical of a discontinuous transition. As the temperature increases the difference in density between the liquid and the gas, which represents the *order parameter* of the system, decreases continuously to zero. Above T_c it is possible to pass continuously from a gas to a liquid as the density is increased at constant temperature. Even starting below T_c, it is always possible to circumvent the critical point by varying the temperature and density accordingly, suggesting that there is no obvious way to distinguish between a liquid and a gas.

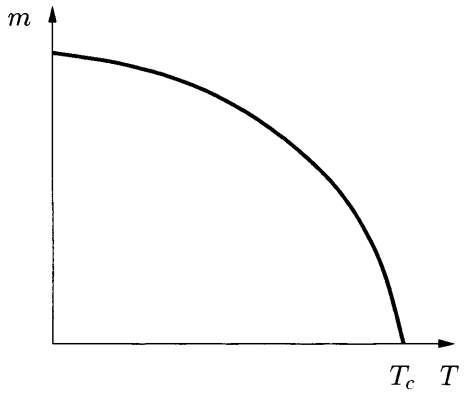

Figure 2.2: Behaviour of the magnetisation as a function of temperature for a simple ferromagnet.

Ferromagnetic Transition

Another example, which is more pertinent to the subject of this Thesis, is the phase transition of a ferromagnet in zero field. It was shown in the previous chapter that a magnet may be regarded as a set of interacting spins residing on the vertices of a crystal lattice. The simplest idealisation of such a system is the Ising ferromagnet, which constrains the spins to point in one of only two directions (see Section 1.4.1). At high temperature the system is in a paramagnetic, or disordered phase, characterised by a net magnetic moment that is zero. Below a critical temperature T_c, however, the spins tend to be aligned with each other, and there is a net magnetisation $m(T)$. The onset of this ferromagnetic behaviour is a continuous phase transition, as the magnetisation rises continuously from zero as the temperature is reduced below T_c, as shown in Figure 2.2. The fact that the magnetisation is zero above the transition and non-zero below the transition temperature identifies it as the order parameter in this case.

2.1.2 Thermodynamic Considerations

A thermodynamic system is described by a set of potentials, each associated with a pair of 'natural' variables[a]. If a particular potential is given as a function of these

[a]The natural variables of a potential X are those that enable dX to be readily separated into components of heat and work, and that lead to physically relevant partial derivatives of X.

Table 2.1: Thermodynamic potentials for a magnetic system at constant volume V, and their associated natural variables.

Thermodynamic Potential	Natural Variables
Internal energy U	Magnetisation M, Entropy S
Enthalpy H	Entropy S, Field h
Gibbs free energy G	Field h, Temperature T
Helmholtz free energy F	Temperature T, Magnetisation M

variables, then all the thermodynamic properties of the system may be found, as it is possible to derive the other potentials by a series of Legendre transforms [32].

Table 2.1 lists the thermodynamic potentials that are relevant to a magnetic system of fixed volume. In this case, the combined first and second laws of thermodynamics can be written as

$$dU = TdS + hdM, \tag{2.1}$$

The internal energy U is a thermodynamic potential in the sense that other interesting properties can be expressed as its derivative:

$$T = \left(\frac{\partial U}{\partial S}\right)_M \quad \text{and} \quad h = \left(\frac{\partial U}{\partial M}\right)_S. \tag{2.2}$$

Of course, certain properties are more easily manipulable in the laboratory than others, so it is of practical use to derive potentials which have easily accessible natural variables. It is straightforward to show that for magnetic systems the most convenient potentials are the Gibbs and the Helmholtz free energies. Recall their thermodynamic definitions:

$$F = U - TS \tag{2.3}$$

$$G = U - TS - Mh. \tag{2.4}$$

Differentiating and using Equation (2.1)

$$dF = dU - TdS - SdT = hdM - SdT \tag{2.5}$$

$$dG = dF - hdM - Mdh = -SdT - Mdh, \tag{2.6}$$

from which it follows that $G \equiv G(h, T)$ and $F \equiv F(M, T)$[b].

A phase transition is signalled by a singularity in one of the thermodynamic potentials. If there is a discontinuity in one or more of the first derivatives of the appropriate thermodynamic potential the transition is termed first order. If first derivatives are continuous but second derivatives are discontinuous or infinite, the transition is described as second-order, or continuous[c].

As an example, consider a simple ferromagnet in a magnetic field. Its (h, T) phase diagram is shown in Figure 2.3(a), and it is characterised by a phase boundary at $h = 0$ extending from $T = 0$ to a finite temperature T_c. The two phases reflect the symmetry of a ferromagnet under reversal of the magnetic field. For the purposes of this discussion it is interesting to describe the field dependence of the free energy and its field derivatives, the magnetisation and the susceptibility, along the three paths 1, 2, and 3 (below, at and above T_c). Crossing the phase boundary by following path 1 results in a discontinuity in the magnetisation $M = -\left(\frac{\partial G}{\partial h}\right)_T$ *i.e.* the transition is first order. Following path 2 does not result in a discontinuity in the magnetisation, but it is found that the susceptibility $\chi = \left(\frac{\partial M}{\partial h}\right)_T$ diverges as $h \to 0$, *i.e.* the transition is continuous at T_c. Finally, it is found that following path 3 does not result in any singularities, neither in the magnetisation nor in the susceptibility.

[b] In many textbooks (*e.g.* Huang [33]), the natural variables of F and G are inverted *i.e.* $G \equiv G(M, T)$ and $F \equiv F(h, T)$. This arises as a consequence of expressing (2.1) in an alternative form $dU = TdS - Mdh$.

[c] The term 'second order' is used synonymously with 'continuous' throughout this Thesis, although strictly speaking they have slightly different meanings. The categorisation of transitions as first order, second order and so on is due to Ehrenfest [34], who categorised transitions according to discontinuities in thermodynamic derivatives. In fact, this classification scheme has turned out to be inappropriate, as it does not correctly recognise divergences.

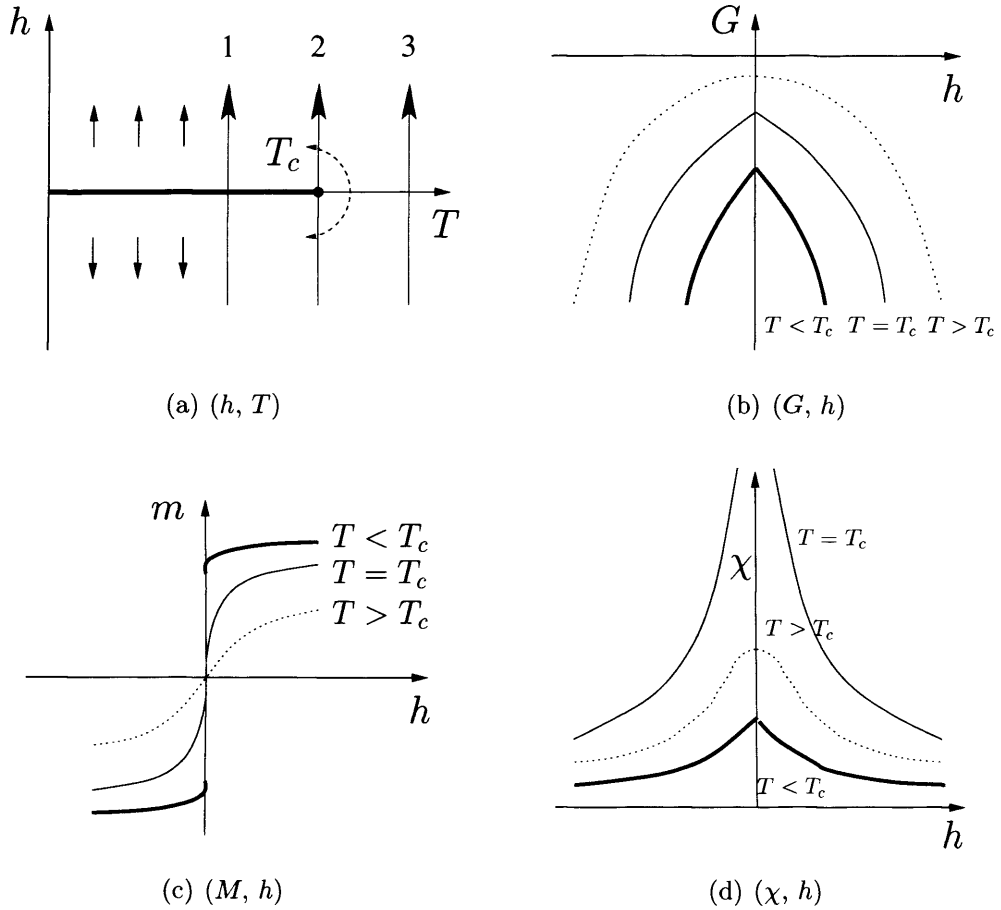

Figure 2.3: (a) Phase diagram for a ferromagnet in the (h, T) plane. (b) Field dependence of the free energy. (c) Field dependence of the magnetisation. (d) Field dependence of the susceptibility.

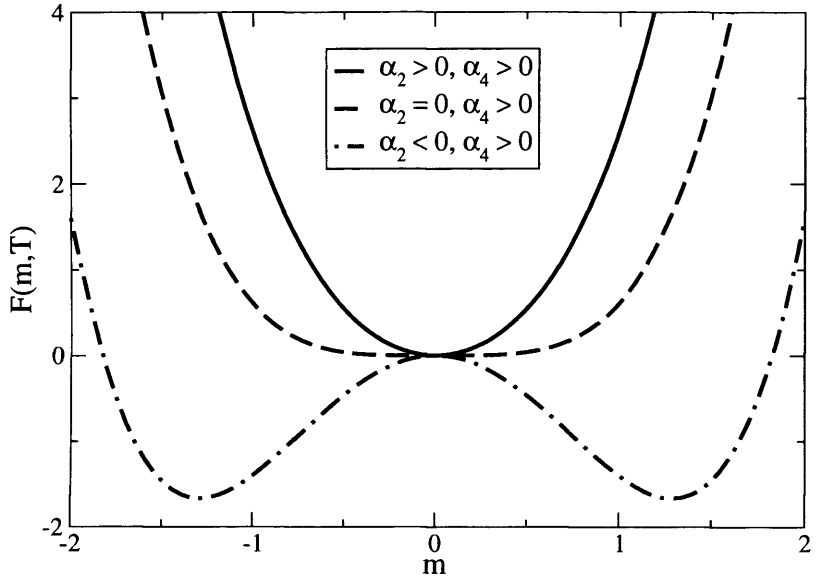

Figure 2.4: Possible shapes of $F(m,T)$ for various signs of the expansion coefficients.

2.1.3 Landau's Mean Field Theory

In 1937 Landau constructed a generalised theory of phase transitions [35,36]. The fundamental hypothesis is that in the vicinity of the critical point the Helmholtz free energy may be expanded in a power series in the order parameter, denoted by m. The equilibrium value of m is then the value that minimises the energy. Furthermore, it is also assumed the Helmholtz free energy has the simple symmetry $F(m,T) = F(-m,T)$, and that the field h which is conjugate to the order parameter is zero. No assumption is made on the exact nature of the order parameter. Thus the most general expansion of $F(m,T)$ is

$$F(m,T) = \alpha_0(T) + \alpha_2(T)m^2 + \alpha_4(T)m^4 + \cdots \tag{2.7}$$

where each of the expansion coefficients is effectively a function T only. The shape of $F(m,T)$ as a function of m, for small m, is shown in Figure 2.4 for a few possible combinations of signs of α_2 and α_4.

A point on the extrapolated coexistence line ('beyond' the critical point) in Figure 2.3(a) is in the paramagnetic region where the Helmholtz potential has a single minimum. This implies that $\alpha_2(T)$ and $\alpha_4(T)$ are positive. As the point of

interest approaches and then passes the critical point along the coexistence line, the function $\alpha_2(T)$ passes through zero and becomes negative (Figure 2.4). The function $\alpha_4(T)$ usually remains positive, and $F(m,T)$ splits into two minima which correspond to the two possible states formed as a result of the two possible field directions. The critical temperature is therefore viewed as the temperature at which α_2 happens to have a zero.

The change in sign of α_2 at the critical point implies it may be written as

$$\alpha_2(T) = (T - T_c)\alpha_2^0. \tag{2.8}$$

It is then straightforward to work out the temperature dependence of the order parameter

$$\frac{\partial F}{\partial m} = 2(T - T_c)\alpha_2^0 m + 4\alpha_4 m^3 + \cdots = 0. \tag{2.9}$$

Below T_c it is found that

$$m = \pm\left[\frac{\alpha_2^0}{2\alpha_4}(T_c - T)\right]^{1/2}. \tag{2.10}$$

The basic conclusion of the classical theory of critical points is therefore that the order parameter spontaneously becomes nonzero and grows as $(T_c - T)^\beta$ for temperatures below T_c. This *critical exponent* β has the value

$$\beta(\text{classical}) = 1/2. \tag{2.11}$$

Using these arguments it is also possible to evaluate the temperature dependence of other thermodynamic quantities (see Table 2.3).

Comparison with Experiment

In light of the mean field prediction, it is of interest to consider the curves in Figures 2.1 and 2.2 and ask what shape they might be near their respective critical points. For example, for the fluid sulphur hexafluoride it is experimentally found that [37]

$$|\rho_g - \rho_l| \propto |T - T_c|^{0.327(6)} \tag{2.12}$$

where $\rho_{g,l}(T)$ are the values of the density at coexistence of the two branches of the coexistence curve below T_c. To within experimental error, the value of the critical exponent is not found to depend on the particular fluid system studied. This remarkable fact was made clear by Guggenheim [38], who observed almost identical coexistence curves for eight different fluids, provided suitable reduced units were adopted. Even more surprisingly, certain categories of magnets also display comparable exponents. For example, near T_c it is found that EuO obeys the power law [39]

$$M \propto (T_c - T)^{0.367(8)}. \tag{2.13}$$

These critical exponents are not obviously simple rational fractions, and are clearly different from the mean field prediction given in Equation (2.11). In fact, it was the overwhelming experimental evidence that the exponents were different from 1/2 that forced the physics community in the 1930s to realise that there was a deep rooted problem lurking in these seemingly unimportant critical exponents.

2.2 Critical Phenomena

2.2.1 Critical Exponents, Power Laws and Scale Invariance

In order to define a critical exponent, it is convenient to define the reduced temperature $t = (T - T_c)/T_c$ as a measure of the distance of the system from the critical point. The variation with temperature of a general thermodynamic function $f(t)$ may thus be approximated by a power law expansion in t such as

$$f(t) = At^{\lambda}(1 + Bt^{\mu} + \cdots), \tag{2.14}$$

where the exponent of the leading term λ is defined as

$$\lambda = \lim_{t \to 0} \frac{\ln[f(t)]}{\ln(t)}. \tag{2.15}$$

To a first approximation the higher order terms in (2.14) may be neglected, yielding a power law

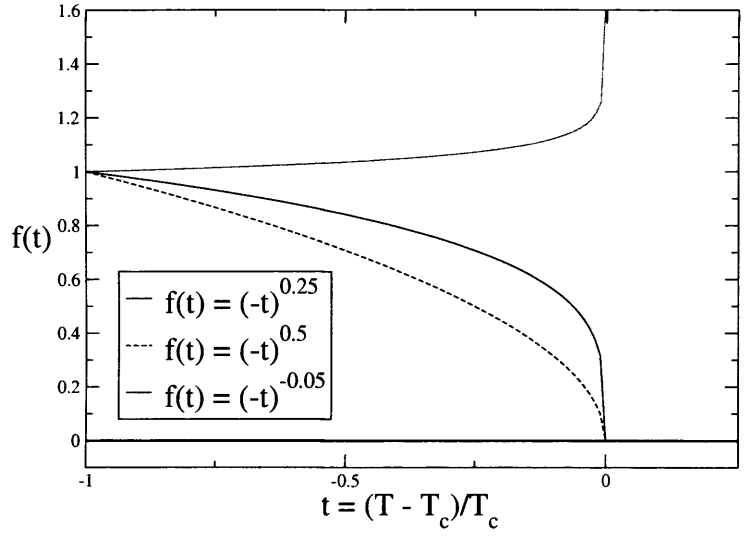

Figure 2.5: Power laws resulting from different critical exponents.

$$f(t) \sim t^{\lambda}, \tag{2.16}$$

in which λ is the critical exponent. The form of (2.16) is such that a negative exponent corresponds to a function that diverges as $t \rightarrow 0$ whereas a positive exponent yields a function which approaches zero. In addition, it is clear from Figure 2.5 that a smaller value of $|\lambda|$ results in a more abrupt change of $f(t)$ as $t \rightarrow 0$.

The observation of power law behaviour is significant as it is a mathematical expression of scale invariance. This becomes clear if one considers the effect of a change of scale on a power law compared to that on some other functional form. A plot of $y = x^n$ may be superimposed on a plot of $y = (ax)^n$ by linear changes in the scale of the two axes by a factor of n, whereas this is manifestly not possible, for example, in the case of an exponential function $y = \exp(x)^n$. In this sense a phenomenon obeying a power law looks the same regardless of the scale one probes it, *i.e.* it is scale invariant. In order to gain further insight into this phenomenon, it is helpful to consider the snapshot of the Ising model on a square lattice at criticality, shown in Figure 2.6. The black and white areas represent the spin-up and spin-down regions, respectively. The difference of the two areas divided by the

Table 2.2: Definitions of the principal critical exponents for magnetic systems. In the expression for the correlation function at T_c, d is the lattice dimensionality.

Zero field specific heat	$C_H \propto \lvert t\rvert^{-\alpha}$
Zero field magnetisation	$m \propto \lvert t\rvert^{\beta}$
Zero field susceptibility	$\chi \propto \lvert t\rvert^{-\gamma}$
Critical isotherm	$m \propto \lvert h\rvert^{1/\delta}$
Correlation length	$\xi \propto \lvert t\rvert^{-\nu}$
Pair correlation function at T_c	$G(r) \propto 1/r^{d-2+\eta}$

total area gives the intensive magnetisation which, given the system is at its critical point, is only nonzero because of its finite size. The self similarity characteristic of a power law is clearly noticeable in terms of the fractal structures that are present. If one were to magnify Figure 2.6, it would be noticeable that within the scaling 'window' limited by the system size and the lattice spacing, the pattern in which the spins lie is statistically indistinguishable from that in the unmagnified picture.

Table 2.2 lists and gives the definitions of the principal critical exponents which characterise the power laws for the thermodynamic properties of a ferromagnet. In principle, one should consider the possibility of different exponents occurring for the quantities which diverge as the transition temperature is approached from either above or below. In practise this is not the case, the singularities are generally symmetric about the transition, making only one exponent necessary. Furthermore, the power laws need not necessarily be functions of the temperature: the exponent δ, for example, is defined with respect to the reduced external field $h = H/k_BT$.

Only two of the six critical exponents defined in the preceding discussion are independent, because of the following scaling laws:

$$\text{Fisher}: \quad \gamma = \nu(2-\eta) \tag{2.17}$$

$$\text{Rushbrooke}: \quad \alpha + 2\beta + \gamma = 2 \tag{2.18}$$

$$\text{Widom}: \quad \gamma = \beta(\delta - 1) \tag{2.19}$$

$$\text{Josephson}: \quad \nu d = 2 - \alpha \tag{2.20}$$

where, in the last relation, d is the dimensionality of space. These relations were

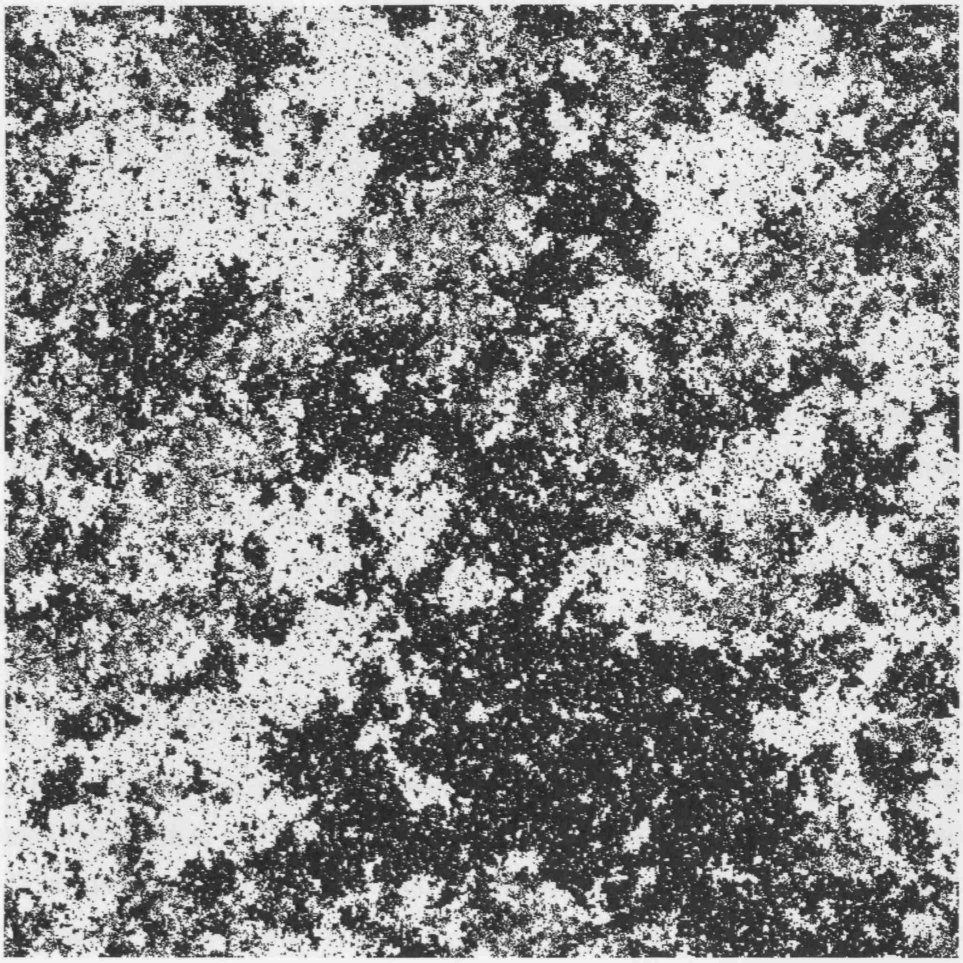

Figure 2.6: Snapshot of the Ising model at the critical point. Self similar, or fractal structures are clearly present, and black or white 'islands' are present in all sizes. The system cannot separate into black and white, so it fluctuates on all scales, exhibiting critical phenomena. After Sethna [40].

Table 2.3: Critical exponent values for systems belonging to the mean field, 2d Ising, 3d Ising and 3d Heisenberg universality classes. The values for the 2d Ising class all follow from Onsager's exact solution [14]. All the categories obey the hyperscaling relations (2.17–2.20), except for the mean field class, which is only self consistent for $d = 4$.

Exponent	MF	2d Ising	3d Ising [41]	3d Heisenberg [42]
α	0 (disc.)	0	0.1106	-0.1336
β	1/2	1/8	0.3264	0.3689
γ	1	7/4	1.2365	1.3960
δ	3	15	4.7883	4.783
ν	1/2	1	0.6298	0.7112
η	0	1/4	0.0366	0.0375
$(2-\alpha)/\nu d$	$4/d$	1	1	1

originally derived as inequalities using dimensional analysis [27], but are experimentally verified as equalities. They also suggest that systems fall into 'universality classes' and that the critical indices are the same only within a particular universality class. The critical exponents of some commonly encountered universality categories are summarised in Table 2.3

2.2.2 Statistical Mechanics

Phase transitions take place in systems of many constituents (or many states) because of statistics, or interactions, or both. It is therefore necessary to adopt a statistical mechanical approach which considers these degrees of freedom explicitly. If a system has a state i with energy E_i, the probability of the system being in this state is, assuming equilibrium Boltzmann statistics,

$$p_i = \frac{1}{Q}\exp(-\beta E_i), \tag{2.21}$$

where $\beta = 1/k_B T$ is the inverse temperature (k is the Boltzmann constant), and the normalising factor Q is the partition function

$$Q(h, \beta) = \sum_i \exp(-\beta E_i). \tag{2.22}$$

All the thermodynamic functions may be obtained by differentiating the Gibbs free energy[d]

$$G(h, \beta) = -\frac{1}{\beta} \ln Q(h, \beta). \tag{2.23}$$

In principle, knowledge of Q is sufficient to completely describe the system. Although there are a number of notable exceptions [43], its evaluation is usually an intractable problem for even the most simple of systems. The expectation of a quantity X for a system in equilibrium is

$$\langle X \rangle = \sum_i X_i p_i = \frac{1}{Q} \sum_i X_i \exp(-\beta E_i). \tag{2.24}$$

This value can be considered as the mean value of a sharply peaked probability distribution of X. For example, the expectation value of the energy $\langle E \rangle$, which is also the thermodynamic quantity known as the internal energy, U, is given by

$$\langle E \rangle = \frac{1}{Q} \sum_i E_i \exp(-\beta E_i). \tag{2.25}$$

Fluctuations

Statistical mechanics also yields information regarding the fluctuations of thermodynamically observable quantities. For the energy, the mean square deviation of individual measurements away from the mean value $U = \langle E \rangle$ is

$$\langle (E - \langle E \rangle)^2 \rangle = \langle E^2 \rangle - \langle E \rangle^2. \tag{2.26}$$

$\langle E^2 \rangle$ can be calculated from derivatives of the partition function in a similar way to $\langle E \rangle$

$$\langle E^2 \rangle = \frac{1}{Q} \sum_i E_i^2 \exp(-\beta E_i) = \frac{1}{Q} \frac{\partial Q^2}{\partial \beta^2}, \tag{2.27}$$

so

[d]This is assuming the canonical ensemble, in which the energy of a system of fixed size and at fixed temperature is free to vary [32].

$$\langle E^2\rangle - \langle E\rangle^2 = \frac{1}{Q}\frac{\partial Q^2}{\partial \beta^2} - \left[\frac{1}{Q}\frac{\partial Q}{\partial \beta}\right]^2 = \frac{\partial^2 \log Q}{\partial \beta^2}. \tag{2.28}$$

By noticing that it conceals the second derivative of the free energy, Equation (2.28) can be rewritten in terms of the specific heat

$$\langle E^2\rangle - \langle E\rangle^2 = \frac{C}{k\beta^2}. \tag{2.29}$$

This is an important result, as it could never have been derived within the framework of thermodynamics. For a general quantity X, its fluctuations can be found by supposing there is a term $-hX$ in the Hamiltonian, where h and X are conjugate variables (this is the case for all spin models in an external magnetic field). The expectation value of X can be found by differentiating $\log Q$ with respect to h, and then setting h to zero

$$\begin{aligned}\langle X\rangle &= \frac{1}{\beta}\frac{\partial \log Q}{\partial h}\bigg|_{h=0} = \frac{1}{\beta Q}\frac{\partial}{\partial h}\bigg|_{h=0}\sum_i \exp\beta(E_i - hX_i) \\ &= \frac{1}{Q}\sum_i X_i \exp(-\beta E_i),\end{aligned} \tag{2.30}$$

and its fluctuations are provided by performing a second differentiation

$$\begin{aligned}\frac{1}{\beta}\frac{\partial\langle X\rangle}{\partial h}\bigg|_{h=0} = \frac{1}{\beta}\frac{\partial^2(\log Q)}{\partial h^2}\bigg|_{h=0} &= \frac{1}{\beta}\frac{\partial}{\partial h}\left(\frac{1}{Q}\frac{\partial Q}{\partial h}\bigg|_{h=0}\right) \\ &= \frac{1}{\beta}\left[\frac{1}{Q}\frac{\partial^2 Q}{\partial h^2}\bigg|_{h=0} - \left(\frac{1}{Q}\frac{\partial Q}{\partial h}\bigg|_{h=0}\right)^2\right] \\ &= \langle X^2\rangle - \langle X\rangle^2 \\ &= \frac{\chi}{\beta},\end{aligned} \tag{2.31}$$

where χ is the susceptibility. This relation between the fluctuations in X and the linear response of $\langle X\rangle$ to h is known as the linear response theorem.

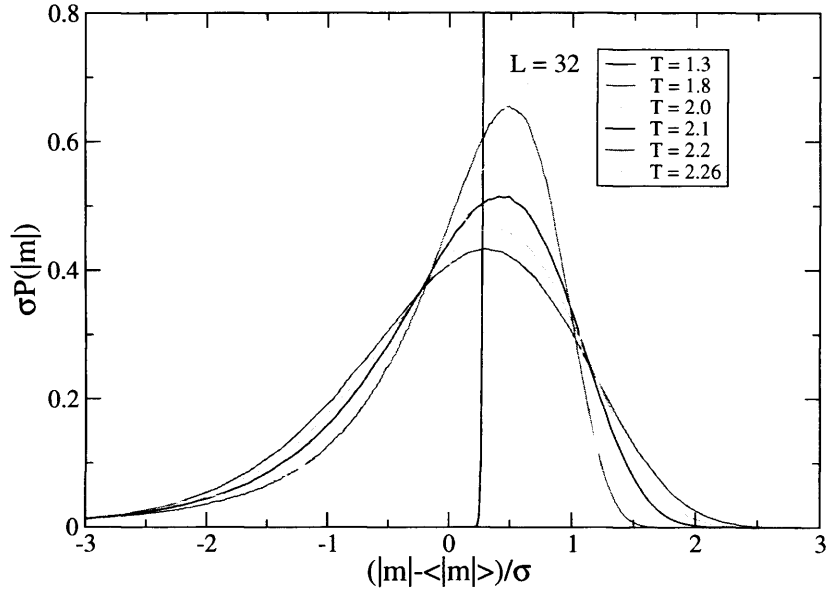

Figure 2.7: Normalised probability density functions of the absolute magnetisation for the finite ($N = 1024$) two-dimensional Ising model at different temperatures [44]. The increasing importance of fluctuations as the critical temperature is approached is made manifest by the increasing skewness of the PDFs.

Importance of Fluctuations Near the Transition Point

The expectation value of a quantity X represents the mean value of its probability distribution. Generally this is very sharp, such that the average in X coincides with its most probable value (the mode). However, in the critical regime the probability distribution becomes much broader, fluctuations become relevant, and the distinction between average and most probable states becomes significant.

To illustrate the consequence of this distinction, Figure 2.7 displays the probability density functions (PDFs) of the absolute magnetisation $|m|$ for the two-dimensional Ising model at varying temperatures [44]. At low temperature the distribution is a δ function, which is a reflection of the fact that the magnetisation is saturated, and that fluctuations are essentially irrelevant. As the critical temperature is approached from below, fluctuations become increasingly important and the mean magnetisation moves away from the mode, *i.e.* the symmetry around $\langle|m|\rangle$ is lost. The PDFs in the vicinity of T_c deviate considerably from the Gaussian form, with a high probability of large fluctuations for small $|m|$. Mean field theory,

in all its various guises, fails to recognise the significance of these fluctuations.

The essential feature of systems near criticality is that fluctuations over *all* length scales are relevant. A celebrated demonstration of this phenomenon is that of critical opalescence, first reported by Andrews following investigations on the liquid/gas transition in carbon dioxide [45]. As the critical point is approached the sizes of the gas and liquid region begin to fluctuate over increasingly large length scales. As the density fluctuations become of a size comparable to the wavelength of light, the light is scattered and causes the fluid to appear cloudy. Tellingly, the opalescence does not diminish as one gets closer to the critical point, where the largest fluctuations can reach even centimetre proportions, thus confirming the physical relevance of smaller fluctuations. Figure 2.8 shows photographs of critical opalescence occurring in a methanol/cyclohexane binary fluid mixture as it undergoes a transition from a single phase to two phases [44]. In this case the opalescence is caused by fluctuations in the fluid's refractive index.

Correlations

As the interactions in many body systems are often taken to be short ranged, one can ask how the correlations behave over larger distances by introducing the *correlation function.* Again, it is useful to have a definite system in mind, so consider a simple spin system. When a particular spin is flipped, what effect does this have on spins in other positions on the lattice? To answer this question, the two-point connected correlation function is defined

$$\begin{aligned} G(r) &\equiv \langle \mathbf{s}_i \mathbf{s}_j \rangle - \langle \mathbf{s}_i \rangle \langle \mathbf{s}_j \rangle \\ &= \langle (\mathbf{s}_i - \langle \mathbf{s}_i \rangle) \times (\mathbf{s}_j - \langle \mathbf{s}_j \rangle) \rangle \end{aligned} \tag{2.32}$$

where it is assumed the system is translationally invariant so that G is a function of only one variable, $r = |\mathbf{r}_i - \mathbf{r}_j|$. Away from the critical point the spins become uncorrelated as $r \to \infty$, hence the correlation function decays to zero exponentially

$$G(r) \sim \exp(-r/\xi). \tag{2.33}$$

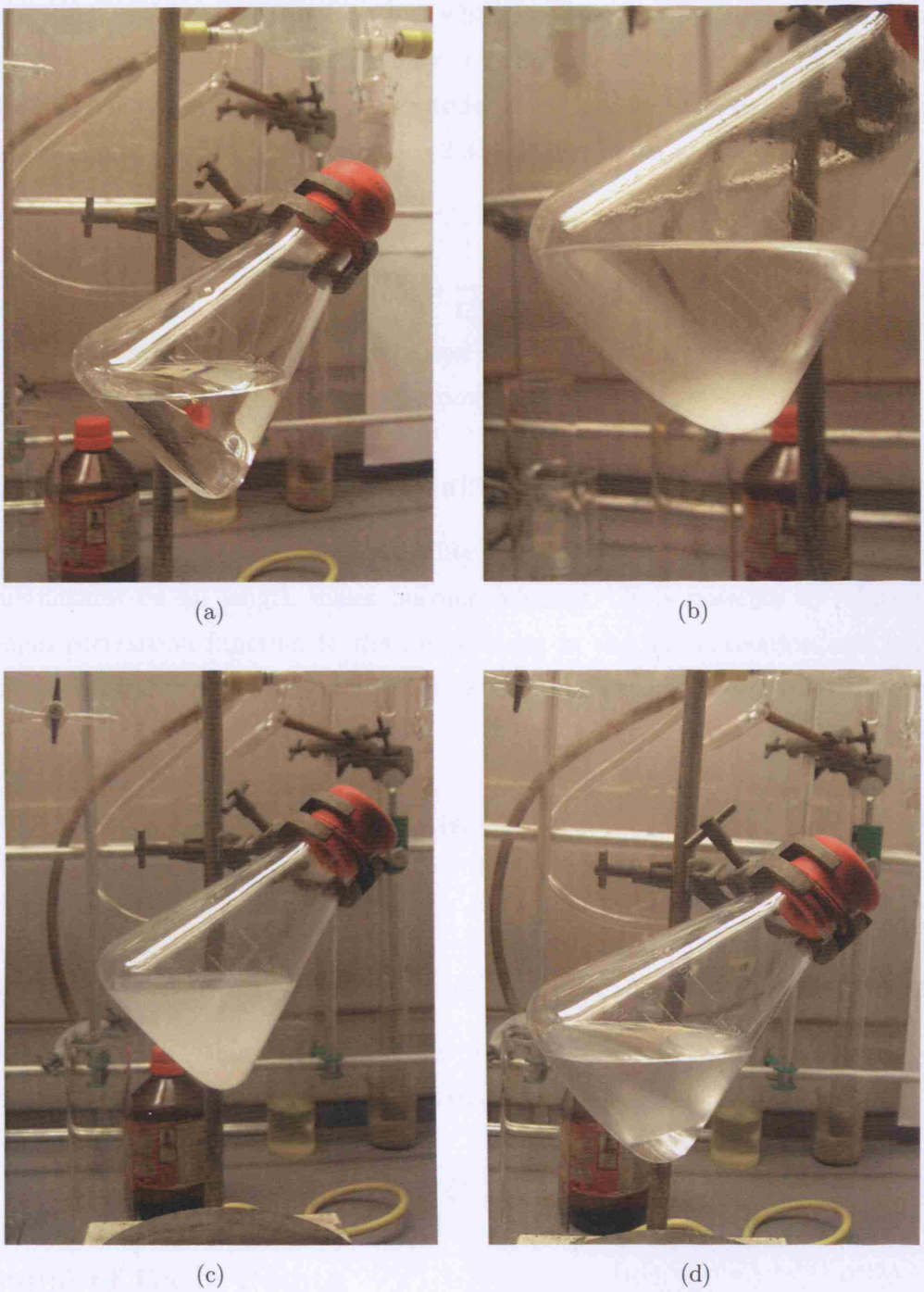

Figure 2.8: Critical opalescence in a methanol/cyclohexane binary fluid mixture [44]. (a) Above the critical temperature $T_c = 42.4$ °C, the two components are miscible in any proportion and form a fluid of uniform composition. (b) and (c) Provided the two components are in the molar ratio 0.435:0.665, the mixture becomes opalescent as T_c is approached. (d) Below T_c the two components are immiscible and separate into two distinct phases.

This introduces the correlation length ξ, which can be regarded as a measure of the range of the correlation function *i.e.* for $r > \xi$ the spins are effectively independent. At the critical point itself, long range order develops and the correlation length becomes infinite, $\xi(T_c) = \infty$. Equation (2.33) breaks down and it is instead found that

$$G(r) \sim \frac{1}{r^{d-2+\eta}} \tag{2.34}$$

where d is the system's dimensionality and η is a system dependent critical exponent. Thus the correlation length has a power law divergence

$$\xi \sim |t|^{-\nu}. \tag{2.35}$$

This really captures the essence of criticality: at T_c the correlation length is infinite, so fluctuations on all length scales become relevant. It is possible to relate the spin-spin correlation function to the fluctuations in the magnetisation and hence to the susceptibility. Recalling Equation (2.31), and writing the magnetisation as a function of spins,

$$G(r) = \sum_i (\mathbf{s}_i - \langle \mathbf{s}_i \rangle) \sum_j (\mathbf{s}_i - \langle \mathbf{s}_i \rangle) = \langle m^2 \rangle - \langle m \rangle^2, \tag{2.36}$$

so

$$\chi = \beta G(r). \tag{2.37}$$

It follows from the Fisher scaling relation (2.17) that the divergence in the susceptibility and the correlation length are related to each other as

$$\chi \sim \xi^{2-\eta}. \tag{2.38}$$

Resumé of Basic Points

Before proceeding further with this discussion, it is worth listing the main points which have occurred so far:

1. A phase transition is a cooperative effect caused by interactions or statistics.

2. The transition marks the onset of spontaneous ordering, characterised by an order parameter which is nonzero in the ordered phase.
3. As temperature increases, the order disappears when entropy overcomes the energy gained by ordering.
4. Fluctuations of all length scales dominate at continuous transitions.
5. Singular ('critical') behaviour occurs at continuous transitions, and is characterised by critical exponents and driven by long range correlations and a divergent correlation length ξ.

The Ising model is the simplest model available which contains all of the above features, making it ubiquitous in areas of physics in which many body effects are relevant. It is consequently with some justification that it has become considered the *drosophila* of physics [30].

2.2.3 Universality

One of the most useful concepts that has come out of the theoretical and experimental study of critical phenomena is that of universality. The critical behaviour of all systems undergoing a continuous phase transition depends only on their dimensionality, the symmetry of the order parameter and the range of the interaction responsible for the cooperative behaviour. For magnetic systems this means that, provided there are no unusual effects present, such as frustration, they can be classified into universality classes according to the dimensionality of the lattice d and that of the spin n. Thus, widely different systems with critical temperatures differing by orders of magnitude, may well belong to the same universality class and share the same critical exponents.

Table 2.4 lists the universality classes most likely to be encountered in experiment, and also indicates whether or not they display long range order at low temperature. A noticeable trend is that with increasing spatial dimensionality, fluctuations become less dominant. In fact, above the *upper critical dimension* $d_c = 4$, fluctuations become so unimportant that mean-field theory provides an analytically correct description[e].

[e]Incidentally, this accounts for the fact that the mean field universality class only obeys the

Table 2.4: Different values of n and d correspond to different universality classes. $\times$ denotes a universality class exhibiting a phase transition to long range order, whereas $\bigcirc$ denotes one that does not. The 2dXY model does undergo a phase transition, but not to long range order.

n	Model	Hamiltonian	$d=1$	$d=2$	$d=3$
1	Ising	$\mathcal{H} = \sum_{\langle i,j \rangle} S_i^x S_j^x$	$\bigcirc$	$\times$	$\times$
2	XY	$\mathcal{H} = \sum_{\langle i,j \rangle} S_i^x S_j^x + S_i^y S_j^y$	$\bigcirc$	$\otimes$	$\times$
3	Heisenberg	$\mathcal{H} = \sum_{\langle i,j \rangle} S_i^x S_j^x + S_i^y S_j^y + S_i^z S_j^z$	$\bigcirc$	$\bigcirc$	$\times$

Below three dimensions, fluctuations become so strong that they can destroy the ordered state and finite temperature phase transitions. In one dimension, fluctuations destroy all long range order and phase transitions. This is essentially a problem of connectivity. The only way information can be transmitted from one end of a one dimensional Ising system to the other is directly through the chain: any fluctuations cut the flow of information and hence the order present. Since there are always fluctuations at finite temperatures, a one dimensional system cannot be ordered except at zero temperature.

In two-dimensional systems, there are many paths that connect one part of the system to others, and the situation is less clear cut. Fluctuations do not suppress long range order in systems with discrete symmetry, yet they are strong enough to destroy it in systems possessing continuous symmetry. However, this does not necessarily rule out a phase transition. As will be discussed in Section 2.4, the 2dXY model undergoes a unique sort of transition to a state of *quasi* long range order.

2.2.4 Finite Size Scaling

A central notion in the theory of phase transitions is that of the thermodynamic limit, in which the system size is taken to be infinitely large. Strictly speaking, phase transitions can only occur in this limit, and in practice most experimental systems behave as if they were infinite, despite actually being finite. Nevertheless,

hyperscaling relations (2.17–2.20) for $d = 4$.

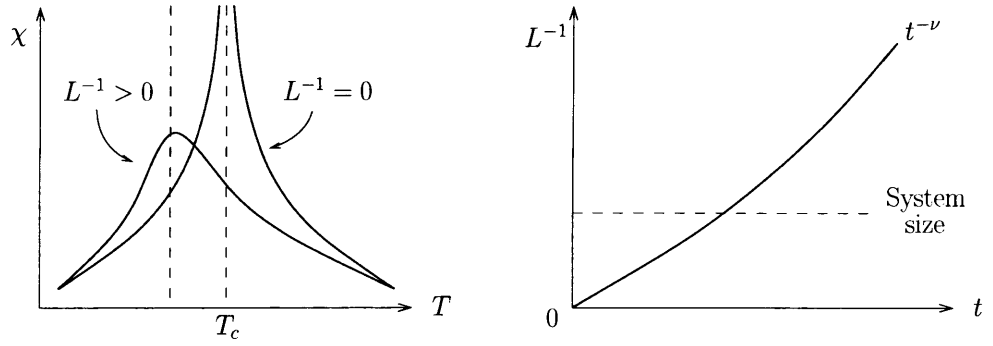

Figure 2.9: Effects of finite size on a phase transition.

there are exceptions to this, and these happen to be of interest in this work.

When dealing with a finite system, such as a spin model simulated on a computer, the singularity associated with the phase transition does not occur, and instead there is a finite peak at a temperature shifted from T_c, as shown in Figure 2.9(a). This can be understood by considering that as the critical temperature $T_c(L)$ is approached, there must be a cutoff in the correlation length divergence $\xi \sim t^{-\nu}$ given by $t \lesssim L^{-1/\nu}$, since the correlation length itself is cut off by the system length L (Figure 2.9(b)).

In a finite system at criticality, the algebraic behaviour of the correlation function $G(r)$ given by Equation (2.34) breaks down and is replaced by a function $g(L/\xi)$ which breaks the scale invariance characteristic of a critical system at the thermodynamic limit. As an illustration of this, Figure 2.10 plots the correlation function for an Ising model on a finite lattice, clearly showing that the algebraic behaviour of $G(r)$ only occurs in the limit of $L \gg \xi$. More generally, one takes into account the effects of finite size by postulating the observables, such as the susceptibility, scale as [46]

$$\chi(L,T) = |t|^{-\gamma} g\left(\frac{L}{\xi(t)}\right) \tag{2.39}$$

where the scaling function g has the limiting behaviour $g(x) \to$ const. as $x \to \infty$ and $g(x) \to x^{\gamma/\nu}$ as $x \to 0$. The first limit ensures that the correct power law behaviour of the infinite system is recovered for $L \to \infty$, whereas the second limit

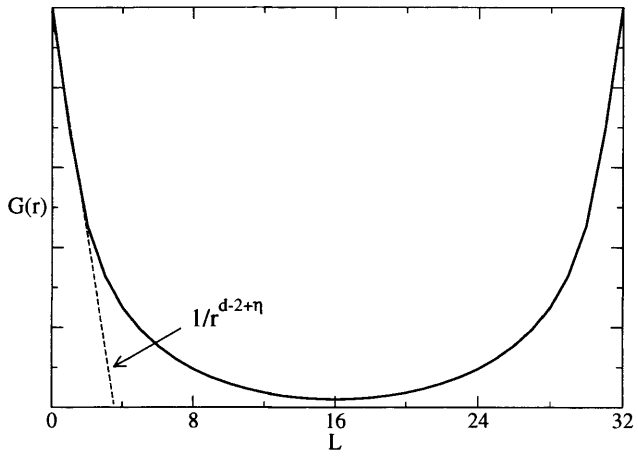

Figure 2.10: Correlation function for a critical 2d Ising system of finite size [44].

gives rise to a temperature independent magnetisation as $\xi \gg L$, since $\xi(t) \sim |t|^{-\nu}$. This form therefore also predicts that the maximum in the susceptibility will grow as

$$\chi_{\max} \sim L^{\gamma/\nu}. \tag{2.40}$$

An identical analysis shows that the specific heat and the order parameter behave similarly in the region of the critical point:

$$C_{\max} \sim L^{\alpha/\nu} \tag{2.41}$$

$$m_{\max} \sim L^{-\beta/\nu}. \tag{2.42}$$

It should be noted that in all these expressions it is assumed the system undergoes a transition at a shifted critical temperature $T_c(L) = T_c(\infty) - aL^{-1/\nu}$, where a is some constant.

More formally, if a general function $F(|t|, L)$ scales as $|t|^y$ in the thermodynamic limit, multiplying it by $L^{y/\nu}$ generates the scaling function

$$L^{y/\nu} F(|t|, L) = \left(L^{1/\nu}|t|\right)^y \widetilde{F}(L^{1/\nu}|t|) \tag{2.43}$$

in which the right hand side is a function of a single variable $L^{1/\nu}|t|$. It is possible to

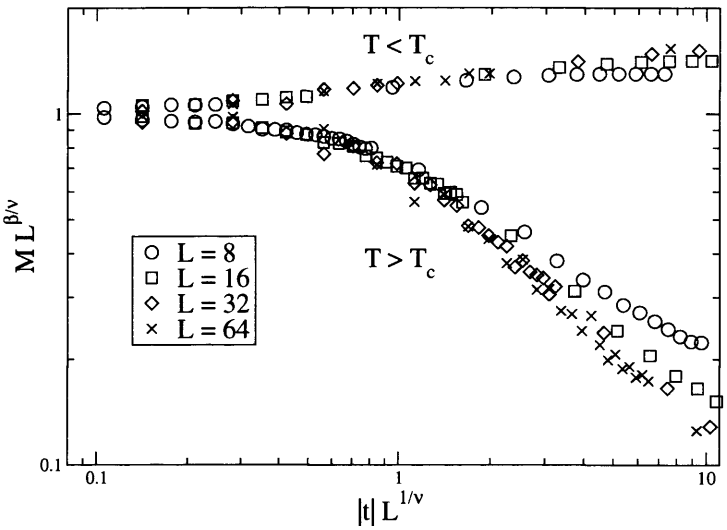

Figure 2.11: Logarithmic plot of $M_L L^{\beta/\nu}$ versus $|t|\, L^{1/\nu}$ for the 2d Ising model on a square lattice of system size $L = 8$, 16, 32 and 64 [44]. A good data collapse is only observed when the critical exponents are of the 2d Ising universality class ($\beta = 1/8$, $\nu = 1$), and $T_c = 2.27\, J$.

get an estimate of the scaling function $\widetilde{F}$ for several different values of the scaling variable $x = L^{1/\nu}|t|$ for each system size. As the scaling function is invariant with system size, these estimates should coincide with one another, assuming the correct values of the exponents and T_c are used. Such a data collapse is shown in Figure 2.11 for the magnetisation $m(|t|, L)$ of the 2d Ising model, for systems of size $L = 8$, 16, 32 and 64. The data for different system sizes only coincide if the correct parameters $\beta = 1/8$, $\nu = 1$ and $T_c = 2.27$ are used, with any other values giving much poorer fits.

It is also possible to construct a finite size scaling form for the correlation length ξ in complete analogy with the discussion given above. This specific case is discussed in Section 2.3.3.

2.2.5 Renormalization Group Theory

The scaling theory described above takes advantage of the most characteristic feature of critical phenomena: the diverging correlation length. Kadanoff [47] argued on intuitive grounds that in the Ising model, when the correlation length ξ is large near T_c, all the spins inside a cell of length $L \ll \xi$ should behave essentially alike

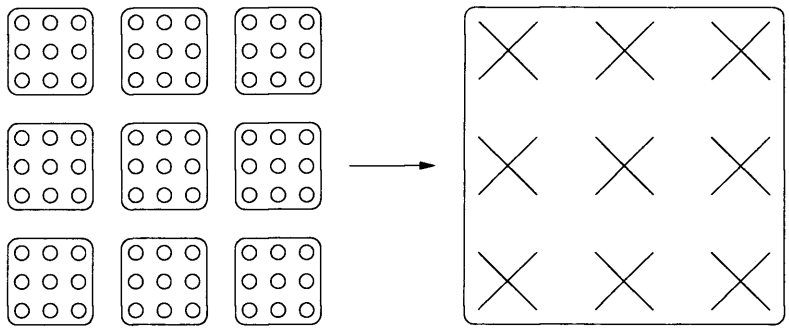

Figure 2.12: Grouping of spins into nine-spin blocks on a square lattice. This is an example of real space renormalization.

and can therefore be replaced by an effective 'block spin', as shown in Figure 2.12. The free energy calculated with interacting effective spins should be the same as that calculated from the original Hamiltonian. By expressing the connection between the original and the effective spins and interactions in terms of power laws of L, Kadanoff was able to show that the critical free energy is a scaling function of only one variable $t/h^{y/x}$

$$g = t^{-d/y}\tilde{g}(t/h^{y/x}) \tag{2.44}$$

where d is the lattice dimensionality, t and h are the reduced temperature and field, and x and y are unknown exponents. All other thermodynamic functions may be obtained from Equation (2.44), and indeed one notes that the scaling function (2.43) is of a similar form. Thus all critical exponents are reducible to combinations of just two, x and y, leading to the scaling relations discussed in Section 2.2.1.

Although Kadanoff's arguments lacked precision, they showed a great degree of intuition. The conceptual importance of his work is that it suggests thinning out or coarse-graining the degrees of freedom may lead to fruitful results, by emphasising the fact that coupling constants vary with a change of length scale. Wilson [48,49] elaborated this idea further by considering how the coupling constants vary under *repeated* elimination of short length scales. The idea is again to find an effective Hamiltonian with N degrees of freedom that gives the same partition function in the critical region

$$\mathrm{Tr}_{N'} \exp\left[-\mathcal{H}'(N')\right] = \mathrm{Tr}_N \exp\left[-\mathcal{H}(N)\right]. \tag{2.45}$$

where

$$\mathcal{H}' = \mathbf{R}[\mathcal{H}] \tag{2.46}$$

is a renormalized Hamiltonian with a reduced number of degrees of freedom N', in which fluctuations of wavelengths shorter than ξ have been integrated out. Since $\xi \to \infty$ at T_c, this procedure can be repeated an infinite number of times

$$\mathcal{H}' = \mathbf{R}[\mathcal{H}], \quad \mathcal{H}'' = \mathbf{R}[\mathcal{H}'], \quad \ldots \tag{2.47}$$

until a *fixed point* is reached where the Hamiltonian remains unchanged

$$\mathcal{H}^* = \mathbf{R}[\mathcal{H}^*]. \tag{2.48}$$

There is a choice of possible Renormalization Group (RG) operators $\mathbf{R}$ that can satisfy these conditions, of which the spin blocking technique described above is only one example. Note that as there is no inverse operation $\mathbf{R}^{-1}$, the term 'group' is in fact a misnomer [31].

Iterative processes of the form

$$x_{n+1} = f(x_n) \tag{2.49}$$

are well known in numerical analysis as a useful method of approximating to a root of the equation

$$x = f(x). \tag{2.50}$$

Such processes have the advantage that the final solution is independent of the starting point of the iteration. A root of Equation (2.50) is called a *fixed point*, x^* of the transformation (2.49). If Equation (2.49) has a number of different roots, each of these fixed points will have a characteristic basin of attraction, or in other words a range of starting points within which convergence will occur to a particular root. Equation (2.46) involves a generalisation of the above process to a multidimensional

space corresponding to a number of parameters in the Hamiltonian. On iterating the RG transformation, a given system represented by its initial set of coupling constants traces out a trajectory in coupling constant space. The set of all such trajectories, generated by different initial sets of coupling constants generates a renormalization group flow in coupling constant space.

These rather general arguments provide, in qualitative terms at least, a basis for the explanation of universality classes. Each fixed point corresponds to one universality class, and Hamiltonians with a wide variety of parameters all converge to the same fixed point. RG theory effectively explains why highly simplified models such as the Ising model yield such realistic results: their Hamiltonians include the most important parameters, the spin and system dimensionality. Most other parameters, which one might intuitively think should be important, are simply 'renormalized out' by the RG transformation.

Epsilon Expansion

In practice, the sums involved in actually carrying out the trace (2.45) are intractable, and it is necessary to resort to some approximation scheme to proceed further. By use of perturbation theory and extensive use of Gaussian integrals, Wilson and Fisher [50] were able to arrive at the recursion relation for a continuous approximation of the Ising model, and show that $\epsilon = 4 - d$ forms a natural small parameter with which to estimate critical exponents. The detailed nature of their calculation is beyond the scope of this work, but in essence it provides a natural framework within which to modify Landau's theory of phase transitions to correctly include the relevant fluctuations. For $\epsilon \leq 0$ ($d \geq 4$), the problem reduces to the so-called Gaussian model, which gives mean field exponents. For $d < 4$, the solution of the problem gives rise to a non-trivial fixed point. The eigenvalues of the renormalization group operator $\mathbf{R}$ linearised about this fixed point also turn out to be the exponents x and y in Equation (2.44). By using the ϵ expansion it is therefore possible to actually calculate x and y, and thereby all the other critical exponents.

2.3 Monte Carlo Method

The numerical simulation of a system involves calculation of its partition function, and consequently its thermodynamic properties. Even for moderately small systems, however, implicit calculation of the partition function is unfeasible. Consequently, one must turn to a method which computes the partition function approximately. The whimsically named Monte Carlo method does so by relying on a stochastic scheme, *i.e.* by drawing random variables. In essence there are two possible sampling schemes.

Simple sampling samples the partition function by generating configurations at random. This method does not get around the fact that the vast majority of these configurations make a negligible contribution to the partition function, and is consequently very inefficient.

Importance sampling, on the other hand, is a biased scheme which focuses on sampling the configurations that are dominant in the expression of the partition function. This is achieved by generating a Markov chain of configurations (or states, or microstates) that are distributed according to the Boltzmann distribution at a given temperature. Starting from a particular configuration σ_o, the chain chooses a new configuration σ_n according to a transition probability $\Pi(o \to n)$ which must satisfy the condition of *detailed balance* or *microreversibility*,

$$P_{\text{eq}}(o)\Pi(o \to n) = P_{\text{eq}}(n)\Pi(n \to o), \tag{2.51}$$

where $P_{\text{eq}}(o)$ and $P_{\text{eq}}(n)$ are the probability of occurrence (often termed the weight) of states o and n in the generated distribution

$$P_{\text{eq}}(o) = \frac{1}{Q} \exp\left(-\beta E_o\right), \tag{2.52}$$

where E_o is the energy of state o.

2.3.1 Metropolis Algorithm

Equation (2.51) implies that the ratio of transition probabilities for a 'move' $o \to n$ and its inverse $n \to o$ depend only on the energy change $\Delta E = E_n - E_o$:

$$\frac{\Pi(o \to n)}{\Pi(n \to o)} = \exp\left(-\beta \Delta E\right). \tag{2.53}$$

However, this still does not specify $\Pi(o \to n)$ completely. In their seminal paper Metropolis *et al.* proposed [51]

$$\Pi(o \to n) \propto \begin{cases} \exp(-\beta \Delta E) & \text{if } \Delta E > 0, \\ 1 & \text{otherwise,} \end{cases} \tag{2.54}$$

although other choices are possible [52]. Whilst it is easy to see that (2.54) satisfies (2.51) and (2.53), it is more complicated to show that a sequence of states $o \to n \to n' \ldots$ generated by (2.54) converges to the Boltzmann equilibrium described by Equation (2.52). A well known heuristic argument is presented by Binder and Heermann [53].

Application to Spin Systems

The Metropolis algorithm lends itself in an obvious manner to lattice spin systems. The essential steps of the scheme are:

1. Pick a spin at random (this is known as the *a priori* choice or *proposed value*).
2. Flip the spin (*move attempt*).
3. Calculate the energy difference $E_n - E_o$, and then the *acceptance rate* $\Pi(o \to n)$.
4. Draw a number $r \in [0, +1)$ at random, and
   - if $r < \Pi(o \to n)$, accept the proposed move (*i.e.* the next configuration in the Markov chain is σ_n.),
   - otherwise reject the move (*i.e.* the next configuration in the Markov chain is the same as the current one, σ_o.).

Once all spins have been given the chance to flip, a Monte Carlo Sweep (MCS) has been completed[f]. Whereas uniaxial (Ising) spins may only point in one of two

[f] A sweep may also referred to as one Monte Carlo Step per Spin, abbreviated to MCS/s.

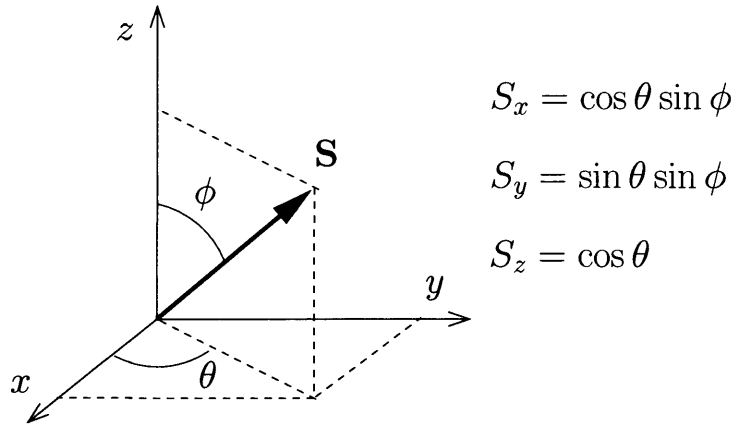

Figure 2.13: Spin coordinates.

orientations, for continuous spins a new spin orientation is chosen by drawing two uniformly distributed random variables: $\theta \in [0, 2\pi)$ for the azimuthal angle, and $\cos\phi = x^r \in [-1, +1)$ for the cosine of the polar angle (Figure 2.13).

Once the Markov process has been set up to sample the important contributions to an average, it is simple to calculate thermodynamic quantities such as the magnetisation

$$m_{\text{rms}} = \sqrt{\left(\frac{1}{N}\sum_{i=1}^{N} S_i^x\right)^2 + \left(\frac{1}{N}\sum_{i=1}^{N} S_i^y\right)^2 + \left(\frac{1}{N}\sum_{i=1}^{N} S_i^z\right)^2}, \tag{2.55}$$

where N is the number of spins in the system. The root mean square magnetisation is evaluated in order to ease a finite size scaling analysis, since $m_{\text{rms}} = 1/\sqrt{N}$ for $T \to \infty$. Using the relations discussed in Section 2.2.2, it is also possible to compute the fluctuations of these properties. For example, the magnetic susceptibility is

$$\chi = \beta N \left(\langle m^2 \rangle - \langle m \rangle^2\right). \tag{2.56}$$

2.3.2 Cluster Algorithms

Although the Metropolis algorithm is adequate for most small scale simulations, it is possible to create other more sophisticated Monte Carlo schemes which provide a substantial increase in computational efficiency, particularly in the vicinity of the

critical temperature. The most successful of these rely on flipping whole clusters of spins, as opposed to a single spin at a time, and are consequently known as cluster algorithms.

A property of all critical systems is that as T_c is approached, they take longer to equilibrate, a phenomenon known as critical slowing down. As the correlation length diverges, the regions of the system, which correspond to fluctuations about the equilibrium state, get increasingly larger, and correspondingly they take longer to relax. These critical relaxation processes are on a time scale which diverges with the correlation length

$$\tau \sim \xi^w, \tag{2.57}$$

where w is the dynamical critical exponent. This quantity provides a rough measure of the scalability of simulations. For example, replacing ξ with L in Equation (2.57), one may ask how long it takes for a particular simulation to complete if the system size is doubled. It turns out w is a non-universal property, and depends heavily on the algorithm adopted. Cluster algorithms generally have lower w exponents than single spin flip algorithms, and it is in this respect that they are more efficient. For example, for the Metropolis algorithm $w \sim 2$, whereas for the Swendsen Wang cluster algorithm [54] $w \sim 0.35$. Although cluster algorithms have not been used during the course of this work, their development and application is increasingly important in the field of critical phenomena.

2.3.3 Practical Issues

The simulations reported in this Thesis were carried out on the Pôle Scientifique de Modélisation Numérique[g] (PSMN) at the École Normale Supérieure in Lyon, using a 2.6 GHz AMD processor. A typical Monte Carlo run is 110 000 MCS/s, with thermodynamic averages taken every sweep in order to minimise the correlations between successive configurations in the Markov chain. Furthermore, the first 10 000 MCS/s are disregarded from the average, since the system is reaching equilibrium during this time, as shown in Figure 2.14. It is generally convenient

[g] `http://www.psmn.ens-lyon.fr/`

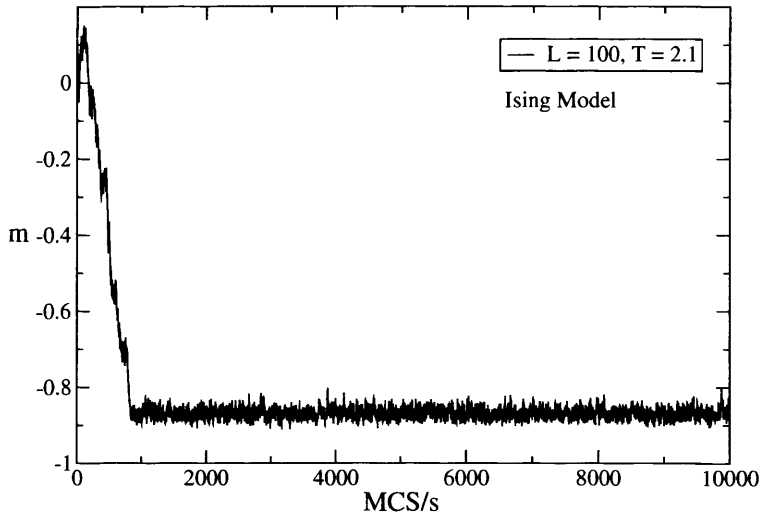

Figure 2.14: Evolution of the magnetisation in Monte Carlo time, for a 10^4 spin Ising system at $T = 2.1$.

to repeat this procedure over a succession of decreasing temperatures. The first simulation is started from a random spin configuration, and the final configuration of each run is conserved and used as the starting point for the next temperature. Better statistics can always be acquired at a greater computational expense.

Determination of Critical Exponents

Since critical exponents play a prominent role in this work, it seems appropriate to discuss how one might go about measuring them. In experiment it is found that instrumental resolution, extraneous effects and the finite size of the system cause a rounding of the divergence associated with the phase transition, such that in practice, one is lucky to obtain two decades of convincing power law behaviour (see for example Figure 4.3). Furthermore, the precise value of T_c is not known *a priori*, so it is often treated as an adjustable parameter along with the background and the corrections to scaling. Despite these difficulties, reasonable estimates are possible, and there is good consistency between the results of independent experiments.

An alternative method for determining T_c and β without having to rely on any guesswork is attributed to Kouvel and Fisher [55]. By taking advantage of the relation

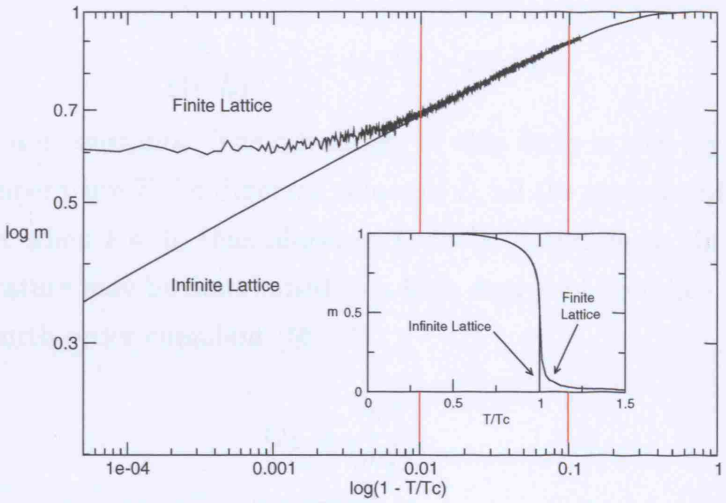

Figure 2.15: Magnetisation of the Ising square model with side $L = 64$ compared with the analytical solution for the infinite system. The arrow marks the onset of finite size effects. Large figure: log-log plot. Inset: linear plot.

$$\frac{M}{dM/dT} = \frac{T - T_c}{\beta} \tag{2.58}$$

one may plot $M/(dM/dT)$ against T and obtain a straight line with slope $1/\beta$, which intersects the abscissa at T_c. In practice, this method is very sensitive to random noise, and is consequently little used.

Data from numerical simulations is, in many respects, no different from experimental data, in that finite size effects are also prominent (see Figure 2.15). However, unlike experiment, it is possible to quantify these by performing an analysis on the basis of the arguments discussed in Section 2.2.4. It can be shown [46] that in the vicinity of the critical point the correlation length may be written in the form

$$\xi(t, L) = Lg(|t|L^{1/\nu}), \tag{2.59}$$

where for $L \to \infty$ one must have $g(x) \to x^{-1}$ so as to recover the $|t|^{1/\nu}$ behaviour. For finite L and $t \to 0$, $g(x)$ tends towards a constant, and since it is perfectly analytic in this limit, it can be expanded about $t = 0$:

$$\frac{L}{\xi(t,L)} = a + btL^{1/\nu} + \mathcal{O}(t^2), \tag{2.60}$$

where a and b are constants. The advantage of this form is that by plotting L/ξ against the temperature T, for different values of L, all the curves will pass through the same point when $t = 0$, thus allowing T_c to be determined. In practice, the critical temperature may be determined to a high degree of accuracy by measuring the reduced fourth order cumulant [56, 57]

$$Q_L = \frac{\langle m_L^4 \rangle}{\langle m_L^2 \rangle^2}. \tag{2.61}$$

Since this quantity is a function of $[L/\xi(T)]$, it also is invariant under renormalization at the transition temperature.

It is a common misconception that critical exponents are only measurable asymptotically close to the critical point. It is in fact an enlightening exercise to estimate the size of the critical region for different systems, which can be done by considering the breakdown of Landau theory near the critical point[h]. One important conclusion from such a consideration is that by lowering the lattice dimensionality, the size of the critical region increases. This fact is attested by the large body of data available for both experimental and theoretical two-dimensional systems considered in the second part of this Thesis.

2.4 2dXY Model

The final part of this chapter is devoted to the 2dXY model, which plays a prominent role in the rest of this work. The seemingly minor difference in the spin dimensionality with respect to the Ising model (the critical behaviour of which is summarised in the third column of Table 2.3) is misleading: this model displays a highly peculiar behaviour which, in order to be understood, requires full use of the theoretical machinery introduced so far.

The 2dXY model describes a set of interacting spins which are constrained to rotate within the plane of a square lattice. The Hamiltonian is

[h] See Goldenfeld [30] (p. 172) for a clear discussion on this issue.

$$\mathcal{H} = -J \sum_{\langle i,j \rangle} \cos(\theta_i - \theta_j), \tag{2.62}$$

where θ_i is the angle of the spin at site i relative to an arbitrary axis. The Hamiltonian is invariant under rotations in the spin plane, in other words it is said to possess $O(2)$ symmetry. Analytic study of the 2dXY model is problematic not least because an exact evaluation of the partition function is impossible. Nevertheless, a combination of theoretical approaches have allowed for a reasonably complete picture to be developed.

High Temperature Behaviour

One might expect on intuitive grounds that the 2dXY model should enter a conventional disordered phase at high enough temperatures, and indeed this is the case. This is confirmed by high temperature series expansions, which involve expanding the energy term (2.62) in the partition function in powers of (J/T) as $T \to \infty$, and identifying the terms giving the lowest power. Using this technique it is found that at high temperature the correlation function decays exponentially

$$G(r) = \exp\left(-r \ln(T/J)\right). \tag{2.63}$$

Interestingly, the first evidence that the 2dXY model undergoes a phase transition arose from early analyses of this sort [58, 59].

Low Temperature Behaviour

At low temperatures it is reasonable to assume that θ varies little from one lattice site to the next, and (2.62) may be replaced by the first two terms of its Taylor expansion

$$\mathcal{H} \simeq -J \left(1 - \frac{1}{2} \sum_{\langle i,j \rangle} (\theta_i - \theta_j)^2 \right). \tag{2.64}$$

In this case the dominant fluctuations are spin waves of long wavelength, and it follows that expression (2.64) is known as the spin wave approximation of the XY

model. As this approach makes it possible to express thermodynamic quantities in terms of solvable Gaussian integrals, it is also known as the Gaussian approximation. In particular, it can be shown that the magnetisation as a function of system size and temperature is

$$M(N,T) = \left\langle \left| \frac{1}{N} \sum_i \mathbf{S}_i \right| \right\rangle = \left(\frac{1}{aN} \right)^{T/8\pi J}, \tag{2.65}$$

where a is a constant equal to ~ 1.86 [60]. In the thermodynamic limit the magnetisation vanishes, reflecting the fact that there is no cost in energy associated with the excitation of infinitely long spin waves, the so-called Goldstone mode. This is true for all continuous spin systems of lattice dimensionality $d \leq 2$, and is a result that has become commonly known as the Mermin-Wagner theorem [1]. However, it is noteworthy that the approach to the thermodynamic limit is very slow in Equation (2.65). Whilst it is obvious that the finite size of a system introduces a cutoff in the spin wave spectrum, the exponent $T/8\pi J$ is so small, even for $T \sim \mathcal{O}(J)$, that the magnetisation remains observable in macroscopic systems at finite temperatures[i]. This is an important indication that the physics of real 2dXY systems are not completely dictated by predictions at the thermodynamic limit.

Another result arising from the spin wave analysis concerns the behaviour of the correlation function, which is found to decay to zero algebraically

$$G(r) = r^{-\eta(T)} \tag{2.66}$$

with

$$\eta(T) = \frac{T}{2\pi J}. \tag{2.67}$$

This result has a number of important implications. Firstly it is consistent with the Mermin-Wagner theorem, because $G(r)$ approaches zero for all T. Secondly, it seems to indicate that the system is critical at any temperature. There is no

[i] A rough estimate of the magnitude of finite size effects can be worked out by putting the 'mean field' value for the transition temperature $T = \pi/2$ (see below) in Equation (2.65). For example, with $N = 10^5$, $M \simeq 0.47$, indicating that finite size effects will always be present in computer simulations. With $N \simeq 10^{16}$, which would correspond to a sample with an area equal to this page, M would still be $\simeq 0.1$, an appreciable value.

characteristic length scale associated with the exponential decay typical of a disordered phase, because $G(r)$ decays as a power law governed by the continuously varying exponent $\eta(T)$. However, this peculiar state of affairs cannot persist up to arbitrary temperatures, because it is known that at high enough temperatures the correlations must fall off exponentially.

Role of Vortices

The inadequacy of the Gaussian approximation at higher temperatures is traceable to the fact that spin waves are not the only possible thermal excitations in the 2dXY model. Low energy configurations known as *vortices* exist in which θ varies very little between neighbouring sites, but where, if one were to follow its behaviour around a large closed curve, θ may in fact change by some non-zero multiple of 2π.

An isolated vortex has an energy that depends logarithmically on the size L of the system

$$U \simeq \pi J \ln L, \tag{2.68}$$

consequently its energy is infinite at the thermodynamic limit. Whilst this fact might appear to lend some justification to neglecting vortices in the spin wave calculation, it can be seen by computing the entropy that this is not the case. Since there are L^2 possible positions for the vortex, its entropy is

$$S \simeq 2 \ln L. \tag{2.69}$$

The free energy to introduce the vortex is therefore

$$F = U - TS \simeq (\pi J - 2T) \ln L. \tag{2.70}$$

Below a temperature $T_{\mathrm{KT}} = \frac{\pi J}{2}$, the internal energy dominates and the occurrence of free vortices is suppressed. For $T > T_{\mathrm{KT}}$, however, the entropy term takes over and isolated vortices may proliferate.

This criterion was put forward by Kosterlitz and Thouless (KT) [61]. However, it does not take into account interactions between vortices. KT realised that vortex-antivortex pairs (as depicted in Figure 2.16) have an energy that depends

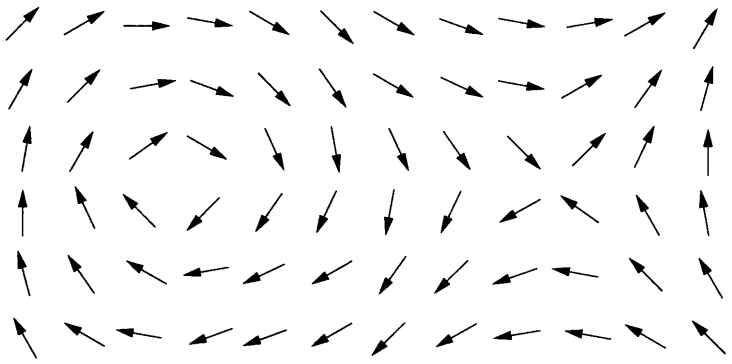

Figure 2.16: A vortex anti-vortex pair. Such a configuration is possible below T_{KT}, unlike a single vortex, which is energetically unfavourable.

logarithmically on their separation, and provided they are tightly bound, they are not excluded from the low temperature phase. Thus the phase transition does not lead to the creation of new vortices, rather it corresponds to a dissociation of bound vortex-antivortex pairs already present, as shown in the Monte Carlo 'snapshots' in Figure 2.17. In this revised picture there is a lowering of the transition temperature. However by the time the temperature has reached $T_{\mathrm{KT}} = \frac{\pi J}{2}$, the vortices will have started to proliferate.

2.4.1 Kosterlitz-Thouless Transition

In their seminal paper [61], KT mapped the vortex problem onto a model of a two-dimensional Coulomb gas, and solved it using an iterated mean field approach. They were able to show that the dissociation of vortex-antivortex pairs drive a transition between two phases which, although both completely disordered, are distinct in so far as topological defects are concerned. At low temperature the system is said to be *topologically ordered* (tightly bound vortex-antivortex pairs are present), whereas at high temperature it becomes *topologically disordered* (free vortices are present). The difference between the two phases is made manifest by the response of the 2dXY model to an applied magnetic field, quantified by the magnetic susceptibility. This is found to take entirely different forms above and below T_{KT}, and is indicative of a change of rigidity: the low temperature state has an elastic rigidity whereas the high temperature state does not. This Kosterlitz-

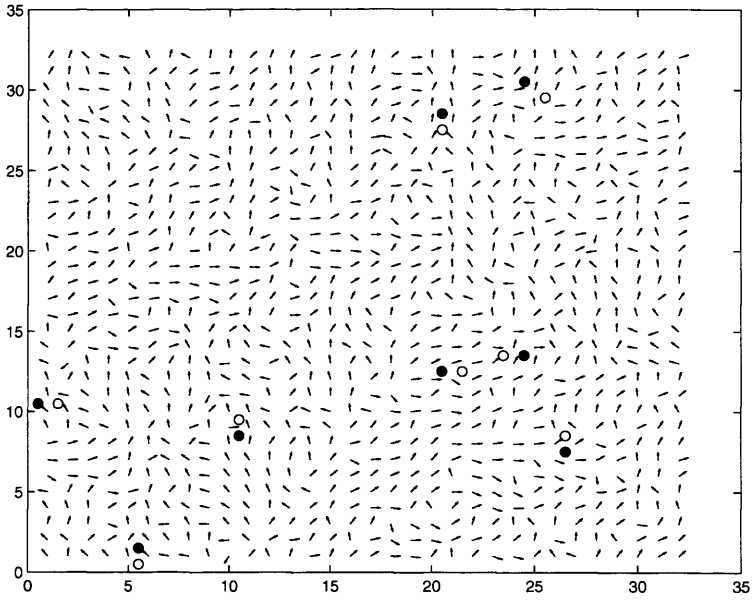

(a)

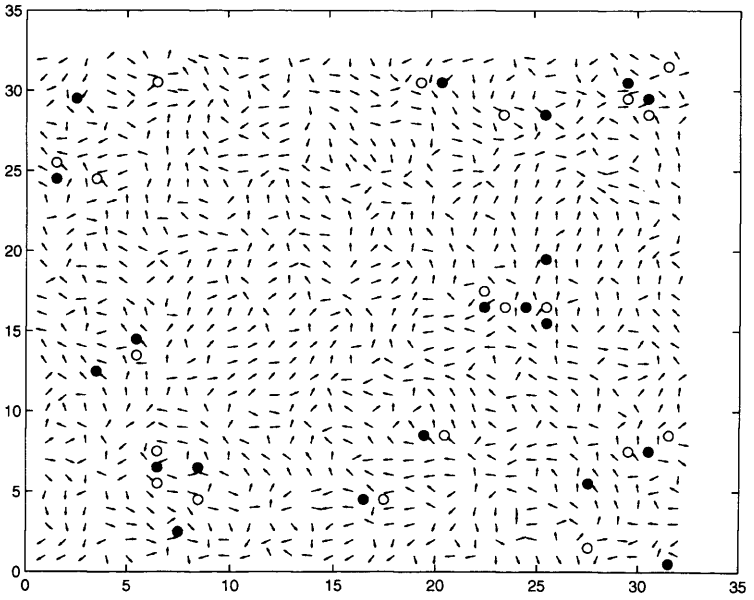

(b)

Figure 2.17: Spin and vortex configurations for the XY model, with $N = 1024$, at (a) T_{KT} and (b) above T_{KT} [44]. The vortex positions are calculated by summing $\theta_i - \theta_{i+1}$ around each square plaquette of the lattice. Solid (open) circles represent positive (negative) vortices centred on plaquettes with a circulation of $+(-)2\pi$.

Thouless mechanism is clearly different from a conventional second order transition to long range order, and is found to occur in a wide range of systems in which topological defects - such as vortices in magnets and dislocations in crystals - are relevant.

Renormalization Group Analysis

A more concrete picture is made by following a more sophisticated renormalization approach first taken by Kosterlitz [62]. The main results from this treatment are that as T_{KT} is approached the correlation length ξ and susceptibility χ diverge according to the power laws

$$\xi \sim \exp\left(bt^{1/2}\right) \qquad t > 0 \tag{2.71}$$

$$\rightarrow \infty \qquad t < 0 \tag{2.72}$$

where $t = (T - T_{\mathrm{c}})/T_{\mathrm{c}}$ and $b \simeq 1.5$, and

$$\chi \sim \xi^{2-\eta} \qquad t > 0 \tag{2.73}$$

$$\rightarrow \infty \qquad t < 0 \tag{2.74}$$

where the exponent $\eta = 1/4$ has the same value as the two-dimensional Ising model. This implies the conventional exponents β, γ and ν are undefined since ξ diverges faster than any power of t. However, since the magnetisation and susceptibility may be expressed in terms of ξ as $m \sim \xi^{-\beta/\nu}$ and $\chi \sim \xi^{\gamma/\nu}$, the ratios

$$\frac{\beta}{\nu} = (d - 2 + \eta)/2 \tag{2.75}$$

$$\frac{\gamma}{\nu} = 2 - \eta \tag{2.76}$$

remain defined. This suggests the standard scaling relations hold at the KT transition, a phenomenon referred to as 'weak' scaling [63]. It is also noteworthy that in the 2dXY model the exponent $\delta = 15$ agrees with the corresponding value for the two-dimensional Ising model, just as for η.

Unlike a single vortex, which has an energy given by Equation (2.68), two

vortices separated by a single lattice spacing have an energy [61]

$$U = \pi^2 J. \tag{2.77}$$

Within the electrostatics analogy with a Coulomb gas, U may be thought of as a chemical potential μ. The basic idea of the Kosterlitz method is to renormalize the free vortex fugacity $y(\ell) = \exp(-\mu/k_B T)$ at each length scale ℓ in terms of the spin wave stiffness $K(\ell) = J(\ell)/T$. This latter quantity, also known as the helicity modulus, describes how much energy it costs to excite a spin wave, and is an example of a generalised rigidity [64]. The inverse of the spin wave stiffness on each length scale ℓ is determined by those vortex pairs whose size is less than ℓ, so that its change when the length scale is varied is proportional to the square of the concentration of free vortices found on the length scales ℓ. This leads to the first of the Kosterlitz equations

$$\frac{dK^{-1}(\ell)}{d\ell} = 4\pi^3 y^2(\ell) + \mathcal{O}[y^4(\ell)]. \tag{2.78}$$

The energy of a vortex on a length scale ℓ depends on the polarisability of the medium on that length scale and on the concentration of free vortices, leading to the second Kosterlitz equation

$$\frac{dy(\ell)}{d\ell} = [2 - \pi K(\ell)]\, y(\ell) + \mathcal{O}[y^3(\ell)]. \tag{2.79}$$

These equations were derived using a method developed by Anderson and Yuval for the Kondo problem [65]. A more detailed derivation may be found in the review article [66] and book [67] by Nelson.

Figure 2.18 shows the renormalization trajectories generated by the Kosterlitz equations in the (K^{-1}, y) plane, together with a temperature dependent locus of initial conditions. Hamiltonians to the left of the incoming separatrix terminating at $K^{-1}(\ell) = 2/\pi$ renormalize toward a series of Gaussian fixed points at $y = 0$, which describe the low temperature phase. At higher temperatures $y(\ell)$ eventually becomes large, indicating that vortices are important even at very long wavelengths, and the flows are toward a high temperature fixed point which controls a truly paramagnetic region.

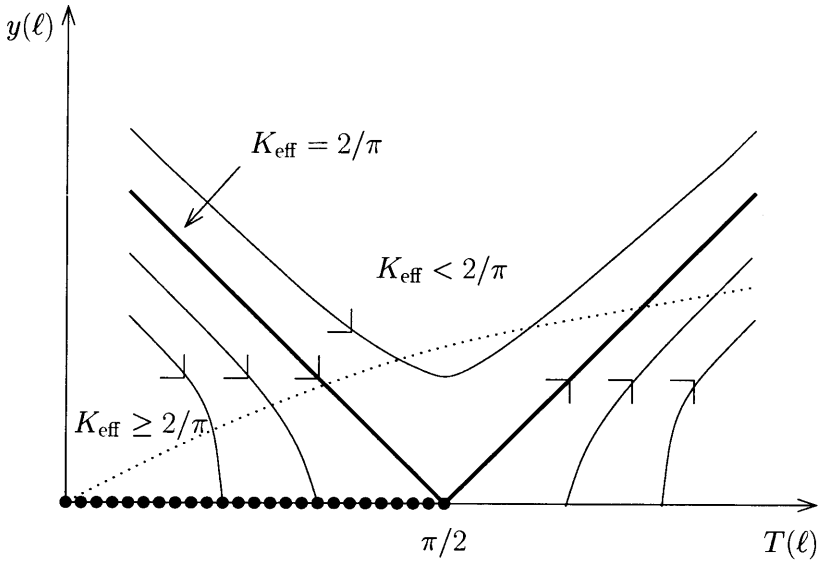

Figure 2.18: RG trajectories for the 2dXY model. A locus of initial conditions is shown as a dotted line. For $T_{\text{KT}} \leq \pi/2$ the flows are toward a continuous line of Gaussian fixed points.

Universal Jump

The physical interpretation of the RG analysis is that vortex excitations are irrelevant below T_{KT}, and that bound pairs of vortices renormalize the spin wave stiffness measured at long length scales to an effective value $K_{\text{eff}} = J_{\text{eff}}/T$. The asymptotic behaviour of the spin correlation function is the same as the Gaussian model (*c.f.* expression (2.67)), so that $\eta = 1/2\pi K_{\text{eff}}$ is a non-universal function of temperature [68]. However, precisely at T_{KT}, $K_{\text{eff}} = 2/\pi$, so that the value of $\eta(T_{\text{KT}}) = 1/4$ is universal. Above T_{KT} the vortices become unbound, and K_{eff} jumps discontinuously from the universal value $2/\pi$ to zero [69]. This phenomenon is termed the universal jump in the spin wave stiffness.

Historical Remark

The notion of topological excitations and phase transitions driven by them was first introduced by Berezinskiĭ in 1971 [70, 71], two years before Kosterlitz and Thouless [61, 62]. He did not find, however, their simple relation between the transition temperature and the transverse stiffness. Other notable theoretical developments include the contributions by Villain [72] and José *et al.* [68], who worked on an

analytically more tractable model in which vortices are completely decoupled from spin waves.

2.4.2 2dXY Model on a Finite Lattice

As will be shown in Chapter 4, the remarkable phenomenology of the 2dXY model occurs in a whole range of two-dimensional systems in which there is a defect mediated transition [67, 73, 74]. For example, elegant experiments on superfluid helium films provide compelling evidence of a universal jump in the superfluid density [75,76]. However, two-dimensional planar magnets are conspicuously absent from the list of 'clean' KT systems. Despite being described by almost ideal 2dXY Hamiltonians, these persist in ordering at low temperature, and display features which, at least superficially, do not appear to be consistent with KT theory. In order to understand why this is the case, it is necessary to consider how the 2dXY model behaves away from the thermodynamic limit, and understand its scaling properties.

Universal Scaling

The behaviour of Equation (2.65) suggests the presence of long range order at appreciable temperatures even in very large 2dXY systems. Bramwell and Holdsworth (BH) [77,78] investigated this magnetisation by means of a finite size scaling analysis of the Kosterlitz renormalization group Equations (2.78) and (2.79) [61], using the system length L as the scaling parameter. In a finite system, the spin wave stiffness K_{eff} does not jump discontinuously to zero at T_{KT}. The universal jump is rounded out as the exclusion of length scales greater than L implies the spin wave stiffness is no longer renormalized to zero above T_{KT}. This in turn gives rise to an observable magnetisation which falls steeply yet continuously with increasing temperature, and renders T_{KT} non-special. However, this analysis yields two other characteristic temperatures. The first, T^*, is defined as the temperature at which $K_{\text{eff}}(T^*(L)) = 2/\pi$. The second, T_{c}, is defined as the point at which the correlation length ξ becomes equal to the system length L. This may be interpreted as the effective Curie temperature for the finite system. It can be shown [77] that T^* and T_{c} are both shifted logarithmically from T_{KT} with respect to L

$$T_c(L) - T_{KT} = 4\left[T^*(L) - T_{KT}\right] = \frac{\pi^2}{c\,(\ln L)^2}. \tag{2.80}$$

The logarithmic dependence on L ensures that, for fixed L, the range of temperature ($\sim T_c - T^*$) over which scaling behaviour occurs is unusually large. As $L \to \infty$ the two temperatures converge on T_{KT}, and the system passes smoothly over to KT behaviour, thus recovering the universal jump in K_{eff} and destroying long range order.

After replacing $K = J/T$ by K_{eff} in Equation (2.65), an effective magnetisation exponent $\tilde{\beta}$ can be defined

$$\tilde{\beta}(L, T) = \left[\frac{\partial \ln M(L, T)}{\partial \ln(t(L))}\right]_L \tag{2.81}$$

where $t = T_c - T$. For most values of t, $\tilde{\beta}$ is a function of the system size. However, for $t^* = T_c - T^*$ it can be shown that $\tilde{\beta}$ takes up a universal value $\tilde{\beta}(L, T^*) = \frac{3\pi^2}{128} \simeq 0.231$. This striking result is clearly observable in numerical simulations (Figure 2.19), and accounts for the behaviour of a whole class of two-dimensional magnetic systems, as will become clear in Chapter 4. One should emphasise that $\tilde{\beta}$ is not a critical exponent in the conventional sense, and is distinct from the true order parameter exponent β, which in any case was shown in Section 2.4.1 to be undefined in the 2dXY model. In practice this distinction is academic: experimentalists measure and treat $\tilde{\beta}$ as if it were a normal exponent, consequently the tilde is generally omitted.

In their original paper BH also remark that their results provide a procedure for choosing T_c for numerical results. One can calculate the temperature at which $M = (1/aN)^{1/16}$, corresponding to $K_{eff} = 2/\pi$. This locates T^* and, following from (2.80) and the fact that T_{KT} is 0.898 [79], also defines T_c. Furthermore, as a test of consistency between systems of different size, one may calculate the constant c from Equation (2.80)[j]. Using this procedure for the system of size $N = 1024$ yields $T^* = 0.943$, $T_c = 1.078$ and $c = 2.48$. This is in good agreement with a

[j]Kosterlitz [62] and Gupta [79] estimate values of $c = 2.1$ and $c = 2.35$, respectively. Given the difference between the Monte Carlo result of $T_{KT} = 0.898$ and the RG result of $T_{KT} = 1.35$ the c values quoted in the main text are derived from the data through Equation (2.80) and multiplied by a factor of 0.898/1.35.

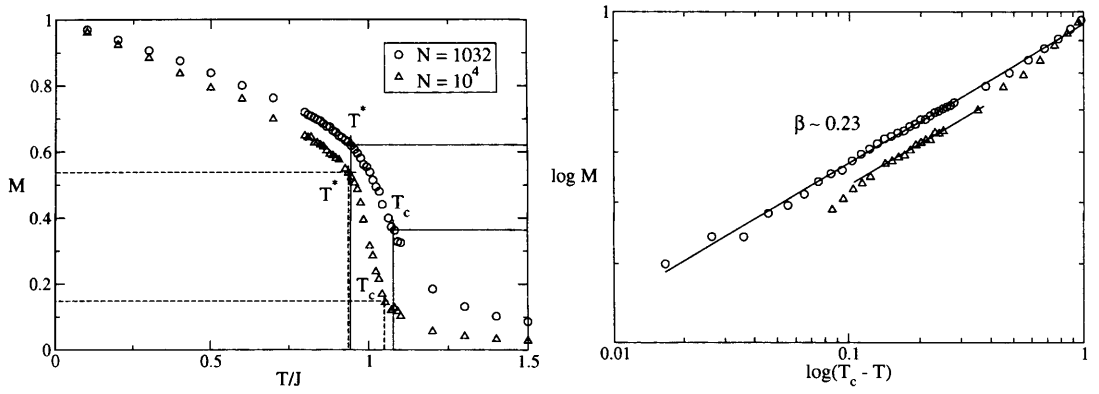

Figure 2.19: Left: Monte Carlo magnetisation versus temperature curves for a system of $N = 1024$ (circles) and $N = 10^4$ (triangles) [44]. T^* and T_c are marked for each curve, with $T_c > T^*$. Right: Logarithmic plot of the same data. The lines are of slope $\beta \simeq 3\pi^2/128$.

pragmatic choice of T_c to give the best power law behaviour. For $N = 10^4$, an identical analysis gives a similar sort of agreement, with $c = 2.2$.

It is somewhat ironic that the characteristic feature of 2dXY behaviour in magnets should be the magnetisation, the very property that is precluded by the Mermin-Wagner theorem. Figure 2.20 shows data from Monte Carlo simulations of the 2dXY model and a related model given by the Hamiltonian

$$\mathcal{H} = -J \sum_{\langle i,j \rangle} \left[1 - \frac{1}{2}(\theta_i - \theta_j - 2\pi n)^2 \right], \tag{2.82}$$

where $n = 0, \pm 1$ is an integer chosen so that $(\theta_i - \theta_j - 2\pi n)$ lies between $\pm\pi$. This model, referred to as the Harmonic XY (HXY) model, has the advantage over the true XY Hamiltonian (2.62) that it only allows for harmonic spin waves and vortex pairs as excitations, and furthermore has them decoupled. As a consequence its low temperature behaviour closely matches that of the spin wave prediction (2.65), only deviating to a '$\beta \simeq 0.23$' regime once vortices become relevant. The 2dXY model (2.62), on the other hand, has a slightly more complex behaviour due to the inclusion of anharmonic terms in the cosine interaction. These reduce the vortex pair fugacity, and consequently reduce both the temperature scale over which the scaling behaviour takes place and the absolute value of T_{KT}. The anharmonic terms also cause the magnetisation to fall below that of the spin wave curve at relatively

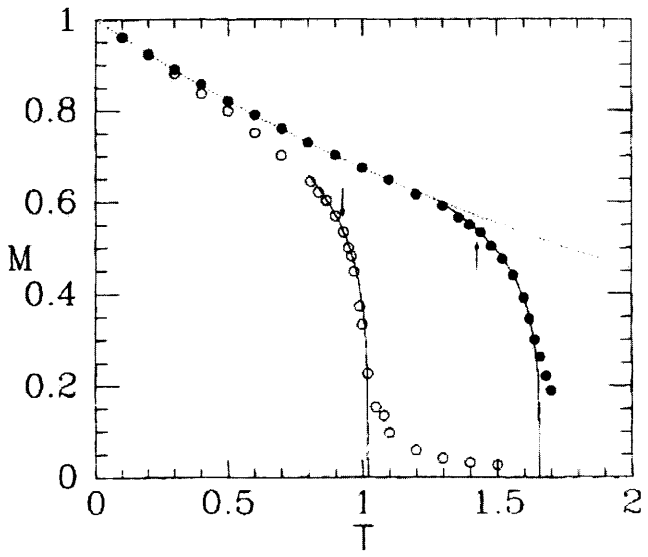

Figure 2.20: Magnetisation versus temperature curves for the HXY model (full circles) and the 2dXY model (empty circles). The dashed curve is the spin wave result of Equation (2.65). The solid curves show, in each case, the fit to the scaling behaviour, with exponent $3\pi^2/128$. After Bramwell and Holdsworth [78].

low temperature, even in the absence of vortex pairs. Thus, with increasing temperature the 2dXY model passes through four different regimes [78]: a linear spin wave regime, an anharmonic spin wave regime, a scaling regime with $\beta \simeq 0.23$, and a regime of finite sized rounding. The conclusion drawn from the work of BH is that only the scaling regime is universal, and that its behaviour acts as a signature of 2dXY behaviour in experiment.

Part II

Investigations of Critical Phenomena in Two-Dimensional Systems

Chapter 3

Aims and Objectives of the Present Work

In two dimensions there are relatively few symmetries possible, and hence few universality classes. Those one might expect to observe include the Ising, XY, XYh_p (where h_p indicates the presence of a p-fold symmetric crystal field, as described by Equation (5.14)), Potts [80] and dipolar [81, 82] classes. The aim of this work is to investigate the incidence and signatures of these universality classes in real systems.

The first step in doing so is to analyse the properties of known experimental systems, and ascertain whether or not a pattern is present in their critical behaviour. The relevant experimental literature is therefore surveyed in Chapter 4. An exhaustive survey is presented, and the information reported for each system includes the transition temperature, critical exponents, nature of the order present and experimental technique used to probe the system. The order parameter critical exponent β is of particular interest, since this is found to act as a signature of the universality class to which any given system belongs, although where there is ambiguity, other exponents are also considered. In this way, a classification scheme is constructed.

The majority of two-dimensional systems are placed in either the Ising or XY universality class, depending on the presence of either uniaxial or planar spin anisotropy. The Potts classes are observed to be absent for magnetic systems,

though they are observable in non-magnetic systems. Surprisingly, the XYh_p ($p > 2$) class also appears to be absent, and the central purpose of this work is to understand this peculiar fact. In particular, the influence of quadratic crystal fields is not at all evident, despite the fact that tetragonal symmetry is common in the systems considered. José *et al.* [68] have predicted non-universal critical behaviour for the XYh_4 model, and the question as to what the precise values of the critical exponents are in this case is examined in Chapter 5. Finally, one may ask what the influence of long range interactions is in two dimensions, especially those of the dipolar type. This question is addressed in Chapter 6.

Chapter 4

Survey and Classification of Experimental Data

The purpose of this chapter is to survey the experimental realisations of two-dimensional systems. The focus is primarily on ultrathin film magnets and layered bulk materials, although other non-magnetic systems are also considered. The systems are classified according to their critical behaviour.

4.1 Universality in Two-Dimensional Magnetic Systems

The onset of spontaneous order in two-dimensional systems with continuous spin symmetry is precluded by the Mermin-Wagner theorem [1], which rigorously proves the validity of Bloch's argument [83] with regard to spin waves destroying long range order in the thermodynamic limit. In real two-dimensional magnets, however, spontaneous order is stabilised by perturbations to the Heisenberg Hamiltonian. For example, the single ion anisotropy arising from spin-orbit coupling can destroy rotational spin invariance in such a way that it induces a crossover to behaviour of the Ising universality class [84, 85].

In fact, the only way a true second order phase transition can occur in two dimensions is if it belongs to the Ising universality class. However, it was shown in the previous chapter that spontaneous order can arise naturally in the 2dXY

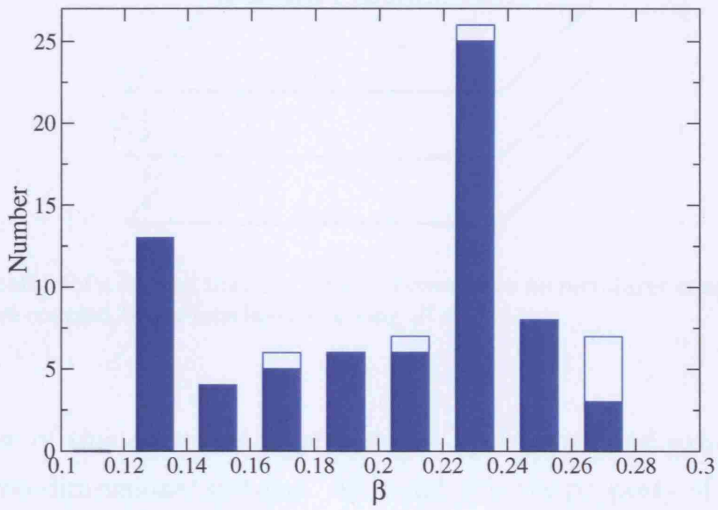

Figure 4.1: Histograms of β values in two-dimensional magnets.

model [77], provided macroscopically large, albeit finite systems are considered. In this case the temperature dependence of the magnetisation is dictated by an effective critical exponent with a value $\tilde{\beta} = \frac{3\pi^2}{128} \simeq 0.231$, independent of system size. The range of reduced temperature $t = (1 - T/T_c)$ over which $\tilde{\beta}$ is close to this value is non-universal, indeed it is zero in the thermodynamic limit where BH theory [77] smoothly passes over to KT theory [61]. Nonetheless, Monte Carlo data lie close to the theoretical value for $0.03 < t < 0.4$ (see Figure 2.19), which is typically in the same range as experimental observations for the materials discussed in this chapter.

Thus, the key experiment on two-dimensional systems is to test the existence and temperature dependence of an order parameter $m(T)$. This quantity is nearly always found to approximate, over a certain range of temperatures, to a power law $m \sim (T_c - T)^{\beta}$, where T_c is the transition temperature. In Figure 4.1 and in Tables 4.1 and 4.2, an extended set of recorded values for the exponent β is collected for two-dimensional magnets. As observed previously on a more limited data sets [86,87], it is noticeable that the distribution of values of β is bimodal, with strong peaks at $\beta = 0.12$ and $\beta = 0.23$, which bound the distribution. The peak values compare well with $\beta = 1/8$, the critical exponent of the Ising model [14,88], and $\tilde{\beta} \simeq 0.23$, observed in systems with planar spin symmetry.

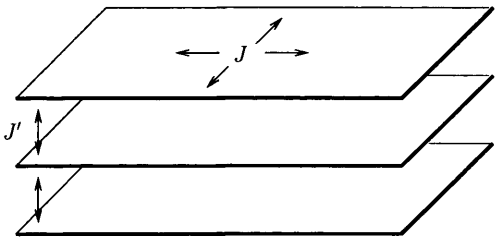

Figure 4.2: Illustration of a layered magnet. The 2d layers have an intralayer coupling J, whereas adjacent layers are coupled by an interlayer coupling $J' \ll J$.

The purpose of this survey is to provide an up to date and exhaustive list of experimental two-dimensional systems. Although β is the property of most interest, the behaviour of other thermodynamic properties is also reported for each system. This allows an unequivocal classification of each system according to its critical behaviour. It is on the basis of these experimental observations that the models discussed in the subsequent chapters are put forward.

4.1.1 Layered Magnets

Historically, the first two-dimensional systems to be studied were layered magnets such as K_2CoF_4 [89]. These are characterised by a *quasi* two-dimensional magnetic structure in which the inter-layer coupling J' is orders of magnitude weaker than the intralayer coupling J, as depicted in Figure 4.2. Such bulk systems lend themselves well to investigation by neutron scattering techniques, and detailed information on their ground state magnetic structure as well as their magnetic properties as a function of external magnetic field and temperature was accessible.

Given the developments in the theory of critical phenomena occurring in the early 1970s [27], there was also an effort to measure the critical exponents of these systems in order to classify them into so-called universality classes. For example, K_2CoF_4 was found to have exponents in agreement with those predicted for the 2d Ising model [89]. On the other hand there were other substances, such as EuS and EuO [39], which were found to display exponents consistent with the three-dimensional models. However there were a number of compounds, such as K_2CuF_4, which displayed unexpected critical behaviour which seemingly did not belong to

any known universality class. Their magnetisation critical exponent $\beta \simeq 0.23$, being roughly intermediate between the 2d Ising value of 1/8 and the 3d value of $\sim 1/3$, was explained by de Jongh and Miedema [90] in terms of "a smeared-out transition range, taking into account that they [the critical exponents] have been determined in a relatively high range of the relative temperature ($t > 0.01$)"[a]. With hindsight these systems are recognisable as belonging to an effective universality class of their own, associated with the 2dXY model on a finite lattice.

In layered magnets the interlayer exchange J' represents the most important perturbation. The ratio of J' to the nearest-neighbour exchange J is typically of order $\sim 10^{-3} - 10^{-4}$ and is sufficient to induce three-dimensional order, with an asymptotic value of β close to either the 3d Ising or 3d Heisenberg values, 0.327 [91] and 0.369 [42] respectively. However, the range over which this critical behaviour is observed is generally very small, and below T_c there is a crossover to a regime, usually at a reduced temperature $t \sim 0.01$, which may be understood in terms of finite size 2d behaviour. Only fluctuations on length scales less than the order of $L_{\text{eff}} = \sqrt{\frac{J}{J'}}$ are two-dimensional [92, 93], which implies that when the correlation length ξ is less than L_{eff}, J' is irrelevant and two-dimensional behaviour occurs. An experimental example of this crossover in barium nickel phosphate is shown in Figure 4.3.

Table 4.1 lists the magnetisation critical exponents measured from all the layered ferromagnets (FMs) and antiferromagnets (AFMs) found in an extensive literature survey. The range of reduced temperature over which they were measured is also reported along with the transition temperatures of the materials. The accuracy of the measured values for β is largely limited by the experimental technique employed: powder neutron diffraction (PND) is generally less accurate than single crystal neutron diffraction (SCND), for example. As discussed above, it is noticeable that the distribution of values of β is not random. One group of compounds, with $\beta \sim 0.13$, is associated with the 2d Ising model, whilst the other group, with $\beta \sim 0.23$, is associated with the 2dXY model.

Nonetheless, a number of materials fall outside of this classification scheme: those with $\beta > 0.23$, and those with $0.125 < \beta \leq 0.23$. The former can be explained

[a]See page 1059 of de Jongh and Miedema [90].

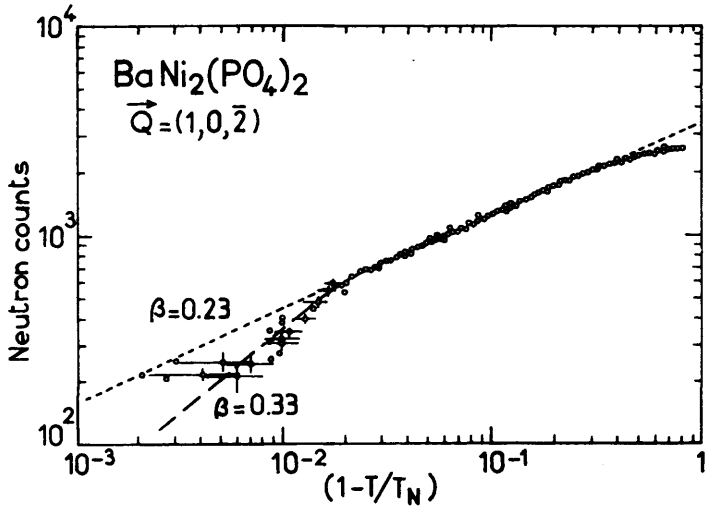

Figure 4.3: Temperature dependence of the magnetic Bragg peak $[1, 0, \bar{2}]$ of $BaNi_2(PO_4)_2$. The abrupt crossover from 2dXY behaviour ($\beta = 0.23$) to 3d behaviour ($\beta = 0.33$) at $T \sim 0.9T_N$ is noteworthy. After Regnault *et al.* [94].

as being intermediate between 2d and 3d behaviour. For example, Rb_2CrCl_3Br [95] is known to possess stronger interlayer coupling than Rb_2CrCl_4 [96], and consequently has a larger β value. The latter are often ascribed to the Ising model with a non-universal correction, possibly due to long range interactions. It will be demonstrated in Chapter 5 that these intermediate materials may in fact be accounted for through another crossover mechanism.

Table 4.1: List of 2d critical exponents β for 54 compounds, mostly measured by neutron diffraction. For more information on the experimental techniques adopted on each system, see main text. Fo = (HCO_2), chdc = *trans*-1,4-cyclohexanedicarboxylate, CSDAB = $Co_4(SO_4)(OH)_6(C_6N_2H_{12})_{0.5} \cdot H_2O$, CSEN = $Co_4(SO_4)(OH)_6(C_2N_2H_8)_{0.5} \cdot 3H_2O$, 5CAP = 2-amino-5-chloropyridinium.

System	β	t range	T_c (K)	Reference	Description
Rb_2CoF_4	0.119(8)	$1 \cdot 10^{-1}$–$2 \cdot 10^{-4}$	102.96	[97]	AFM
$ErBa_2Cu_3O_7$	0.122(4)	0.11–$1 \cdot 10^{-4}$	0.618	[98]	AFM
K_2CoF_4	0.123(8)	$1 \cdot 10^{-1}$–$8 \cdot 10^{-4}$	107.85	[89]	AFM
$BaNi_2(AsO_4)_2$	0.135	$3 \cdot 10^{-1}$–$1 \cdot 10^{-2}$	19.2	[94]	AFM
Ba_2FeF_6	0.135(3)	$7 \cdot 10^{-1}$–$4 \cdot 10^{-3}$	47.96(4)	[99]	AFM

Continued on next page

Table 4.1 – continued from previous page

System	β	t range	T_c (K)	Reference	Description
K_2NiF_4	0.138(4)	$2 \cdot 10^{-1}$–$3 \cdot 10^{-4}$	97.23	[100]	AFM
$K_3Mn_2F_7$	0.154(6)	$1 \cdot 10^{-1}$–$1 \cdot 10^{-3}$	58.3(2)	[101]	AFM
Rb_2MnCl_4 (B < 5.8 T)*	0.15(1)	$1 \cdot 10^{-1}$–$1 \cdot 10^{-3}$	54	[102, 103]	AFM
K_2MnF_4	0.15(1)	$1 \cdot 10^{-1}$–$1 \cdot 10^{-3}$	42.14	[104]	AFM
K_2FeF_4	0.15(1)	–	63.0(3)	[105]	AFM
Rb_2MnF_4	0.16(2)	$1 \cdot 10^{-1}$–$3 \cdot 10^{-3}$	38.4	[100]	AFM
$Pb_2Sr_2TbCu_3O_8$†	0.165(5)	–	5.30(2)	[106]	AFM
$BaFeF_4$	0.17	$3 \cdot 10^{-1}$–$1 \cdot 10^{-2}$		[90]	AFM
$Cr_2Si_2Te_6$	0.17(1)	$6 \cdot 10^{-1}$–$3 \cdot 10^{-2}$	32.1(1)	[107]	FM
$CsDy(MoO_4)_2$	0.17(1)	–	1.36	[108]	AFM
$CoCl_2 \cdot 6H_2O$	0.18	$4 \cdot 10^{-1}$–$4 \cdot 10^{-2}$	2.29	[90]	AFM
$MnC_3H_7PO_3 \cdot H_2O$	0.18(1)	$4 \cdot 10^{-1}$–$1 \cdot 10^{-2}$	~ 15	[109]	FM
$MnC_4H_9PO_3 \cdot H_2O$	0.18(1)	$4 \cdot 10^{-1}$–$2 \cdot 10^{-2}$	~ 15	[109]	FM
$KFeF_4$	0.185(5)	$3 \cdot 10^{-1}$–$1 \cdot 10^{-2}$	137.2(1)	[90, 110]	AFM
$Fe(NCS)_2(pyrazine)_2$‡	0.19(2)	$2 \cdot 10^{-1}$–$3 \cdot 10^{-2}$	6.8	[111]	AFM
Rb_2FeF_4	0.2	$3 \cdot 10^{-1}$–$2 \cdot 10^{-3}$	56.3	[100]	AFM
La_2CoO_4	0.20(2)	–	274.7(6)	[112]	AFM
CSDAB‡§	0.20(4)	$7 \cdot 10^{-1}$–$4 \cdot 10^{-2}$	21	[113]	AFM
$MnC_2H_5PO_3 \cdot H_2O$	0.21(2)	$6 \cdot 10^{-1}$–$9 \cdot 10^{-2}$	~ 15	[109]	AFM
$NH_4MnPO_4 \cdot H_2O$†	0.21(3)	$8 \cdot 10^{-1}$–$2 \cdot 10^{-2}$	17.5(1)	[109, 114]	AFM
K_2CuF_4	0.22	$3 \cdot 10^{-1}$–$3 \cdot 10^{-2}$	6.25	[115]	FM
$CuFo_2 \cdot 4D_2O$	0.22(2)	$5 \cdot 10^{-1}$–$5 \cdot 10^{-2}$	16.72	[116]	AFM
$CuFo_2 \cdot CO(ND_2)_2 \cdot 2D_2O$	0.22(1)	$4 \cdot 10^{-1}$–$1 \cdot 10^{-3}$	15.31	[116]	AFM
Tanol suberate‡	0.22	$7 \cdot 10^{-1}$–$2 \cdot 10^{-2}$	0.7	[117]	FM
$Sr_2CuO_2Cl_2$	0.22(1)	$2 \cdot 10^{-1}$–$1 \cdot 10^{-2}$	265.5(5)	[118]	AFM
La_2NiO_4	0.22(2)	$8 \cdot 10^{-2}$–$2 \cdot 10^{-3}$	327.5(5)	[119]	AFM
CSEN‡§	0.22(2)	$7 \cdot 10^{-1}$–$3 \cdot 10^{-2}$	14	[113]	AFM
$BaNi_2(PO_4)_2$	0.23	$3 \cdot 10^{-1}$–$2 \cdot 10^{-2}$	23.5(5)	[94]	AFM
$Cu(DCO_2)_2 \cdot 4D_2O$	0.23(1)	$t > 6 \cdot 10^{-}2$	16.54(5)	[120]	AFM
$MnFo_2 \cdot 2H_2O$	0.23(1)	$4 \cdot 10^{-1}$–$4 \cdot 10^{-2}$	3.6	[121]	AFM
Rb_2CrCl_4	0.230(2)	$2 \cdot 10^{-1}$–$1 \cdot 10^{-2}$	52.3	[96]	FM
Gd_2CuO_4	0.23	$7 \cdot 10^{-1}$–$3 \cdot 10^{-3}$	6.4	[122]	AFM
$(C_6H_5CH_2NH_3)_2CrBr_4$	0.23	$7 \cdot 10^{-1}$–$1 \cdot 10^{-1}$	52.0(1)	[123]	FM
$KMnPO_4 \cdot H_2O$†	0.23(2)	$t > 9 \cdot 10^{-2}$	~ 15	[109]	AFM
$(CH_3NH_3)_2MnCl_4$	0.23(2)	$1 \cdot 10^{-2}$–$1 \cdot 10^{-3}$	44.75	[124]	FM
$ErCl_3$	0.23(2)	$4 \cdot 10^{-1}$–$1 \cdot 10^{-2}$	0.350(5)	[125]	AFM

Continued on next page

Table 4.1 – continued from previous page

System	β	t range	T_c (K)	Reference	Description
$(d_6\text{-}5CAP)_2CuBr_4$	0.23(4)	$4\cdot10^{-2}$–$6\cdot10^{-3}$	5.18(1)	[126]	AFM
Li_2VOSiO_4	0.235(9)	$4\cdot10^{-1}$–$2\cdot10^{-2}$	2.85	[127]	AFM
Li_2VOGeO_4	0.236	–	1.95	[128]	AFM
$La_{0.04}Sr_{2.96}Mn_2O_7$	0.24(2)	–	145.0(5)	[129]	AFM
$La_{0.525}Sr_{1.475}MnO_4$	0.24(3)	–	110(1)	[130]	AFM
$RbFeF_4$	0.245(5)	$6\cdot10^{-1}$–$1\cdot10^{-2}$	133(2)	[90]	AFM
$MnPS_3$	0.25(1)	$t > 3\cdot10^{-2}$	78.6	[131,132]	AFM
$Co_5(OH)_8(chdc)\cdot4H_2O$‡	0.25(3)	–	60.5	[133]	FM
$YBa_2Cu_3O_{6+x}$	0.26(1)	$5\cdot10^{-2}$–$5\cdot10^{-3}$	410	[134]	AFM
Rb_2MnCl_4 (B > 5.8 T)*	0.26(1)	$1\cdot10^{-1}$–$2\cdot10^{-3}$	54	[102,103]	AFM
Rb_2CrCl_3Br†	0.26(1)	$9\cdot10^{-1}$–$1\cdot10^{-2}$	55	[95,135]	FM
$Rb_2CrCl_2Br_2$†	0.26(1)	$9\cdot10^{-1}$–$3\cdot10^{-2}$	57	[95,135]	FM
$KMnF_4$†	0.26(1)	$3\cdot10^{-1}$–$3\cdot10^{-2}$	5.2(1)	[136]	AFM
$RbMnF_4$†	0.26(1)	$3\cdot10^{-1}$–$3\cdot10^{-2}$	3.7(1)	[136]	AFM

Temperature Dependence of Magnetic Order in Selected Systems

The antiferromagnetic and ferromagnetic layer-type compounds gathered in Table 4.1 display a wide range of experimental properties which merit further consideration. Many of these materials have been discussed in previous books and reviews [90, 137], consequently only the most salient facts shall be reported, with a bias towards 2dXY and recently discovered systems.

Inorganic Magnets

The most common source of quasi two-dimensional layered magnets are systems with the formula A_2BX_4, where A is a non magnetic cation of single charge, B is a doubly charged magnetic cation and X is a halide anion. The crystal structure of such compounds is tetragonal and the magnetic ions reside on a square lattice in two

*Rb_2MnCl_4 undergoes a spin-flop transition in an external magnetic field.
†Studied by powder neutron diffraction, hence the large degree of uncertainty in β.
‡Molecular magnet.
§CSDAB and CSEN undergo a metamagnetic transition in a critical field.

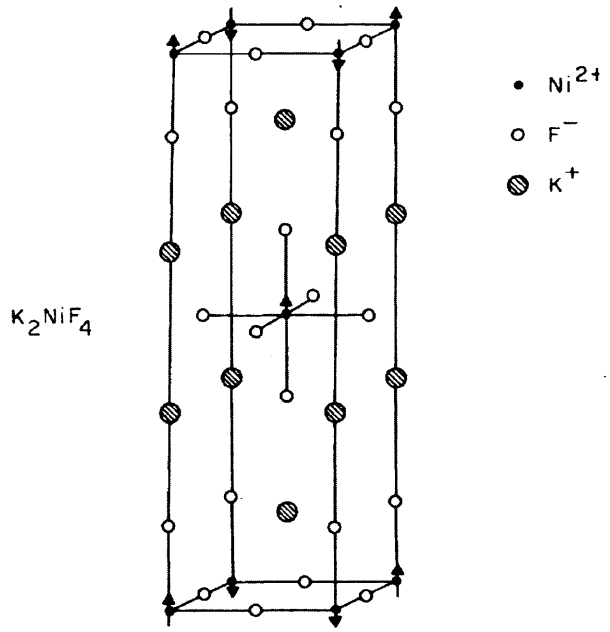

Figure 4.4: Tetragonal crystal structure of K_2NiF_4. The large distance between the Ni layers gives rise to a quasi 2d magnetic structure. After Birgeneau *et al.* [100].

dimensions. A typical material is K_2NiF_4 (see Figure 4.4), indeed these systems are often said to have the K_2NiF_4 structure. It is noteworthy that high temperature superconductors based on doped copper oxides La_2CuO_4 also have the K_2NiF_4 structure. It is thought that low dimensionality, combined with the proximity to a Mott insulating phase, is crucial in causing doped materials to display this fundamentally different behaviour not explicable in terms of conventional metal physics [138, 139]. However, it will become clear as this discussion progresses that materials displaying 2d magnetic properties are not confined to being only K_2NiF_4-like, and that their structures may be surprisingly varied.

Rb_2CoF_4 and K_2CoF_4 The critical behaviour of these antiferromagnets has been investigated by single crystal neutron diffraction experiments (SCND) by Samuelsen [97] (Rb_2CoF_4) and Ikeda and Hirakawa [89] (K_2CoF_4). In both cases the evidence strongly suggests a pronounced two-dimensional Ising nature. The data measured from rubidium cobalt fluoride is of particularly high quality. The sublattice magnetisation determined from the magnetic scattering intensity clearly

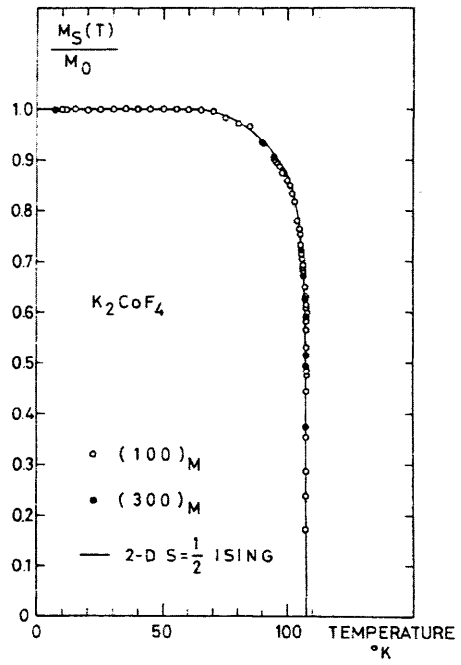

Figure 4.5: The critical behaviour of the order parameter of K_2CoF_4 is clearly of two-dimensional Ising nature over a wide temperature range. After Ikeda and Hirakawa [89].

obeys the Onsager solution for the 2d Ising model over a wide range of temperatures, as shown in Figure 4.5. The least squares fitted value of β for $1 \cdot 10^{-1} > t > 8 \cdot 10^{-4}$ is 0.123(8) which is in excellent agreement with theory. The determined values for ν, γ and η are 0.97(5), 1.71(4) and 0.2(1), respectively, and are in good agreement with the theoretically expected values of 1.0, 1.75 an 0.25. No evidence of crossover to three-dimensional behaviour is found for either system, suggesting the 3d region is very narrow.

$ErBa_2Cu_3O_7$ The magnetic order of the erbium ions in this superconducting compound has been studied by SCND by Lynn *et al.* [98]. Both above and below the Néel temperature there is evidence that the magnetic interactions are highly anisotropic, and the temperature dependence of the order parameter below T_N is in excellent agreement with the 2d Ising model, despite the presence of the long range dipolar interactions associated with erbium. Indeed, the authors note that their data is very similar to the prototypical 2d Ising system K_2CoF_4. Numerical

simulations by De'Bell and Whitehead [140] confirms that the behaviour of the 2d Ising antiferromagnet remains virtually unaffected by the dipolar interaction (see Section 6.2.3).

$BaNi_2(AsO_4)_2$ The magnetic properties of $BaNi_2(AsO_4)_2$ are summarised by Regnault and Rossat-Mignod [94]. The system is based on a layered honeycomb lattice and elastic neutron scattering experiments confirm antiferromagnetic ordering below $T_N = 18.7(3)$ K, with a significant degree of frustration arising. The temperature dependence of the order parameter is consistent with the 2d Ising model, with a critical exponent $\beta_{2d} \simeq 0.135$ in the reduced temperature region $3 \cdot 10^{-1} > t > 1 \cdot 10^{-2}$. Closer to $T_N = 18.7(3)$ K there is a crossover to three-dimensional behaviour, with $\beta_{3d} \simeq 0.33$. Whilst the 2d Ising nature of the system is corroborated by the obtained values for ν and η, there is some contradictory evidence, particularly with regards to the behaviour of the low temperature specific heat, which suggests Kawamura's theory for frustrated triangular antiferromagnets may be relevant [141,142].

Ba_2FeF_6 Brennan and co-workers [99] have used the Mössbauer effect to measure the critical behaviour of the layered antiferromagnet Ba_2FeF_6. They measure an exponent $\beta = 0.135(3)$ over a temperature range $7 \cdot 10^{-1} > t > 4 \cdot 10^{-3}$.

K_2NiF_4 The SCND study by Birgeneau *et al.* [100] of K_2NiF_4 and its two isostructural compounds Rb_2MnF_4 and Rb_2FeF_4 (both described below) represents a watershed in the study of low dimensional magnetism. In all three compounds the diffuse scattering above the phase transition takes the form of a ridge rather than a peak, giving the first piece of concrete evidence for two-dimensional nature of the magnetism in such systems. The sublattice magnetisation measurements made on K_2NiF_4 yield $\beta = 0.138(4)$ in the temperature region $2 \cdot 10^{-1} > t > 3 \cdot 10^{-4}$, with $T_N = 97.23$ K.

$K_3Mn_2F_7$ The magnetic structure elucidated by SCND of $K_3Mn_2F_7$ consists of a double-layer with nearest neighbour Heisenberg interactions that are weakly

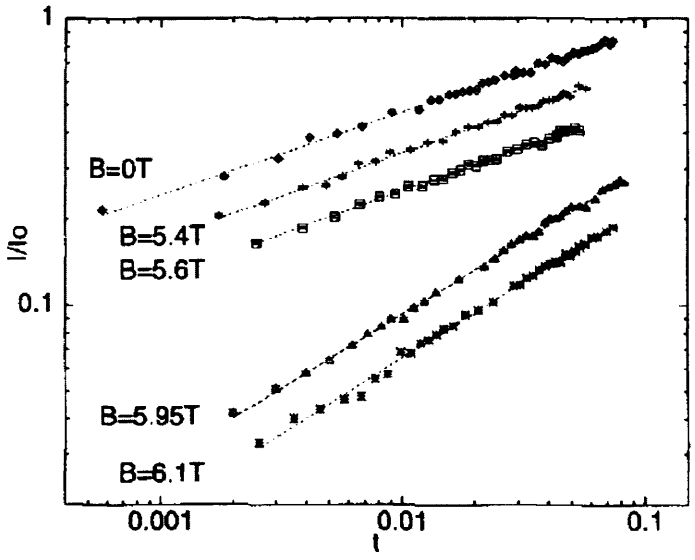

Figure 4.6: Field-dependent critical behaviour of Rb_2MnCl_4. The dashed lines represent fits to power laws, with $\beta = 0.15(1)$ ($\beta = 0.26(1)$) below (above) $B = 5.8$ T. After van de Kamp *et al.* [103].

anisotropic [101]. At $T_N = 58.3(2)$ K the system exhibits a second order phase transition to antiferromagnetic order. As one might expect, there is strong evidence that the paired magnetic layers interfere strongly with each other. The critical behaviour in the vicinity of T_N is comparable to that of the the single layer systems such as K_2NiF_4, and does not differ substantially from exact two-dimensional Ising results.

Rb_2MnCl_4 SCND experiments by van de Kamp *et al.* [103] have shown that an applied external magnetic field can induce a spin flop from Ising to XY behaviour in the weakly anisotropic Heisenberg antiferromagnet Rb_2MnCl_4. As is clear in Figure 4.6, below $B = 5.8$ T a critical exponent of $\beta = 0.15(1)$ is measured, whereas above $\beta = 0.26(1)$.

K_2MnF_4 and Rb_2MnF_4 Potassium manganese fluoride and its rubidium analogue have been extensively studied using SCND by a number of authors. Rb_2MnF_4 was found to have two distinct magnetic phases with identical ordering within the

plane but different stacking arrangements [100]. Within experimental error, both phases were found to have identical transition temperatures and follow a power law t^{β} with $\beta = 0.16(2)$, within the temperature range $1 \cdot 10^{-1} > t > 3 \cdot 10^{-3}$.

K_2MnF_4 was the subject of two separate studies, the results of which are largely in agreement with each other and with the observed behaviour in other quadratic layered antiferromagnets. There were, however, two important differences. Firstly, Ikeda and Hirakawa (IH) [143] observed two distinct 3d magnetic phases as in Rb_2MnF_4, but in their case with very different Néel temperatures, suggesting the 3d coupling is quite different for the two phases. Birgeneau *et al.* [100], on the other hand, observe no evidence of a second phase. Secondly, the two research groups find contrasting behaviours for the sublattice magnetisation in the vicinity of T_N. Whereas IH report a changeover from 2d to 3d critical behaviour at $t = 5 \cdot 10^{-3}$, with $\beta = 0.15(1)$, Birgeneau and co-workers find a single exponent $\beta = 0.15(1)$ over the range $3 \cdot 10^{-1} > t > 6 \cdot 10^{-4}$. The Birgeneau group discuss the effects of the distribution of the Néel temperatures on neutron order parameter determinations, and make a convicing argument that the crossover observed by IH can be accounted for on this basis.

K_2FeF_4 and Rb_2FeF_4 Thurlings *et al.* [105] have carried out a detailed examination of the quadratic-layer antiferromagnet K_2FeF_4 by SCND. They observe a phase transition at $T_N = 63.0(3)$ K, and measure critical exponents $\beta = 0.15(1)$, $\gamma = 1.5(5)$ and $\nu = 0.9(2)$, which are comparable with experimental findings in other quadratic layer systems. This system is considered in more detail in Section 5.3, since it will be argued it represents an experimental example of non-universal exponents occurring as a result of a crossover from 2dXY to 2d Ising behaviour due to the presence of four-fold crystal fields.

Rb_2FeF_4 has been found to have a rather high order parameter critical exponent, $\beta \simeq 0.2$ over the temperature range $3 \cdot 10^{-1} > t > 2 \cdot 10^{-2}$ [100]. Whilst this confirms the 2d nature of the material, it appears to rule out the relevance of the 2d Ising model. However, it should be noted that the slope of $\log m$ against $\log t$ increases rapidly as the phase transition is approached. This change may arise from extraneous effects such as the distribution of the Néel temperatures or from a

fundamental change in the critical behaviour due to a crossover to the 3d regime.

$Pb_2Sr_2TbCu_3O_8$ Wu and co-workers [106] have carried out a powder neutron diffraction (PND) study of $Pb_2Sr_2TbCu_3O_8$ and have found the magnetic correlations to be predominantly 2d in nature. Whilst the value obtained for the critical exponent of the correlation length $\nu = 1.00(5)$ agrees very well with the 2d Ising theoretical prediction, there is a significant departure for the magnetisation, with $\beta = 0.165(5)$. Given the polycrystalline nature of the powder sample examined, one might expect a refinement of this estimate by studying a single crystal. The presence of a strong dipolar interaction may also be relevant.

$Cr_2Si_2Te_6$ The lamellar compound $Cr_2Si_2Te_6$ represents the first realisation of a quasi 2d Ising ferromagnet [107]. SCND experiments have allowed close examination of the thermal evolution of the order parameter and reveal a critical exponent $\beta \simeq 0.17$, which is claimed to be comparable to the 2d Ising theoretical prediction.

$CsDy(MoO_4)_2$ An approximate magnetic structure for this quasi two-dimensional antiferromagnet has been determined by neutron diffraction by Khatsko *et al.* [108]. In the ordered phase the order parameter critical exponent, the correlation length exponent and the staggered susceptibility index were measured as $\beta = 0.17(1)$, $\nu = 0.94(7)$ and $\gamma = 1.01(4)$, respectively. Although two-dimensional behaviour is apparent, there are clear deviations from the simple 2d Ising model. The authors suggest the strong nature of the dipole-dipole interactions between the dysprosium atoms may be relevant. One may remark here that compounds of general formula $MR(MoO_4)_2$ (M = rare-earth, M = alkali metal), crystallise in a variety of layered structures and have hitherto received little attention by neutron diffraction techniques. These materials, sometimes referred to as double rare-earth molybdenates (DRMs), are worthy of further consideration as 2d magnetic systems.

$MnC_nH_{(2n+1)}PO_3 \cdot H_2O$, n=2−4 The magnetisation critical exponent β for the weakly ferromagnetic layer compounds $MnC_nH_{(2n+1)}PO_3 \cdot H_2O$ have been measured by bulk magnetometry for $n = 2-4$ by Carling *et al.* [109]. In all three compounds crossovers were observed in β as follows (β_1, β_2): 0.21(2), 0.73(2) ($n = 2$), 0.18(1),

0.42(6) ($n = 3$) and 0.18(1), 0.6(2) ($n = 4$). Varying the chain length of the alkyl group leads to a variation of the interlayer spacing, and it is found that with increasing magnetic layer spacing the crossover occurs at decreasing values of the reduced temperature t. Whilst the β_2 values are considerably bigger than typical 3d values of ~ 0.33, they seem likely to represent a departure from 2d magnetic correlations. The β_1 values appear to tend to the 0.23 value predicted by 2dXY theory.

La_2CoO_4 SCND measurements carried out by Yamada *et al.* [112] on this K_2NiF_4-like material reveal an order parameter critical exponent $\beta = 0.20(2)$. Coupled with evidence from susceptibility measurements that suggests the spins possess an XY anisotropy, it seems likely this system belongs to the 2dXY class.

$NH_4MnPO_4 \cdot H_2O$ and $KMnPO_4 \cdot H_2O$ In a study related to their work on the manganese alkylphophonate hydrates described above, Carling *et al.* [114] have measured by magnetometry and PND measurements the critical exponents of the magnetisation below T_N for the 2d canted antiferromagnets $MMnPO_4 \cdot H_2O$ (M = K, NH_4 and ND_4). In all three cases a change in the value of the critical exponent β is observed which is attributed to a crossover in dimensionality from 2d to 3d. The values approaching $\beta = 0.23$ in the 2d regime suggest a 2dXY-like nature.

K_2CuF_4 The magnetic properties of this insulating Heisenberg ferromagnet have been studied by Hirakawa and Ikeda by SCND [115]. Despite a very weak ($< 1\%$) XY anisotropy, K_2CuF_4 displays all the features of a 2dXY system. The two-dimensional nature of the compound is supported by the observation of strong paramagnetic diffuse scattering in the form of a ridge near $T_c = 6.25$ K. The ratio of intra- and interlayer exchange is determined as $J'/J = 0.00066$. Despite having the same crystal structure as K_2NiF_4, the material displays a quite different critical behaviour in the magnetisation, with $\beta_{2d} = 0.22$ over the range $3 \cdot 10^{-1} > t > 3 \cdot 10^{-2}$ (see Figure 4.7), followed by a crossover to typical 3d critical behaviour with $\beta_{3d} = 0.33(3)$ in the range $2 \cdot 10^{-2} > t > 1 \cdot 10^{-3}$. Further investigation [144] by measuring the critical parameters $\delta(T)$, $\chi(T)$, $\xi(T)$ and $\eta(T)$ confirmed the Kosterlitz-Thouless nature of the observed transition.

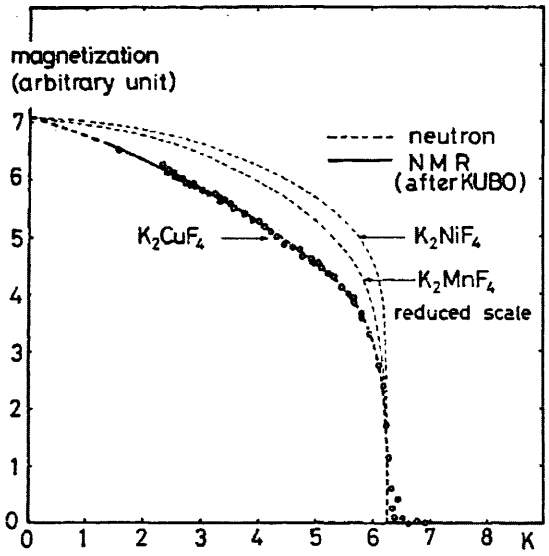

Figure 4.7: Magnetisation as a function of temperature for K_2CuF_4. After Hirakawa and Ikeda [115].

$CuFo_2 \cdot 4D_2O$ and $CuFo_2 \cdot CO(ND_2)_2 \cdot 2D_2O$ These $S = 1/2$ square Heisenberg antiferromagnets were first studied by Koyama *et al.* using proton NMR techniques [116]. Copper formate tetradeuterate (CFTD) was found to crossover from $\beta_{2d} = 0.22$ for $t > 5 \cdot 10^{-2}$ to $\beta_{3d} = 0.30$ for $t < 5 \cdot 10^{-2}$, whereas copper formate urea dihydrate (CFUTD) was found to exhibit a single power law with $\beta = 0.22$. This difference in behaviour is likely to be due to the interplane interaction J' in CFTD being about 20 times larger than that for CFUTD. A later SCND study by Clarke *et al.* [120] on the fully deuterated analogue of copper formate tetrahydrate, $Cu(DCO_2)_2 \cdot 4D_2O$, confirmed the crossover in β observed in CFTD. Koyama *et al.* interpreted their smaller exponent value as evidence for the chiral universality class proposed by Kawamura [141] to exist in canted Heisenberg ferro- and antiferromagnets. However, it is not clear there is any canting in the magnetic ground state of CFTD with no external applied magnetic field. Furthermore the canting that has been suggested to be present is not thought to give rise to Kawamura's chiral universality class [120]. Thus, despite the extremely weak anisotropy present, it would appear the critical behaviour of these systems is 2dXY-like.

$Sr_2CuO_2Cl_2$ and La_2NiO_4 The lanthanum copper oxide analogues La_2NiO_4 and $Sr_2CuO_2Cl_2$ are very good approximations to the $S = 1/2$ and $S = 1$ square Heisenberg antiferromagnets, respectively. In a series of single crystal neutron diffraction studies [118, 119], Birgeneau and co-workers measure, amongst other things, the critical behaviour of the order parameter of these systems. In both cases $\beta = 0.22$, and to account for this the authors suggest two possibilities: either it may indicate finite size two-dimensional XY behaviour or it may reflect tricriticality as outlined by Thio and Aharony in the case of La_2CuO_4 [145]. How one might go about distinguishing experimentally between these two theories is discussed in Section 4.1.2, but it is worth making a couple of remarks on $Sr_2CuO_2Cl_2$ here.

Firstly, the mean field theory discussed by Thio and Aharony [145] explicitly includes the Dzyaloshinskii-Moriya (DM) anisotropic exchange interaction given by Equation (1.27) [146,147], which is allowed in the spin Hamiltonian of La_2CuO_4 as a result of a distortion from tetragonal to orthorombic symmetry occurring at low temperature. There is no evidence of such a distortion in $Sr_2CuO_2Cl_2$ [148, 149], and hence no reason to believe the DM interaction should be relevant, thus refuting the mean field tricritical explanation in this context. Secondly, the behaviour of the correlation length ξ as a function of temperature is impressively accounted for by two-dimensional non-linear sigma model, and not by KT theory (*c.f.* Equation (2.71)) [150]. Consequently this material is by no means an ideal 2dXY magnet, either. Nonetheless, it is noteworthy that 2dXY critical behaviour has been shown to persist in systems with very small XY spin anisotropy [151].

$BaNi_2(PO_4)_2$ The magnetic properties of this honeycomb layered material are summarised in reference [94]. Elastic neutron scattering data confirm antiferromagnetic ordering below $T_N = 23.5(5)$ K and the XY anisotropy of the spins. The temperature dependence of the staggered magnetisation derived from the magnetic peak intensities is shown in Figure 4.3, and a crossover from $\beta_{2d} \simeq 0.23$ to $\beta_{3d} \simeq 0.33$ is clearly observable, suggesting this system belongs to the 2dXY class. An analogue of this material, $BaNi_2(VO_4)_2$, has also been studied recently by SCND [152] and electron spin resonance (ESR) [153], and has been found to display characteristics compatible with the 2dXY model.

$MnFo_2 \cdot 2H_2O$ This Heisenberg antiferromagnet was first studied using SCND by Skalyo *et al.* [121] who observed a sublattice magnetisation varying according to a power law with $\beta = 0.23(1)$ over the temperature range $4 \cdot 10^{-1} > t > 4 \cdot 10^{-2}$. In a subsequent study Matsuura *et al.* [154] confirmed this by neutron and magnetometry techniques, and in addition found that below $0.98\,T_N = 1.7(1)$ K there is a crossover to three-dimensional behaviour with $\beta_{3d} = 0.31$.

Rb_2CrCl_4, Rb_2CrCl_3Br and $Rb_2CrCl_2Br_2$ The ionic ferromagnet Rb_2CrCl_4 was studied in depth by Als-Nielsen *et al.* [96] using SCND and represents the first experimental system compellingly found to be described in its entirety by the 2dXY model. The material is characterised by a layered structure with a very weak 3d exchange coupling ($J'/J \sim 10^{-4}$), which explains why two-dimensional fluctuations remain dominant up to a surprisingly high temperatures. The consistency of the data within the framework of KT and BH theory is impressive. In particular, the authors were able to locate the three distinct temperatures T_c, T_{KT} and T^*, and measure the critical behaviour of the magnetisation. In two separate experiments this was found to take the 2dXY value $\beta_{2d} \simeq 0.23$ in the region $2 \cdot 10^{-1} > t > 1 \cdot 10^{-2}$ and a 3d value $\beta_{3d} \sim 0.33$ in the region $1 \cdot 10^{-2} > t > 5 \cdot 10^{-4}$. Furthermore the correlation length was found to scale with temperature according to the Kosterlitz expression (2.71), as shown in Figure 4.8.

In addition to Rb_2CrCl_4, SCND and bulk magnetometry measurements have also been made on its structural analogues Rb_2CrCl_3Br and $Rb_2CrCl_2Br_2$ [95,135]. For Rb_2CrCl_3Br β was found to be 0.26(1), whereas for $Rb_2CrCl_2Br_2$ an abrupt crossover was observed from 0.26(1) to 0.41(3) as T_c is approached.

Gd_2CuO_4 SCND measurements on this compound suggest magnetic ordering of gadolinium below $T_N = 6.4$ K, with a magnetic structure consisting of ferromagnetic planes stacked antiferromagnetically [122]. The sublattice magnetisation was found to obey a power law with a critical index $\beta = 0.234(9)$. Following a more recent investigation using dc magnetisation techniques [155], it appears that weak ferromagnetism occurs as a result of a canting of the Cu moments from the ideal antiferromagnetic structure. In this other study the magnetisation critical exponent was found to crossover from $\beta_{3d} = 0.34(1)$ to $\beta_{2d} = 0.19$ further away from the

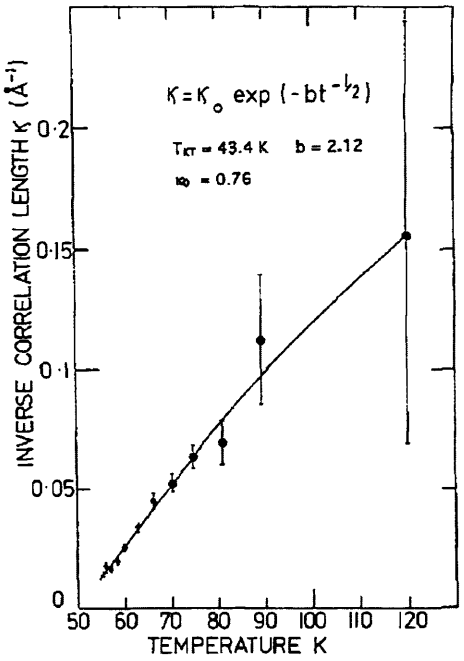

Figure 4.8: Temperature dependence of the inverse correlation length κ of Rb_2CrCl_4, fitted to the inverse of expression (2.71). After Als-Nielsen *et al.* [96].

critical temperature, in a manner that is qualitatively consistent with the 2dXY picture.

$(C_6H_5CH_2NH_3)_2CrBr_4$ This two-dimensional ionic ferromagnet has been investigated using ac magnetic susceptibility measurements [123]. The critical behaviour of the magnetisation was reported as $\beta = 0.23$ in the range $7 \cdot 10^{-1} > t > 1 \cdot 10^{-1}$, with $T_c = 52.0(1)$ K. As the critical temperature is approached, a change over to a larger value of β was observed, suggesting a crossover from 2d to 3d behaviour.

$(CH_3NH_3)_2MnCl_4$ A crossover in β from 0.17 to 0.23 has been reported for this square-layered material, *as the critical temperature is approached* [124]. Further investigation is desireable in order to account for these perplexing measurements.

$ErCl_3$ Single crystal neutron diffraction measurements on the honeycomb layer material $ErCl_3$ have revealed triangular antiferromagnetic order [125] below $T_N =$ 350 mK. From the temperature dependence of the integrated neutron magnetic

peak intensity a critical exponent $\beta = 0.23(2)$ was derived for the magnetic phase transition, over the temperature range $4 \cdot 10^{-1} > t > 1 \cdot 10^{-2}$. Whilst this system bears a number of similarities with other 2dXY honeycomb systems such as $BaNi_2(PO_4)_2$, the potential relevance of Kawamura's theory for Heisenberg antiferromagnets on triangular lattices has so far not been established.

Li_2VOSiO_4 and Li_2VOGeO_4 Vanadates such as Li_2VOSiO_4 and Li_2VOGeO_4 represent prototypes of frustrated two-dimensional $S = 1/2$ antiferromagnets on a square lattice [128]. Their phase diagrams are characteristically complex as their low dimensionality and low spin values give rise to an enhancement of quantum fluctuations. The temperature dependence of the sublattice magnetisations measured by muon spin rotation (μSR) techniques for both these systems obey a power law with a critical exponent $\beta \simeq 0.236$. The close agreement with the 2dXY prediction suggests that the 3d ordering is onset by the divergence of the in-plane correlations caused by a small XY anisotropy. This is consistent with a recent quantum Monte Carlo study in which it was shown that 2dXY critical behaviour persists even in the presence very small spin anisotropy [151].

$La_{0.04}Sr_{2.96}Mn_2O_7$ The double layered manganites $La_{2-2x}Sr_{1+2x}Mn_2O_7$ ($0.4 \leq x \leq 1$) have been the subject of much interest in recent years [156, 157], as under specific doping conditions they display Colossal Magneto Resistance (CMR)[b]. A μSR study investigating the local magnetic structure of these systems by Coldea *et al.* [129] has revealed a transition temperature $T_N = 145.0(5)$ K and a critical index $\beta = 0.24(2)$ for the $x = 0.98$ compound, in agreement with previous neutron powder diffraction measurements [158].

$La_{0.525}Sr_{1.475}MnO_4$ The single layered manganite $La_{1-x}Sr_{1+x}MnO_4$ ($0 \leq x \leq 0.7$) has also been studied by single crystal x-ray and neutron scattering techniques [130]. For $x = 0.475$, 2dXY critical behaviour was observed, with $\beta = 0.24(3)$.

[b]CMR is a property which is characterised by extremely large changes in electrical response to an applied magnetic field, and is observed in many manganese-based perovskite oxides. It has a large technological potential for the development of magnetic memory and switching devices.

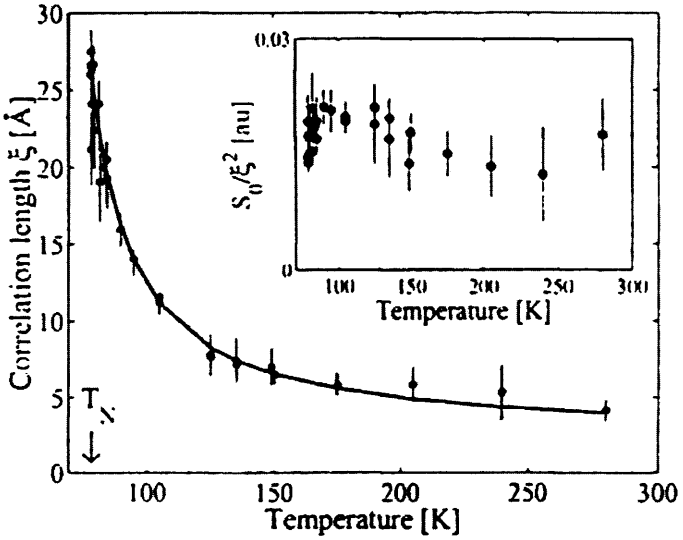

Figure 4.9: Temperature dependence of the correlation length ξ of $MnPS_3$, fitted to expression (2.71). After Rønnow *et al.* [131].

$MnPS_3$ The 2d $S = 5/2$ honeycomb antiferromagnet $MnPS_3$ has been the subject of a SCND study in which it was convincingly shown to be 2dXY-like [131]. The temperature dependence of the correlation length ξ was found to follow the Kosterlitz expression (2.71) (see Figure 4.9), with parameters which are described by a Heisenberg system with interplane coupling $J'/J = \frac{1}{405}$ and weak XY anisotropy. Furthermore, below $T_N = 78.6$ K the critical exponent β_{2d} was measured as 0.24(1), with a crossover to $\beta_{3d} = 0.32(1)$ for $t < 2 \cdot 10^{-2}$. A later study [132] has confirmed these results, concluding that the 2d Heisenberg model with XY anisotropy provides the best description of the system. The exact origin of the anisotropy is a matter for future investigation.

$YBa_2Cu_3O_{6+x}$ The tetragonal compound $YBa_2Cu_3O_{6+x}$ (with $x \leq 0.1$) is a bilayer Heisenberg antiferromagnet with a weak XY anisotropy. A single crystal neutron diffraction experiment [134] has established that this system undergoes a dimensional crossover at $T \sim 0.995T_N$ ($T_N = 410$ K). The critical exponent of the sublattice magnetisation takes a value $\beta_{2d} = 0.26(1)$ in the region $5 \cdot 10^{-2} > t > 5 \cdot 10^{-3}$ and a value $\beta_{3d} = 0.35(5)$ in the region $5 \cdot 10^{-3} > t > 5 \cdot 10^{-4}$.

Molecular Magnets

Table 4.1 also contains some examples of chemically more complex molecular and organic magnets. These are a relatively recent topic of interest and challenge the traditional solid-state physics notion that magnetic materials should necessarily be inorganic [159]. Their building blocks are not atoms but molecules, and as these may be rather complicated, the initiatives in this field have come from organic and coordination chemistry. Purely organic ferromagnets may be based on nitronyl nitroxide or sulphur based radicals, and it is also possible to prepare molecule based magnets in which transition metal ions are used to provide the magnetic moment, but organic groups mediate the interactions. The shape of molecules and their electronic structure play a pivotal role in the resulting crystallographic structure, and it follows that there is a rich variety of magnetic behaviours observable in molecular chains, layers and three-dimensional networks. Intermolecular forces are in general weaker than interatomic forces and are also rather short range. Consequently they differ markedly from the type of strong, long range Coulombic forces typical of ionic crystals. As a result molecular crystals are rather soft and their properties are tunable by applying pressure.

Tanol Suberate Despite their chemical complexity, molecular magnets may display strikingly clear-cut critical behaviour. One early example of an organic magnet is based on tanol suberate, which is a biradical with formula $(C_{13}H_{23}O_2NO)_2$ (Figure 4.10). The spin density is found to be located on the NO group and is almost equally shared between the oxygen and the nitrogen atoms. The molecules are arranged in sheet-like structures and neutron scattering studies confirm that the magnetic moments lie in the plane, aligning parallel to each other within the plane of the sheets and antiparallel within adjacent sheets [160]. The susceptibility has been shown to be well described by a two-dimensional ferromagnetic square lattice with weak interlayer coupling [161]. Elegant muon spin rotation (μSR) experiments [117] yield clear spin precession oscillations with the temperature dependence of the oscillation frequency fitting the power law $\nu_\mu(T) = \nu_\mu(0)(1 - T/T_c)^\beta$, with $\beta \simeq 0.22$, consistent with a 2dXY magnet.

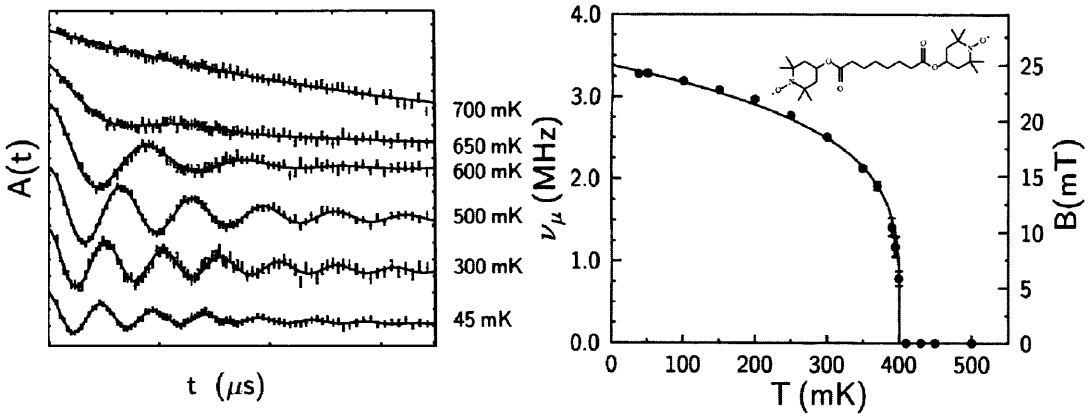

Figure 4.10: Left: Zero-field muon-spin rotation frequency in the organic antiferromagnet tanol suberate. Right: Temperature dependence of the zero-field muon-spin rotation in tanol suberate, found to obey the power law $\nu_\mu(T) = \nu_\mu(0)(1 - T/T_c)^{0.22}$. After Blundell *et al.* [117].

$Fe(NCS)_2(pyrazine)_2$ Powder neutron diffraction measurements have shown that $Fe(NCS)_2(pyrazine)_2$ displays three-dimensional long range magnetic ordering below $T_N = 6.8$ K [111]. Below T_N the sublattice magnetisation varies as $(T - T_N)^\beta$ with $\beta = 0.19$, which is claimed to be an indication of 2d Ising behaviour. The 2d behaviour is further substantiated by evidence indicating long range correlations within the planes, and no measurable correlations between them.

CSDAB and CSEN The porous materials CSDAB and CSEN (of chemical formula $Co_4(SO_4)(OH)_6(C_6N_2H_{12})_{0.5} \cdot H_2O$ and $Co_4(SO_4)(OH)_6(C_2N_2H_8)_{0.5} \cdot 3H_2O$, respectively) consist of two-dimensional hydroxy-sulfate arrays linked by ethylenediamine molecules via tetrahedral cobalt ions, and exhibit antiferromagnetic coupling at low temperatures [113]. In an applied field the compounds behave as metamagnets, with the magnetisation isotherms becoming characteristically S-shaped below T_N, as shown in Figure 4.11. The metamagnetic critical field, defined as the lowest field in which the onset of the S-shaped isotherm becomes observable, increases with decreasing temperature up until saturation, with CSDAB exhibiting a higher critical field for the metamagnetic transition. In both cases the isotherms allow the $h_c - T$ phase diagrams to be deduced. Fits to the power law $h_c(T) = h_c(0)((T_N - T)/T_N)^\beta$ gave the following parameters for CS-

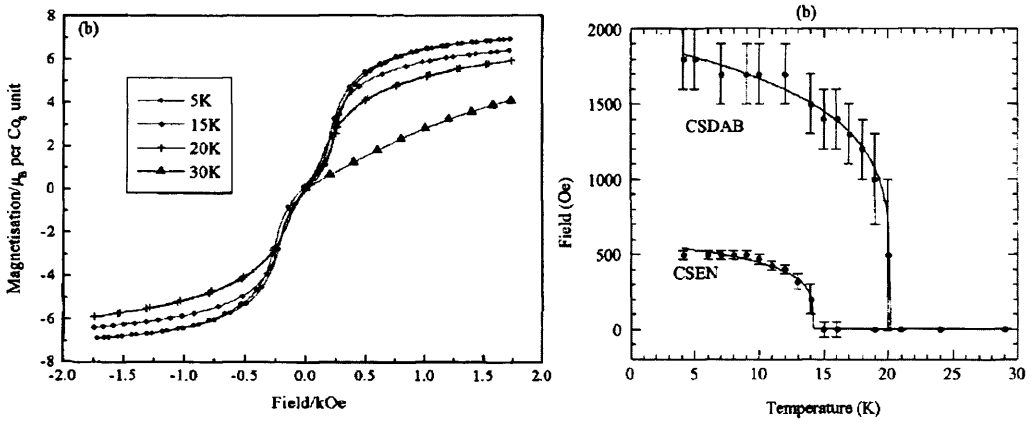

Figure 4.11: Left: Isothermal transitions for CSDAB collected at temperatures between 5 and 30 K showing increased curvature with decreasing temperature. Right: Critical field as a function of temperature for the metamagnetic transitions observed in CSDAB and CSEN. The fits to $h_c(T) = h_c(0)((T_N - T)/T_N)^\beta$ are shown as the solid lines, and the derived parameters are given in the text. After Rujiwatra *et al.* [113].

DAB, $h_c(0) = 1900(200)$ Oe, $T_N = 20.2(2)$ K and $\beta = 0.20(4)$; and for CSEN, $h_c(0) = 580(20)$ Oe, $T_N = 14.2(2)$ K and $\beta = 0.22(2)$. The critical exponents derived for the two materials are within experimental error of each other, and are consistent with their layered structure and coercive field measurements which suggest the moments possess a planar anisotropy. On the other hand, one cannot rule out tricritical behaviour, which is known to exist in some materials displaying metamagnetic-antiferromagnetic transitions, such as dysprosium aluminium garnet [162].

$Co_5(OH)_8(chdc) \cdot 4H_2O$ This cobalt based layered material has been found to order ferrimagnetically at $T_c = 60.5$ K [133]. Susceptibility data suggest an enhanced 2d correlation within the layers just above T_c, and magnetisation data on single crystals indicate a pronounced anisotropy. A measured critical exponent $\beta = 0.25(3)$ suggests 2dXY behaviour.

4.1.2 2dXY Layered Magnets

The sheer structural variety of 2dXY-like materials is noteworthy. As well as systems based on square layered K_2NiF_4-like lattices, there are also materials based on

honeycomb layered lattices, such as $BaNi_2(PO_4)_2$ and $MnPS_3$. More exotic systems are also present, most notably the highly frustrated antiferromagnets Li_2VOSiO_4 and Li_2VOGeO_4. Many so-called '2dXY' systems are actually better described by the 2d Heisenberg model with a very weak anisotropy. This is consistent with recent quantum Monte Carlo results which suggest that even in the presence of anisotropies as small as 10^{-3} times the coupling constant J, finite temperature transitions with clear Ising or KT critical behaviour persist, depending on the orientation of the anisotropy [151].

The variety of structures is such that one is entitled to wonder whether all quasi two-dimensional magnets which display $\beta \sim 0.23$ are necessarily only described by the 2dXY model. In fact there are two other theories which predict a similar exponent value. Thio and Aharony [145] have suggested that the transition to 3d Néel order in La_2CuO_4 is very close to a tricritical point, and it follows from their argument that β should be close to its mean field tricritical value of 0.25. In addition, Kawamura has put forward a theory for triangular antiferromagnets which also predicts $\beta \simeq 1/4$ [141, 142]. This theory, which has recently been reviewed in reference [163], is successful in accounting for the behaviour of a large number materials in which geometrical frustration plays a prominent role, such as $CsMnBr_3$ [164].

In light of these competing theories, it is desirable to have a set of criteria in order to conclusively establish the 2dXY nature of a particular system, helping one to discriminate between 2dXY and other types of magnets. BH 2dXY theory makes a number of predictions beyond that of the critical behaviour of the order parameter, which can be tested against experiment. These include:

1. An abrupt crossover from two-dimensional to three-dimensional behaviour very close to T_c, as shown in Figure 4.3 for $BaNi_2(PO_4)_2$. This is a result of the interplay between the intralayer (J) and interlayer (J') coupling, as explained previously. Whilst this phenomenon is not exclusive to planar magnets, it nonetheless adds credence to the fact that there is a 2dXY regime to cross over to.

2. The correlation length scales with temperature according to Equation (2.71). Furthermore, on finite systems the relation (2.80) holds, which provides a

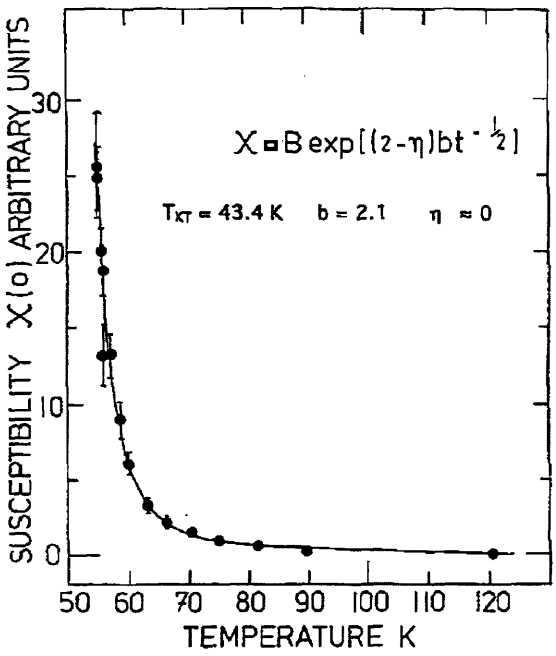

Figure 4.12: Temperature dependence of the susceptibility χ of Rb_2CrCl_4. After Als-Nielsen *et al.* [96].

means to verify that for a particular system the 2dXY description is consistent. In addition the measured magnetic susceptibility χ may also be compared with theory, by applying the scaling law $\chi \sim \xi^{2-\eta}$ (see Figure 4.12).

3. At low temperatures, the magnetisation as a function of applied magnetic field h scales according to the power law $m \propto h^{1/\delta}$, with δ decreasing slowly with increasing temperature. The temperature at which $\delta = 15$ locates an effective Kosterlitz-Thouless temperature T_{KT}. In practice it is not possible to create staggered magnetic fields in the laboratory, so this behaviour is only observable in ferromagnets such as Rb_2CrCl_4 [165] (see Figure 4.13) and K_2CuF_4 [144].

The only materials known to display the complete behavioural picture outlined above are Rb_2CrCl_4 [96] and K_2CuF_4 [115], and as a consequence they are considered to be canonical experimental realisations of the 2dXY model. However, on the basis of the above criteria, a number of other systems in Table 4.1 may be

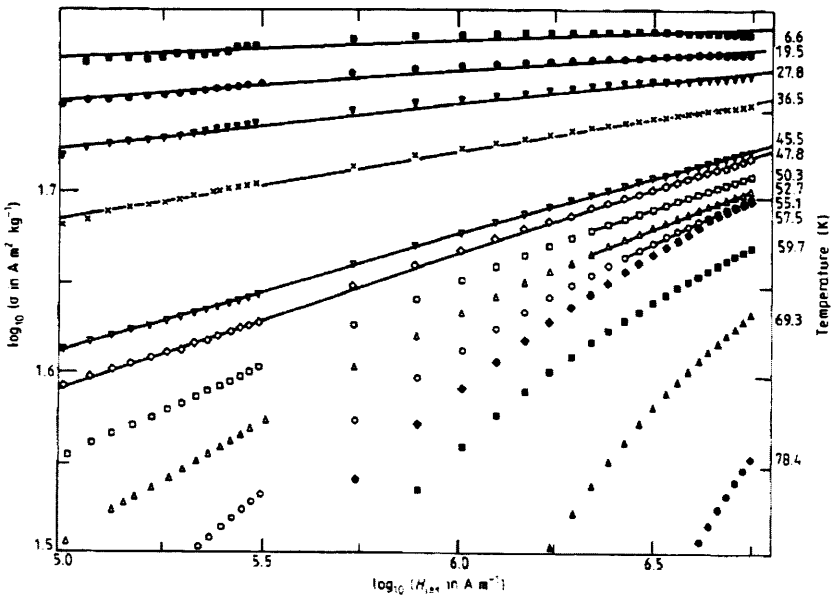

Figure 4.13: Magnetisation m as a function of field $h \parallel [110]$ at high fields and low temperatures. The temperature at which $\delta = 15$ locates T_{KT} and was found to be 45.5 K in this case. After Cornelius *et al.* [165].

classified with some confidence as belonging to the the 2dXY class. For example, $BaNi_2(PO_4)_2$ [94] fulfils all the criteria, except for the behaviour of $\delta(T)$, which cannot be measured in antiferromagnets. For other systems the evidence in favour of 2dXY-like behaviour is suggestive rather than compelling, and it is necessary to consider alternative explanations with attention.

Mean Field Tricritical Behaviour

It is straightforward to obtain from mean field theory the main features of tricritical behaviour[c]. These include the prediction that $\beta = 0.25$, which is of course rather close to the BH prediction of 0.23. Given that the upper critical dimension for a system near tricriticality is 3, it would appear unlikely that a mean field description should be relevant in systems strongly affected by two-dimensional fluctuations such as the ones discussed here. However, in order to account for observation in the Heisenberg antiferromagnet La_2CuO_4, a theory has been put forward which

[c]See for example Chapter 4 in Cardy's book [31].

treats the interlayer coupling using a mean field approach [145]. Whether or not this theory is applicable to other lanthanum cuprate analogues is unclear, since there is no reason to expect the tricritical points of any two systems to occur in similar thermodynamic conditions. In order to highlight this, consider the case of the alkali halides NX_4Cl and NX_4Br, where X is either H or D [166]. These are structurally and chemically very similar compounds, and are characterised by well attested tricritical points in their (P, T) phase diagrams. Nevertheless, the positions of the tricritical points are very different, with NH_4Cl having one at 1500 bar, and ND_4Cl having one an order of magnitude lower, at 150 bar. Changes in chemistry clearly have a profound influence on the positions of tricritical points, and one would expect this argument to hold for the lanthanum cuprate analogues.

Chiral Universality Class

In an attempt to explain observation in layered triangular antiferromagnets with continuous spin symmetry, Kawamura has advanced the possibility of their belonging to a new universality category of their own, termed the chiral universality class [141, 142]. The origin of the name lies in the fact that in XY systems of this sort, depicted in Figure 4.14, there are two distinct ground states which cannot be transformed into each other through any global spin rotation in the XY plane. Thus, the ground-state manifold of these frustrated magnets possesses a chirality, which may also be thought of as a hidden Ising symmetry, in addition to the continuous degeneracy associated with the XY spins. In the instance of Heisenberg spins, there is no longer a discrete chiral degeneracy as the two spin configurations depicted in Figure 4.14 may be transformed into each other via the third dimension. Nontheless, a chirality vector may still be defined and it would appear the $n = 3$ spin system shares much in common with its $n = 2$ counterpart.

The primary prediction by Kawamura, substantiated by Monte Carlo calculations, regards the critical behaviour of these systems. For the XY antiferromagnet, the critical exponents are $\alpha = 0.34(6)$, $\beta = 0.253(1)$, $\gamma = 1.13(5)$ and $\nu = 0.54(2)$, whereas for its Heisenberg counterpart $\alpha = 0.24(8)$, $\beta = 0.30(2)$, $\gamma = 1.17(7)$ and $\nu = 0.59(20)$ [167]. Whilst these values would appear to satisfy the hyperscaling relations, it is also worth noting their similarity with the mean field tricritical values

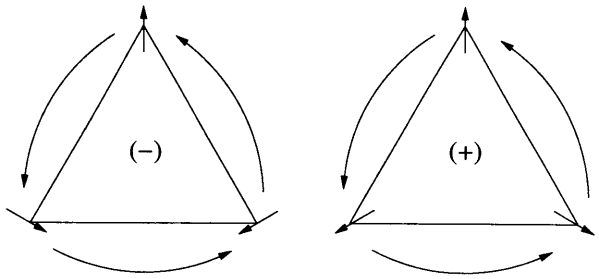

Figure 4.14: Chirality associated with XY spins antiferromagnetically coupled on a triangular lattice. The ground state of such a system can be seen to be two-fold degenerate.

$\alpha = 0.5$, $\beta = 0.25$, $\gamma = 1$ and $\nu = 0.5$. Indeed, the chiral universality class has been put into question by authors favouring a mean field tricritical interpretation [168]. Nonetheless it is undoubtedly true that certain experimental triangular antiferromagnets are well described by Kawamura's theory, most notably $CsMnBr_3$ [164] and $CsBiCl_3$ [169].

Despite their almost coincident predictions for the critical index β, it seems clear that distingushing between Kawamura and 2dXY systems is a relatively straightforward task. Whereas Kawamura's theory considers three-dimensional systems in which $J = J'$, 2dXY systems invariably possess a pronounced two-dimensional character, with J' being orders of magnitude smaller than J. Furthermore, as will be discussed in Chapter 5, the measured values of γ and ν in 2dXY systems are very different from those typical of chiral systems. It is interesting to note that there is evidence suggesting that a slightly modified KT behaviour occurs 2d triangular antiferromagnetic systems [170]. Further investigation on this front would be desirable, particularly in order to resolve doubts which persist in the classification of compounds with hexagonal lattices such as $ErCl_3$ [125].

4.1.3 Ultrathin Film Magnets

The preparation and characterisation of thin film magnets down to a monolayer precision has been a comparatively recent breakthrough, largely due to technological advances in both their methods of preparation and the high precision optical tools employed to characterise them. Consequently one can focus on their intrinsic properties and consider them as experimental realisations of truly two-dimensional

magnets. Ultrathin magnets are now routinely grown by Molecular Beam Epitaxy (MBE) and sputtering techniques, whereas the most common tool employed to probe their magnetic properties relies on the Magneto-Optic Kerr Effect (MOKE). Although it is not the aim to present such techniques here[d], one should stress their exquisite sensitivity: one can routinely gain magnetic information on ultrathin films by applying magnetic fields of the order of a few microtesla.

The thin film community had also noticed that the critical behaviour of magnetic thin films falls into two classes, depending on the orientation of the anisotropy present. The surface anisotropy usually consists of two terms, one perpendicular and the other parallel to the plane of the film. If the surface has a more than a two-fold rotational axis the in-plane term vanishes. The next higher order term in the magnetic anisotropy, usually identified with the volume anisotropy, is quadratic in the Cartesian components of the spin vector. Consequently Qiu and Bader [87] have classified magnetic thin films with cubic symmetry according to the presence or not of a uniaxial anisotropy, be it perpendicular or parallel to the film plane.

The first scenario is associated with the two-dimensional Heisenberg model with a uniaxial anisotropy term, which behaves like the Ising model [85]. The other case can be described by a 2dXY model with a four-fold field contribution. José, Kadanoff, Kirkpatrick and Nelson (JKKN) [68] have predicted that a quadratic anisotropy gives rise to a unique sort of second order phase transition, characterised by non-universal exponents which vary with the anisotropy strength. In practice, the finite nature of experimental systems ensures an unexpected robustness to the presence of such a perturbation, such that $\beta \simeq 0.23$ 2dXY behaviour persists. This subtlety is observed in computer simulations [173–175], and is studied in depth in Chapter 5.

Table 4.2 summarises the values of β and T_c for all known systems of thickness $d_{\min}$ where both quantities have been measured. Wherever given, the measured anisotropy and easy axis is also quoted. Like layered magnets, ultrathin film magnets fall into one of two groupings: those with β close to the Ising value of 1/8, and those with β close to the XY value of 0.23. Ising systems with an anisotropy perpendicular to the plane of the film display slightly lower exponents than those

[d]See the articles by Elmers [171] and Gradmann [172] for introductory reviews on the experimental techniques employed to synthesise and characterise ultrathin magnets.

with in-plane anisotropy. The similarity of behaviour between ultrathin films and layered magnets is hardly surprising: as BH theory [86] only requires that the *effective* system size L_{eff} be finite, it is irrelevant whether finite size effects arise directly or through other perturbations.

Table 4.2: Summary of transition temperatures T_c and magnetisation critical exponents β for epitaxial magnetic films grown on a range of substrates. The thickness d_{min} denotes the thickness at which these quantities were measured and t range indicates the range of reduced temperature over which β was measured. The magnetic anisotropy is indicated by the direction of the easy axis, and can either be perpendicular ($\perp$) or parallel ($\parallel$) to the film plane.

System	Structure	d_{min} (ML)	β	t range	T_c (K)	Anisotropy	Method*	Reference
Fe on								
Pd(100)	bct, 1 × 1	2.0	0.125(10)	$t < 3 \cdot 10^{-2}$	613.1	$\perp$	ECS	[176]
		1.2	0.127(4)	$1 \cdot 10^{-1}$–$3 \cdot 10^{-3}$	< 100	$\perp$	MOKE	[177]
Ag(100)	bcc, 1 × 1	2.5-2.7†	0.124(2)	$1 \cdot 10^{-1}$–$1 \cdot 10^{-3}$	324	$\perp$	MOKE	[87,178]
W(110)	bcc, 1 × 1	0.8	0.124(1)	$1 \cdot 10^{-1}$–$4 \cdot 10^{-3}$	221.1(1)	$\parallel$ [1$\bar{1}$0]	SPLEED	[179,180]
		1.0	0.134(3)	$1 \cdot 10^{-1}$–$5 \cdot 10^{-2}$	224	$\parallel$ [1$\bar{1}$0]	SPLEED	[181]
		1.7	0.13(2)	–	317	$\parallel$ [1$\bar{1}$0]	MOKE	[182]
Ag(111)	bcc, 1 × 1	1.8	0.139(6)	$1 \cdot 10^{-1}$–$1 \cdot 10^{-3}$	∼ 450	$\parallel$	MOKE	[183]
		2.0	0.130(3)	$1 \cdot 10^{-1}$–$1 \cdot 10^{-3}$	∼ 450	$\parallel$	MOKE	[183]
Cu(100)	fct, 4 × 1	∼ 2.5†	0.17(3)	$1 \cdot 10^{-1}$–$1 \cdot 10^{-2}$	370	$\perp$‡	MOKE	[184–186]
W(110)§	bcc, 1 × 1	0.82	0.18(1)	$3 \cdot 10^{-1}$–$1 \cdot 10^{-2}$	282(3)	$\parallel$ [1$\bar{1}$0]	TOM, CEMS	[187–189]
$Cu_{84}Al_{16}$(100)	fcc, 1 × 1	4.0	0.212(5)	$3 \cdot 10^{-1}$–$1 \cdot 10^{-2}$	288(2)	$\parallel$	LMDAD	[190]
W(100)	bcc, 1 × 1	1.6	0.217(2)	$1 \cdot 10^{-1}$–$1 \cdot 10^{-2}$	207.8(1)	$\parallel$ [001]	CEMS, SPLEED	[191,192]
Au(100)	bcc, 1 × 1	1.0	0.22(1)	$1 \cdot 10^{-1}$–$1 \cdot 10^{-3}$	300	$\parallel$ [001]	SPLEED	[193]
		2.0	0.25(1)	$2 \cdot 10^{-1}$–$1 \cdot 10^{-4}$	290	$\parallel$ [001]	ECS	[194]
W(100)§	bcc, 1 × 1	1.5	0.22(2)	–	282(1)	$\parallel$ [001]	CEMS	[171]
V(001)	bcc	3	0.23(1)	$2 \cdot 10^{-1}$–$2 \cdot 10^{-2}$	∼ 190	$\parallel$	MOKE	[195]
Pd¶	–	0.2-0.4†	0.23(1)	$2 \cdot 10^{-1}$–$2 \cdot 10^{-2}$	> 50	$\parallel$	MOKE	[196]
GaAs(100)	bcc, 2 × 6	3.4	0.26(2)	$1 \cdot 10^{-1}$–$1 \cdot 10^{-3}$	254.8(2)	$\parallel$	MOKE	[197]

Continued on next page

Table 4.2 – continued from previous page

System	Structure	$d_{\min}$ (ML)	β	t range	T_c (K)	Anisotropy	Method*	Reference
Co on								
Cu(111)	fcc, 1 × 1	1.0	0.125	–	433	⊥	TOM	[198]
		1.5	0.15(8)	–	460	⊥	MOKE	[199]
Cu(100)	fcc	2.0	0.24	–	∼ 240	∥	MOKE	[200, 201]
Ni on								
W(110)	fcc, 7 × 1	2.0	0.13(6)	$1 \cdot 10^{-1}$–$1 \cdot 10^{-3}$	325	∥ [001]	FMR	[202]
Cu(111)	fcc, 1 × 1	2.0-3.0†	0.24(7)	$3 \cdot 10^{-1}$–$6 \cdot 10^{-3}$	380	∥	MOKE	[203]
Cu(100)	fcc, 1 × 1	4.1	0.23(5)	$3 \cdot 10^{-1}$–$1 \cdot 10^{-2}$	284	∥	MOKE	[199, 204]
V on								
Ag(100)	bcc, 1 × 1	5.0	0.128(10)	$3 \cdot 10^{-1}$–$2 \cdot 10^{-4}$	475.1	∥ [001]	ECS	[205]
Gd on								
Y(0001)	hcp	1.0	0.23(5)	$1 \cdot 10^{-1}$–$8 \cdot 10^{-3}$	156	∥	MOKE	[206]
Mn_5Ge_3 on								
Ge(111)		1.0	0.244	$2 \cdot 10^{-1}$–$4 \cdot 10^{-3}$	296	∥	SQUID	[207]
CoAl(100)	bcc, 1 × 1		0.22(2)	$2 \cdot 10^{-1}$–$7 \cdot 10^{-3}$	∼ 90	∥	MOKE	[208]

*Experimental properties were measured by the following techniques: Electron Capture Spectroscopy (ECS), Magneto Optical Kerr Effect (MOKE), Spin Polarised Low Energy Electron Diffraction (SPLEED), Torsion Oscillation Magnetometry (TOM), Convertion Electron Mössbauer Spectroscopy (CEMS), Linear Magnetic Dichroism in the Angular Distribution of photoelectron intensity (LMDAD) and Superconducting QUantum Interference Device (SQUID).

†Exponent determined by averaging over values of a range of films of different thickness.

‡Reversible spin reorientation transition from ∥ to ⊥ with increasing T.

§Coated with Ag.

¶Pd layers δ-doped with Fe.

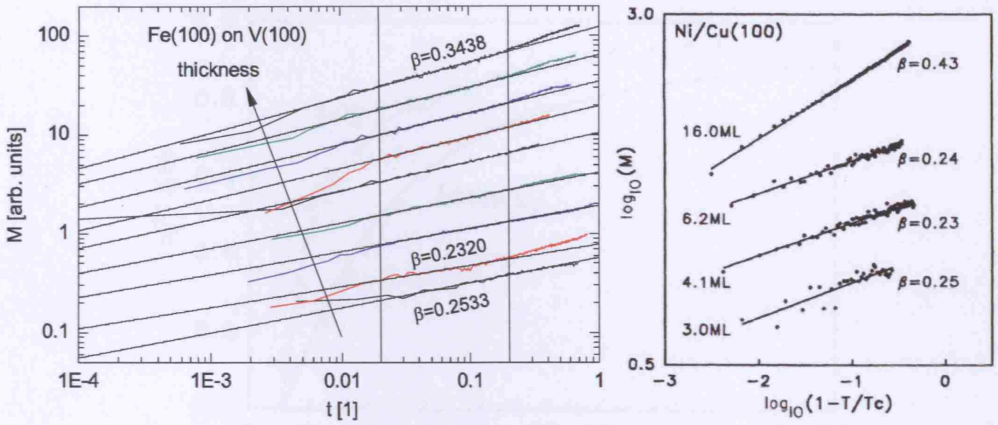

Figure 4.15: Left: Experimentally determined values of β for Fe(100) on V(100) [211]. With increasing thickness the value of β deviates from the 2dXY value towards the 3d Heisenberg value. The critical exponents were measured within the area delimited by the two black vertical lines. Right: Similar data measured by Huang *et al.* [199] for the Ni/Cu(100) system.

Although the error in the determination of the exponent β may be large in some cases, once the film thickness is larger than a certain (system dependent) threshold value, a sudden transition of the exponent is observed in experiment. This crossover from two-dimensional to three-dimensional behaviour is observable in all the systems listed in Table 4.2. Figure 4.15 displays an example of this phenomenon for the case of iron deposited on vanadium. Another system in which such a switch is observed at a thickness of about six and seven monolayers is Ni/Cu(100) [199]. A theoretical estimate of this crossover has been derived from an argument involving the excitation spectrum of spin waves [209, 210]. When confined to a thin film, spin waves are quantised in a manner analogous to electron energy bands. The energy spacing between these quantised states increases as the thickness of the film decreases. When it exceeds k_BT, only the lowest state is thermally accessible and the system becomes two-dimensional.

The transition temperature T_c is also characteristic of the dimensionality in ultrathin magnets as it reduces with decreasing film thickness. This reflects the cooperative nature of ferromagnetism, where the absence of layers on the vacuum side is felt by the deeper layers. Typically, T_c is reduced to half its bulk value at a film thickness of about five monolayers. Furthermore, Huang *et al.* [199, 204] have

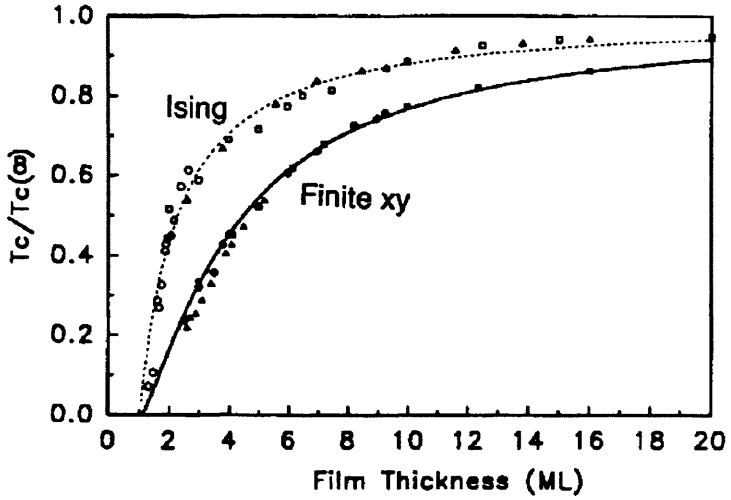

Figure 4.16: Decrease in T_c with the number of layers in a film caused by the decreasing number of neighbours. The symbols are associated with the following systems: □, Ni(111)/W(110); ○, Fe(110)/Ag(111); △, Ni(111)/Re(0001); ■, Ni/Cu(100); •, Ni_9Co_1/Cu(100); ▲, Ni_3Co_1/Cu(100). After renormalisation of T_c to the bulk value $T_c(\infty)$, the Ising and XY classes of materials can be distinguished. After Huang *et al.* [199], and references therein.

observed that Ising films have a significantly higher T_c than in-plane magnetised 2dXY films, and it is possible to distinguish between the two classes by following the values of T_c as a function of film thickness, as shown in Figure 4.16. This difference presumably arises due to the strong anisotropy present in Ising-like magnets, which keeps the ordered phase 'locked in' up to higher temperatures. An intriguing result is that all of the data extrapolate to $T_c = 0$ in the monolayer limit.

Temperature Dependence of Magnetic Order in Selected Systems

As there are a number of reviews on ultrathin magnets [171,172,212], the focus here is only on a limited number of case studies which highlight the range of scenarios in which ultrathin films display magnetic behaviour. For detailed information on other systems, the reader is invited to follow up the references cited in Table 4.2.

Fe(100) on Au(100) Magnetic order was first detected in the Fe(100) on Au(100) system by Bader and Moog using MOKE [213], although the temperature dependence of the magnetic order in the monolayer regime was first investigated by

Dürr *et al.* using SPLEED and spin-polarised secondary electron emission techniques [193]. They observed rounded phase transitions, which they fitted by a power law with exponent $\beta = 0.22(5)$ for a range of film thicknesses between 1 and 3 monolayers. For each individual film, the Curie temperature was determined as a fitting parameter which was chosen to maximise the linear range in the logarithmic plot of the order parameter as a function of temperature, and the exponents were determined with a high accuracy. At the time of publication, these results were difficult to interpret theoretically. They undoubtedly provided evidence of a two-dimensional phase transition, yet there were significant deviations from the 2d Ising picture. These observations are conclusively explained within the framework of the 2dXY model on a finite lattice. Another study by Rau and Xing yielded a power law with $\beta = 0.25(1)$ [194], which is in reasonable agreement with the work of Dürr *et al* [193].

V(100) on Ag(100) Vanadium deposited on silver is a remarkable example of unexpected behaviour in two-dimensional magnetic systems. Rau *et al.* investigated this system by use of Electronic Capture Spectroscopy (ECS) [205], and found that vanadium, a non-magnetic metal in the bulk, becomes ferromagnetic as a thin film up to 7 monolayers thick. The temperature dependence of magnetic order was shown to fit remarkably well to the exact solution of the 2d Ising model, with an exponent $\beta = 0.128(10)$. The explanation most generally invoked for the ferromagnetic behaviour of elements which are non-magnetic in the bulk is based on the argument that the reduced coordination number and epitaxial stress of thin films result in a reduced bandwidth. This implies an increased density of states near the Fermi level, and consequently results in enhanced magnetic moments [214].

Fe(100) on W(100) Iron forms a thermodynamically stable ferromagnetic monolayer on tungsten. As a consequence Fe monolayers on W can be prepared to an unusually high degree of perfection, and their magnetic properties have been extensively studied [171]. Of particular interest in the context of the 2dXY model is the work on the in-plane magnetised double-layer Fe on W(100) reported by Elmers and co-workers [191]. Using diffraction of spin polarised electrons and conversion electron Mössbauer spectroscopy, the authors investigated the temperature depen-

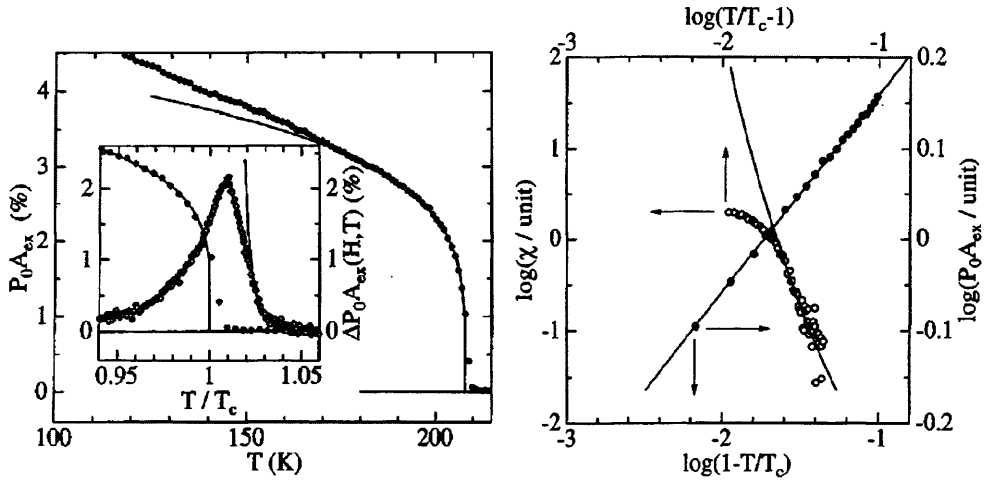

Figure 4.17: Magnetisation M (•) and susceptibility χ (○) data of Fe(100) on W(100), after Elmers *et al.* [191]. The left hand figure plots the remanent magnetisation as a function of temperature, with the susceptibility as a function of temperature in the inset. The right hand figure plots the same experimental data as a function of reduced temperature in a logarithmic scale.

dence of the spontaneous magnetisation and the susceptibility. Averaging over all their measurements, they found that the magnetisation follows a power law with an exponent $\beta = 0.22 \pm 0.03$ in the temperature regime $0.3 < T/T_c < 0.99$, consistent with the presence of planar anisotropy. More impressively, the 2dXY explanation was substantiated further by fitting the susceptibility χ to the exponential law $\chi \propto \exp(b/\sqrt{T - T_c})$ (*c.f.* Equation (2.71)) predicted by theory, with $b = 1.6$. These results are summarised in Figure 4.17, and provide compelling evidence that this system belongs to the 2dXY class. Indeed, it is arguable that the Fe/W(100) system represents the most convincing example of an ultrathin XY magnet currently known.

Pd Layers δ-doped with Fe Recently, Pärnaste *et al.* have studied palladium δ-doped with iron by introducing Fe atoms within a single monolayer sandwiched between Pd atoms [196]. As Pd possesses a high magnetic susceptibility and long range polarisability, Fe can induce in it a large magnetic moment. For example, a single Fe impurity in bulk Pd polarises a sphere with a radius of about 10 Å, resulting in a total magnetic moment of 9-12 μ_B per Fe atom. Thus, the effective thickness of the ferromagnetic layer can be tuned simply by controlling the con-

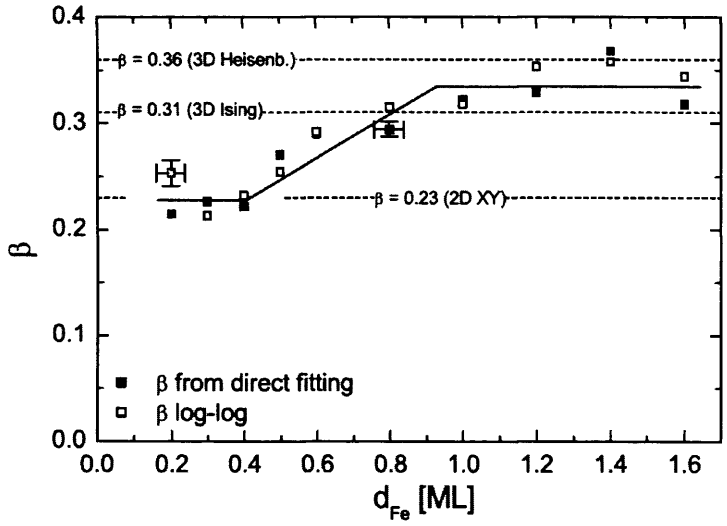

Figure 4.18: Exponent β as a function of d_{Fe} for all Pd layers δ-doped with Fe studied by Pärnaste *et al.* [196]. A dimensionality crossover clearly occurs at $0.4 < d_{\mathrm{Fe}} < 1.0$.

centration of Fe. The idea behind this experiment is to bypass any problems with structural imperfections and defects by ensuring that the range of the induced magnetisation is much larger than the length scale of the atomic imperfections, thus achieving perfect layered magnetisation.

The samples studied consisted of a single Fe layer with nominal thickness $0.2 \leq d_{\mathrm{Fe}} \leq 1.6$ monolayers sandwiched between two 20 ML Pd layers. It is found that a dimensionality crossover from two-dimensional XY to three-dimensional behaviour occurs as d_{Fe} is increased from 0.4 to 1.0 ML, shown in Figure 4.18. This can be qualitatively understood in terms of the spin wave quantum well model mentioned above [209, 210]. Whilst the authors acknowledge that a more quantitative description is desirable, their work clearly demonstrates the existence of a dimensionality crossover in the induced magnetisation.

4.1.4 Other Two-Dimensional Magnetic Systems

There are other experimental realisations of two-dimensional magnetic structures which have so far received less attention than layered and ultrathin film magnets. These include magnetic films grown using the Langmuir-Blodgett (LB) tech-

nique [215] and two-dimensional nuclear magnets [216].

Magnetic LB films consist of magnetic ions (*e.g.* Mn^{2+}, Fe^{2+} and Co^{2+}) attached to lipid monolayers deposited on water. Although the two-dimensional nature of these materials was immediately recognised, there has recently been a renewed interest in their magnetic properties. Studies on gadolinium stereate LB films [217,218], although finding no evidence for spontaneous magnetisation, reveal interesting magnetic behaviour as a function of temperature and applied field: the net magnetisation is found to increase exponentially with decreasing temperature, at constant field. A complete understanding of this behaviour is still forthcoming and further investigations of these remarkably stable structures[e] is desirable.

Two-dimensional nuclear magnets obtained by the physisorption of ^3He atoms on solid substrates are reviewed by Godfrin and Rapp [216]. They also represent exceptionally good experimental realisations of Heisenberg Hamiltonians. It is simply remarked here that ferromagnetic order has been observed in a variety of conditions in applied fields [219], and that a recent study has found evidence for a finite temperature ferromagnetic transition as $H \rightarrow 0$ [220].

4.1.5 Further Remarks

Figure 4.19 represents in the form of histograms the data listed in Tables 4.1 and 4.2. The distribution of exponent values in the bottom histogram is noticeably far from random, and confirms the view that there are two distinct groups of values associated with the 2d Ising and the 2dXY models [86,87]. Any deviations from either one of these two values of β can be explained by the onset of three-dimensional character, the presence of non-universal corrections, or, as discussed in the next chapter, by a crossover induced by the presence of symmetry breaking crystal fields. In principle there are two further two-dimensional universality classes, the three- and four-state Potts models [43], with $\beta = 1/9$ and $1/12$, respectively. However, as there appear to be no known magnetic systems in which $\beta < 0.12$, one can conclude from the literature that there are no magnetic systems which map onto these two models.

[e]Under ordinary storage conditions, LB films are said to show no noticeable deterioration over periods of years [215].

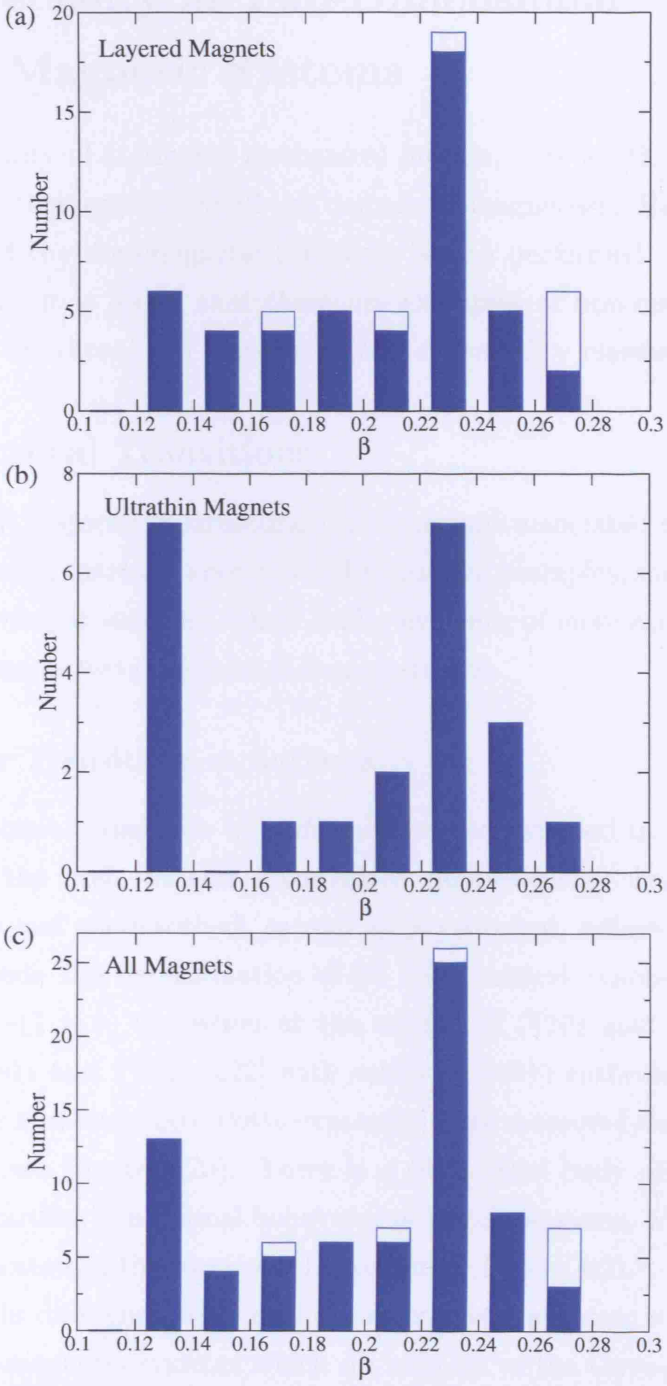

Figure 4.19: Histograms of the data in Tables 4.1 and 4.2. The white bars stacked on top of the blue ones represent compounds studied by powder neutron diffraction, resulting in the exponents being determined with a large degree of uncertainty.

4.2 Universality in Two-Dimensional Non-Magnetic Systems

Given the generality of statistical mechanical models, it is worth considering situations in which they apply beyond the domain of magnetism. Hence, a comprehensive review of the non-magnetic literature is also performed. As opposed to magnetic systems, it is found that there *are* examples of non-magnetic systems which belong to the three- and four-state Potts universality classes.

4.2.1 Structural Transitions

Although the vast majority of structural transitions are associated with bulk three-dimensional systems, there are known two-dimensional examples, such order-disorder transitions occurring at surfaces. There is also evidence of more exotic spin-Peierls transitions displaying two-dimensional characteristics.

Order-Disorder Transitions at Surfaces

Order-disorder phase transitions at surfaces have been studied in detail since the 1980s. Among the first systems investigated quantitatively were clean reconstructed surfaces and chemisorbed, as well as physisorbed, adlayers. Noteworthy experiments include the determination of 2d Ising critical exponents for the reversible $(1 \times 2) \leftrightarrow (1 \times 1)$ transition at the surface of (110) gold [221][f], and the work of Sokolowski and Pfnür [222] with sulfur on (001) ruthenium surfaces, in which three-state and four-state Potts exponents were measured depending on the conditions [222] (see Figure 4.20). There is a substantial body of information in the literature regarding the critical behaviour of similar systems, which is listed in Table 4.3, and plotted in the form of a histogram in Figure 4.21.

One noticeable difference with respect to magnetic systems is that there are examples of non-magnetic systems which do map on to the three-state and four-state Potts models. Heuristically, one can imagine that in the simplest cases, structural order-disorder phase transitions of commensurate chemisorbed adlayers

[f]See Appendix B for a summary of the conventions adopted to describe the structures of ordered surfaces.

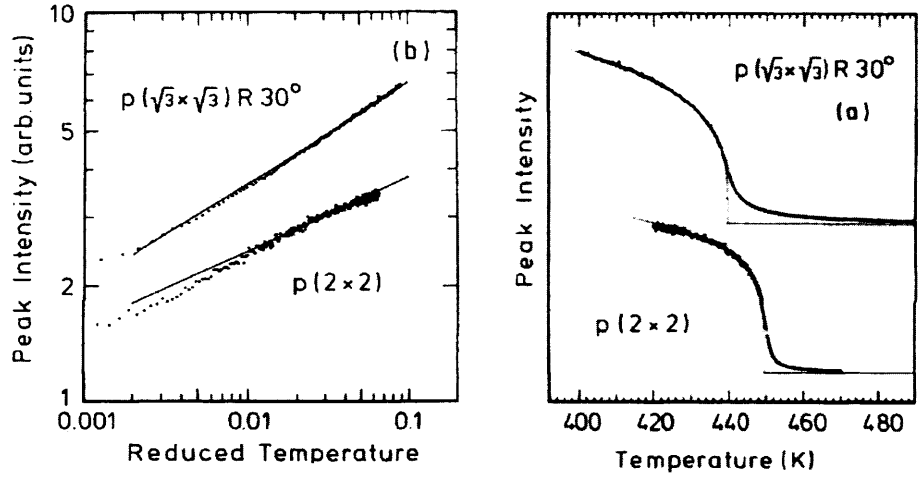

Figure 4.20: Critical behaviour in the order-disorder phase transition of the $p(2\times2)$ and $(\sqrt{3}\times\sqrt{3})R30°$ sulfur structures chemisorbed on ruthenium. The former belongs to the four-state Potts universality class, and the latter to the three-state Potts class. After Sokolowski and Pfnür [222].

may be well described by lattice-gas models, and it is therefore plausible that more complicated surfaces may lead to the Potts models being more realistic. This view is indeed substantiated by numerical work [223].

There are also examples of experimental systems which display the critical behaviour of the 2dXY model. In their pioneering work on the on the W(011)$p(1\times1)$-H system, Lyuksyutov and Fedorus [224] observed that depending on the coverage of hydrogen on a tungsten surface, different critical exponents are measured: $\beta = 0.13(4)$ for the $p(2\times1)$ structure and $\beta = 0.25(7)$ for the $p(2\times2)$ structure. Despite the large errors, these results remain an impressive example of a switch from 2d Ising behaviour to what is now known to be 2dXY behaviour. Systems belonging to the 2dXY class with strong four-fold anisotropy fields are also known, the transition in the (2×2) lattice of oxygen on a (110) molybdenum surface [228] being an example . The measured values of β in these cases is closer to 0.19 than 0.23, which suggests the presence of a strong four-fold anisotropy capable of pushing the system away from the 2dXY universality class and towards the non-universal exponents predicted by JKKN [68]. A complete discussion on this issue is a central part of this work, and is deferred to Chapter 5.

Remarkably, two-dimensional order-disorder transitions may also be manifested

Table 4.3: Selection of experimental systems displaying two-dimensional order-disorder phase transitions. The systems are classified according to the findings of the authors who studied them. See Appendix B for a summary of the conventions adopted to describe the structures of ordered surfaces.

System	β	Model Ascribed	Method	Reference
W(011)$p(2 \times 1)$-H	0.13(4)	2d Ising*	LEED†	[224]
W(011)$p(2 \times 2)$-H	0.25(7)	2dXY*	LEED	[224]
$p(1 \times 2) \leftrightarrow (1 \times 1)$-Au(110)	0.13(2)	2d Ising	LEED	[221]
W(112)$p(2 \times 1)$-O	0.13(1)	2d Ising	LEED	[225]
$p(2 \times 2)$-O disordering on Ru(001)	0.13(2)	3-state Potts	LEED	[226]
$p(2 \times 1)$-O disordering on Ru(001)	0.085(15)	4-state Potts	LEED	[227]
$p(2 \times 2)$-O disordering on Mo(110)	0.19(2)	2dXY	LEED	[228]
$p(2 \times 1)$-O disordering on W(110)	0.19(5)	2dXY	LEED	[229]
Ru(001)$p(2 \times 2)$-S	0.11(2)	4-state Potts	LEED	[222]
Ru(001)$(\sqrt{3} \times \sqrt{3})R30°$-S	0.14(3)	3-state Potts	LEED	[222]
(3×3)-Sn disordering on Ge(111)	0.11(1)	3-state Potts	HAS‡, XRD§	[230]
$\begin{pmatrix} 2 & 1 \\ 0 & 6 \end{pmatrix} \leftrightarrow \begin{pmatrix} 2 & 1 \\ 0 & 3 \end{pmatrix}$-Pb on Ge(001)	–	2d Ising	HAS, XRD	[231]
$\begin{pmatrix} 2 & 1 \\ 0 & 6 \end{pmatrix} \leftrightarrow (2 \times 1)$-Pb on Ge(001)	–	3-state Potts	HAS, XRD	[231]

* Model not ascribed by original authors.
† LEED: Low Energy Electron Diffraction.
‡ HAS: Helium diffraction.
§ XRD: X-ray diffraction.

in bulk systems. For example, the phase transition of both calcite ($CaCO_3$) and nitratine ($NaNO_3$), which had long been thought to be anomalous, have been suggested by Harris to be consistent with the two-dimensional XY model [232]. In these systems, the orientational order-disorder is driven by continuous planar rotations of the carbonate and nitrate groups, and the nature of the interaction is strongly two-dimensional.

Charge Ordering Transitions

In recent years there has been an increased interest in materials displaying the spin-Peierls (SP) transition, which corresponds to the dimerisation of a one-dimensional antiferromagnetic $S = 1/2$ chain coupled to a three-dimensional elastic medium. It is the magnetic analogue of the Peierls transition, the metal-insulator transition

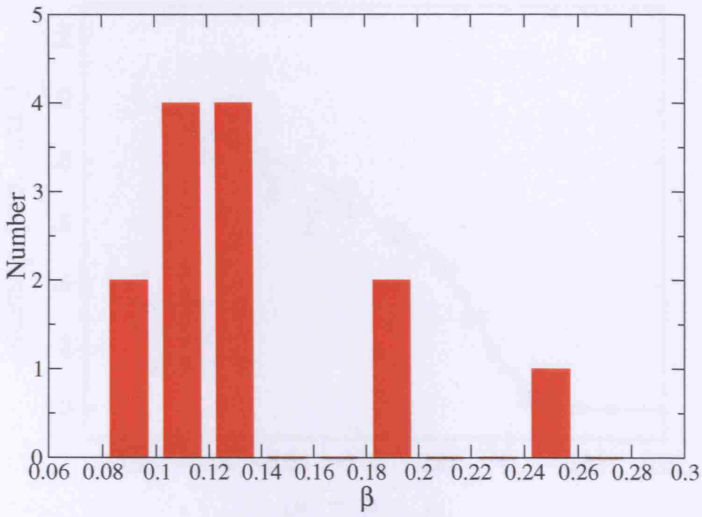

Figure 4.21: Histogram of β values for the systems reported in Table 4.3.

which occurs in quasi one-dimensional solids, and in some sense may be thought of as a three-dimensional structural transition driven by one-dimensional magnetic fluctuations. Intriguingly, it has been suggested that the critical behaviour of the order parameter of the first inorganic SP material $CuGeO_3$ is characterised by a 2dXY to 3dXY crossover as T_{SP} is approached, with the 2d region characterised by an exponent $\beta = 0.21(2)$ [233][g]. Another system believed to undergo an SP transition, α'-NaV_2O_5, has also been shown to be strongly affected by two-dimensional fluctuations [235], and has been measured to have an order parameter exponent $\beta = 0.17(3)$.

4.2.2 Melting at Surfaces

In the context of two-dimensional melting, Halperin, Nelson [236] and Young [237] have extended the 2dXY theory of Kosterlitz and Thouless [61] and put forward a mechanism in which melting occurs in two successive transitions, each driven by the unbinding of pairs of topological defects. The first transition corresponds to the loss of translational periodicity on passing from the solid to an orientationally

[g]However it should be noted that other interpretations for this material's critical behaviour have also been put forward. For example, Birgeneau *et al.* [234] have suggested $CuGeO_3$ undergoes a tricritical to mean field crossover.

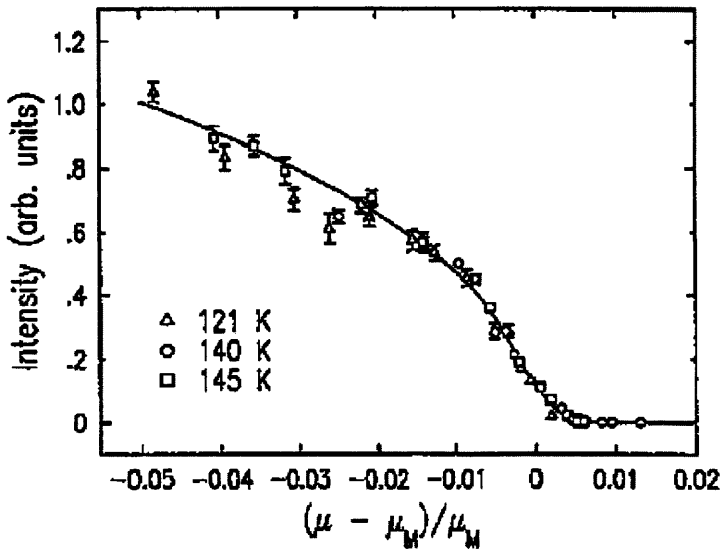

Figure 4.22: Effective order parameter for a finite sized 2d solid against the reduced chemical potential $(\mu - \mu_M)/\mu_M$ for xenon physisorbed on graphite. The solid line is characterised by a power law with $\beta = 0.23$, characteristic of the finite-sized 2dXY model. After Nuttall *et al.* [238].

aligned liquid similar to the hexatic phase observed in free-standing liquid crystal films. The second corresponds to the loss of orientational order on passing from the aligned liquid into the isotropic liquid state. Each of these transitions proceed in a continuous manner, quite unlike one's everyday experience of the melting transition in bulk systems.

Xenon physisorbed on graphite provides a good example of an experimental system which undergoes this kind of melting, with the transition driven by varying the chemical potential, μ_A. This conclusion was reached by Nuttall *et al.* [238] in a study concentrating only on a part of the two-stage melting process of near-monolayer xenon on a single layer of graphite, that of the loss of translational order. The authors analysed their data in terms of an effective order parameter for a finite sized 2d solid, and found that at temperatures of 121 K, 140 K and 145 K there was a satisfying degree of consistency between their measurements and the value of β consistent with the finite sized 2dXY model. In particular, at 140 K the fit is observed to be remarkably good with an observed value $\beta = 0.23(4)$ [239], as shown in Figure 4.22.

It has been argued [240] that thin free-standing liquid crystal films which have

an XY order parameter should also behave proportional to the power law $(T_c - T)^{0.23}$ in an intermediate range below the relevant transition temperature T_c. Examples of order parameters analogous to the XY magnetisation are the in-plane projection of the director in the smetic-C liquid crystals and the hexatic order parameter in hexatic smetic liquid crystals. In principle, these quantities are measurable in experiment, and given the similarities with topological melting one might expect to observe finite sized 2dXY behaviour in thin liquid crystals. To date, there have been no such experimental reports.

4.2.3 Quantum Systems

KT theory provides a successful description of superfluid ^{4}He films, in which the order parameter is the condensate wave function $\Psi(\mathbf{r})$, a complex scalar quantity. Nelson and Kosterlitz [69] have predicted a discontinuous jump in the superfluid density[h] $\rho_s(T)$ of such films at a temperature T_{KT}, which occurs as the vortex-antivortex pairs dissociate into free vortices. The observation of the universal jump in experimental superfluid helium films [75, 76] was therefore seen as conclusive evidence in favour of the validity of the 2dXY theory. In fact, finite size effects are strongly prominent in these systems [241], such that the jump in $\rho_s(T)$ is rounded. However, since the condensate wave function is not a property accessible experimentally, the effective critical behaviour of the 2dXY model is not observable in practice.

Similarly, the order parameter is also not experimentally accessible in two-dimensional superconductors. There is an enormous literature concerning these systems [242]. One particularly original example of a superconducting XY model has been created and studied by Resnick *et al.* [243]. Photolithography was used to create an extremely regular array of Josephson junctions, consisting of over a million tiny lead disks, embedded in a tin matrix. The disks were 1.4 μm apart, and each was 150 nm thick and 13 μm in diameter. Below the bulk superconducting transition of the lead, but above that of the tin, the condensate phases within each lead disk are coupled just as in the 2dXY model. Although the vortex driven transition has been shown to undergo a universal jump rounded by finite size effects,

[h]The superfluid density is exactly analogous to the spin wave stiffness in magnetic systems.

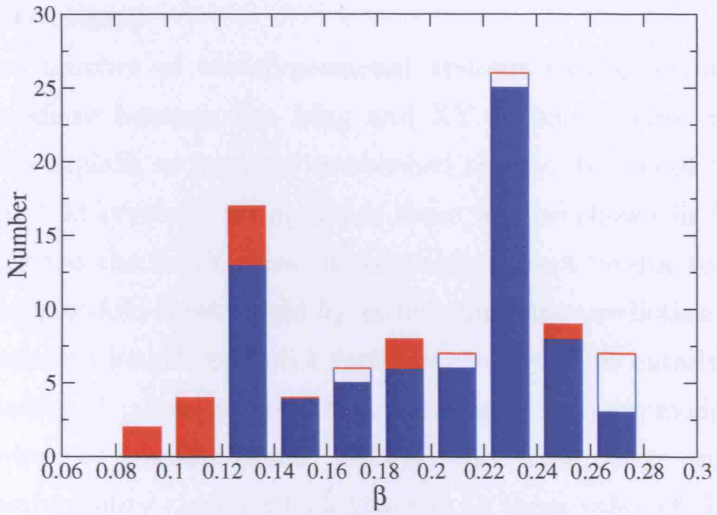

Figure 4.23: Histogram of β values for all two-dimensional systems reported in this chapter. Blue bars represent magnetic systems, empty bars represent systems studied by powder neutron diffraction and red bars represent non-magnetic systems.

$\beta \simeq 0.23$ critical behaviour is not observable.

It has recently been argued that the order parameter should be measurable in Bose-Einstein condensates confined to two-dimensional optical lattices [244, 245], in which case a finite sized 2dXY critical regime should be measurable. Recent experiments have confirmed that such systems are well described by the 2dXY model [246], although unfortunately no data has yet been reported for the critical behaviour of the order parameter.

4.3 Conclusions

The purpose of this literature review has been to classify a vast list of two-dimensional systems according to their critical behaviour. Empirically, the measured β values are found to be distributed according to the histogram shown in Figure 4.23. The bimodal nature of the distribution identifies two relevant universality classes, namely the 2d Ising and the 2dXY categories, which bound the observable critical behaviour. Unlike thin films and layered magnets, physisorbed surfaces are also observed to undergo structural transitions which belong to the three- and four-state

Potts universality classes.

A significant number of two-dimensional systems exhibit critical behaviour which is intermediate between the Ising and XY regimes. This middle ground is problematic to explain in terms of established theory. It cannot be due to XY systems with six-fold crystal field h_6, since these will be shown in Section 5.2 to effectively belong the the 2dXY class. It seemingly cannot be due to XY model in the presence of a four-fold crystal field h_4, either, since the prediction of JKKN [68] is that the correlation length exponent varies as $\nu \sim \frac{1}{h_4}$. This entails a continuous spectrum of possible β values, whereas the histogram 4.23 quite evidently suggests a bounded envelope of possible values. On the other hand, there appear to be no other possible universality classes which give rise to these value of β.

The central issue addressed in this work is to test the predictions of JKKN concerning the XYh_4 model. This can only be achieved either by a statistical sampling of systems with different four-fold fields (which has been the purpose of the present survey), or on a system in which the field h_4 can be tuned. Given the absence of such an experimental system, this is studied by use of Monte Carlo simulations in the next chapter.

Chapter 5

Long Range Order in Two-Dimensional Systems

On the basis of the discussion in Chapter 1, an effective Hamiltonian appropriate for a two-dimensional insulating solid may be formulated as

$$\mathcal{H} = \mathcal{H}_{\text{Heis}} + \mathcal{H}_{\text{anis}} + \mathcal{H}_{\text{dipolar}}. \tag{5.1}$$

where $\mathcal{H}_{\text{Heis}}$ is the Heisenberg exchange term, $\mathcal{H}_{\text{anis}}$ is a single ion anisotropy term, and $\mathcal{H}_{\text{dipolar}}$ is the dipolar interaction. The central question addressed in this chapter is how perturbations to the Heisenberg Hamiltonian such as $\mathcal{H}_{\text{anis}}$ induce long range order, deferring a discussion on the influence of the dipolar interaction to Chapter 6. This is achieved principally by using the Monte Carlo (MC) techniques presented in Section 2.3, but also analytically where necessary.

Following an analysis of the Heisenberg model itself, the simplest possible type of single ion anisotropy is examined, which may give rise to a crossover to either Ising or XY symmetry. Subsequently, a more complex form of anisotropy is considered, which is known to account for the behaviour of layered systems such as Rb_2CrCl_4 and K_2FeF_4. Crossover resulting in XY critical behaviour is studied with particular attention, and compared with the finite size 2dXY behaviour discussed in Section 2.4.2.

An outstanding question which arises from this discussion is the precise influence four-fold crystal fields in XY-like systems. To this end, the behaviour of the 2dXY

model in the presence of symmetry breaking fields is analysed in detail. Following José, Kadanoff, Kirkpatrick and Nelson (JKKN) [68], the value of the magnetisation exponent β as a function of anisotropy strength is calculated analytically, and compared with the results of Monte Carlo simulations. As predicted by JKKN, β is found to be non-universal. However, by considering finite size effects it is shown that in practice, the possible values of β are restricted to the range observed in Figure 4.19. In light of these these ideas, specific experimental candidates of XY systems with four-fold fields are reconsidered at the end of the chapter, and their observed behaviour is shown to be consistent with this mechanism.

5.1 Two-Dimensional Heisenberg Model

Unlike the Ising and XY models, in two dimensions the Heisenberg model

$$\mathcal{H}_{\text{Heis}} = -J \sum_{\langle i,j \rangle} \mathbf{S}_i \cdot \mathbf{S}_j \tag{5.2}$$

is not thought to undergo a phase transition at finite temperature. Support for this view comes from analytical [247–249] and Monte Carlo Renormalization Group [250] investigations. The difference between the 2dXY and the 2d Heisenberg models is fundamentally due to topology, and is highlighted by considering what happens when the spins are free to point in any direction in space [61], as opposed to anywhere in the xy plane. In this case there is no longer a metastable vortex, a singular point around which the spin rotates by an angle 2π, because the spin is free to be directed anywhere in the sphere. This allows the vortex to be replaced by a texture in which the spins near the centre are tilted out of the xy plane toward the z direction, so that the direction of the spins is a smooth function of position. The energy of this texture, instead of being proportional to $\ln(L/a_0)$, where a_0 is the order of the lattice spacing, is proportional to $\ln(L/\xi_0)$, where ξ_0 is the length scale of this central region in which the spins are tilted out of the plane. Since ξ_0 is continuously variable, this energy is continuously variable down to zero, and so there is no energy barrier to the creation or annihilation of vortex pairs. Thus, there is no finite temperature phase transition for the two-dimensional

Heisenberg model, at the thermodynamic limit. To illustrate this situation, MC 'snapshots' of the Heisenberg model were recorded at varying temperatures. As Figure 5.1(a) confirms, vortex pairs remain common even at low temperature, at odds with the KT mechanism described in Section 2.4.

Nevertheless, in some respects the Heisenberg model does share similarities with the XY model. The classical spin wave analysis carried out in Appendix A finds the low temperature expression for the magnetisation to be

$$M(N,T) = \left(\frac{1}{aN}\right)^{T/4\pi J} . \tag{5.3}$$

This differs from the equivalent expression for the XY model only by a factor of two in the exponent (*c.f.* Equation (2.65)), a fact that can be directly ascribed to there being an extra mode for the fluctuations in the Heisenberg model, in the z direction (*c.f.* Equation (A.12)). It has been argued [251] that in finite systems this also implies the presence of quasi long range order at low temperatures, characterised by a correlation decay exponent $\eta(T) = 2\eta^{\mathrm{XY}}(T)$. This follows because in the XY model the spin wave stiffness $K = J/T$ can be related to η by Equation (2.67).

The top hand plot in Figure 5.2 displays magnetisation data obtained from MC simulations on the 2d Heisenberg model with $N = 4096$. The finite nature of the system ensures that a transition to long range order to occurs at finite temperature. This is also confirmed in the behaviour of the susceptibility (middle plot of Figure 5.2). At low temperature, the MC magnetisation data is in surprisingly good agreement with (5.3), thus lending evidence to the quasi long range order mechanism suggested in reference [251].

The misleading nature of the Heisenberg model is also apparent from the behaviour of the susceptibility χ as a function of system size L, shown on the middle plot in Figure 5.2. With increasing L, one expects the transition temperature T_{c}, defined as the peak in χ, to tend to zero. However, the exact functional form of $T_{\mathrm{c}}(L)$ is not immediately apparent. At low temperature one might expect the correlation length to display exponential behaviour

$$\xi \sim \exp\left(\frac{aJ}{k_B T}\right), \tag{5.4}$$

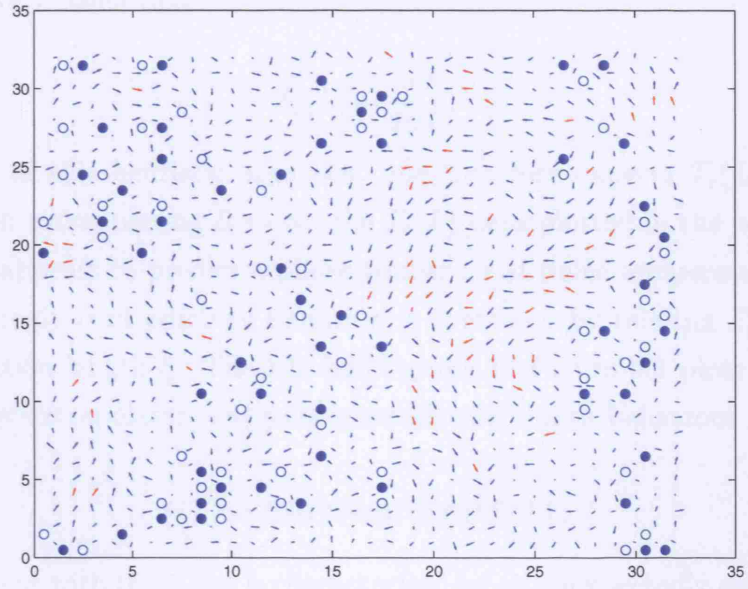

(a)

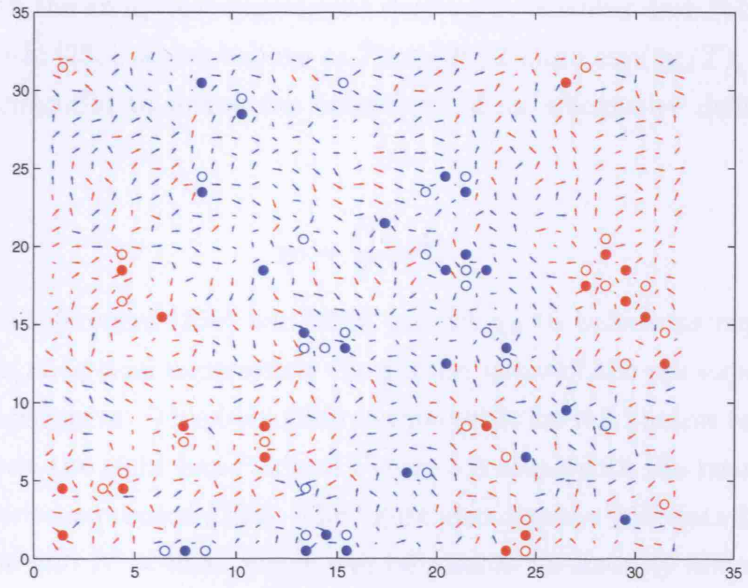

(b)

Figure 5.1: Spin and vortex configurations for the 2d Heisenberg model, with $N = 1024$, at (a) $T = 0.4$ and (b) $T = 0.65$. Red and blue indicate whether the z component of a spin point upward or downward, respectively. Unlike the XY model (Figure 2.17), at low temperature there is no barrier to the creation or annihilation of vortex pairs.

a being a constant of order unity. At $T_c(L)$ the correlation length ξ is limited by the system size L, such that

$$T_c(L) \sim \frac{aJ}{\ln L}. \tag{5.5}$$

On the basis of this heuristic argument one therefore expects $T_c(L) \propto 1/\ln L$. However, upon extrapolating $L \to \infty$, the $T_c(L)$ data plotted in the bottom graph of Figure 5.2 appears to predict a phase transition at finite temperature [252].

This seemingly contradictory situation is overcome by relating $T_c(L)$ directly to the correlation length ξ. The left hand graph in Figure 5.3 plots $\ln L$ against $1/T_c$, which by extrapolation suggests a correlation length behaviour given by

$$\xi(T) = 0.0195 \exp\left(5.0156/T\right). \tag{5.6}$$

This is consistent with (5.4), but is characterised by an unexpectedly small prefactor and large numerator in the exponential. It is noteworthy that (5.6) also compares favourably with the analytical expressions derived by Shenker and Tobochnik [250] and by Takahashi [253], which behave as $T\exp(2\pi/T)$ and $\exp(2\pi/T)$, respectively.

It is also insightful to follow the behaviour of an alternative definition of the susceptibility

$$\chi_0 = \frac{N}{T}\langle m^2 \rangle. \tag{5.7}$$

The authors in references [250] and [253] predict χ_0 to behave as $\exp(4\pi/T)$, although in their analytical expressions the precise value of the pre-exponential factors are in disagreement. This behaviour is thought to be valid at low temperatures, and is plotted on the right hand side of Figure 5.3 along with the results of a high temperature series expansion [254]. The figure also displays MC data from systems of size $N = 256$ and $N = 4096$, which can be seen to be strongly affected by finite size at low temperature. However, up until the point at which it tails away, the Monte Carlo data appears to favour a crossover from the high temperature regime to the low temperature behaviour predicted by Shenker and Tobochnik [250].

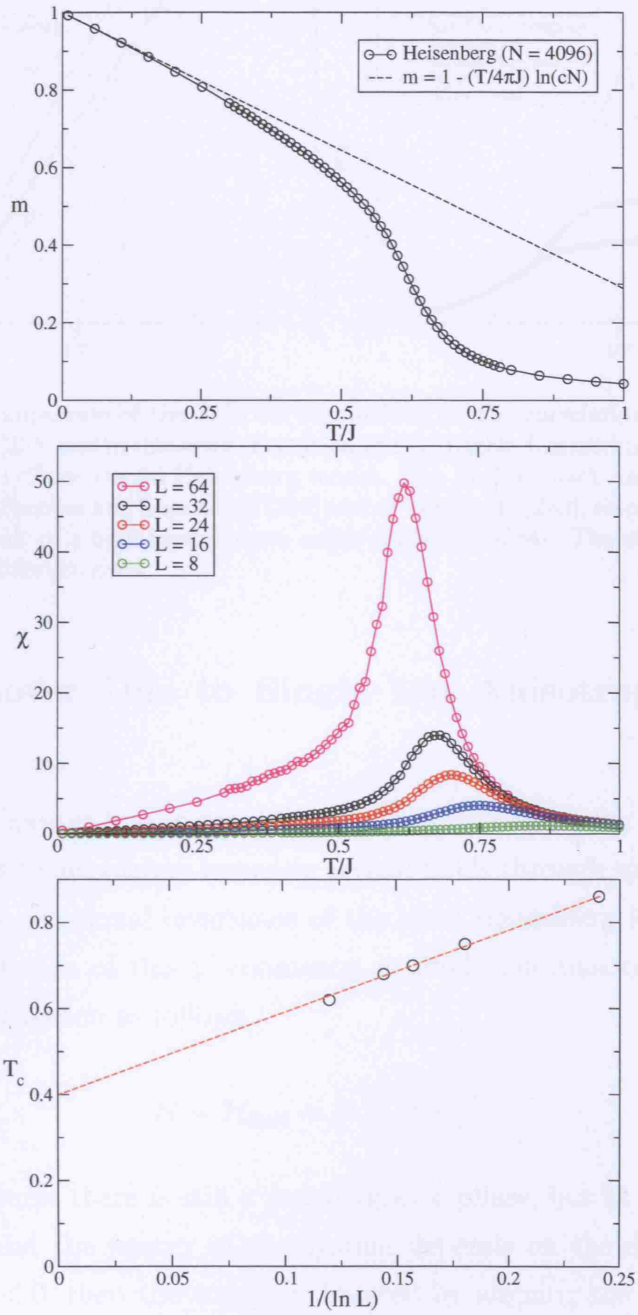

Figure 5.2: Top: Magnetisation data for a 2d Heisenberg system of size $L = 64$, compared with the spin wave expression (5.3). Middle: Susceptibility data for the same model for a number of system sizes. Bottom: Variation of T_c, determined from the peaks in the susceptibility curves, as a function of system size L. On this basis one is misled to the conclusion that the 2d Heisenberg model undergoes a phase transition.

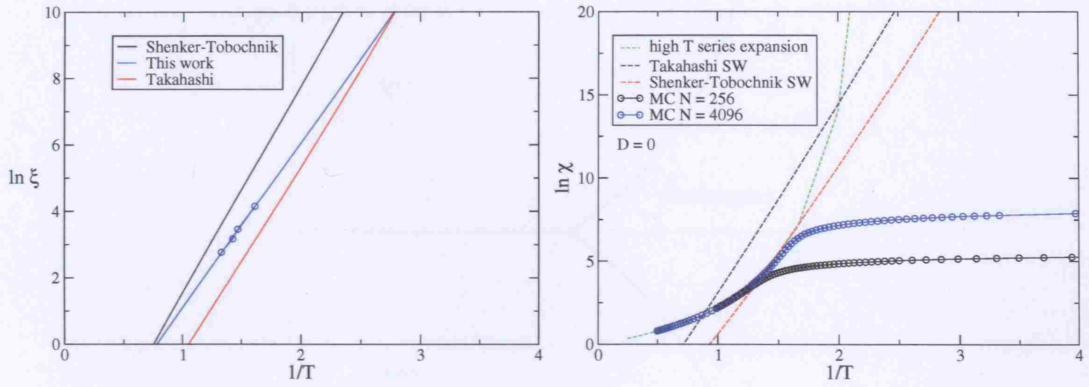

Figure 5.3: Left: Comparison of the different expressions for the correlation length ξ derived in references [250] and [253] and in this work (Equation (5.6)). Right: Logarithm of the susceptibility χ_0 as a function of $1/T$ for the 2d Heisenberg model. The dashed black and red lines show the analytical results of Shenker and Tobochnik [250] and of Takahashi [253], respectively. The dashed green line is the result of a high temperature series expansion [254]. The circles show MC data for two systems of different sizes.

5.1.1 Crossover Due to Single Ion Anisotropy I. Simple Case

As discussed in Chapter 1, it is generally the case that the spins lying on a crystal lattice are subject to anisotropy inducing crystal fields through spin-orbit coupling, which destroy the rotational invariance of the ideal Heisenberg Hamiltonian. One common manifestation of this phenomenon is single ion anisotropy which corresponds to a perturbation as follows

$$\mathcal{H} = \mathcal{H}_{\text{Heis}} + D \sum_i (S_i^z)^2 \,. \tag{5.8}$$

At high temperatures there is still a paramagnetic phase, but at low temperatures the spins order and the energy of the system depends on the direction in which they align. If $D < 0$, then the energy is lowered by aligning the spins along the z axis and at low enough temperatures

$$\langle S_i^z \rangle = \pm 1 \tag{5.9}$$

a state analogous to the low temperature behaviour of the Ising model. Conversely,

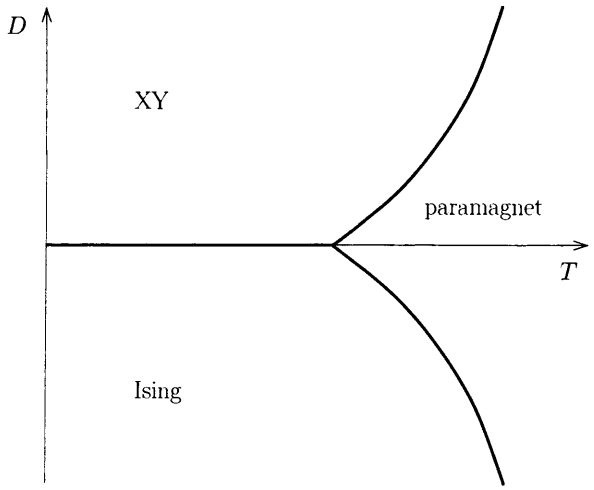

Figure 5.4: Phase diagram for the Heisenberg model in the presence of single ion anisotropy.

if $D > 0$, then the spins order in the xy plane, writing $\mathbf{S}_\perp \equiv (S^x, S^y)$, at low temperatures it is found that

$$\langle |\mathbf{S}_\perp|^2 \rangle = 1, \tag{5.10}$$

which is behaviour characteristic of the XY model.

A consequence of these considerations is that for large D, the phase transition from the paramagnetic phase as T is reduced will be either Ising or XY like, depending on the sign of D. For $D = 0$ the transition is in the Heisenberg universality class, but for any finite D, the RG flows will end up at the stable low temperature Ising or XY fixed points. In the language of the Renormalization Group, the symmetry breaking term is said to be relevant at the Heisenberg fixed point. Small values of D will grow under renormalization, and will push the system towards a new fixed point, either Ising or XY, as shown schematically in the phase diagram in Figure 5.4. Around each of these fixed points there will be different scaling phenomena from those of the Heisenberg fixed point.

To test these ideas, Monte Carlo simulations were performed on the model defined by (5.8) on a range of different system sizes. The magnetisation curves for different values of D for a system of size $L = 32$ are plotted in Figure 5.5. As expected, for negative D a crossover is observed toward Ising behaviour, whereas

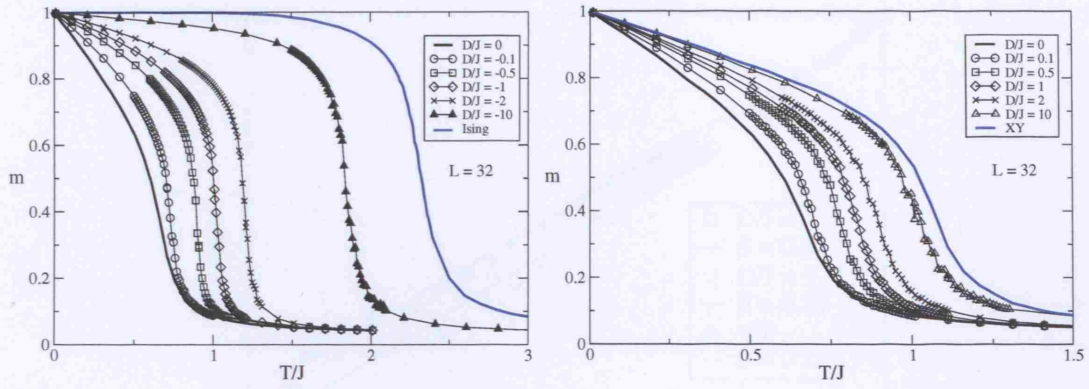

Figure 5.5: Monte Carlo magnetisation curves for the Heisenberg model in the presence of single ion anisotropy. For negative D the crossover is toward Ising behaviour, for positive D it is toward XY behaviour.

for positive D the crossover is toward XY behaviour. The crossover toward the Ising regime has been studied in the past [84], the main conclusion being that in so far as the critical behaviour of the order parameter is concerned, the Ising value of $\beta = 0.125$ remains observable even for very small anisotropies $|D/J| \sim \mathcal{O}(0.01)$.

The question naturally arises as to whether the crossover toward the XY limit is equally fast. As discussed in Section 2.4.2, the signature of XY critical behaviour is an effective critical exponent $\tilde{\beta} \simeq 0.23$ [77], which, as shown in Figure 2.19, is observable in numerical simulations. Figure 5.6 plots the logarithm of m against the logarithm of the reduced temperature $t = |1 - T/T_c|$, where T_c has been located as the point at which there is a peak in the susceptibility. For all the values of D studied, $0.1 < D < 10$, the slope of these curves has been determined to be $\beta \sim 0.23$, thus confirming the important influence of planar anisotropy.

5.1.2 Crossover Due to Single Ion Anisotropy II. Complex Case

Another form of anisotropy which is commonly encountered is cubic anisotropy, specified by the Hamiltonian

$$\mathcal{H} = \mathcal{H}_{\text{Heis}} + E \sum_i \left[(S_i^x)^4 + (S_i^y)^4 + (S_i^z)^4 \right]. \tag{5.11}$$

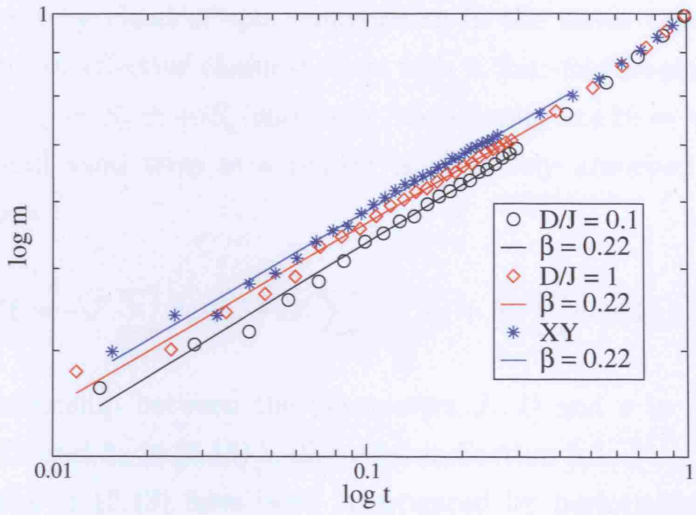

Figure 5.6: Log-log plot of the order parameter m against the reduced temperature t of the data on the right hand side of Figure 5.5. For all the values of D studied, 2dXY critical behaviour is observed.

This is not invariant under continuous rotations, but is invariant under discrete rotations of the spins through $\pi/2$. Cubic anisotropy turns out to be irrelevant at the Heisenberg fixed point in $d = 3$ [255]. A two-dimensional system cannot have cubic anisotropy but may instead have tetragonal anisotropy, as defined in the following Hamiltonian derived from crystal field theory [105]

$$\mathcal{H} = -J\mathbf{S}_1 \cdot \mathbf{S}_2 + \sum_{i=1,2} \left[D(S_i^z)^2 + a(S_i^z)^4 + \frac{1}{2}e(S_{i+}^4 + S_{i-}^4) \right], \qquad (5.12)$$

where $D > 0$ represents an axial anisotropy that confines the spins to the xy plane, as observed for the Hamiltonian (5.8), a is a quartic axial anisotropy and e is a four-fold in plane anisotropy.

The expression (5.12) turns out to convincingly describe the behaviour of quasi two-dimensional insulators such as K_2FeF_4 and Rb_2CrCl_4 [105, 256]. J is found to be positive (ferromagnetic) for Rb_2CrCl_4 and negative (antiferromagnetic) for K_2FeF_4. Although this does lead to important experimental consequences (see Section 5.3), this difference is irrelevant for the purposes of the present discussion, therefore only the ferromagnet is considered for now. Furthermore, although (5.12) could represent either a quantum mechanical or a classical Hamiltonian, with the

operators replaced by classical spin components in the latter case, it is helpful to reduce it into an effective classical form with a four-fold in-plane anisotropy by substituting $S_{\pm} = S_x \pm +iS_y$ and using the identity $\cos 2\theta = \cos^2\theta - \sin^2\theta$. Ignoring the small axial term in a (which is effectively absorbed into D), one eventually obtains

$$\mathcal{H} = -J' \sum_{\langle i,j \rangle} \mathbf{S}_i \cdot \mathbf{S}_j + D' \sum_i \cos^2\phi_i + h_4 \sum_i \cos(4\theta_i). \tag{5.13}$$

The precise relationship between the parameters J, D and e in (5.12) and the parameters J', D' and h_4 in (5.13) is discussed in Section 5.3.

The properties of (5.13) have been investigated by performing Monte Carlo calculations on system of different sizes, with different values of D' and h_4[a]. Some typical magnetisation curves are displayed in Figure 5.7. The most noticeable feature is that for small four-fold anisotropies, the critical regime appears to be unaffected. A departure from XY-like behaviour is only observed for stronger values of h_4, of the same order of D'. This raises a number of issues. Does the Monte Carlo data imply XY behaviour is robust to four-fold crystal field effects in experiment? If so, can this stability be quantified? Can the nature of the apparent crossover undergone in the presence of strong h_4 be elucidated? In particular, to what universality class is the crossover to? It is in order to address these questions that the next section turns to the XY model in the presence of symmetry breaking crystal fields.

5.2 Influence of Symmetry Breaking Fields on the 2dXY Model

The relevant Hamiltonian for two-dimensional XY spins on a periodic lattice subject to symmetry breaking crystal fields is the XYh_p model

[a]Note that, in keeping with the rest of the numerical work presented in this Thesis, spins of unit length are assumed.

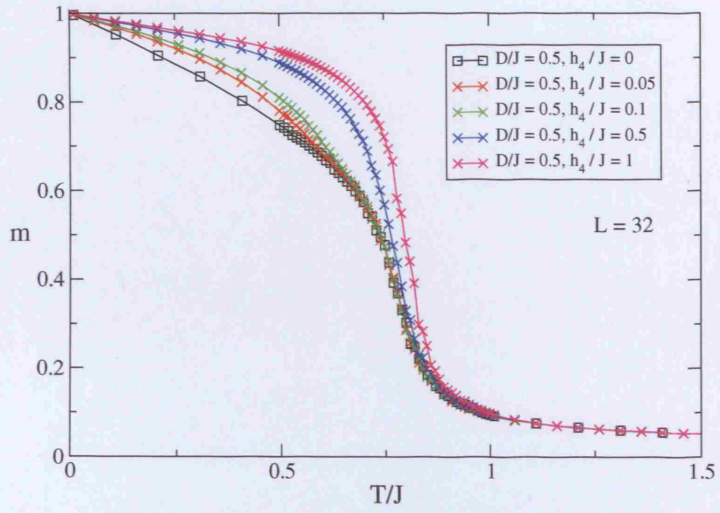

Figure 5.7: Monte Carlo magnetisation data for the model described by (5.13) with $D' = 0.5$ and different values of h_4.

$$\mathcal{H}_{\{h_p\}} = -J \sum_{\langle i,j \rangle} \cos\left(\theta_i - \theta_j\right) - h_p \sum_i \cos\left(p\theta_i\right). \tag{5.14}$$

From an experimental point of view, the most interesting scenarios are $p = 1 - 4$ and $p = 6$. Setting $p = 1$ corresponds to the application of an external magnetic field. If there is a two-fold symmetry - two equivalent minima in the energy at an angle π apart - the system has the critical behaviour of the Ising model. With a three-fold symmetry axis, so that the minima in energy are at an angle $2\pi/3$ apart, the critical behaviour is that of the three-state Potts model.

The properties of systems with four-fold or higher symmetry are more complex, and have been considered in an approximation of the Hamiltonian (5.14) by JKKN [68]. Their main predictions are as follows. If the symmetry axis perpendicular to the plane has a five-fold or higher symmetry, as it will if the anisotropy is due to crystal fields in a triangular lattice ($p = 6$), then the anisotropy can be shown to lock the magnetisation into one of the preferred directions at sufficiently low temperatures. At intermediate temperatures the anisotropy becomes irrelevant, so that the system behaves as if it were isotropic, with algebraically decaying long range order, whose exponent changes continuously with temperature until it

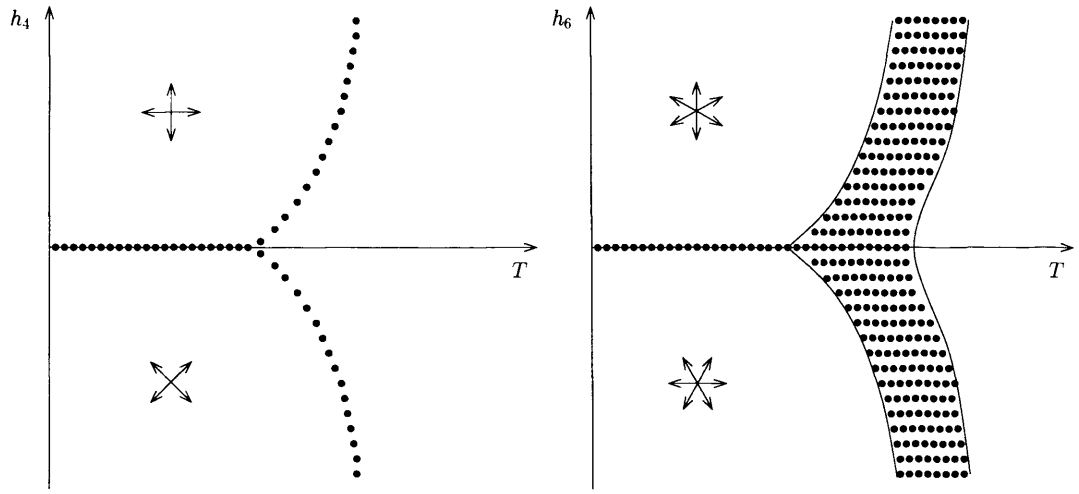

Figure 5.8: Temperature-field phase diagram for the XY model in the presence of a four-fold and six-fold crystal fields. The filled circles denote critical points with continuously varying critical exponents.

reaches a critical value at which free vortices can form spontaneously. The case of anisotropy with four equivalent axes in the plane lies on the boundary between these two types of behaviour: algebraically decaying order occurs at only one temperature, but the exponent at this temperature has a non-universal value. The physical origin stems from the fact that, for $p > 4$, thermal fluctuations can take spins from one crystal field minimum to another without destroying the local ordering. For $p = 4$ the required jumps, $\Delta\theta = \pi/4$ are the same as those required, on average, to create a vortex around a square plaquette. Hence, the temperature at which the spins jump the crystal field barriers is the same as the KT transition temperature. The phase diagrams for systems with four-fold and six-fold crystal fields are shown in Figure 5.8.

5.2.1 Numerical Results

To test the predictions of JKKN, Monte Carlo simulations were performed on the XYh_p model (5.14), placing the spins on a square lattice with periodic boundary conditions. The model was studied for different values of p and field strengths h_p, and for a variety of system sizes L. At each temperature, the thermodynamic quantities were measured by averaging the results of 5 independent runs of 10^5

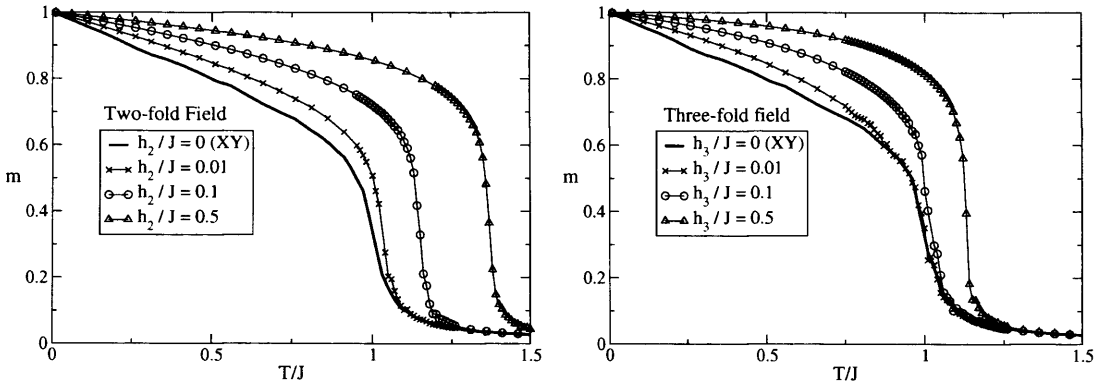

Figure 5.9: Magnetisation data for the XYh_2 and XYh_3 models with $N = 10^4$, with anisotropies of strength $h_p = 0, 0.01, 0.1$ and 0.5.

MCS/s, disregarding the first 10^4 MCS/s for equilibration. Near the transition temperature, simulations with 10^6 MCS/s were performed.

Two- and Three-fold Field

Figure 5.9(a) displays magnetisation data obtained from MC simulations of the XYh_2 model, for anisotropies of strength $h_2/J = 0$, 0.01, 0.1 and 0.5. It is apparent that 2dXY critical behaviour is destroyed even for very weak values of h_2, and there is a rapid crossover to 2d Ising critical behaviour as $h_2 \to \infty$. Thus, the XYh_2 model is unstable with respect to the two-fold anisotropy, consistent with the predictions of JKKN. A similar instability is observed in the XYh_3 model (Figure 5.9(b)), although in this case the crossover is toward the three-state Potts class.

Six-fold Field

The effect six-fold crystal fields have on the finite sized 2dXY model is more peculiar. With increasing anisotropy strength the three phase behaviour predicted by JKKN becomes apparent. As the temperature is increased the system goes through a low temperature phase in which the spins order in one of the directions preferred by the anisotropy, an intermediate regime in which it behaves as if it were isotropic, and a high temperature paramagnetic phase. However, whereas at the thermodynamic limit the intermediate phase is dictated by the low temperature

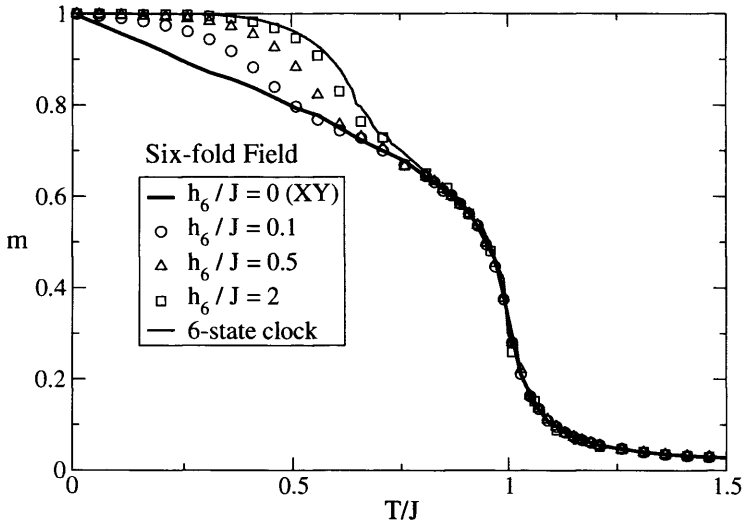

Figure 5.10: Magnetisation data for the XYh_6 model with anisotropies varying strength, with $N = 10^4$. With increasing h_p/J the three phase behaviour of the system becomes apparent. However, the critical behaviour of the magnetisation is characterised by the exponent $\beta \simeq 0.23$ for all values of h_6.

prediction of $\eta(T)$ given by Equation (2.66), on a finite lattice the work of BH implies a $\beta = 0.23$ regime. This restoration of continuous spin symmetry is clearly observable in numerical simulations. Figure 5.10 compares magnetisation data of the XY model with crystal fields of increasing strength. For all values of h_6, the critical behaviour of the magnetisation is characterised by the exponent $\beta \simeq 0.23$. The conclusion is therefore that the six-fold crystal field acts as an irrelevant perturbation on the 2dXY model, on any length scale: the XYh_6 model does not define a new universality class.

It is remarked that the XYh_6 model behaves in a manner closely related to the mechanism of two-dimensional melting proposed by Halperin, Nelson [236] and Young [237]. This accounts for the observation of XY-like critical behaviour in the xenon physisorbed on graphite system discussed in Section 4.2.2.

Four-fold Field

Figure 5.11(a) displays the magnetisation versus temperature for the XYh_4 model with different crystal field perturbations, for a system with $N = 10^4$ spins. A number of features are immediately apparent. For $h_4/J = 0$, the finite size 2dXY

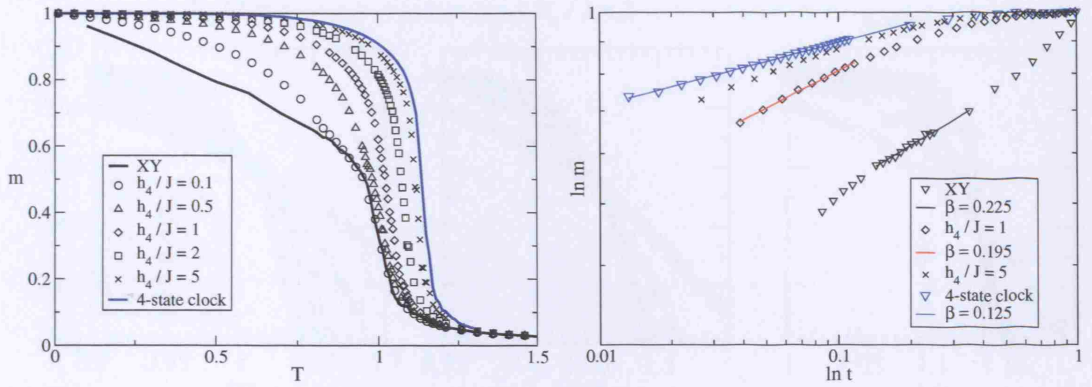

(a) (b)

Figure 5.11: Monte Carlo data for the XY model in the presence of a four-fold crystal field, with $N = 10^4$. Plot (a) displays the magnetisation of the XY model in the presence of increasingly strong anisotropies. Plot (b) displays the same data as a function of the reduced temperature t, in a logarithmic scale.

behaviour described in Section 2.4.2 is recovered. For $h_4/J \to \infty$, on the other hand, the four-state clock model is recovered, which reduces to two perpendicular Ising models and is consequently in the Ising class (see page 161). In between these two limiting regimes, the MC data suggests the occurrence of critical behaviour intermediate between the XY and Ising models, which presumably represents an example of the non-universal exponents anticipated by JKKN. However, the onset of non-universal behaviour is not immediate. For small values of h_4/J, a restoration of continuous spin symmetry analogous to that seen in the XYh_6 model is observed, and the magnetisation falls exactly on the data for zero field. A departure from XY critical behaviour only occurs in the presence of anisotropies as strong as $h_4/J \simeq 0.5$. Figure 5.11(b) displays $\ln(m)$ against $\ln(T - T_c(L))$, which confirms that the magnetisation exponents lie in the interval $1/8 < \beta(h_4) < 0.23$. The crossover to Ising exponents is slow: for $h_4/J = 1$, $\beta(h_4) \approx 0.2$ and to approach $\beta \approx 1/8$ requires h_4/J in excess of 5.

Determination of Non-Universal Exponents From Numerical Data Although the main method to estimate β from experimental data is likely to be the direct measurement of the gradient of the magnetisation plotted in a logarithmic scale, Monte Carlo data allows a more thorough scaling analysis to be performed,

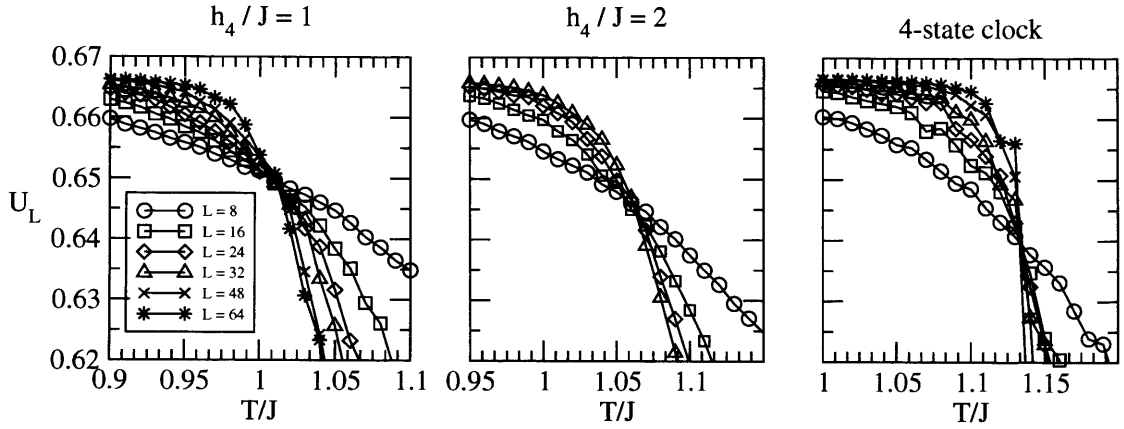

Figure 5.12: Fourth order cumulant U_L plotted against temperature for the XYh_4 model, with different h_4 and different lattice sizes.

as introduced in Section 2.2.4. Here, the critical exponents of the XYh_4 model with $h_4 = 1$, 2 and $h_4 \to \infty$ (four-state clock model) are determined, and compared with the results of Rastelli *et al.* [174].

A useful quantity to consider is the fourth-order ('Binder') cumulant [56, 57]

$$U_L = 1 - \frac{\langle m_L^4 \rangle}{3\langle m_L^2 \rangle^2}, \tag{5.15}$$

which takes a universal value in the limit $L \to \infty$. For temperatures above the critical temperature T_c, the cumulant approaches the Gaussian value $U_L = 0$ and for temperatures below T_c it approaches a maximum value $U_L = 2/3$. As discussed in Section 2.3.3 for the related quantity Q_L, the Binder cumulant is invariant under renormalization [56, 57], allowing the critical temperature to be located by monitoring the crossing point of U_L for different lattice sizes. In Figure 5.12, the cumulant is plotted against temperature for different lattice sizes with $h_4 = 1$, 2 and ∞. The critical temperature is located at $T_c = 1.008(2)$, $1.065(2)$ and $1.135(3)$ for $h_4 = 1$, 2 and ∞, respectively, in good agreement with previous measurements [174, 257].

In order to evaluate the critical exponents, it is necessary to first obtain the correlation length exponent ν. This is notoriously problematic to extract from numerical simulations [53]. Based on the renormalization arguments in Section 2.3.3 it can be shown [56] that an estimation of ν that is independent of other

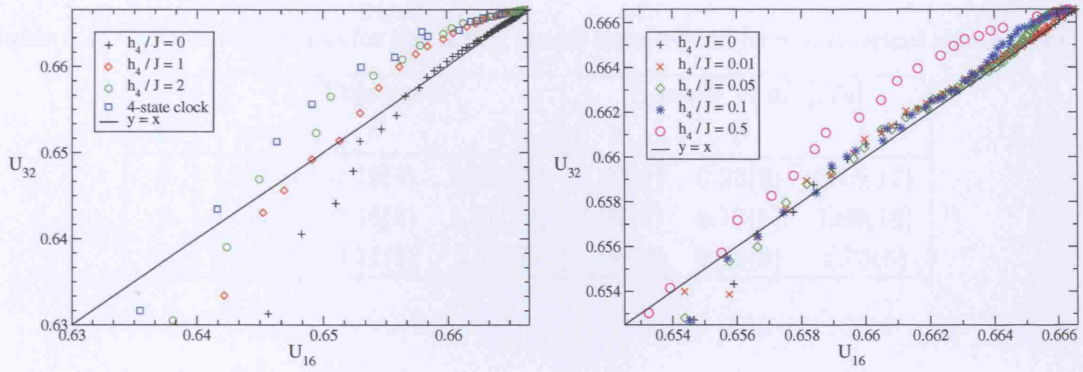

Figure 5.13: Fourth order cumulant U_{32} plotted against U_{32} for different values of h_4.

exponents may be achieved by using the relationship

$$\left(\frac{\partial U_{L'}}{\partial U_L}\right)_{T=T_c} = b^{1/\nu}, \tag{5.16}$$

where $L' = bL$ and b is a scale factor greater than unity. In this way, ν may be computed by evaluating the slope of $U_{L'}$ against U_L at the intersection point with the diagonal line given by $y = x$.

Figure 5.13(a) plots U_{32} against U_{16} for $h_4 = 0$, 1, 2 and ∞. It is noteworthy that the data for $h_4 = 0$ falls onto the diagonal line up until a temperature $T = 0.94$, which is close to typical values of T^* for the finite size 2dXY model. This implies the slope of the curve $(\partial U_{L'}/\partial U_L) = b^{1/\nu} = 1$ in the temperature range $0 < T < T^*$, and that $\nu \to \infty$, consistent with the exponentially divergent correlation length predicted by KT theory [61]. Figure 5.13(b) shows that this behaviour remains present in the presence of fields $h_4 \leq 0.5$. This persistence of the KT phase to four-fold fields is also observable in other thermodynamic quantities (such as the magnetisation in Figure 5.11), and is discussed further in the next section.

For stronger nonzero fields, a single crossing point with the $y = x$ line is observed. The coordinates of this point were determined numerically by a least-squares fit of the data to second, third and fourth order polynomials. The derivative of each polynomial at the crossing point was also determined, thus allowing ν to be estimated. This procedure was repeated for $L' = 16$, 24 and 32, and $L = 32$, 48 and 64. As a measure of the reliability of the method, the four-state clock model

Table 5.1: Critical exponents for the XYh_4 model determined from numerical simulations.

	This work			Rastelli *et al.* [174]		
h_4	ν	β	γ	ν	β	γ
1	1.19(4)	0.19(4)	2.00(15)	1.22(3)	0.23(3)	2.15(17)
2	1.09(8)	0.16(3)	1.87(10)	1.07(9)	0.17(5)	1.89(13)
∞	1.00(5)	0.11(2)	1.76(7)	1.00(3)	0.14(2)	1.75(6)

was considered, which as will be discussed in Section 5.2.2, belongs to the Ising universality class. For the systems studied, ν was found to range from 1.03 to 0.97. A noticeable feature of these estimates is that for decreasing system sizes, higher values of the exponent are obtained. Nevertheless, once averaged they compare favourably with the theoretical value $\nu = 1$. On this basis, the measured values of ν reported in Table 5.1 for the XYh_4 model with $h_4 = 1$ and $h_4 = 2$ are to be considered reliable.

Table 5.1 also reports estimates for the exponents β and γ. These were obtained by taking advantage of the relationships (2.40) and (2.42): plotting the logarithm of the maximum in the susceptibility against the logarithm of the lattice size L, gives a line with a slope equal to γ/ν. Similarly, plotting the magnetisation measured at the temperature at which the susceptibility has its maximum against the logarithm of L yields the ratio β/ν. The non-universal field dependent nature of the exponents is thus clearly confirmed, provided $h_4 > 0.5$, and the estimates are in good agreement with previous work [174]. In particular, it is noteworthy that in the limit $h_4 \to \infty$, critical behaviour of the 2d Ising model is recovered, as expected theoretically.

Marginal Nature of the Four-fold Field

For $h_4 < 0.5$, the numerical data presented in this and in previous works [173–175] suggest there is a re-establishment of continuous symmetry, such that XY-like behaviour remains present. This special phenomenon is consistent with h_4 being a marginal perturbation. In general, a system susceptible to a perturbation scales as [258]

$$\left(\frac{h_p}{J}\right)' = \ell^{y_p}\left(\frac{h_p}{J}\right), \tag{5.17}$$

where ℓ is the scaling factor. If the perturbation is relevant ($y_p > 0$) it grows under rescaling and a crossover to the universality class of reduced symmetry occurs at a characteristic crossover length scale ℓ_c

$$\left(\frac{h_p}{J}\right)' = \ell_c^{y_p}\left(\frac{h_p}{J}\right) \simeq 1 \tag{5.18}$$

$$\ell_c \simeq \left(\frac{J}{h_p}\right)^{1/y_p}. \tag{5.19}$$

On the other hand, if $y_p < 0$ the perturbation is irrelevant. For a marginal perturbation, such as the four-fold field in the 2dXY model, the crossover exponent $y_4 = 0$. In this case crossover can only occur, at best, due to logarithmic corrections to scaling

$$\left(\frac{h_4}{J}\right)' = \alpha \log(\ell)\left(\frac{h_4}{J}\right), \tag{5.20}$$

and will consequently be only observable on exponentially large length scales

$$\ell_c \simeq \exp\left(\frac{J}{\alpha h_4}\right). \tag{5.21}$$

If this length scale is larger than the effective system size, 2dXY behaviour persists. Hence, for small and intermediate crystal field strengths the finite size scaling appears compatible with that of the continuous symmetry of the 2dXY model, as in the six-fold case. This fact is substantiated by the detailed finite size scaling analysis performed above, which shows no evidence of any crossover occurring for small fields. This is an experimentally relevant point, since it provides a satisfactory explanation as to why the crossover to the non-universal behaviour predicted by JKKN is suppressed in many magnetic 2dXY systems. For example, the canonical 2dXY system Rb_2CrCl_4 [96] is in effect subject to four-fold crystal fields, yet it displays $\beta \simeq 0.23$. Given it has a coupling constant $J \approx 14$ K, this particular material would require unphysically strong fields $h_4 \approx 7$ K in order for this behaviour to be altered. This fact is discussed further in Section 5.3.

5.2.2 Clock Models and Extended Universality

In the $h_p \rightarrow \infty$ limit, the Hamiltonian (5.14) is called a clock model since the only allowed states consist of spins pointing in p discrete directions symmetrically distributed around a circle

$$\mathcal{H}_p = -J \sum_{\langle i,j \rangle} \cos\left(\theta_i - \theta_j\right) \text{ with } \theta_i = 2\pi \left(\frac{\delta}{p}\right) \quad (\delta = 1, \ldots, p). \tag{5.22}$$

This model interpolates between the spin-up or -down Ising limit ($p = 2$) and the continuous 2dXY limit ($p = \infty$). It may consequently be studied to track how the phase transition of the Ising model, characterised by spontaneous broken symmetry in the ordered phase, gives way to the Kosterlitz-Thouless transition, in which broken symmetry is absent.

The model has a diverse phase diagram [259]: for $p = 2, 4$ it belongs to the Ising universality class, with a low temperature ferromagnetic phase and a high temperature paramagnetic phase; for $p > 4$ it has three phases - a low temperature ordered and a high temperature disordered phase, as in the Ising model, and also a 'quasi-liquid' intermediate phase. MC simulations performed on the model (5.22) confirm this behaviour: the specific heat data for the $p = 6$ and $p = 8$ models clearly has two peaks. Focusing on the $p = 8$ data, the quasi-liquid regime is shown to lie in the region $T_1 < T < T_2$.

The transition at T_2 has been conjectured to be KT-like by various authors [259–262]. Indeed, in its vicinity the specific heat and magnetisation data obtained from the MC calculations for the six- and eight-state clock models is shown in Figure 5.14 to match exactly on to that of the XY model. With regards to the magnetisation data, the restoration of continuous spin symmetry is identical to that described for the XYh_6 model. Lapilli, Pfeifer and Wexler (LPW) [263] have recently presented a more rigid argument in order to verify this equivalence. On the basis of known results on the generalised Villain model [68], they define a temperature

$$T_{\text{eu}}(p) = \frac{4\pi^2}{p^2 T_{\text{KT}}}, \tag{5.23}$$

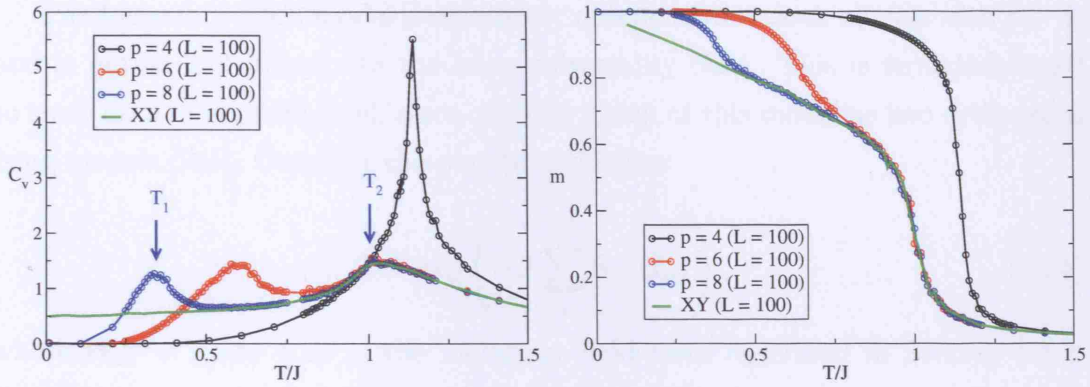

Figure 5.14: Comparison of p-state clock models for $p = 4$, 6 and 8. Left: specific head data; Right: magnetisation data. The quasi liquid phase for the eight-state clock model lies between the temperatures T_1 and T_2.

above which the macroscopic thermal averages of discrete clock models with $p > 4$ become *identical* to those of the continuous XY system. This collapse of thermodynamic observables creates a regime of what LPW refer to as *extended universality*, and an emergent symmetry not present in the original Hamiltonian. This remarkable phenomenon is distinct from conventional universality, because the symmetry is present over an extended range of temperatures and not just at the critical point.

Equation (5.23) thus provides a criterion which allows for the nature of the transition at T_2 to be established, depending on the value of p. For $p \geq 8$, T_{eu} lies in the quasi liquid phase below T_2, thus guaranteeing that the transition $T_2(p \geq 8)$ is of the KT type. Conversely, for $p \leq 7$, T_{eu} lies above T_2, which implies that the transition $T_2(p \leq 7)$ is not a KT transition. LPW substantiate these predictions by showing that, following a free energy stability argument proposed by Minnhagen and Kim [264], a twist of the spins at T_2^+ costs much more in energy for $p \leq 7$ than it does for $p \geq 8$, suggesting that the spin wave stiffness does not jump discontinuously to zero as $L \to \infty$ for $p \leq 7$. The Monte Carlo simulations performed in this work, summarised by the magnetisation data shown in Figure 5.14, also confirm the predictions of LPW. An important observation is that, despite not strictly undergoing a KT transition according to the LPW criterion (5.23), the six-state clock model remains indistinguishable from the XY model, in so far as the measurable critical behaviour is concerned.

The four-state clock model is manifestly different from clock models with $p > 4$, and in actual fact belongs to the Ising universality class. This is straightforward to show on a mean field level, since one may think of this model as two orthogonal Ising models [265]. Consider the partition function

$$Q = \exp\left(-J\sum_i \mathbf{S}_i \cdot \mathbf{H}_{\text{mf}}\right), \tag{5.24}$$

where $\mathbf{H}_{\text{mf}} = zJM + H$ is the molecular field term described in Section 1.4.2. For the two state Ising model the summations in (5.24) are trivial since $\mathbf{S_i} = \pm 1$. Therefore

$$\begin{aligned} Q_{\text{Ising}} &= \text{Tr}\, \exp\left(-\beta \mathbf{S}_i \cdot \mathbf{H}_{\text{eff}}\right) \\ &= \exp\left(\beta \mathbf{H}_{\text{eff}}\right) + \left(-\beta \mathbf{H}_{\text{eff}}\right) = 2\cosh\left(\beta \mathbf{H}_{\text{eff}}\right). \end{aligned} \tag{5.25}$$

For the four-state clock model $\mathbf{S}_i$ may take up four values, two of which are degenerate: $\mathbf{S_i} = \pm S_x, \pm S_y = \pm 1, 0, 0$ (see the bottom left hand diagram in Figure 5.16). Consequently

$$\begin{aligned} Q_{4\,\text{states}} &= \text{Tr}\, \exp\left(-\beta \mathbf{S}_i \cdot \mathbf{H}_{\text{eff}}\right) \\ &= \exp\left(\beta \mathbf{H}_{\text{eff}}\right) + \exp\left(-\beta \mathbf{H}_{\text{eff}}\right) + 2 \\ &= \left[\exp\left(\frac{\beta \mathbf{H}_{\text{eff}}}{2}\right) + \left(-\frac{\beta \mathbf{H}_{\text{eff}}}{2}\right)\right]^2 = 2\left[1 + \cosh\left(\beta \mathbf{H}_{\text{eff}}\right)\right]. \end{aligned} \tag{5.26}$$

Thus the partition function of the four-state clock model is simply the square of the partition function of the Ising model with an interaction potential $J/2$:

$$Q_{4\,\text{states}}(\beta, J) = \left[Q_{\text{Ising}}\left(\frac{\beta, J}{2}\right)\right]^2. \tag{5.27}$$

To test this equivalence, MC simulations of the four-state clock model were performed. The results for the magnetisation are plotted in Figure 5.15, and clearly illustrate that the data for the 2d Ising model falls exactly on top of that of the clock model, provided the energy scale is halved.

Another generalisation of the Ising model is the Potts model, which is defined by the Hamiltonian

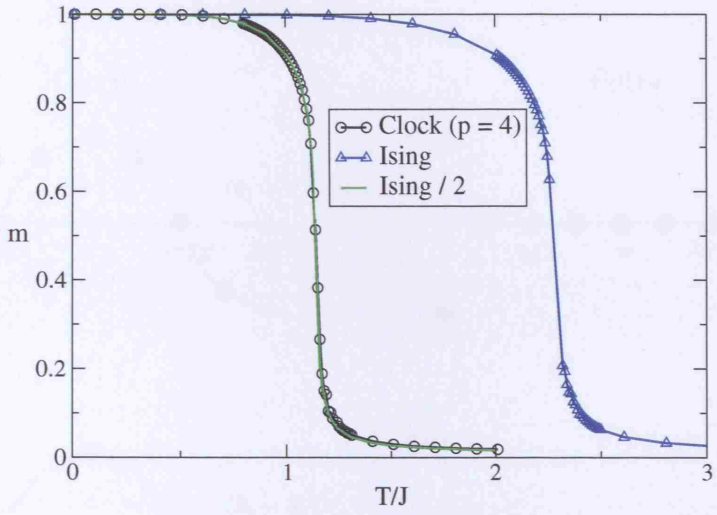

Figure 5.15: Comparison of the four-state clock model and the Ising model. By changing the temperature scale of the Ising model by a factor of $\frac{1}{2}$, the magnetisation curves (and indeed all other thermodynamic quantities) are identical to each other for both models.

$$\mathcal{H} = -J \sum_{\langle i,j \rangle} \delta\left(\theta_i, \theta_j\right). \tag{5.28}$$

δ is a Kronecker delta function so the energy of the neighbouring spins is $-J$ if they are in the same state and zero otherwise. With increasing p this model remains a two level system, but becomes characterised by a large degeneracy. This is in contrast to the clock model, in which the energy is given by the vectorial product of the two neighbouring spins.

Despite their obvious difference, illustrated clearly in Figure 5.16, there is a degree of confusion in the literature between the clock and the Potts models[b], possibly due to the fact that in his original paper [80] Potts investigated both. In fact, for $p = 2$ and 3, the clock and Potts models are equivalent, and belong to the Ising and three-state Potts universality classes, respectively. For $p \geq 4$, however, the two models are different. With $p = 4$ the Potts model belongs to a universality class of its own, characterised by its own critical exponents [43], distinct from those of the four-state clock model, which belongs to the Ising universality class. With

[b]See for example Won *et al.* [266].

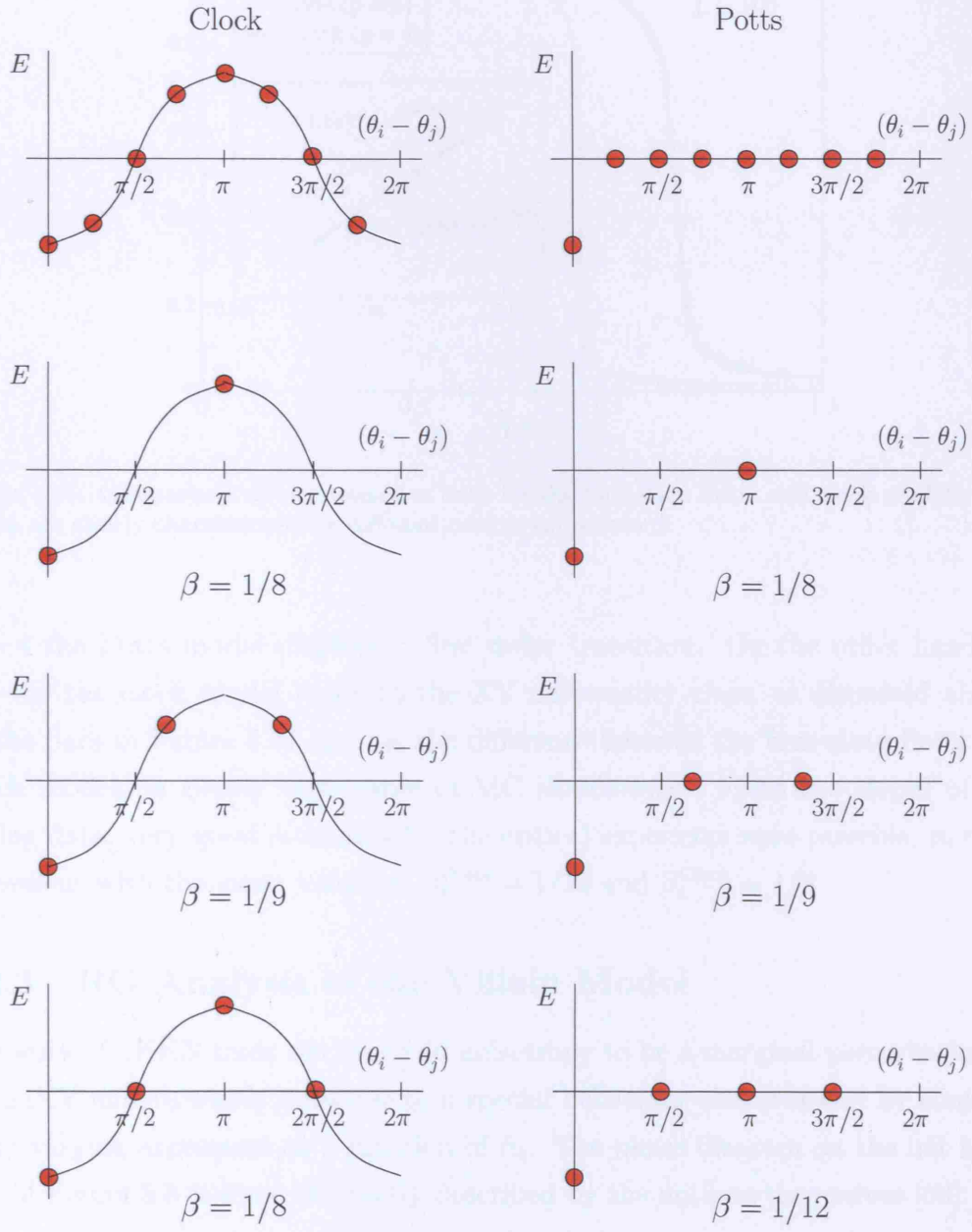

Figure 5.16: Comparison of the energy profiles for the clock and the Potts models. The former is characterised by a vectorial product between the spins, whereas the latter is characterised by a large degeneracy. For $p = 2$ and 3 it can be seen that the two models happen to be equivalent. For $p = 4$ this is not the case: the four-state clock model belongs to the Ising universality class whereas the four-state Potts model belongs to a universality category of its own.

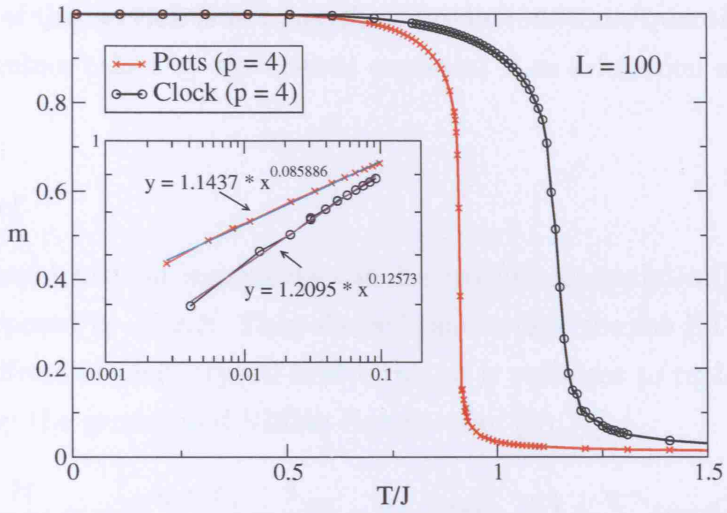

Figure 5.17: Comparison of magnetisation data for the four-state Potts and clock models. The curves are clearly characterised by different critical exponents β.

$p > 4$ the Potts model displays a first order transition. On the other hand, as $p \to \infty$ the clock model tends to the XY universality class, as discussed above. As the data in Figure 5.17 attests, the difference between the four-state Potts and Clock models is clearly observable in MC simulations. From the slopes of the log-log data, very good estimates for the critical exponents were possible, in close agreement with the exact values of $\beta_4^{\text{Potts}} = 1/12$ and $\beta_4^{\text{Clock}} = 1/8$.

5.2.3 RG Analysis of the Villain Model

The work of JKKN finds the four-fold anisotropy to be a marginal perturbation to the 2dXY model, which gives rise to a special behaviour characterised by continuously varying exponents as a function of h_4. The phase diagram on the left hand side of Figure 5.8 is most succinctly described by the authors themselves [68]:

> All three lines display continuously variable critical exponents with a conventional phase transition across $T_c(h_4)$. Although the exponent $\eta(h_4)$ remains fixed at $\frac{1}{4}$ to lowest order in h_4, we find that the correlation length exponent $\nu(h_4)$ diverges, $\nu(h_4) \sim 1/|h_4|$, as $h_4 \to \infty$.

The objective of this section is to make these predictions more quantitative, and to calculate the values taken by the critical exponent β as a function of crystal field strength h_4.

Villain Model

The non-universal critical exponents can be calculated analytically within the framework proposed by JKKN. They showed that to describe the KT phase transition and the effects of weak crystal field terms, it is sufficient to replace the 2dXY Hamiltonian by the generalised Villain Hamiltonian [68, 72]

$$\begin{aligned}\frac{\mathcal{H}}{k_BT} = -K\sum_{\langle i,j\rangle}\left(1-\frac{1}{2}(\theta_i-\theta_j-2\pi m_{ij})^2\right)+\sum_i ipn_i\theta_i \\ +\ln(y_0)\sum_i S_R^2+\ln(y_p)\sum_i n_i^2.\end{aligned} \tag{5.29}$$

where $K = J/k_BT$. The first term is recognisable as the HXY model (2.82), in which the integers m_{ij} maintain the periodicity of the original XY Hamiltonian for rotations over an angle 2π. S_R is a directed sum of integers m_{ij} around a square plaquette of four sites centred at $\vec{R}$: $S_R = m_{41} + m_{12} - m_{32} - m_{43}$, takes the values $S_R = 0, \pm1, \pm2\ldots$ and is therefore a quantum number for a vortex of spin circulation centred on the dual lattice site $\vec{R}$. y_0 is a small parameter related to the chemical potential μ and fugacity y for the creation of a vortex anti-vortex pair on neighbouring dual lattice sites: $y = y_0\exp(-\beta\mu) \approx y_0\exp(-\pi^2K/2)$. In the original Villain model $y_0 = 1$ but it is introduced here as a phenomenological small parameter which is renormalized in the subsequent flows. Similarly, y_p is a fugacity for a locking process of spins along one of the p-fold field directions with integer n_i being a measure of the strength of this process at site i.

The justification for using the generalised Villain model relies on a duality theorem, which holds provided the term $\exp[h_p\cos(p\theta)]$ in the partition function of the XY model can be replaced by a periodic function with the same symmetry [72]:

$$e^{h_p\cos[p\theta(\boldsymbol{r})]} \longrightarrow \sum_{n(\boldsymbol{r})=-\infty}^{\infty} e^{ipn(\boldsymbol{r})\theta(\boldsymbol{r})}e^{(\ln y_p)n^2(\boldsymbol{r})}. \tag{5.30}$$

Since terms with $|n(\boldsymbol{r})| > 1$ contribute negligibly for small y_p, it is possible to make the identification

$$y_p \approx \frac{1}{2} h_p \tag{5.31}$$

in this limit. By invoking the hypothesis of universality, whereby the precise form of the interaction should be immaterial provided the correct symmetry is maintained, Villain has argued [72] that no important physics is lost by considering the analytically more tractable Hamiltonian (5.29), which has the additional advantage of allowing vortices to be introduced explicitly into the problem, separately from spin waves.

Thus, for weak crystal fields $y_p = \frac{1}{2} h_p$, reproducing the field contribution to the partition function of the 2dXY model to leading order in y_p. On the other hand, for strong fields $y_p \to 1$, and (5.29) transforms into a discrete p-states model. However, it must be stressed that this model is not the p-state clock model: although the Villain model maintains the global rotational symmetry, it destroys the local $O(2)$ symmetry of the pair interaction. This results in the neighbouring spins orientated perpendicularly having an energy less than half that of antiparallel spins, which in turn means the ordered state has lower lying excitations than the corresponding clock model. The difference between the two models is highlighted in Figure 5.18, and makes it clear that for quantitative studies of the strong field limit one should use Hamiltonian (5.14) rather than (5.29).

With y_p set equal to zero, a real space renormalization analysis for the spin-spin correlation functions resulting from (5.29) leads to the Kosterlitz RG flow equations (2.78) and (2.79) for an effective coupling constant K_{eff} and vortex fugacity y. For $K_{\text{eff}} = 2/\pi$ and $y = 0$, the flows yield the KT transition. In the presence of a p-fold field the flow equations are modified and a third equation is generated[c].

[c] Note that in the original paper [68], JKKN omit a factor of 2 in a number of their expressions. This is pointed out in a list of errata [267].

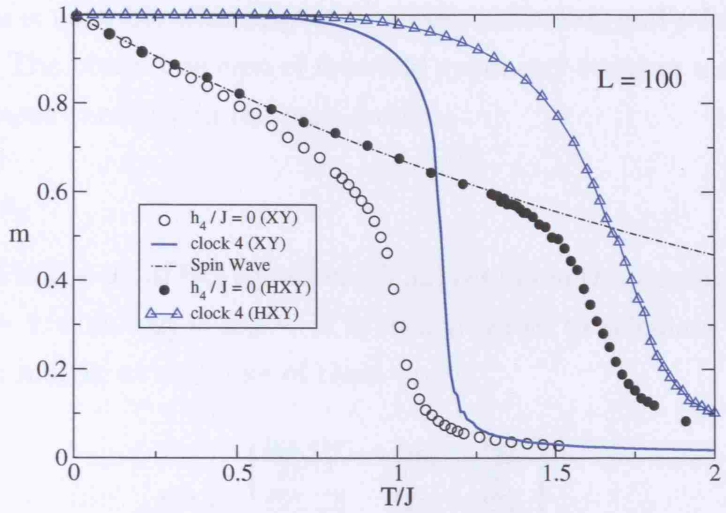

Figure 5.18: Comparison between the XY and HXY (Villain) models in the $h_4 \to \infty$ limit.

$$(K^{-1})' = K^{-1} + \left(4\pi^3 y_0^2 e^{-\pi^2 K} - \frac{1}{2}p^2 y_p^2 K^{-2} e^{-p^2 K^{-1}/4}\right)\ln(b), \tag{5.32a}$$

$$y_0' = y_0 + (2 - \pi K) y_0 \ln(b), \tag{5.32b}$$

$$y_p' = y_p + \left(2 - \frac{p^2}{\pi}K^{-1}\right) y_p \ln(b), \tag{5.32c}$$

where b is the scale factor and where the equations are valid as $b \to 1$. These recursion relations imply that y_p will grow under renormalization below a temperature given by $p^2/(4\pi^2 K) \approx 2\pi$, which is consistent with the fact that the magnetisation locks into one of the p directions favoured by the perturbation. There is a series of temperatures

$$\frac{2}{\pi} \leq K_{\text{eff}} \leq \frac{p^2}{8\pi}, \tag{5.33}$$

in which only Gaussian spin waves are present, and *both* the symmetry breaking perturbation and vortex excitations are unimportant. This intermediate phase is characterised by algebraically decaying correlations, and upon substituting (5.33) into (2.67) it is found that $\eta(T)$ ranges from $\eta = \frac{1}{4}$ to $\eta = 4/p^2$, as the temperature is decreased. Evidently this stability region is only present in systems with $p > 4$,

and the system is unstable with respect to vortex unbinding and p-fold fields when $p = 1$, 2, or 3. The borderline case of four-fold symmetry requires more study, and is considered more carefully in the next section.

Influence of h_4

Inserting $p = 4$ in the set of RG equations (5.32) results in the identification of fixed points at $K^* = 2/\pi$ and $y_0^* = \pm y^{*4}$. It is then possible to calculate the linearised transformation matrix at each one of these points

$$M^* = \begin{bmatrix} \frac{\partial (K^{-1})'}{\partial K^{-1}} & \frac{\partial y_0'}{\partial K^{-1}} & \frac{\partial y_4'}{\partial K^{-1}} \\ \frac{\partial (K^{-1})'}{\partial y_0} & \frac{\partial y_0'}{\partial y_0} & \frac{\partial y_4'}{\partial y_0} \\ \frac{\partial (K^{-1})'}{\partial y_4} & \frac{\partial y_0'}{\partial y_4} & \frac{\partial y_4'}{\partial y_4} \end{bmatrix}, \tag{5.34}$$

where the asterisk denotes that the matrix is evaluated at the fixed point. It is found that [268]

$$M^* = \begin{bmatrix} 1+\alpha & \delta & -\delta \\ \gamma & 1 & 0 \\ -\gamma & 0 & 1 \end{bmatrix}, \tag{5.35}$$

with

$$\alpha = 16\pi^2(2\pi - 1)\tilde{y}^2 e^{-2\pi} \ln(b) \tag{5.36a}$$

$$\gamma = 8\pi^3 \tilde{y} e^{-2\pi} \ln(b) \tag{5.36b}$$

$$\delta = \frac{4}{\pi}\tilde{y} \ln(b), \tag{5.36c}$$

and where $y_0 = y_4 = \tilde{y}$. Solving for the eigenvalues it is found that

$$\lambda = 1, 1 + \frac{\alpha}{2} \pm \frac{1}{2}\sqrt{\alpha^2 + 8\gamma\delta}. \tag{5.37}$$

Upon writing $\lambda = b^\sigma$, the three scaling exponents corresponding to the RG flow are extracted. One relevant exponent is found, which is interpreted as $\sigma_1 = 1/\nu$, the index which takes the coupling constant away from the critical value at the now regular second order phase transition. An irrelevant variable σ_2 is also found,

which is interpreted as driving the vortex fugacity to zero. Finally, a marginal variable, σ_3, is found, which corresponds to the scaling exponent of the four-fold crystal field. Taking $h_4 = 0$, all eigenvalues become marginal in a manner consistent with the particular scaling properties of the 2dXY model. In the small field limit, $\sigma_1 = 4\pi e^{-\pi} h_4$, $\sigma_2 = 0$ and $\sigma_3 = -4\pi e^{-\pi} h_4$. This gives the non-universal correlation length exponent $\nu \approx 1.8/h_4$. In the strong field limit, $y_4 = 1$ yields $\nu \approx 0.47$, which should be compared with the exact result for the Ising model, $\nu = 1$. The agreement is not good, as might be expected given the distortion of the four-fold interaction imposed by the Villain model. This result further emphasises the fact that a quantitative calculation for the strong field limit requires a different starting Hamiltonian to Equation (5.29).

Calculation of the Critical Exponents

To calculate β from the scaling relations, a second relevant scaling exponent, or critical exponent, is required. In this case the anomalous dimension exponent η may be calculated directly from the correlation function. At the KT transition $\eta = 1/4$, giving the universal jump in the spin stiffness, $K = 2/\pi$. On the basis of the weak scaling properties of the 2dXY model discussed in page 82, the finite size scaling exponent $\beta/\nu = 1/8$ is a universal number despite the fact that the true β and ν are not defined. Furthermore, a striking result in the presence of a four-fold field is that η remains unchanged to lowest order in h_4. Therefore, since $\eta = 1/4$ also for the two-dimensional Ising model, it is reasonable to assume $\eta = 1/4$ and $\beta/\nu = 1/8$ for all values of h_4 [174, 269].

The Villain model therefore predicts a range of non-universal magnetisation exponents ranging from

$$\beta \approx \frac{1}{8}\left(\frac{1.8}{h_4}\right) \tag{5.38}$$

for weak field, to $\beta = 1/8$ in the strong field limit. For weak crystal fields, β is large and the magnetisation would develop very slowly with temperature below the transition, if this were the dominant scaling. However, as shown numerically, there is no crossover for accessible system sizes and the large β values are masked by

the finite size magnetisation of the 2dXY model itself. It is only for larger values of h_4 that one can expect to see non-universal exponents for $1/8 < \beta(h_4) < 0.23$, confirming both numerical and experimental observations above. Putting $\beta(h_4) = 0.23$ in Equation (5.38) gives $h_4/J \approx 1$, a ratio of order unity, in agreement with the above general arguments, and comparable with the numerics, where the change of regime occurs for $h_4/J \approx 0.5$.

5.2.4 Critical Isotherms

The magnetisation-field exponent δ is related to the anomalous dimension exponent η through the hyperscaling relation

$$\delta = \frac{d+2-\eta}{d-2+\eta}, \tag{5.39}$$

which in two dimensions implies $\delta = 4/\eta - 1$. From Equation (2.67) it follows that the spin wave magnetisation (2.65) may be rewritten as

$$M(N,T) = \left(\frac{1}{aN}\right)^{\eta(T)/4} = \left(\frac{1}{aN}\right)^{1/(\delta(T)+1)}. \tag{5.40}$$

i.e. δ is related to the spin wave stiffness by $\delta = 8\pi K_{\text{eff}} - 1$. Indeed, this relation has been used in order to precisely locate T^* from measurements of $\delta(T)$ in Rb_2CrCl_4 [270, 271], since $\delta(T^*) = 15$, by definition.

To gain a more complete picture of the scaling behaviour of the XYh_4 model, it is therefore informative to follow the behaviour of $\delta(T)$, and hence $\eta(T)$, as a function of the strength of the four-fold anisotropy. The plot 5.19(a) displays magnetisation versus field data collected from Monte Carlo simulations on a pure XY model of size $N = 1032$. From the procedure described in Section 2.4.2, $T^*(L = 32) = 0.943$. At this temperature, measurement of the slope of the isotherm in the log-log plot 5.19(b) yields an estimated value $\delta = 14.3$, which is consistent with the value predicted by theory, $\delta = 15$. On a finite size XY model, the effective Curie temperature is shifted logarithmically with system size, $T_c(L) - T_{KT} \sim \frac{1}{\ln^2(L)}$ (*c.f.* Equation (2.80)). As δ decreases continuously through the transition, at $T_c(L = 32) = 1.078$, which is in the vicinity of the peak in the susceptibility χ, a much lower value $\delta = 10.3$ is obtained. In turn this implies $\eta \sim 0.35$, a number

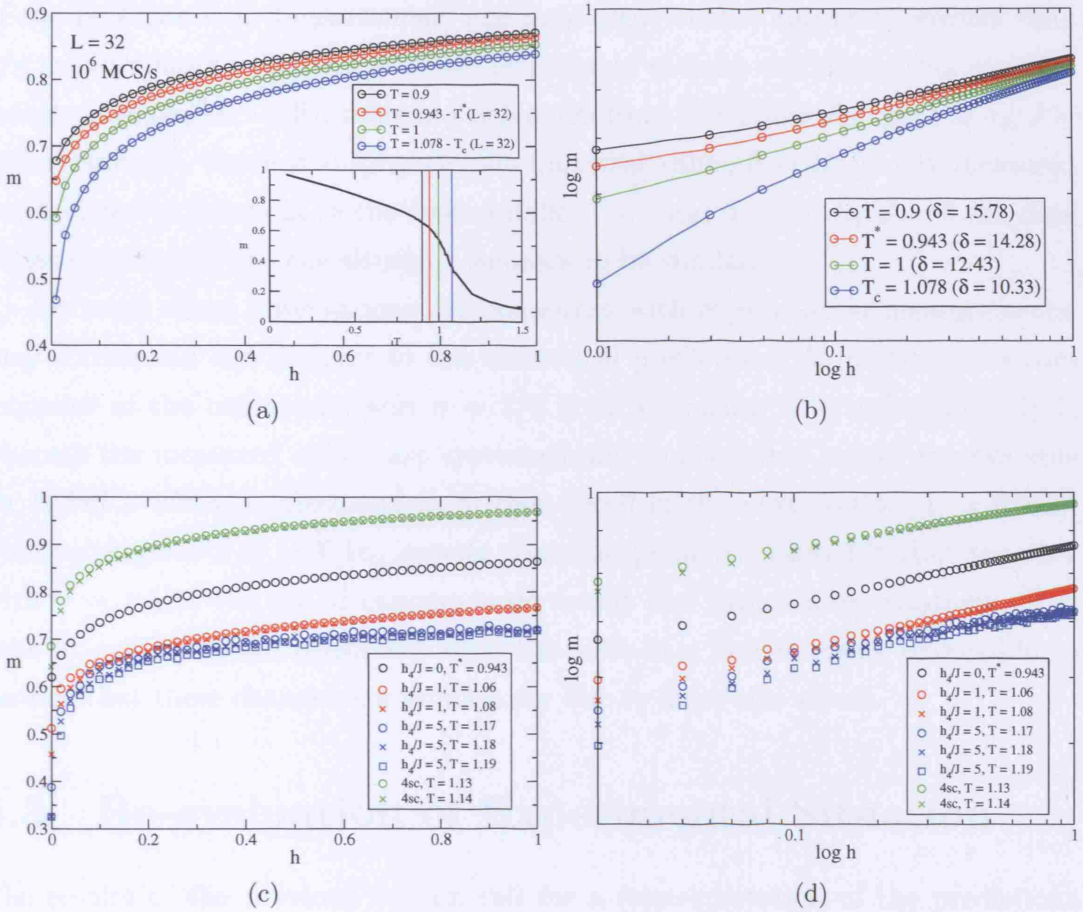

Figure 5.19: Magnetisation-field Monte Carlo data for a 2dXY system of $N = 1032$ spins. Plots (a) and (b) display data for the pure 2dXY Hamiltonian in linear and logarithmic scales, respectively. Plots (c) and (d) display isotherms for the 2dXY model in the presence of different crystal fields.

considerably in excess of the value $\eta = 1/4$ expected at the thermodynamic limit, where $T_c = T^* = T_{KT}$.

In the limit of the four-state clock (Ising) model, on the other hand, an isotherm with slope $\sim 1/15$ is only measured in the vicinity of the critical temperature $T_c(L = 32) = 1.14$ (plots 5.19(c) and 5.19(d)), which is consistent with the truly ordering nature of the 2d Ising phase transition. In this regime the finite size shift is a more conventional power law, $T_c(L) - T_c \sim \frac{1}{L^{1/\nu}}$, as discussed in Section 2.2.4.

In the presence of h_4, the finite size shift of the XY model is seen to cross over to that of the Ising model. Nevertheless for small fields ($h_4/J \lesssim 0.5$), $\nu \sim 1/h_4$ is large, and finite size effects remain dominant, consistent with the marginal nature

of the perturbation. In particular, one may argue that η appearing greater than 1/4 in experiment is an indication of the presence of finite size effects. For stronger anisotropies ($h_4/J > 0.5$), there is a departure from 2dXY-like scaling. For $h_4/J = 1$, for example, where β displays a non-universal value, $\delta = 15$ is only measured much closer to the peak in the susceptibility, *i.e.* near T_c. For $h_4/J = 5$ the data is less convincing, but the situation appears to be similar.

Although these observations are consistent with experimental measurements, they correspond less directly to the theoretical predictions. In particular, a consequence of the universal result $\eta = 1/4$ is an unusually large value for $\nu \geq 1$, whereas the measured values are systematically smaller than unity. For example for K_2FeF_4, which is discussed in further detail in the next section, $\nu = 0.9(2)$. This value gives $\beta/\nu = 0.16$, greater than the predicted ratio 1/8, but together with $\gamma = 1.5(5)$ the set of exponents do satisfy the hyperscaling relations. The shift in ν is therefore consistent with the shift in η and it seems reasonable to assume that these changes are uniformally due to finite size effects.

5.3 Re-evaluation of Experimental Situation

The results of the previous section call for a reinterpretation of the predictions made by JKKN regarding the behaviour of the XY model with four-fold crystal fields. The non-universal exponents predicted by their theory are in fact bounded by the Ising and XY limits, which in practical terms means that the measured exponent β lies in the range 0.125 – 0.23. In addition, the extraordinary scaling properties of the XY model ensure a stability region in which pure XY critical behaviour persists, despite the presence of weak fields. Non-universal exponents are only observable with much stronger anisotropies. Experimental evidence for this strong field–weak field divide comes from making head to head comparisons between systems classified in Chapter 4.

5.3.1 Layered Magnets

One of the advantages of layered magnets is that in many cases their properties have been experimentally investigated to a high degree of precision. Hence, a *quantitative*

head to head comes from a comparison between the quasi two-dimensional $S = 2$ ferromagnet Rb_2CrCl_4 [256] and the $S = 2$ antiferromagnet, K_2FeF_4 [105]. While the ferromagnet shows the characteristics of the pure XY universality class, the antiferromagnet has non-universal exponents, with $\beta = 0.15$, consistent with XYh_4 behaviour. In both cases the spatial anisotropy of the exchange, with the interplane coupling J much bigger than the intra-plane coupling J', gives rise to an extended temperature range with two-dimensional critical fluctuations. A detailed analysis of both materials [105, 256] yields a clear picture of the spins being confined to the XY plane by a crystal field D which breaks the O(3) spin symmetry. There is also an in-plane crystal field e with four-fold symmetry. For the purposes of fitting the spin wave spectra, both Hutchings *et al.* [256] and Thurlings *et al.* [105] applied a low temperature approximation to the Hamiltonian (5.12), which involves omitting the negligible quartic axial anisotropy, and decoupling the quartic in-layer anisotropy into an effective quadratic term:

$$\begin{aligned} \frac{1}{2}e(S_{i+}^4 - S_{i-}^4) &= 6e\langle (S^x)^2 - (S^y)^2 \rangle [(S_i^x)^2 - (S_i^y)^2] \\ &= E[(S_i^x)^2 - (S_i^y)^2]. \end{aligned} \tag{5.41}$$

The neutron scatterring data (see Figure 5.20) may then fitted to the effective Hamiltonian

$$\mathcal{H} = -J \sum_{\langle i,j \rangle} \mathbf{S}_i \cdot \mathbf{S}_j + D \sum_i (S_i^z)^2 + E \sum_i [(S_i^x)^2 + (S_i^y)^2]. \tag{5.42}$$

The fitted parameters J, D and E can be used to derive estimates for e and h_4 in Equations (5.12) and (5.13). The results are summarised in Table 5.2.

For both K_2FeF_4 and Rb_2CrCl_4, the values of h_4/J derived from e/J are much smaller than the values required to lie in the non-universal regime of Figure 5.11. Hence, at first sight it seems that both compounds should fall into the weak field category. Although this is true for Rb_2CrCl_4, the observed critical exponents for K_2FeF_4 are clearly inconsistent with this scenario. An explanation for the anomalous behaviour of the antiferromagnet must therfore be included if the theoretical description is to be made complete. A plausible mechanism which leads to a larger effective h_4, and consequently non-universal critical behaviour, has been identified

Table 5.2: Main parameters for K_2FeF_4 and Rb_2CrCl_4, as determined from experiment [105, 256]. The theoretical values of the spin wave gaps Δ_1 and Δ_2 have been determined from the expressions (5.43) and (A.22).

	K_2FeF_4	Rb_2CrCl_4
S	2	2
J(K)	-15.7	15.12†
D(K)	5.7	1.12
E(K)	-0.49	0.062
D/JS^2	0.363	0.07
e/JS^2	-0.0024	0.02
h_4/JS^2‡	-0.0094	0.0026
Δ_1(K)	71(2)	-
Δ_2(K)	24(4)	0.638(70)
Δ_1(K) (theoretical)	75.68	-
Δ_2(K) (theoretical)	31.36	1.49
β	0.15(1)	0.230(2)

using spin wave theory, as follows.

Antiferromagnetic Case

The spin wave analysis reported in Appendix A shows that the simple Heisenberg antiferromagnet has two degenerate spin wave branches, which become dispersionless at long wavelength. Applying the crystal fields D and E lifts the degeneracy of the branches and introduces two gaps for the spin wave frequencies at the magnetic Brillouin zone centre. For the case $E \ll D$ one finds

$$\Delta_1 = 2S\sqrt{zDJ} \tag{5.43a}$$

$$\Delta_2 = 2S\sqrt{2zEJ}. \tag{5.43b}$$

The first branch, with gap Δ_1, corresponds to the out-of-plane fluctuations and the

†To ensure a consistent definition of J with the data for K_2FeF_4, the parameter reported here for Rb_2CrCl_4 has been multiplied by a factor of two with respect to that of Hutchings *et al.* [256].

‡To compare these results with simulations of systems with unit spins, values of h_4/JS^2 are quoted, which are equivalent to h_4/J in the simulations.

second, with Δ_2, to in-plane fluctuations. The gaps open rapidly with perturbation strength: for K_2FeF_4 it is found from experiment that $\Delta_1 = 71.04$ K and $\Delta_2 = 24$ K [105]. Δ_1 is larger than the transition temperature, $T_N = 63$ K $\approx JS^2$, such that out-of-plane spin fluctuations are largely frozen out over the whole of the ordered phase. The spins will therefore be truly confined to the plane with an effective crystal field, h_4, of the order of Δ_2. This gives $h_4 \sim JS^2/3$ (or $h_4/J \sim 0.3$) which is the right order of magnitude to fall into the strong field category. One can further speculate that quantum fluctuations for the in-plane branch and non-linear corrections to the spin wave calculation will renormalize it to even higher values. In this case, K_2FeF_4 would clearly be a candidate for non-universal criticality characteristic of the XYh_4 model. In this respect, it is noteworthy that a 'spin dimensional reduction' due to quantum suppression of fluctuations has recently been observed in quantum Monte Carlo simulations with a Hamiltonian similar to (5.42) [272].

Ferromagnetic Case

In the case of the ferromagnet Rb_2CrCl_4, the field D changes the dispersion relation $\omega(q)$ at small wave vector from quadratic to linear in q. It does not, however, introduce a gap at zero wave vector. Upon the application of the second crystal field, a gap is opened, which varies as $\sqrt{DE}$, and is hence an order of magnitude smaller than those appearing for the antiferromagnetic system. This difference is emphasised by the experimental data shown in Figure 5.20. The effective field h_4 appearing in (5.14) is therefore small for Rb_2CrCl_4, which is perfectly consistent with the observation of the 2dXY critical behaviour in this case.

Criterion for Onset of Non-Universality

The above results may also be obtained using the standard Holstein–Primakoff approach [273]. In either case, the main conclusion is that the zero wave vector spin wave gap is determined by the geometric mean of E and D for the ferromagnet, and the geometric mean of E and zJ for the antiferromagnet. Since, $E \ll D \ll J$, it follows that $\Delta_2^{FM} \ll \Delta_2^{AFM}$, explaining why fluctuations re-establish XY symmetry in ferromagnetic Rb_2CrCl_4 but not in antiferromagnetic K_2FeF_4. On the basis of this argument, one is also led to the prediction that systems falling into the

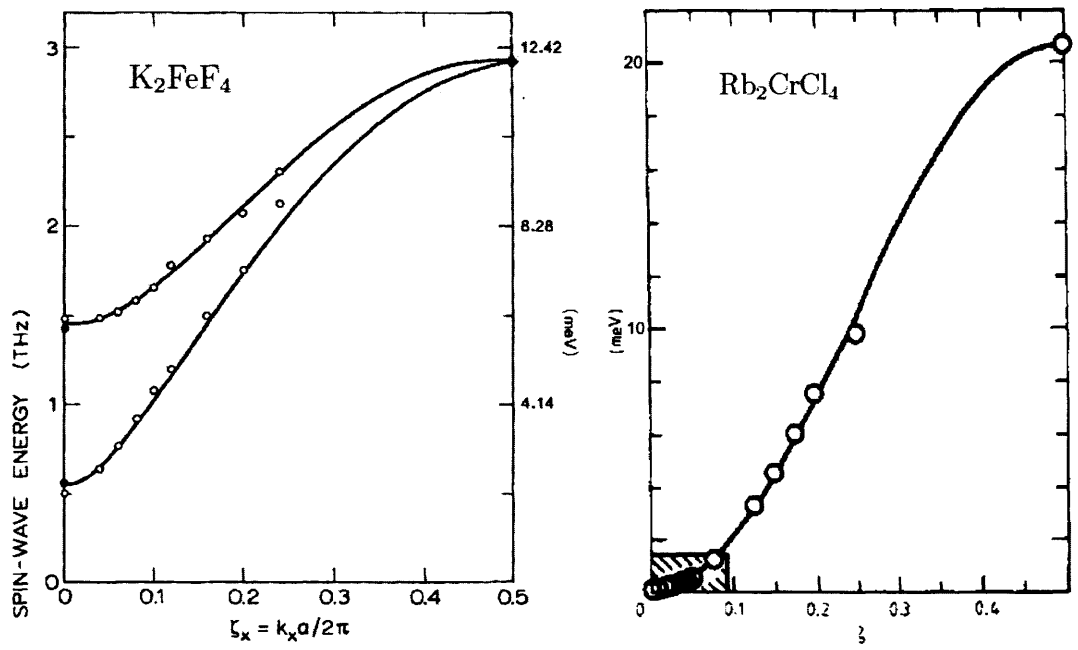

Figure 5.20: Spin wave energy dispersion in K_2FeF_4 and Rb_2CrCl_4 along the in-plane direction, as measured with inelastic neutron scattering. The data for K_2FeF_4 and Rb_2CrCl_4 was measured at 4.2 and 20 K, respectively. The points are experimental and the curves calculated from the best fit of the Hamiltonian (5.42). Note the entirely different energies for the two compounds at small vectors (1 THz $\simeq$ 4.14 meV). After Thurlings *et al.* [105] and Hutchings *et al.* [256].

non-universal window of critical exponents will mostly be antiferromagnetic.

5.3.2 Ultrathin Magnets

The critical behaviour of ultrathin magnets is also consistent with the mechanism discussed in this Thesis. Many of the systems listed in Table 4.2 possess four-fold symmetry, and their measured order parameter exponents have in the past been explined as non-universal (see for example the work of Rau and Robert [274, 275]). This direct interpretation of the work of JKKN cannot be correct, however, since the prediction $\beta \propto J/h_4$ would give, over many experiments, an unbounded distribution of exponents β, extending to infinity for limitingly small crystal fields. It is clear from the observations in Section 4.1.3 that in reality there is a clustering of values at $\beta \sim 0.23$. In light of the present work, these may be classified into the weak field regime of the XYh_4 class, which is a consequence of the unique scaling

properties of the 2dXY model and the marginal nature of the h_4 perturbation.

5.3.3 Structural Transitions at Surfaces

Oxygen absorbed onto Mo(110) [228] or W(110) [229] and hydrogen on W(110) [224] have both been claimed to fall into the XYh_4 class, representing four-fold equivalents of the two stage melting process for hexagonally coordinated systems [236]. Electron hybridisation between absorbed and substrate particles will result in the generation of electronic dipoles aligned perpendicularly to the (110) surface. The resulting $1/r^3$ interaction between the particles is repulsive and of sufficiently long range to ensure crystallisation into a square lattice structure in the absence of a substrate. The (110) surface provides a substrate potential of the same topology and which can be made commensurate with the free standing array by tuning the absorbate density, the clearest example being the (2×2) lattice structure. The result is claimed to be the XYh_4 universality class and the measured exponent, $\beta = 0.19$ [228,229], is, in light of the current work, seen to be consistent with this. The same should, in principle, be true for the (2×2) ordering transition for hydrogen on W(110), but the measured β is consistent with the pure XY model [224]. Hydrogen being so much lighter that oxygen, larger zero point fluctuations should make the substrate potential less effective at pinning the crystal, putting it in the category of systems with a weak field h_4, consistent with the experimental observation.

Another Mechanism

A mechanism which has been put forward in order to account for the observed behaviour of adsorbed monolayers on cubic (100) surfaces occurs through the Ising antiferromagnet with nearest and next nearest neighbours J_{nn} and J_{nnn} (Figure 5.21(a)). Provided $J_{nnn}/J_{nn} > 0.5$, this model undergoes a transition to a layered antiferromagnetic structure, belonging to the XYh_4 class [276]. This becomes evident if one considers that the ground state of this system consists of ferromagnetically aligned rows of up spins alternating with ferromagnetically aligned rows of down spins. Since there are two ways to achieve this ordering (Figures 5.21(b) and 5.21(c)), a degeneracy is present which should be considered as the two compo-

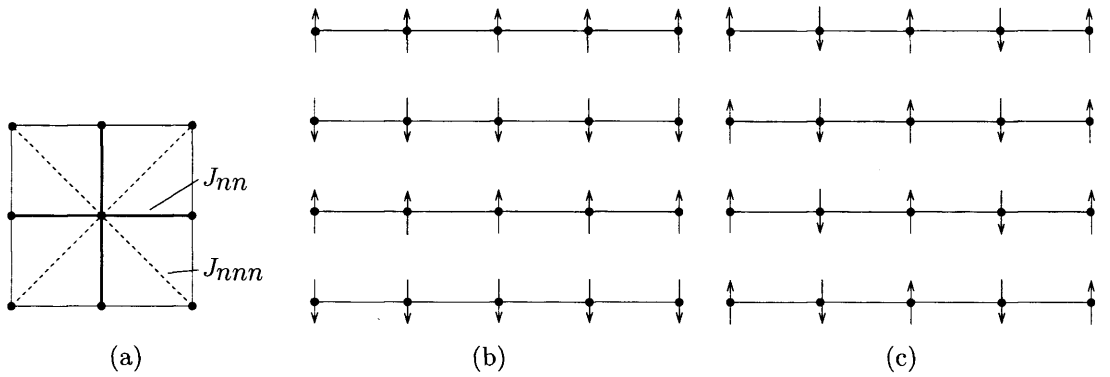

Figure 5.21: Ising lattice with nearest and next-nearest neighbour interactions J_{nn} and J_{nnn}. (b,c) Spin arrangements in the antiferromagnetic structure, in which ferromagnetically aligned rows of up spins alternate with ferromagnetically aligned rows of down spins. These rows can be oriented in either the x or the y direction.

nents of an XY order parameter. Landau and Binder [277] have studied the critical behaviour of this model using the same numerical techniques adopted in Section 5.2.1, and have confirmed a non-universal behaviour typical of the XYh_4 class.

5.4 Discussion

This chapter has examined how long range order may arise in two-dimensional spin systems with continuous spin symmetry. An analysis of the pure Heisenberg model finds its peculiar scaling properties to be consistent with previous studies in the literature [250, 253]. Despite certain similarities with the XY model, most notably the low temperature behaviour given by the spin wave expression (5.3), the Heisenberg model does not undergo a phase transition in the thermodynamic limit, and does not exhibit an effective critical behaviour akin to that observed in the finite size 2dXY model. Long range order is invariably found to be induced through any mechanism which destroys the rotational invariance of the Heisenberg spin, such as single ion anisotropy. The spins may either be constrained to lie perpendicular to the plane of the lattice (uniaxial symmetry) or parallel to it (planar symmetry). The former scenario gives rise to a conventional second order phase transition and critical behaviour belonging to the Ising universality class. The latter gives rise to a KT transition [61] to a peculiar state of quasi long range order. However,

on a finite lattice a spontaneous magnetisation is possible, and furthermore it is characterised by an exponent $\tilde{\beta} \simeq 0.23$. This acts as a signature of 2dXY behaviour in experiment, and indicates that the physics of many layered and ultrathin magnets is not dictated by predictions at the thermodynamic limit [77].

The main question explored has been how higher order contributions to the Heisenberg Hamiltonian influence the behaviour of the model in the XY regime. This was achieved by considering the XY model in the presence of symmetry breaking crystal fields. The XYh_2 and XYh_6 models do not define new universality classes, and belong to the Ising and XY class, respectively. The XYh_3 model belongs to the three-state Potts universality class. Although this is distinct from the Ising and XY classes, three-fold symmetry breaks time reversal symmetry, and consequently does not occur in simple magnetic systems. Much more common is the four-fold symmetry of the XYh_4 model, which exhibits a far richer behaviour involving continuously changing critical exponents as a function of h_4. The detailed numerical and analytical analysis presented in this chapter has shown that in practice the regime in which β is non-universal is restricted to an envelope of values $0.125 \geq \beta \geq 0.23$, as illustrated in Figure 5.11, ruling out the relevance of the four-state Potts class. This finally explains the histogram of measured β values shown in Figure 4.19. Furthermore, on the basis of the RG calculation it is predicted that the exponent η remains constant at 0.25. However, experimental values are systematically found to be higher due to the finite size effects associated with the XY model, both in zero and in weak field. The actual values of the four-fold crystal field that occur in magnetic systems are, at first sight, too small to take any system away from the XY limit. However, a mechanism has been identified in antiferromagnets whereby the four fold field is effectively amplified by quantum confinement of the spins to the easy plane.

In light of the work by Lapilli *et al.* [263], the links and similarities between the XY and the clock models have also been investigated. The fact that, above a certain temperature T_{eu}, *discrete* p-state clock models with $p > 4$ produce identical thermodynamics to the *continuous* XY model, provides an example of extended universality. The restoration of continuous spin symmetry observable in XYh_p systems with $p \geq 4$ may be interpreted as the remanence of this phenomenon.

Chapter 6

Competing Long and Short Range Interactions

This chapter addresses the question of competing length scales in spin models. Specifically, the aim is to understand the influence of the dipolar interaction (1.8) in Heisenberg spin systems using the following Hamiltonian

$$\mathcal{H} = -J \sum_{\langle i,j \rangle} \mathbf{s}_i \cdot \mathbf{s}_j \qquad \text{Exchange} \qquad (6.1a)$$

$$- D \sum_i (s_i^z)^2 \qquad \text{Single ion anisotropy} \qquad (6.1b)$$

$$+ g \sum_{i>j} \left[\frac{\mathbf{s}_i \cdot \mathbf{s}_j}{\mathbf{r}_{ij}^3} - \frac{3\,(\mathbf{s}_i \cdot \mathbf{r}_{ij})\,(\mathbf{s}_j \cdot \mathbf{r}_{ij})}{\mathbf{r}_{ij}^5} \right] \qquad \text{Dipolar interaction} \qquad (6.1c)$$

where J is the nearest neighbour exchange coupling, D is the strength of the single ion anisotropy, which depending on the sign favours either Ising ($D < 0$) or XY ($D > 0$) anisotropy, and g is the strength of the dipolar energy. Although generally very weak, the dipolar interaction decays slowly as a function of the distance between spins $\mathbf{r}_{ij}$, and consequently may dominate the physics of certain systems.

The complex nature of the Hamiltonian above raises a number of difficulties. The competition between the exchange and dipolar terms leads to an inherent frustration due to their having different ground states. The dipolar term represents

a remarkably difficult object to handle in itself, let alone in competition with other interactions. It is therefore helpful to construct an increasingly sophisticated model in steps, by analysing various limiting cases of the above Hamiltonian. The pure dipolar model is considered first, by setting $J = 0$ and $g \neq 0$, and by looking at its behaviour in the context of either discrete ($D \to -\infty$) or continuous ($D = 0$ or $D \to \infty$) spins. Furthermore, the two main features of the dipolar interaction, namely its long range nature and its anisotropy, are examined separately. Only subsequently is the competition between the dipolar term and the short range exchange term considered. In keeping with the rest of this work, the focus is on two-dimensional systems [278].

6.1 Long Range Interactions

Consider the simplified Hamiltonian

$$\mathcal{H} = -g \sum_{i,j} \frac{\mathbf{s}_i \cdot \mathbf{s}_j}{\mathbf{r}_{ij}^{\alpha}}, \tag{6.2}$$

in which the interaction decays isotropically with respect to the orientations of the spins. The special cases $\alpha = 0$ and $\alpha \to \infty$ correspond to equivalent neighbour models and nearest neighbour, respectively. The latter scenario corresponds to a model of infinite range weak interactions, and is shown in Appendix C to belong to the mean field universality class. For Boltzmann-Gibbs statistical mechanics to be applicable it is necessary that the potential (6.2) be integrable,

$$\int_1^{\infty} dr\ r^{d-1} r^{-\alpha} < \infty. \tag{6.3}$$

This implies that $\alpha > d$, which is of course the case for the scenario most pertinent in the present work, which has $d = 2$ and $\alpha = 3$. The full dipolar interaction is more complicated, since it is anisotropic

$$\mathcal{H} = -g \sum_{i,j} \frac{\mathbf{s}_i \cdot \mathbf{s}_j}{\mathbf{r}_{ij}^3} - \frac{3\,(\mathbf{s}_i \cdot \mathbf{r}_{ij})\,(\mathbf{s}_j \cdot \mathbf{r}_{ij})}{\mathbf{r}_{ij}^5}. \tag{6.4}$$

It is this anisotropy which renders the integral (6.3) conditionally convergent in

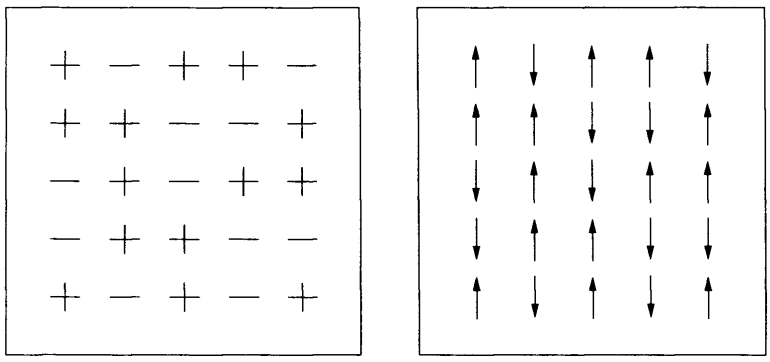

Figure 6.1: Symmetry breaking between the in-plane and out-of-plane orientation of the spins in the two-dimensional Ising model. Left: isotropic interaction (6.2). Right: anisotropic interaction (6.4).

three dimensions, as opposed to logarithmically divergent as would be the case if the interaction were isotropic.

6.1.1 Discrete Systems

For two-dimensional Ising systems with scalar spin s_i, the dipolar interaction breaks the symmetry between the in-plane and out-of-plane orientation of the spins because of the angle dependent term in (6.4). Consequently, if the axis of anisotropy is perpendicular to the plane of the lattice, the Hamiltonian (6.4) is equivalent to (6.2) with $\alpha = 3$. If, on the the other hand, the axis of anisotropy is parallel to the plane, then the two models are different. This situation is depicted in Figure 6.1.

Isotropic Decay

The critical behaviour of the spin models based on Equation (6.2) was considered within the framework of renormalization group theory in an influential paper by Fisher *et al.* [279]. As one of their central results emerged an explicit dependence of the upper critical dimension on the decay power of the interaction. It is convenient to employ the standard notation for the spin-spin interaction

$$g(r) = r^{-(d+\sigma)}. \tag{6.5}$$

According to the analysis in [279], universality classes are parameterised by σ,

identifying three distinct regimes: (a) A classical mean-field regime for $\sigma \leq d/2$ (*i.e.* the upper critical dimension is given by $d_{\rm uc} = 2\sigma$). (b) An intermediate regime $d/2 < \sigma < 2$, in which the critical exponents are continuous functions of σ. (c) A short range regime, in which the critical properties are those of the model with nearest neighbour interactions only. One therefore observes that for $d = 2$, the dipolar interaction lies in regime (a), close to the boundary with regime (b), and is consequently predicted to have classical exponents in the thermodynamic limit.

Numerical work on this model was until recently restricted to very small systems as a result of prohibitively large computational requirements. To illustrate this problem, the left hand plot in Figure 6.2 displays magnetisation data for the interesting case in which $d = 2$ and $\sigma = 1$, with all interactions ignored beyond a cutoff $r_{\rm cut}$ such that

$$g^{\rm trunc}(r) = \begin{cases} g(r) & r \leq r_{\rm cut} \\ 0 & r \geq r_{\rm cut}. \end{cases} \tag{6.6}$$

Setting $r_{\rm cut} = 1$ recovers the nearest neighbour Ising limit, whereas higher cutoffs result in qualitatively different curves with considerably higher transition temperatures and critical exponents which approach the mean field value of $\beta = 1/2$. If the potential is nonzero at $r \geq r_{\rm cut}$, truncation results in a systematic error in $g(r)$. One may correct for this by adding a tail contribution

$$g^{\rm tail}(r) = \int_{r_{\rm cut}}^{\infty} 4\pi g(r) r^{d-1}\, dr. \tag{6.7}$$

For $d = 2$ the integral is finite, therefore as $r_{\rm cut} \to \infty$, $g^{\rm tail} \to 0$. This is clearly observable in Figure 6.2, since with increasing cutoffs the magnetisation curves become increasingly hard to discern from each other.

One way to monitor the crossover between the two regimes is to follow the behaviour of the Binder cumulant defined by (5.15) as a function of $r_{\rm cut}$. At the critical temperature $T_{\rm c}$, the amplitude ratio is known exactly for the mean field case, $U_L = 0.275\ldots$ [280] (see Appendix C), and to a high degree of accuracy in the 2d Ising case, $U_L \simeq 0.609$ [281]. These values are indicated by the horizontal lines on the right hand graph in Figure 6.2. It is clear that for increasing cutoffs,

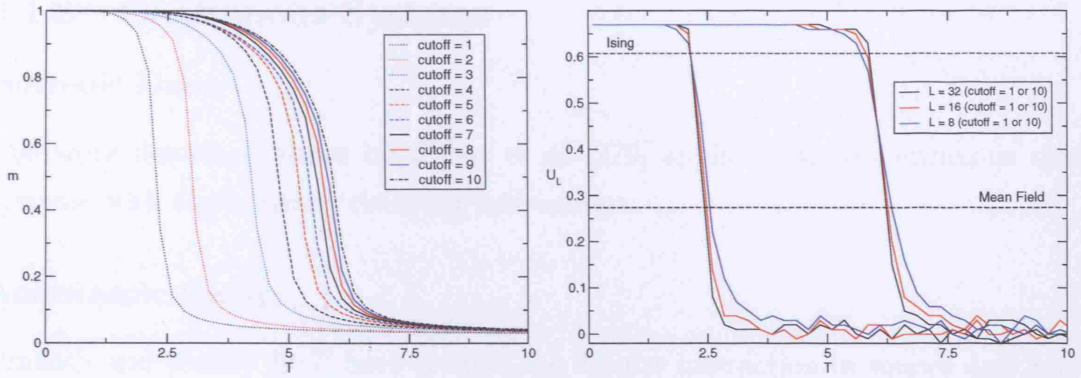

Figure 6.2: Effects of the increasing range of interaction (6.5) with $d = 2$ and $\sigma = 1$, for different cutoffs. Left: magnetisation curves. Right: Binder cumulants. In both plots an approach to mean field-like behaviour is clearly observed as a function of increasing cutoff.

$U_L(T_c)$ tends away from the Ising value towards the mean field value, although the latter is not actually reached. This is due to finite size effects: in order to observe the rest of the crossover toward classical behaviour, much larger systems must be studied, using larger cutoff values.

The Metropolis algorithm, which scales as a function of spin interactions present in the system, is clearly unsuitable for a large scale study of this kind. A more fruitful approach is to employ a cluster algorithm that is independent of the number of interactions per spin [282]. By taking advantage of this method, Luijten and Blöte [283, 284] have confirmed the RG picture of Fisher *et al* [279]. They have also been able to resolve a long standing controversy regarding the precise location of the boundary between regimes (b) and (c), locating the crossover at $\sigma = 2 - \eta_{\rm sr}$, *i.e.* at $\sigma = \frac{7}{4}$ for $d = 2$ [284].

Anisotropic Decay

The Ising spin system based on the full dipolar interaction (6.4) has an antiferromagnetic ground state configuration. Monte Carlo calculations [285, 286] suggest this model is in the same universality class as the 2d Ising model with nearest neighbour interactions. Indeed, a recent finite size scaling analysis [286] is almost identical to that shown in Section 2.2.4, with $\gamma = 1.75(2)$, $\nu = 1.00(2)$ and $\beta = 0.125(5)$.

6.1.2 Continuous Systems

Isotropic Decay

The work described above by Fisher *et al.* [279] applies also to continuous spin systems with algebraically decaying interactions.

Anisotropic Decay

Prakash and Henley [287] have studied the dipolar interaction in square and honeycomb lattices with XY dipoles confined to rotate in the plane of the lattice. For simplicity, they restricted themselves to a nearest neighbour interaction, thus focusing on the anisotropic nature of the dipolar interaction. In this case the interaction (6.1c) may be written as

$$\mathcal{H} = J \sum_{\langle i,j \rangle} \left[\cos(\theta_i - \theta_j) - 3\cos(\theta_i - \psi_{ij})\cos(\theta_j - \psi_{ij}) \right], \tag{6.8}$$

where θ_i and ψ_{ij} are the angles that the dipole at site i and the vector $\mathbf{r}_{ij}$ make with an arbitrary axis in the plane of the lattice. As the authors point out, confining the dipoles to the XY plane does not lose any of the physics of the three-dimensional dipolar interaction, essentially because its main effect is precisely that of confining the spins to the plane of the lattice [288, 289].

Due to the competition between antiferromagnetic and ferromagnetic behaviour of the two terms in (6.8), the continuous degeneracy of the ground state is reduced to a discrete symmetry, reflecting that of the underlying lattice. This occurs through an order by disorder mechanism by which thermal fluctuations select particular states over others. Intriguingly, Prakash and Henley have argued that the role of the dipolar anisotropy on the square lattice may be understood by considering the nearest neighbour XY model in the presence of p-fold anisotropies [68]. This presumably implies the applicability of the results obtained in the previous chapter. Later work [290, 291] on the full dipolar interaction (6.1c) appears to confirm this conjecture. Critical exponents determined by numerical simulations on the square planar lattice, $\beta = 0.19(4)$ and $\gamma = 1.37(7)$ [291], are consistent with an XY model in the presence of a relatively strong four-fold crystal field, undergoing

the kind of crossover discussed in Chapter 5. It is interesting to note that these exponent values are close to those observed in K_2FeF_4 [105] and the O/Mo(110) physisorbed system [228], both of which represent experimental examples of non-universal behaviour induced by four-fold crystal fields.

6.1.3 Problems in Simulation

The inclusion of long range interactions is problematic in Monte Carlo simulation. With regard to dipolar interactions, the problem is complicated by their slowly convergent nature. Such summations are usually done by implementing the Ewald technique, which separates the sum into a real-space part and a reciprocal space part, both of which are quickly convergent. An alternative option is to employ the cluster algorithm introduced by Luijten and Blöte (LB) [282]. With this method, the number of operations per spin flip is independent of the number of interactions between a spin and all the other spins in the system. Thus, the computational effort for a simulation of an N particle system is $\mathcal{O}(N)$ rather than $\mathcal{O}(N^2)$. In addition, since the suppression of critical slowing down brings about an additional efficiency improvement $\mathcal{O}(L^z)$, where z is the dynamical critical exponent, this algorithm is roughly a factor $NL^z = L^{d+z}$ more efficient than a conventional Metropolis algorithm, in the critical regime. The method is also generalisable to vector spin models. Although both the Ewald technique and the LB algorithm bring tangible advantages to simulations of systems with long range interactions, neither has been adopted in this work.

6.2 Competing Length Scales in the Ising Model

This section addresses the question of interactions with competing length scales in the Ising model. In the first instance, the influence of infinitely long range interactions is considered, since these map on to mean field theory. Subsequently other types of long range interactions are examined.

6.2.1 Equivalent Neighbour Model

The equivalent neighbour model is defined as

$$\mathcal{H}_{\text{mf}}\{s_k\} = -\frac{J}{N}\sum_{i,j} s_i \cdot s_j \tag{6.9}$$

where the summation is performed over all spins, and not only over the nearest neighbours of s_i. The factor $1/N$ is introduced in order to ensure sensible thermodynamic behaviour. At the thermodynamic limit the interactions in this model are vanishingly weak and infinitely long ranged, and it is shown in Appendix C that this is equivalent to the application of a molecular field, *i.e.* the model is mean field-like and exactly soluble. In order to address the question of competing length scales, Equations (1.31) and (6.9) may be combined

$$\begin{aligned}\mathcal{H}_{\text{tot}}\{s_k\} &= \mathcal{H}_{\text{Ising}} + \mathcal{H}_{\text{mf}} \\ &= -J\sum_{\langle i,j\rangle} s_i \cdot s_j - \frac{J'}{N}\sum_{i,j} s_i \cdot s_j,\end{aligned} \tag{6.10}$$

with $J + J' = 1$ in order to keep track of the energy scale. By varying the ratio J/J' one would expect to observe some sort of crossover from the nearest neighbour regime to the equivalent neighbour regime. This Hamiltonian has been studied in the past for the case in which the short range and long range interactions are cooperating [292] and for the case in which they are competing [293]. The work of Baker [292] is of particular relevance, as it highlights the fact that *any* presence of such long range interactions is sufficient to force the nature of the phase transition to be of the Bragg-Williams type *i.e.* continuous in the energy and discontinuous in the specific heat.

It should be noted that the Metropolis algorithm remains a relatively efficient choice for the equivalent neighbour model, since the total interaction energy between one spin s_i and all the other spins is given by

$$-\frac{J}{N}\sum_{i\neq j} s_j = -\frac{J}{N}\left(M^2 - s_i\right), \tag{6.11}$$

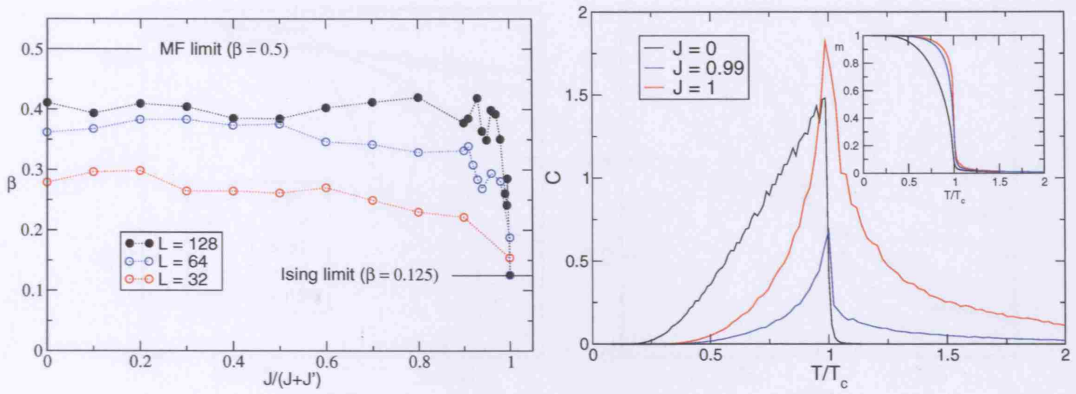

Figure 6.3: Left: magnetisation exponents β measured as a function of $\frac{J}{J+J'}$ for different system sizes. Right: Specific heat curves for a system of size $L = 128$ with different values of J. For $J = 0$ there is a discontinuous peak of height $C = 3/2$, and for $J = 1$ there is an Ising-like singularity. To illustrate the impact of long range interactions, the curve for $J = 0.99$ is also shown. Inset: Corresponding magnetisation curves.

where $M = Nm = \sum_{i=1}^{N} s_i$ is the extensive magnetisation. This is only possible because the coupling between all spin pairs is equal.

The observed values of β, measured from the slopes of the magnetisation curves near T_c, are plotted in Figure 6.3 as a function of $\frac{J}{J+J'}$, for systems of size $L = 32$, 64 and 128. It is clear that the impact of long range interactions is immediate. However, exponents in the mean field regime are seen to depend on the system size: for $L = 128$, $\beta \sim 0.4$ whilst for $L = 32$, $\beta \sim 0.3$. The abrupt crossover to mean field-like behaviour in the model described by (6.10) is perhaps best illustrated in the specific heat plot in Figure 6.3: even a small equivalent neighbour contribution forces a mean field-like discontinuity. That the value of the exponent β depends on system size in the equivalent neighbour limit is explained by the fact that Equation (6.9) only becomes equivalent to the Weiss molecular field theory when $L \to \infty$. When L is large but finite, mean field theory describes the behaviour of the model quite well, except in a very narrow region around the critical point. There mean field theory ultimately breaks down, and a crossover from mean field critical behaviour to critical behaviour of the Ising universality class is observed. The nature of this crossover (which is distinct from the competing length scales crossover of interest in the present discussion) was clarified by Luijten, Blöte and Binder [294]. Their measured β values as a function of system size are in good

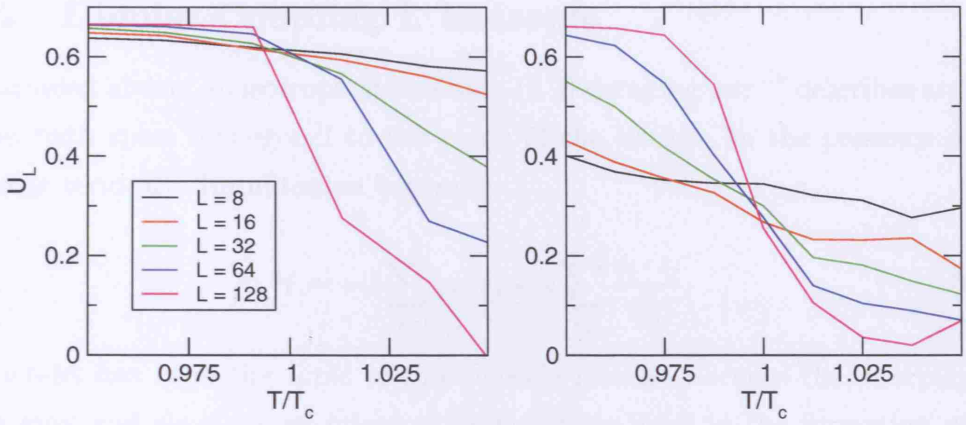

Figure 6.4: The dimensionless cumulant ratio U_L as a function of temperature for several system sizes. Left: nearest neighbour (Ising) model. Right: equivalent neighbour model. The values of U_L at the critical point are comparable to the values reported in the literature [280, 281].

agreement with those presented here.

For the same reasons discussed in Section 6.1.1, the Binder cumulant is also a useful quantity for this model, since it may be monitored to follow the crossover of the system from the pure Ising to the pure mean field regime as a function of $J/(J + J')$ (Figure 6.4). U_L is found to interpolate between the theoretically expected limits abruptly, with the mean field value approached very quickly once the equivalent neighbour interaction is present. However, the nature of the crossover is somewhat complicated by finite size effects. Finite size scaling theory predicts the curves of U_L for different system sizes intersect exactly at the critical temperature of the infinite system, assuming higher order corrections can be disregarded. This assumption is not valid for the model described by Equation (6.10), except for the two limiting cases when $J = 0$ or 1. For any other value of J, the model displays nontrivial behaviour at criticality, and $U(\infty)$ is no longer identified by the 'cumulant crossing point'. This is also the reason why it is not possible to obtain good data collapses for thermodynamic properties such as the magnetisation: the moments are not governed by simple power laws such as $\langle |m|^k \rangle \propto L^{-k\beta/\nu}$. Despite these issues, it is clear from this study that the impact of long range interactions may be dramatic.

6.2.2 Dipolar Coupling I. Isotropic

As discussed above, an isotropic interaction (6.2) decaying as r^{-3} describes an Ising system with spins orthogonal to the plane of the lattice. In the presence of the exchange term, the Hamiltonian becomes

$$\mathcal{H} = -J\sum_{\langle i,j\rangle} s_i \cdot s_j + g\sum_{i,j} \frac{s_i \cdot s_j}{r_{ij}^3}. \tag{6.12}$$

This model has been the topic of considerable interest because the interplay between long and short range interactions manifests itself in the formation of unusual patterns. Provided the exchange interaction exceeds a positive critical value $J/g = 0.85$ [295], the ground state consists of stripes of up and down spins, with the stripe width increasing with increasing exchange. If J is less than this critical value, the ground state is a simple antiferromagnetic configuration. Magnetic striped phases have been observed in ferrimagnetic garnet films [296] and ultrathin films such as Co/Au(111) [297] and Fe/Cu(100) [298].

Qualitatively one can understand the stability of the stripe domains as a compromise between the increase in exchange energy due to the formation of domain walls and the decrease in the dipolar energy due to the interaction between magnetisation currents generated at the domain walls [299]. Monte Carlo simulations reveal a number of stages in the evolution of the system as the temperature is increased [300], as illustrated in the snapshots shown in Figure 6.5. At low temperature the domain walls are essentially rigid until the thermal energy becomes of the order of the energy of an elementary excitation of a domain wall. Above this threshold, the internal energy of the system increases rapidly along with the fluidity of the domain walls, although the symmetry between the vertical and horizontal directions remains broken.

A suitable order parameter to quantify this symmetry breaking is [300]

$$\eta = \frac{n_h - n_v}{n_h + n_v}, \tag{6.13}$$

where n_h (n_v) are the number of horizontal (vertical) bonds between nearest neighbour anti-aligned spins. The fact that this order parameter vanishes implies a restoration of the symmetry between the horizontal and vertical directions, and

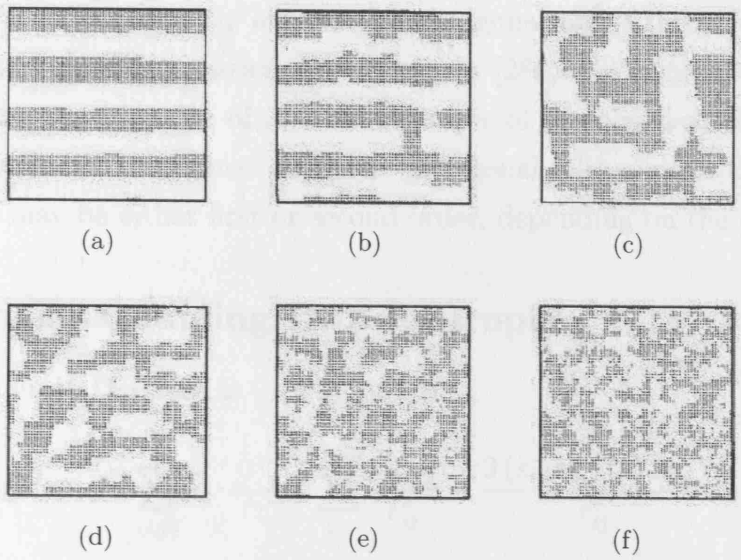

Figure 6.5: Typical spin configurations for the dipolar uniaxial model on a square lattice with $J/g = 8.9$. The configurations were generated by Monte Carlo simulations at temperatures $T/g =$ (a) 3.0, (b) 4.8, (c) 5.2, (d) 6.4, (e) 10.0 and (f) 13.0. (c) and (d) display the so-called tetragonal phase occurring just above the transition. After Booth *et al.* [300].

indeed at high temperatures the system does enter a fully disordered phase. However, in between the striped and paramagnetic phases, just above the transition temperature, the situation is much less clear. Spin configurations in this temperature region (Figures 6.5(c) and 6.5(d)) consist of a patchwork of domains of spins of a given orientation, forming a labyrinthine pattern Booth *et al.* [300] refer to as the tetragonal phase, since it reflects the underlying symmetry of the square lattice. No sharp phase transition between the tetragonal and paramagnetic phases is observed.

The precise nature of the phase diagram for this model is currently open to debate. Work based on a continuous version of the model [301] recognises the phases in terms of topological defects, analogous to the dislocations and disinclinations found in liquid crystals. Depending on the parameters of the model, two distinct scenarios are predicted. In the first one a low temperature smetic-like phase with *quasi* long range order undergoes a Kosterlitz-Thouless transition to a nematic-like phase due to the unbinding of dislocations. At higher temperatures still, orientational symmetry is lost as the system passes over to the tetragonal phase. In the second scenario the system cannot sustain a nematic phase, and the system

passes from the smetic directly over to the tetragonal phase through a first-order transition. More recent numerical investigations [286, 302] suggest a similar picture: depending on the value of J/g the sequence of the observed phases may be either smetic-nematic-tetragonal or smetic-tetragonal, although in the latter case the transition may be either first or second order, depending on the conditions.

6.2.3 Dipolar Coupling II. Anisotropic

The Hamiltonian in this case is

$$\mathcal{H} = -J \sum_{\langle i,j \rangle} s_i \cdot s_j + g \sum_{i,j} \frac{s_i \cdot s_j}{r_{ij}^3} - \frac{3\,(s_i \cdot r_{ij})\,(s_j \cdot r_{ij})}{r_{ij}^5}. \tag{6.14}$$

The $J = 0$ limit, discussed in Section 6.1.1, is characterised by an antiferromagnetic ground state and belongs to the 2d Ising universality class. This explains why the long range character of the dipolar interaction does not affect the universality class of the two-dimensional Ising antiferromagnet ($J < 0$) [285], an experimental example of such a system being the lanthanide material $ErBa_2Cu_3O_7$ [98]. On the other hand, the presence of ferromagnetic exchange ($J > 0$) leads to an inherent frustration since the two terms have different ground states. Due to its problematic nature, there appears to be little in the literature with regard to this scenario.

6.3 Competing Length Scales in Continuous Spin Systems

The effect of the dipolar interaction (6.1c) in the two-dimensional Heisenberg system (6.1a) is to constrain the spins to the plane of the lattice. This can be understood in terms of the following qualitative consideration. Since the dipolar energy is minimised for in-plane spins, and since the zero temperature ordered state must simultaneously minimise the dipolar and the exchange energies, it is favourable for the average magnetisation not to have a component normal to the plane. Furthermore, Maleev [288] has shown by way of a spin wave analysis that in this case long range order is also stabilised at finite temperatures. Unlike the

pure Heisenberg system, which has a $1/q^2$ divergence in the long wavelength limit (see Appendix A), the inclusion of the dipolar term introduces an anisotropy which leads to the longitudinal mode (the mode parallel to the wave vector $\mathbf{q}$) diverging as $1/q$. This is sufficient to suppress the fluctuations which would otherwise destroy the magnetisation.

The inclusion of the magneto-crystalline anisotropy term (6.1b) introduces a further complication because in this case the tendency of the dipole term to align the spins in the plane may be counteracted by a preference for perpendicular alignment, provided D is positive. This leads to the well known reorientation transition [303, 304], where the magnetisation switches from out-of-plane to in-plane anisotropy with increasing temperature [178, 186, 298, 305].

6.3.1 Dipolar XY Model

Maier and Schwabl [81, 82] have recently investigated the low temperature behaviour of the dipolar XY (dXY) model, namely an XY model in the presence of the full dipolar interaction. Despite its anisotropic character, the authors are able to show that, within the framework of the non-linear σ model, it is renormalizable, and that it undergoes a phase transition to the ferromagnetic state governed by a low temperature fixed point with infinite dipolar coupling. The nature and flow diagram of the ferromagnetic transition in the dXY model are qualitatively similar to the Kosterlitz-Thouless transition. However, unlike the short range model the transition is not driven by vortices, but by the dipolar interaction. The authors also attempt to investigate the role of topological excitations, but conclude that there cannot be a vortex unbinding transition as long as the dipolar interaction is present.

The similarities with the 2dXY model extend also to the critical properties, which obey weak scaling identical to that discussed in page 82. Both the correlation length ξ and the magnetisation m exhibit exponential rather than power law divergences, for example. However, by expressing the thermodynamic quantities in terms of the correlation length one obtains power laws analogous to (2.75) and (2.76), such that the ratios β/ν, γ/ν, $\alpha/\nu \ldots$ *are* defined, and the hyperscaling relations (2.17)–(2.20) obeyed. It should be noted, however, that the predicted

values of $\delta = 3$ and $\eta = 1$ for the dXY model are very different to those of the 2dXY model, and are in fact the same as those of the mean field class.

Given its abstract nature, it is difficult to assess the experimental relevance of Maier and Schwabl's analysis at present. An outstanding question that certainly warrants further investigation is that of the scaling behaviour of the dXY model. Since the renormalization group flow diagram appears to be similar to that of the short range XY model, and furthermore, since weak scaling is present, then one might expect similar finite size scaling properties. A Monte Carlo study of the dXY model as a function of temperature for different dipolar coupling strengths would consequently provide a much needed experimental handle on the situation. In particular, one might wish to explore how Prakash and Henley's [287] order by disorder mechanism in the pure dipolar limit is affected by the presence of the exchange interaction. These possibilities are discussed further in the concluding section.

6.4 Heisenberg Model in the Presence of Shape Anisotropy

Another approach to dipolar interactions is to recognise that their leading order effect is shape anisotropy *i.e.* to constrain the spins to the plane of the lattice. This naturally leads to asking whether shape anisotropy alone is sufficient to account for XY behaviour. To investigate this issue, a very simple, though little studied model is investigated. This shape anisotropic (SA) Heisenberg model is defined by the Hamiltonian

$$\mathcal{H} = -J \sum_{\langle i,j \rangle} \mathbf{s}_i \cdot \mathbf{s}_j + \frac{g_{\mathrm{sa}}}{N^2} \left(\sum_i s_i^z \right)^2 , \tag{6.15}$$

where the N^2 factor in front of the second term ensures sensible thermodynamic behaviour. The shape anisotropy applies an overall energy penalty to the spins lying out of the plane of the lattice. In this sense it is mean field-like, and should be distinguished from the single ion anisotropy (6.1b), which acts as a perturbation localised on each individual spin.

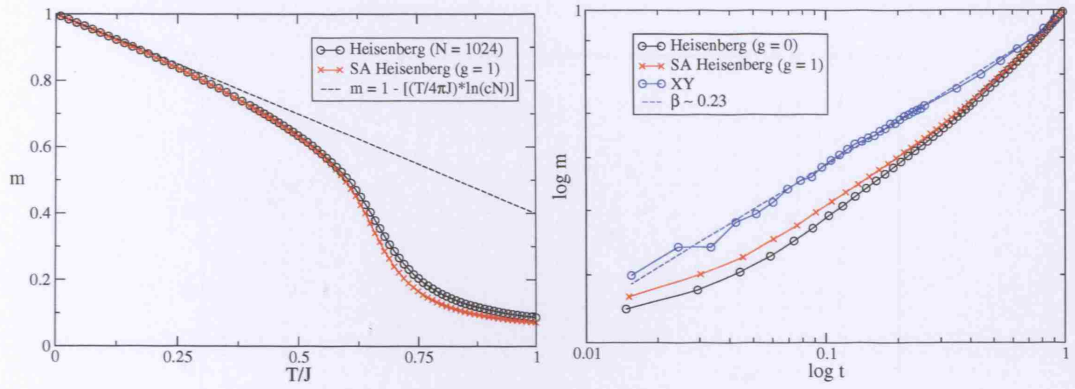

Figure 6.6: Left: Monte Carlo magnetisation data of the pure and SA Heisenberg models with $g_{\rm sa} = 1$, for systems of size $L = 32$. Right: log-log plot.

6.4.1 Influence of Shape Anisotropy

The presence of the shape anisotropy term has a subtle influence on the 2d Heisenberg model. Figure 6.6 illustrates that whereas the low temperature behaviour of the model remains unaffected, a positive value of $g_{\rm sa}$ greater than $\mathcal{O}(J)$ changes the behaviour of the 'critical regime', where the magnetisation descends abruptly to zero.

The nature of this new behaviour is difficult to ascertain. It is important to realise that the shape anisotropy only attenuates the z component of the average magnetisation, despite the fact that individually each spin may point out of the xy plane. This is not the case in the presence of single ion anisotropy. Alternatively, this situation may be thought of in terms of spin waves: whereas the single ion anisotropy attenuates all excitations with a z component, the shape anisotropy only suppresses the mode with the longest wavelength, $q = 1/L$. This is sufficient to single out the xy plane in spin space, and identifies topological excitations which appear to behave in a fashion analogous to the vortices of the 2dXY model, despite not being confined to the xy plane. Figure 6.7 displays Monte Carlo snapshots of the spin configurations at three temperatures in the vicinity of the critical region. With increasing temperature the appearance of vortex pairs is observed. At higher temperatures still, these are seen to dissociate.

This mechanism is more reminiscent of the Kosterlitz-Thouless transition in the

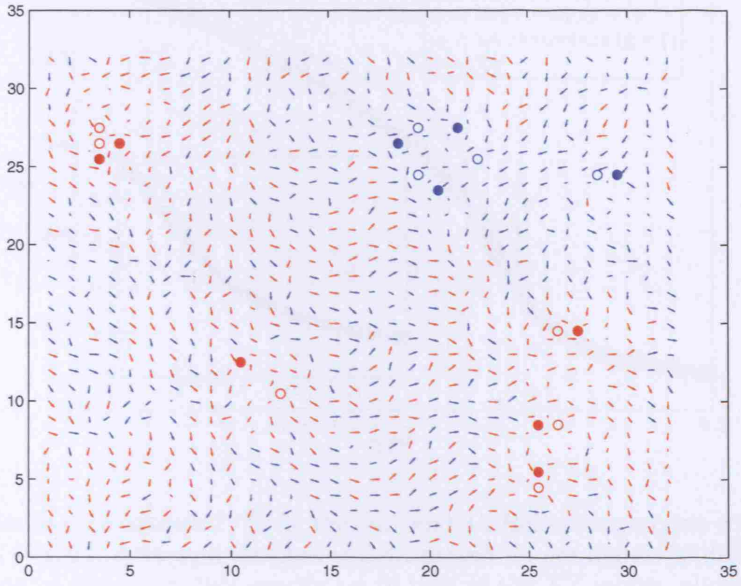

(a)

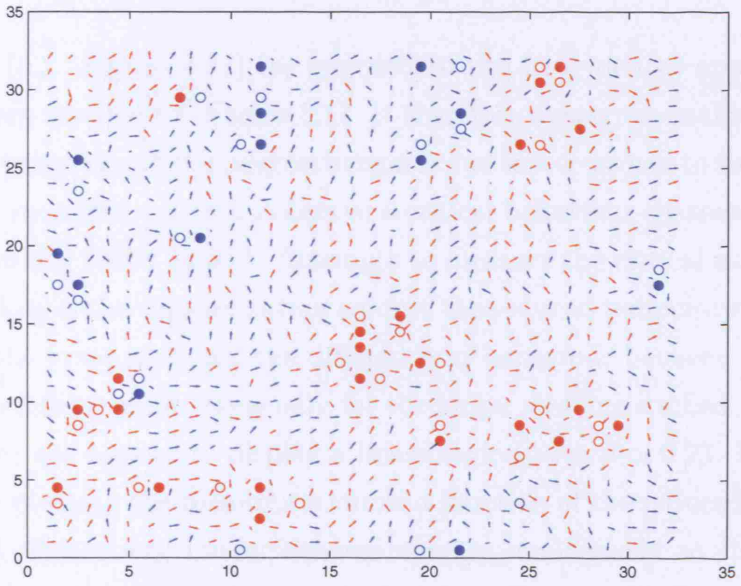

(b)

Figure 6.7: Lattice configurations for an SA Heisenberg system of size $N = 1024$ with $g_{\text{sa}} = 1$, at (a) $T = 0.5$ and (b) $T = 0.65$. The arrows coloured in red point upward, and the blue ones point downward. Vortex(○)-antivortex(●) pairs can be seen to be more common with increasing temperature, and it is also possible to see them dissociate at higher temperatures still. This behaviour is reminiscent of a Kosterlitz-Thouless transition (*c.f.* Figure 2.17).

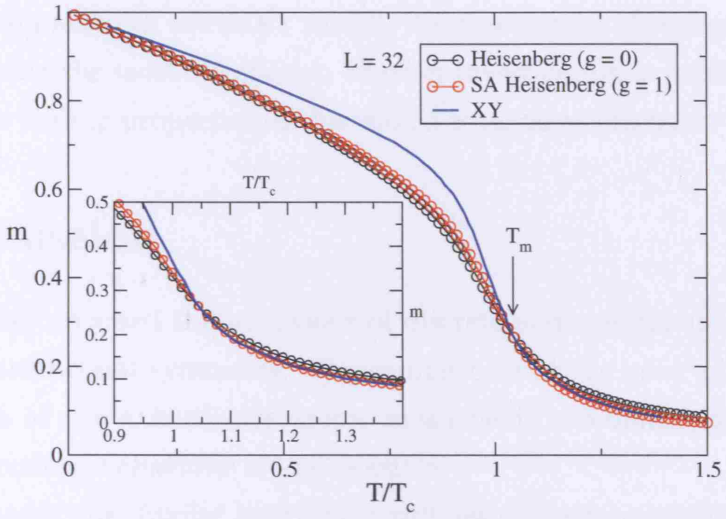

Figure 6.8: Magnetisation against T/T_c for the pure and SA Heisenberg models with $g_{sa} = 1$, for a system of size $N = 1024$. Although the pure and SA models do not appear to differ substantially, the magnetisation of the latter falls exactly on to that of the XY model, above a temperature T_m. Inset: magnification of the region above $T/T_c = 1$.

2dXY model (*c.f.* Figure 2.17), as opposed to the free vortices appearing in the pure Heisenberg model (*c.f.* Figure 5.1). It therefore seems reasonable to ask if the change in the behaviour of the magnetisation is due to a crossover to such a scenario. In particular one might expect to observe a critical behaviour characterised by $\beta \simeq 0.23$, as seen in the 2dXY model. Attempts to measure the critical exponents from logarithmic plots of the magnetisation against the reduced temperature have found that, within the error margins, the difference in behaviour between the pure and the SA case is indiscernible, especially for the larger systems studied. Nevertheless the model does not appear to display a linear region with $\beta \simeq 0.23$. However, it is found that by plotting the magnetisation as a function of the reduced temperature T/T_c, the SA Heisenberg model behaves exactly analogously to the XY model above a certain temperature T_m, as displayed in Figure 6.8. Despite appearing very similar, the data for the pure Heisenberg model does not fall onto that of the XY model.

On the basis of these observations, it is concluded that shape anisotropy alone is not sufficient to induce 2dXY-like critical behaviour. Nevertheless, the fact that it uniquely singles out the plane of the lattice does lend the model features

which are in common with the 2dXY model, the observation of vortices disordering (Figure 6.7) being the most significant. Further investigation is necessary in order to quantify the scaling properties of this model with more precision.

6.5 Discussion

This chapter has reviewed the behaviour of discrete and continuous 'dipolar' spin systems with tetragonal symmetry. Depending on the the spin anisotropy, and the orientation of the axis of anisotropy, mean field, two-dimensional Ising and non-universal critical behaviour are all possible.

In real systems, the dipolar interaction will always be in competition with the exchange coupling, and this question of competing length scales has also been addressed. In Section 6.2, a simplified model with uniaxial spins was studied, and it was found that the long range interaction always dominates the short range one. More realistic systems are more problematic to analyse. However a number of experimentally relevant observations can be made:

1. The primary influence of the dipolar interaction is to constrain the spins to the plane of the lattice [288, 289].
2. For Ising spins interacting through the dipolar coupling, the ground state of the system is antiferromagnetic, and Ising-like critical behaviour is displayed [286]. Consequently, the dipolar interaction does not affect the critical behaviour of antiferromagnetically coupled systems, and accounts for the Ising nature of rare earth materials, such as $ErBa_2Cu_3O_7$ [98].
3. For XY spins interacting through the dipolar coupling, Prakash and Henley [287] have shown that non-universal behaviour occurs, which is reminiscent of that observed in Chapter 5 for the XY model with four-fold fields. Other simulations [291] have confirmed a behaviour which is remarkably similar to that observed in K_2FeF_4 [105].

Thus, the effect of the dipolar interaction in XY quadratic systems is intriguingly similar to that of four-fold fields. The question is immediately raised as to what

happens if the exchange interaction is also present. The work of Maier and Schwabl [81] on the dXY model suggests a behaviour superficially similar to the XY transition, but that is not borne out of the presence of defects. Whether finite size 2dXY behaviour survives the presence of the dipolar coupling is an open question. Although this has not been directly confronted in this work, an algorithm [282] which should allow the limitations of the Metropolis scheme to be overcome has been presented.

To test the influence of the dipolar interaction, the shape anisotropic Heisenberg model was studied. The shape anisotropy term was chosen to mimic the effect of the dipolar coupling and simultaneously maintain numerical tractability. Although its presence subtly alters the behaviour of the Heisenberg model, it alone is not found to induce 2dXY critical behaviour. In pragmatic terms, the conclusion this leads to is that for 2dXY behaviour to be observed, a degree of XY single ion anisotropy must be present. Tautological though this may seem, one must bear in mind that in real two-dimensional systems an axial anisoptropy must *always* occur. This follows from the fact that in two-dimensions the highest possible symmetry is either tetragonal or hexagonal, which identifies at least one unique axis of symmetry. Furthermore, this fact confirms the validity of the work of Prakash and Henley [287] and of Maier and Schwabl [81]: they are correct in considering the influence of the dipolar interaction in XY systems.

Referring to the complexity of dipolar interactions in many-body systems, Lars Onsager is said to have commented that "the theory of dielectrics has more pitfalls than the gamma function has poles!" [306]. The work reported in this chapter provides a rather more optimistic view, at least in the context of two-dimensional systems. A combination of analytical and numerical approaches have proven to be effective in giving a reasonably complete picture. Furthermore, the development of the Luijten-Blöte algorithm [282] provides an ideal tool with which to explore outstanding questions, such as the scaling properties of the dXY model.

Chapter 7

Conclusions and Perspectives

The work presented in this Thesis has addressed the nature of phase transitions and critical phenomena occurring in two-dimensions. The main achievements are summarised below.

7.1 Experimental Classification

An exhaustive classification of the experimental literature concerning layered magnets, thin film magnets and physisorbed surfaces has been performed. The critical behaviour of these systems has been considered in detail, and shown to be dominated by two-dimensional fluctuations. In particular, their order parameter critical exponents β have been reported. These are summarised in the histogram in Figure 4.23. The main feature of this distribution is its bimodal nature, associated with the 2d Ising and 2dXY classes, characterised by $\beta = 0.125$ and $\beta = 0.23$, respectively. Nevertheless, a significant number of systems fall outside of these two categories. In particular:

- Systems with $\beta > 0.23$ are found to possess a significant degree of three-dimensional character.
- Certain non-magnetic systems exhibit three- and four-state Potts critical behaviour, and display $\beta < 0.125$. No magnetic examples of this kind have been found.

- There is a middle ground of observed exponents intermediate between Ising and XY values.

7.2 Theoretical Results

A detailed investigation of the thermodynamic behaviour of two-dimensional spin systems has been performed, leading to a comprehensive understanding of the large data set of experimental results summarised in Figure 4.23.

7.2.1 Symmetry Breaking Anisotropies

An analysis of the two-dimensional Heisenberg Hamiltonian has confirmed that spontaneous ordering can only arise through the presence of perturbations, such as single ion anisotropy. This leads naturally to a crossover to either uniaxial or planar spin symmetry, and consequently to the 2d Ising and 2dXY models being relevant. Although in the latter case the Mermin-Wagner theorem [1] applies, in practice such systems are not dictated by predictions at the thermodynamic limit, and their behaviour is dominated by the unique scaling properties of the 2dXY model.

The model is, however, susceptible to symmetry breaking crystal fields, and the resulting XYh_p model has been studied in detail. The case with four-fold symmetry is of particular relevance to a great number of experimental two-dimensional systems, and has been analysed using two different approaches:

- Analytically, within the framework of the generalised Villain model [72];
- Numerically, by performing a finite size scaling analysis.

In both cases the critical exponents have been calculated as a function of the four-fold anisotropy h_4, and a consistent picture developed. The main features of the XYh_4 model are summarised in Figure 5.11. Due to the marginal nature of h_4, the model undergoes a unique kind of crossover, characterised by continuously varying critical exponents. However, the range of possible exponents is restricted. For $h_4 \rightarrow 0$, the extraordinary scaling properties of the 2dXY model are recovered,

the hallmark of which is an exponent $\tilde{\beta} = 0.23$. For $h_4 \to \infty$, critical behaviour of the 2d Ising model is recovered, characterised by $\beta = 0.125$. Furthermore, 2dXY behaviour is found to remain unaffected by the presence of weak fields: non-universal critical behaviour can only occur in strong fields. Thus a 'universal window' of possible exponent values is identified, bound by the values $\beta = 0.125 - 0.23$.

Hence, depending on the effective strength of h_4, experimental systems may lie either side of the weak field–strong field divide. For example, many magnetic transitions such as those occurring in Rb_2CrCl_4 [256] and Fe on W(100) [191] lie in the weak field region. However, at least one mechanism has been identified, in antiferromagnetic K_2FeF_4 [105], whereby the four-fold field is effectively amplified by the quantum confinement of spins to the easy plane. Other systems which appear to lie in the strong-field region, possibly due to the influence of the underlying substrate, are tungsten and molybdenum surfaces undergoing structural transitions [228,229].

Other symmetries encountered in experiment are not found to lead to new universality classes: the XYh_2 and XYh_6 models belong to the Ising and XY categories, respectively. The much rarer three-fold symmetry of the XYh_3 model leads to three-state Potts behaviour. Importantly, the XYh_p model cannot give rise to four-state Potts model critical behaviour. Hence the disordering transition observed in oxygen physisorbed on ruthenium [227] must occur through a different mechanism, which does not appear to be relevant in magnetic systems.

7.2.2 Long Range Interactions

The influence of the dipolar interaction has been more problematic to analyse, due to its long range and anisotropic nature. Nevertheless, the following simplified models have been studied and characterised numerically:

- The 'isotropic dipolar' Ising model defined by (6.2) has been shown to undergo a crossover from Ising to mean field behaviour as a function of increasing interaction range.
- The 'competing length scales' model (6.10) has been shown to undergo an abrupt crossover from Ising to mean field behaviour, depending on the pres-

ence of a long range interaction term.

- The shape anisotropic Heisenberg model (6.15), chosen to mimic the influence of the dipolar interaction on the Heisenberg model, has been found to be subtly different from the pure Heisenberg model in two-dimensions. Despite tantalising evidence in favour of a possible KT mechanism being present, the model does not exhibit 2dXY-like critical behaviour.

Furthermore, the literature concerning two-dimensional spin models in the presence of the dipolar interaction has been comprehensively reviewed and summarised. Of particular significance are the works concerning dipolar XY models [81, 287]. The results of Prakash and Henley [287] are especially interesting, given their similarity with those reported in this work regarding the XYh_4 model.

7.3 Future Work

Having identified the general mechanism responsible for the 'middle ground' critical behaviour for two-dimensional experimental systems, shown in Figure 4.23, future work should focus on individual systems to see if a more accurate quantitative connection between the physical h_4 and observed critical behaviour can be clearly established.

A number of other avenues for future work address more general questions. An analytical study of the shape anisotropic Heisenberg model would hopefully shed light on the nature of the topological excitations observed in Figure 6.7, which appear to behave consistently with the KT mechanism discussed in Section 2.4. Another system which has been suggested to undergo a slightly modified KT behavior is the two-dimensional continous antiferromagnet on a triangular lattice [170], and it would also be interesting to investigate if these results may be rationalised within the framework discussed in this work.

Finally, a detailed finite size scaling analysis of the XY model in the presence of the dipolar interaction is certainly warranted. In light of the Prakash-Henley conjecture [287], it would be interesting to establish the critical behaviour of this system, and conclusively ascertain whether it ultimately reduces to the unique crossover mechanism of the XYh_4 model, or if there is a crossover to the dipolar

class suggested by Maier and Schwabl [81,82]. In principle, numerical investigations of this system could be aided by a successful implementation of the Luijten-Blöte algorithm [282].

Appendix A

Spin Wave Analysis of the Classical Heisenberg Model

The purpose of this appendix is to derive some basic spin wave results for the Heisenberg model in two dimensions. The simple Heisenberg ferromagnet is considered first, since it is both well known and can be compared to the Monte Carlo simulations presented in Chapter 6. Subsequently, the influence of other perturbations is considered in both ferro- and antiferromagnetic Heisenberg systems, and the results discussed in Section 5.3 are derived.

A.1 Heisenberg Ferromagnet

The basic Heisenberg Hamiltonian is

$$\begin{aligned} \mathcal{H} &= -J \sum_{\langle i,j \rangle} \mathbf{S}_i \cdot \mathbf{S}_j \\ &= -J \sum_{\langle i,j \rangle} s_i^x s_j^x + s_i^y s_j^y + s_i^z s_j^z, \end{aligned} \tag{A.1}$$

in which i and j indicate nearest neighbour spins, and $J > 0$. In the spin wave approximation, one considers a small deviation from the ferromagnetic ground state by an amount $\varepsilon_{(x,y)}$ for each spin

$$\begin{aligned} s_i^x &= \varepsilon_{x_i} \\ s_i^y &= \varepsilon_{y_i} \\ s_i^z &= \sqrt{1-\varepsilon_{x_i}^2-\varepsilon_{y_i}^2} \simeq 1-\frac{1}{2}\left(\varepsilon_{x_i}^2+\varepsilon_{y_i}^2\right), \end{aligned} \tag{A.2}$$

and their effect on the Hamiltonian

$$\begin{aligned} \mathcal{H} &= -J\sum_{\langle i,j\rangle}\varepsilon_{x_i}\varepsilon_{x_j}+\varepsilon_{y_i}\varepsilon_{y_j}+\left[1-\frac{1}{2}\left(\varepsilon_{x_i}^2+\varepsilon_{y_i}^2\right)\right]\left[1-\frac{1}{2}\left(\varepsilon_{x_j}^2+\varepsilon_{y_j}^2\right)\right] \\ &= -J\sum_{\langle i,j\rangle}\varepsilon_{x_i}\varepsilon_{x_j}+\varepsilon_{y_i}\varepsilon_{y_j}+1-\frac{1}{2}\left(\varepsilon_{x_i}^2+\varepsilon_{x_j}^2+\varepsilon_{y_i}^2+\varepsilon_{y_j}^2\right)+\mathcal{O}\left(\varepsilon_x^4,\varepsilon_y^4\right) \\ &= -\frac{JzN}{2}-J\sum_{\langle i,j\rangle}\left(\varepsilon_{x_i}\varepsilon_{x_j}+\varepsilon_{y_i}\varepsilon_{y_j}\right)+\frac{J}{2}\sum_{\langle i,j\rangle}\left(\varepsilon_{x_i}^2+\varepsilon_{x_j}^2+\varepsilon_{y_i}^2+\varepsilon_{y_j}^2\right), \end{aligned} \tag{A.3}$$

where z is the number of nearest neighbours. Defining $\boldsymbol{\delta} = |\mathbf{r}_i - \mathbf{j}_j|$, in which $\mathbf{r}_i$ and $\mathbf{r}_j$ define the vectorial position of the spins i and j, and since

$$\frac{J}{2}z\sum_{\langle i,j\rangle}\left(\varepsilon_{x_i}^2+\varepsilon_{x_j}^2+\varepsilon_{y_i}^2+\varepsilon_{y_j}^2\right)=\frac{J}{2}z\sum_i\left(\varepsilon_{x_i}^2+\varepsilon_{y_i}^2\right), \tag{A.4}$$

the Hamiltonian can be rewritten as

$$\begin{aligned} \mathcal{H} = -\frac{JzN}{2}&+\frac{J}{2}\left[z\sum_i\varepsilon_{x_i}^2-\sum_i\sum_{\boldsymbol{\delta}}\varepsilon_{x_i}\varepsilon_{x_{(i+\delta)}}\right] \\ &+\frac{J}{2}\left[z\sum_i\varepsilon_{y_i}^2-\sum_i\sum_{\boldsymbol{\delta}}\varepsilon_{y_i}\varepsilon_{y_{(i+\delta)}}\right]. \end{aligned} \tag{A.5}$$

In turn, (A.5) can be expressed in matrix form

$$\mathcal{H} = -\frac{JzN}{2}+\frac{J}{2}\sum_i\sum_j\left(\varepsilon_{x_i}\mathbf{M}_{ij}\varepsilon_{x_j}+\varepsilon_{y_i}\mathbf{L}_{ij}\varepsilon_{y_j}\right), \tag{A.6}$$

in which $\mathbf{M}_{ij} = \mathbf{L}_{ij}$, provided the diagonal elements $M_{ii} = z$, and the off-diagonal elements $M_{ij} = -1$ if i and j are nearest neighbours ($|\mathbf{r}_i - \mathbf{r}_j| = \boldsymbol{\delta}$), and 0 otherwise. Defining the pair of Fourier Transforms

$$\varepsilon_{\mathbf{r}} = \frac{1}{N}\sum_{\mathbf{q}} \exp\left(i\mathbf{q}\cdot\mathbf{r}_i\right)\varepsilon^*_{\mathbf{q}}, \tag{A.7a}$$

$$\varepsilon^*_{\mathbf{q}} = \sum_{i} \exp\left(-i\mathbf{q}\cdot\mathbf{r}_i\right)\varepsilon_{\mathbf{r}}, \tag{A.7b}$$

one can express (A.6) as

$$\begin{aligned}\sum_i\sum_j \varepsilon_{x_i}\mathbf{M}_{ij}\varepsilon_{x_j} &= \frac{1}{N^2}\sum_{i,j}\sum_{\mathbf{q},\mathbf{q}'} e^{i\mathbf{q}\cdot\mathbf{r}_i}\varepsilon^x_{\mathbf{q}}\,\mathbf{M}_{ij}\,e^{i\mathbf{q}'\cdot\mathbf{r}_j}\varepsilon^x_{\mathbf{q}'} \\ &= \frac{1}{N^2}\sum_{i}\sum_{\mathbf{q},\mathbf{q}'} e^{i(\mathbf{q}+\mathbf{q}')\cdot\mathbf{r}_i}\sum_{\boldsymbol{\delta}}\varepsilon^x_{\mathbf{q}}\varepsilon^x_{\mathbf{q}'}\,\mathbf{M}_{i\boldsymbol{\delta}}\,e^{i\mathbf{q}'\cdot\boldsymbol{\delta}}.\end{aligned} \tag{A.8}$$

Using the standard relation

$$\lim_{N\to\infty}\sum_i \exp\left(i\mathbf{q}\cdot\mathbf{r}_i\right) = N\delta_{\mathbf{q},0} \tag{A.9}$$

ensures that the only non-zero terms occur when $\mathbf{q}' = -\mathbf{q}$. Furthermore, since $\varepsilon^x_{\mathbf{q}}\varepsilon^x_{\mathbf{q}'} = |\varepsilon^x_{\mathbf{q}}|^2$, one obtains

$$\begin{aligned}\sum_i\sum_j \varepsilon_{x_i}\mathbf{M}_{ij}\varepsilon_{x_j} &= \sum_{\mathbf{q}}\sum_{\boldsymbol{\delta}} |\varepsilon^x_{\mathbf{q}}|^2\,\mathbf{M}_{i\boldsymbol{\delta}}\,e^{i\mathbf{q}\cdot\boldsymbol{\delta}} \\ &= \sum_{\mathbf{q}} |\varepsilon^x_{\mathbf{q}}|^2\left(z - \sum_{\boldsymbol{\delta}} e^{i\mathbf{q}\cdot\boldsymbol{\delta}}\right) \\ &= \sum_{\mathbf{q}} z|\varepsilon^x_{\mathbf{q}}|^2\left(1 + \frac{1}{z}\sum_{\boldsymbol{\delta}} e^{i\mathbf{q}\cdot\boldsymbol{\delta}}\right) \\ &= \sum_{\mathbf{q}} |\varepsilon^x_{\mathbf{q}}|^2\gamma_{\mathbf{q}},\end{aligned} \tag{A.10}$$

where

$$\begin{aligned}\gamma_{\mathbf{q}} &= z - \sum_{\boldsymbol{\delta}} e^{i\mathbf{q}\cdot\boldsymbol{\delta}} \\ &= 4 - 2\cos(q_x a) - 2\cos(q_y a) \qquad \text{in 2d,}\end{aligned} \tag{A.11}$$

and a is the lattice constant. $\mathbf{M}_{ij}$ is thus diagonalised by $\mathbf{q}$ with eigenvalues

$\lambda_{\mathbf{q}}^x = \lambda_{\mathbf{q}}^y = \gamma_{\mathbf{q}}$. Substituting back into (A.6) finally gives

$$\boxed{\mathcal{H} = -\frac{JzN}{2} + \frac{J}{2}\left\{\sum_{\mathbf{q}} \left[\gamma_{\mathbf{q}}|\varepsilon_{\mathbf{q}}^x|^2 + \gamma_{\mathbf{q}}|\varepsilon_{\mathbf{q}}^y|^2\right]\right\}}. \tag{A.12}$$

Expression (A.12) is essentially the Hamiltonian for an array of coupled harmonic oscillators, in which $|\varepsilon_{\mathbf{q}}^x|^2$ and $|\varepsilon_{\mathbf{q}}^y|^2$ are canonically conjugate pairs of variables. By analogy with the simple harmonic oscillator, in which the position x and the momentum p are the conjugate variables and the frequency of oscillation is $\omega = \sqrt{k/m}$, one arrives at the familiar result for the dispersion relation of the spin waves

$$\omega(\mathbf{q}) = J\gamma_{\mathbf{q}} = 2 - 2\cos(\mathbf{q}a) \simeq J\mathbf{q}^2a^2, \tag{A.13}$$

which is valid for small $\mathbf{q}$.

A.1.1 Expression for the Magnetisation

Equation (A.12) allows for the evaluation of the correlation function, and therefore of thermodynamic averages such as the magnetisation, in terms of solvable Gaussian integrals. Such a derivation is carried out explicitly for the 2dXY model in references [307] and [308], in which case the magnetisation is found to be $\langle m \rangle = (1/aN)^{T/8\pi J}$, where $a = 1.86$. Since the Hamiltonian of 2dXY model is

$$\mathcal{H}_{\mathrm{XY}} = -\frac{JzN}{2} + \frac{J}{2}\left[\sum_{\mathbf{q}} \gamma_{\mathbf{q}}|\varepsilon_{\mathbf{q}}^x|^2\right], \tag{A.14}$$

it is argued here that the extra degree of freedom in (A.12) leads to a factor of two being introduced in the relevant expression for the Heisenberg model

$$\langle m \rangle = \left(\frac{1}{aN}\right)^{T/4\pi J}. \tag{A.15}$$

As the Monte Carlo simulations in Chapter 6 show, this expression is accurate at low temperature. A formal derivation of this result is presented in reference [251].

A.1.2 Influence of Anisotropies

In Section 5.3 a more complex Hamiltonian than (A.1) is considered, which includes the terms

$$D\sum_i (S_i^z)^2 + E\sum_i [(S_i^x)^2 - (S_i^y)^2]. \tag{A.16}$$

It is of experimental relevance to understand how the results of the previous section are altered by the presence of these anisotropies. Setting $D > 0$, $E = 0$ and $s_i^y = \varepsilon_{y_i}$, $s_i^z = \varepsilon_{z_i}$ and $s_i^x = \sqrt{1 - \varepsilon_{y_i}^2 - \varepsilon_{z_i}^2}$ is found to eventually lead to the expression

$$\mathcal{H} = -\frac{JzN}{2} + \frac{J}{2}\left\{\sum_{\mathbf{q}}\left[\left(\gamma_{\mathbf{q}} + \frac{2D}{J}\right)|\varepsilon_{\mathbf{q}}^x|^2 + \gamma_{\mathbf{q}}|\varepsilon_{\mathbf{q}}^y|^2\right]\right\}. \tag{A.17}$$

This leads to the following dispersion relation

$$\omega(\mathbf{q}) = J\sqrt{\left(\gamma_{\mathbf{q}} + \frac{2D}{J}\right)\gamma_{\mathbf{q}}}. \tag{A.18}$$

For $q \ll 2D/J$

$$\omega(\mathbf{q}) \simeq J\sqrt{\frac{2D}{J}}\,\mathbf{q} = \sqrt{2DJ}\,\mathbf{q}. \tag{A.19}$$

which is linear in $\mathbf{q}$. If, in addition to the presence of D, $E < 0$, determination of the eigenvalues of $\mathbf{M}_{ij}$ and $\mathbf{L}_{ij}$ gives

$$\lambda_{\mathbf{q}}^x = \gamma_{\mathbf{q}} + \frac{2(D+E)}{J} \tag{A.20a}$$

$$\lambda_{\mathbf{q}}^y = \gamma_{\mathbf{q}} + \frac{4E}{J}. \tag{A.20b}$$

Thus

$$\omega(\mathbf{q}) = J\sqrt{\left(\gamma_{\mathbf{q}} + \frac{2(D+E)}{J}\right)\left(\gamma_{\mathbf{q}} + \frac{4E}{J}\right)}. \tag{A.21}$$

In the limit in which $\mathbf{q} \to 0$ and $E \ll D$, (A.21) approximates to

$$\omega(\mathbf{q} \to \mathbf{0}) \simeq 2\sqrt{2DE}, \tag{A.22}$$

i.e. the presence of the four-fold field term E opens up a gap in the spin wave spectrum.

A.2 Heisenberg Antiferromagnet

The calculation for the Heisenberg antiferromagnet ($J < 0$) proceeds in a similar fashion, with the additional complexity that it is necessary to define two sublattices A and B in which the spins point in opposite directions. The total Hamiltonian is therefore

$$\mathcal{H} = \frac{J}{2}\sum_{i_A}\sum_{\delta}\mathbf{S}_i^A \cdot \mathbf{S}_{i+\delta}^B + \frac{J}{2}\sum_{i_B}\sum_{\delta}\mathbf{S}_i^B \cdot \mathbf{S}_{i+\delta}^A. \tag{A.23}$$

It can be shown that

$$\begin{aligned}\mathcal{H} = -\frac{JzN}{2} &+ \frac{J}{2}\left[z\sum_{i_A}(\varepsilon_{z_i}^A)^2 + (\varepsilon_{y_i}^A)^2 - \sum_{i_A}\sum_{\delta}\varepsilon_{z_i}^A\varepsilon_{z_{(i+\delta)}}^B + \varepsilon_{y_i}^A\varepsilon_{y_{(i+\delta)}}^B\right] \\ &+ \frac{J}{2}\left[z\sum_{i_B}(\varepsilon_{z_i}^B)^2 + (\varepsilon_{y_i}^B)^2 - \sum_{i_B}\sum_{\delta}\varepsilon_{z_i}^B\varepsilon_{z_{(i+\delta)}}^A + \varepsilon_{y_i}^B\varepsilon_{y_{(i+\delta)}}^A\right].\end{aligned} \tag{A.24}$$

It is convenient to define the Bravais lattice vectors as $\mathbf{R} = n_1 a_1 + n_2 a_2$, where, in terms of the unit vectors $\hat{x}$, $\hat{y}$ along the x, y axes, $a_1 = a(\hat{x} + \hat{y})$ and $a_2 = a(\hat{x} - \hat{y})$ (see Figure A.1).

The matrix form of the Hamiltonian is

$$\mathcal{H} = -\frac{JzN}{2} + \frac{J}{2}\sum_{i,j}\sum_{\alpha,\beta}\varepsilon_{z_i}^{\alpha}\mathbf{M}_{ij}^{\alpha\beta}\varepsilon_{z_j}^{\beta} + \varepsilon_{y_i}^{\alpha}\mathbf{L}_{ij}^{\alpha\beta}\varepsilon_{y_j}^{\beta}. \tag{A.25}$$

The tensor $\mathbf{M}_{ij}^{\alpha\beta} = \mathbf{L}_{ij}^{\alpha\beta}$, in which i and j are the Bravais lattice site indices and α and β are the sublattice indices, is essentially made up of four different two-dimensional matrices: $\mathbf{M}_{ij}^{AA}$, $\mathbf{M}_{ij}^{AB}$, $\mathbf{M}_{ij}^{BA}$ and $\mathbf{M}_{ij}^{BB}$. The elements of these matrices are derived in a manner analogous to the previous section. The diagonal elements are

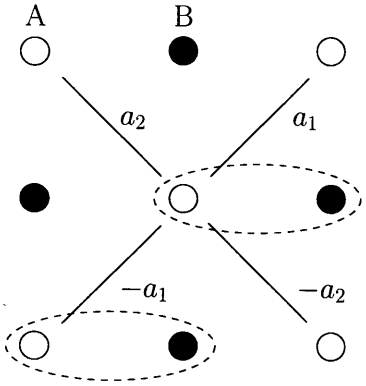

Figure A.1: Bravais lattices for the square antiferromagnet.

$$\begin{aligned} \mathbf{M}_{ii}^{AA} &= \mathbf{M}_{ii}^{BB} = z \\ \mathbf{M}_{ii}^{AB} &= \mathbf{M}_{ii}^{BA} = \frac{J}{2}, \end{aligned} \tag{A.26}$$

and the off-diagonal elements are

$$\begin{aligned} &\mathbf{M}_{ij}^{AA} = \mathbf{M}_{ij}^{BB} = 0 \\ &\mathbf{M}_{ij}^{AB} = \frac{J}{2}, \qquad \text{where} \qquad i-j = \mathbf{a}_2,\ -\mathbf{a}_1,\ a_2 - a_1 \\ &\mathbf{M}_{ij}^{BA} = \frac{J}{2}, \qquad \text{where} \qquad i-j = \mathbf{a}_1,\ -\mathbf{a}_2,\ a_1 - a_2. \end{aligned} \tag{A.27}$$

Defining

$$\varepsilon_{\mathbf{r}}^{A/B} = \frac{1}{N} \sum_{\mathbf{q}} \exp\left(i\mathbf{q} \cdot \mathbf{r}_{i_{A/B}}\right) \varepsilon_{\mathbf{q}}^{A/B}, \tag{A.28}$$

in which $\mathbf{r}_{i_A} = \mathbf{R}$ and $\mathbf{r}_{i_B} = \mathbf{R} + \mathbf{d}$, allows the Hamiltonian to be rewritten as

$$\mathcal{H} = -\frac{JzN}{2} + \frac{J}{2} \left\{ \sum_{\mathbf{q}} \left[\lambda_{\mathbf{q}}^{y} |\varepsilon_{\mathbf{q}}^{y}|^2 + \lambda_{\mathbf{q}}^{z} |\varepsilon_{\mathbf{q}}^{z}|^2 \right] \right\}, \tag{A.29}$$

where

$$\lambda_{\mathbf{q}}^{y} = \lambda_{\mathbf{q}}^{z} = z \pm \gamma_{\mathbf{q}}. \tag{A.30}$$

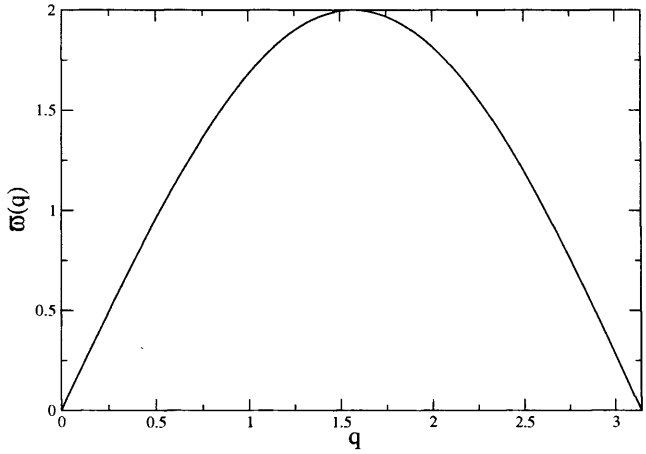

Figure A.2: Dispersion relation (A.32) for a one-dimensional antiferromagnet.

Calculating the frequencies for each $\mathbf{q}$ demands knowledge of the conjugate variables. A systematic method for doing so is beyond the scope of this work, however it is known that as $\mathbf{q} \to 0$, two degenerate branches are expected. This infers $\lambda^y_{\mathbf{q}} = z + \gamma_{\mathbf{q}}$ is conjugate with $\lambda^z_{\mathbf{q}} = z + \gamma_{\mathbf{q}}$ and *vice versa*. Therefore

$$\omega(\mathbf{q}) = J\sqrt{(z + \gamma_{\mathbf{q}})\,(z - \gamma_{\mathbf{q}})}. \tag{A.31}$$

The degeneracy becomes clear by considering a one-dimensional antiferromagnet, in which case $\gamma_{\mathbf{q}} = 2\cos(qa)$ and $z = 2$, such that

$$\omega_{1\mathrm{d}}(\mathbf{q}) = 2J\sqrt{[1 + \cos(qa)]\,[1 - \cos(qa)]}, \tag{A.32}$$

which is plotted in Figure A.2.

A.2.1 Influence of Anisotropies

The inclusion of the terms in (A.16) leads to a behaviour which is altogether different from the ferromagnetic model. Setting $D \neq 0$ leaves $\mathbf{L}(\mathbf{q})$ unaffected, but changes $\mathbf{M}(\mathbf{q})$ in such a way that determination of the eigenvalues gives the solutions

$$\lambda_{\mathbf{q}}^{x} = \gamma_{\mathbf{q}} \tag{A.33a}$$

$$\lambda_{\mathbf{q}}^{y} = z + \frac{2D}{J} \pm \gamma_{\mathbf{q}}. \tag{A.33b}$$

In turn, this leads to the frequency spectrum

$$\omega(\mathbf{q}) = J\sqrt{\left(z + \frac{2D}{J} \pm \gamma_{\mathbf{q}}\right)(z \mp \gamma_{\mathbf{q}})}. \tag{A.34}$$

Thus, the presence of D lifts the degeneracy of the two branches

$$\omega(\mathbf{q}_1 \to 0) = J\sqrt{\left(z + \frac{2D}{J} + \gamma_{\mathbf{q}}\right)(z - \gamma_{\mathbf{q}})} = J\sqrt{\left(2z + \frac{2D}{J}\right)}\mathbf{q}\,a \tag{A.35a}$$

$$\omega(\mathbf{q}_2 \to 0) = J\sqrt{\left(z - \frac{2D}{J} - \gamma_{\mathbf{q}}\right)(z + \gamma_{\mathbf{q}})} = 2\sqrt{2DJ}, \tag{A.35b}$$

introducing a gap in one of them. For D and $E \neq 0$, the eigenvalues for $\mathbf{M}(\mathbf{q})$ are

$$\lambda_{\mathbf{q}}^{x} = \gamma_{\mathbf{q}} \tag{A.36a}$$

$$\lambda_{\mathbf{q}}^{y} = z + \frac{2(D+E)}{J} \pm \gamma_{\mathbf{q}}, \tag{A.36b}$$

and those for $\mathbf{L}(\mathbf{q})$ are

$$\lambda_{\mathbf{q}}^{x} = \gamma_{\mathbf{q}} \tag{A.37a}$$

$$\lambda_{\mathbf{q}}^{y} = z + \frac{4E}{J} \pm \gamma_{\mathbf{q}}. \tag{A.37b}$$

The dispersion relations therefore become

$$\omega(\mathbf{q}_1) = J\sqrt{\left(z + \frac{2(D+E)}{J} + \gamma_{\mathbf{q}}\right)(z - \gamma_{\mathbf{q}})} \tag{A.38a}$$

$$\omega(\mathbf{q}_2) = J\sqrt{\left(z + \frac{4E}{J} - \frac{2D}{J} - \gamma_{\mathbf{q}}\right)(z + \gamma_{\mathbf{q}})}. \tag{A.38b}$$

In the limit $\mathbf{q} \to 0$, and to leading order in D and E two gaps appear,

$$\omega(\mathbf{q}_1 \to 0) = 2z\sqrt{2zEJ} \tag{A.39a}$$

$$\omega(\mathbf{q}_2 \to 0) = 2\sqrt{z(D+E)J}, \tag{A.39b}$$

as in Thurlings *et al.* [105].

A.3 Concluding Remarks

The above results can be reproduced using the more common Holstein–Primakoff operator method [273]. Nevertheless, it is interesting to find that this fundamental difference in behaviour between the ferro- and antiferromagnetic Heisenberg models is observable in a classical calculation.

Appendix B

Conventions for Describing Ordered Surface Structures

The classification of ordered surface structures involves describing the overlayer structure (defined by the two vectors $\mathbf{b}_1$ and $\mathbf{b}_2$) in terms of the underlying structure of the substrate (defined by $\mathbf{a}_1$ and $\mathbf{a}_2$). There are two commonly adopted conventions in order to achieve this.

B.1 Wood's Notation

Wood's notation involves specifying the lengths of the two overlayer vectors, $\mathbf{b}_1$ and $\mathbf{b}_2$, in terms of $\mathbf{a}_1$ and $\mathbf{a}_2$ respectively. This is written in the format

$$\left(\frac{|\mathbf{b}_1|}{|\mathbf{a}_1|} \times \frac{|\mathbf{b}_2|}{|\mathbf{a}_2|}\right), \tag{B.1}$$

e.g. a (2×2) structure on an fcc(100) surface, such as the one depicted in Figure B.1, has $|\mathbf{b}_1| = 2\mathbf{a}_1$ and $|\mathbf{b}_2| = 2|\mathbf{a}_2|$. However, because the overlayer mesh contains an atom in the centre, its full description is $c(2 \times 2)$ (centred two by two). One could equally well define the unit cell of the overlayer in terms of a primitive cell (the vectors $\mathbf{b}'_1$ and $\mathbf{b}'_2$). In this case, the overlayer structure is rotated with respect to the substrate unit cell, so the angle of rotation of $\mathbf{b}'_1$ from $\mathbf{a}'_1$ is also included. Hence, an alternative name for this overlayer is $p(\sqrt{2} \times \sqrt{2})$R45°, where the '$p$' stands for primitive (although often this is simply omitted).

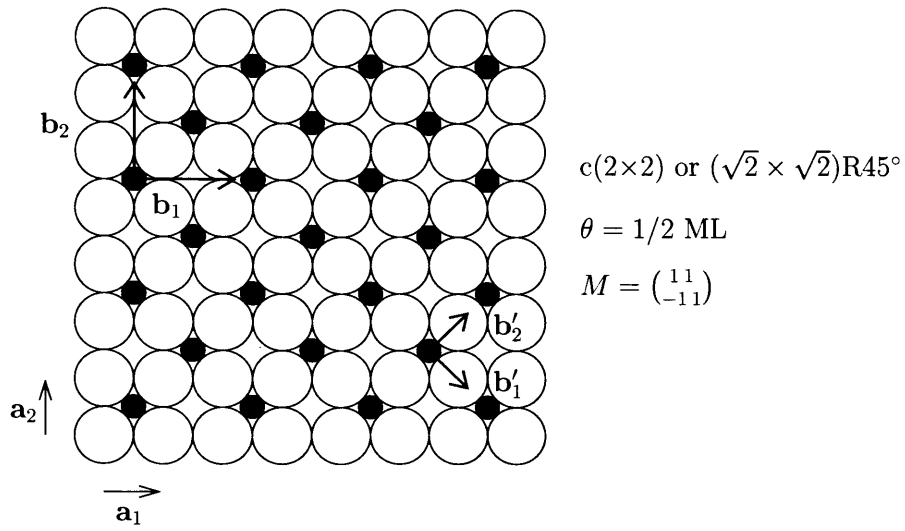

Figure B.1: Adsorbed monolayer on an fcc(100) surface. The relation of the substrate vectors with respect to the overlayer vectors may be expressed in two different ways.

To summarise, Wood's notation may be described as

$$\boxed{\mathrm{M}(hkl)\left(\frac{|\mathbf{b}_1|}{|\mathbf{a}_1|}\times\frac{|\mathbf{b}_2|}{|\mathbf{a}_2|}\right)-\mathrm{R}\alpha^\circ-\mathrm{A}} \tag{B.2}$$

where M is the chemical symbol of the substrate, (hkl) is the Miller index of the surface plane, α is the angle between the substrate and overlayer meshes, and A is the chemical symbol of the surface species. For example, Pt(100)$(\sqrt{2}\times\sqrt{2})$R45°-S should be read as "sulphur chemisorbed on Pt(100) adopting a $(\sqrt{2}\times\sqrt{2})$R45° structural arrangement".

It is important to note that Wood's notation is only appliccable if the angle between $\mathbf{b}_1$ and $\mathbf{b}_2$ is the same as that between $\mathbf{a}_1$ and $\mathbf{a}_2$.

B.2 Matrix Notation

The more general matrix notation defines the vectors $\mathbf{b}_1$ and $\mathbf{b}_2$ independently, as linear combinations of to the substrate vectors $\mathbf{a}_1$ and $\mathbf{a}_2$, and expresses these relationships in a matrix format. For example, the $(\sqrt{2}\times\sqrt{2})$R45° phase in Figure B.1 is written as

$$\begin{pmatrix} \mathbf{b}_1 \\ \mathbf{b}_2 \end{pmatrix} = \begin{pmatrix} 1 & 1 \\ -1 & 1 \end{pmatrix} \begin{pmatrix} \mathbf{a}_1 \\ \mathbf{a}_2 \end{pmatrix}, \tag{B.3}$$

implying that

$$\mathbf{b}_1 = 1 \cdot \mathbf{a}_1 + 1 \cdot \mathbf{a}_2 \tag{B.4a}$$

$$\mathbf{b}_2 = -1 \cdot \mathbf{a}_1 + 1 \cdot \mathbf{a}_2. \tag{B.4b}$$

Appendix C

Some Notes on Mean Field Theory

The aim of this appendix is to show that mean field theory becomes exact for the Ising model, provided the same interaction acts between all pairs of spins. Assuming there are N spins (and $N \gg 1$), then there are $N^2/2$ pairs of spins, and the interaction must be proportional to $1/N$ in order for the energy to be proportional to N. The Hamiltonian of the model is given in Equation (6.9) but is reproduced here for convenience

$$\mathcal{H}\{s_i\} = -\frac{J}{N}\sum_{i,j} s_i \cdot s_j, \tag{C.1}$$

where the sum runs over all pairs of spins, and not merely over nearest neighbours. Equivalently, by using (6.11) one can write

$$\begin{aligned}\mathcal{H}\{s_i\} &= -\frac{J}{2N}\left[\left(\sum_{i=1}^{N} s_i\right)^2 - N\right] \\ &= -\frac{J}{2N}\left(M^2 - N\right) \\ &= -\frac{J}{2}\left(Nm^2 - 1\right),\end{aligned} \tag{C.2}$$

since the total magnetization is $m = \sum_{i=1}^{N} s_i/N$ and $s_i^2 = 1$. Thus in this model the energy of each configuration depends on $s_1, \ldots, s_N$ only via m. This simplification

allows the sum over spin values in the partition function to be replaced by a sum over the allowed values of m, weighted by the number of spin configurations for each value

$$Z = \sum_{-m}^{+m} W(m) \exp\left[-\frac{J}{2kT}(Nm^2 - 1)\right]. \tag{C.3}$$

In a given configuration, if N_+ spins are oriented upwards and $N_- = N - N_+$ are oriented downwards, then the total magnetic moment is

$$m = \frac{N_+ - N_-}{N} = \frac{2N_+ - N}{N}. \tag{C.4}$$

There are $C_{N_+}^N$ such arrangements of spins

$$\begin{aligned} W(m) = C_{N_+}^N &= \binom{N}{N_+} = \binom{N}{\frac{N}{2}(1+m)} \\ &= \frac{N!}{\left[\frac{N}{2}(1+m)\right]!\left[\frac{N}{2}(1-m)\right]!}, \end{aligned} \tag{C.5}$$

so the partition function is

$$Z = \sum_{-m}^{+m} \frac{N!}{\left[\frac{N}{2}(1+m)\right]!\left[\frac{N}{2}(1-m)\right]!} \exp\left[-\frac{J}{2kT}(Nm^2 - 1)\right]. \tag{C.6}$$

This is effectively the approximation made by Bragg and Williams in 1934 [309]. The free energy is

$$F = -kT \ln Z = \frac{J}{2}\left(Nm^2 - 1\right) - kT \ln W(m). \tag{C.7}$$

As $N \to \infty$, one may use Stirling's approximation $x! \simeq x^x e^{-x}$ which gives

$$F = -\frac{1}{2}JNm^2 + NkT\left[\frac{1+m}{2}\ln\left(\frac{1+m}{2}\right) + \frac{1-m}{2}\ln\left(\frac{1-m}{2}\right)\right], \tag{C.8}$$

in which the second term is recognised as the entropy of mixing. By minimising F with respect to m

$$\frac{\partial F}{\partial m} = 0 = -Jm + \frac{1}{2}kT \ln \frac{(1+m)}{(1-m)}. \tag{C.9}$$

Since $\tanh^{-1} x = \frac{1}{2}\ln[(1+x)/(1-x)]$, the familiar mean field expression (1.41) is recovered

$$m = \tanh\left(\frac{Jm}{kT}\right), \tag{C.10}$$

which displays a phase transition at a critical temperature $T_c = J/k$. In the vicinity of the transition, where $m \to 0$, F may be expanded in a power series to obtain the form anticipated by Landau [35]

$$F(m,T) = \frac{m^2}{2}(kT - J) + \frac{kT}{12}m^4 + \cdots \tag{C.11}$$

with all higher order terms of even power in m having positive coefficients.

A number of useful results may be derived by replacing the sum in Equation (C.3) by an integral (which introduces an error of order $1/N$)

$$Z = \int_{-m}^{+m} dm\, W(m)\,[1 + \mathcal{O}(1/N)]\,. \tag{C.12}$$

In particular, the value of the dimensionless ratio $Q = \langle m^2\rangle^2/\langle m^4\rangle$ at criticality may be found [280, 282, 310], by expressing the average square magnetisation and the fourth power of the magnetisation as

$$\langle m^2\rangle = \int_{-m}^{+m} dm\, m^2 W(m)\,[1 + \mathcal{O}(1/N)]\,, \tag{C.13}$$

$$\langle m^4\rangle = \int_{-m}^{+m} dm\, m^4 W(m)\,[1 + \mathcal{O}(1/N)]\,. \tag{C.14}$$

By expanding $\ln W(m)$ for $N \to \infty$ as shown above, and expressing the resulting integrals in terms of the Gamma function, it can be shown following some laborious algebra that [282]

$$
\begin{aligned}
Q &= 4\left[\frac{\Gamma(\frac{3}{4})}{\Gamma(\frac{1}{4})}\right]^2 + \frac{16}{5}\sqrt{3}\left[\frac{\Gamma(\frac{3}{4})}{\Gamma(\frac{1}{4})}\right]^3 \frac{1}{\sqrt{N}} + \mathcal{O}\left(\frac{1}{N}\right) \\
&\simeq 0.456947 + 0.214002\frac{1}{\sqrt{N}} + \mathcal{O}\left(\frac{1}{N}\right).
\end{aligned}
\tag{C.15}
$$

Bibliography

[1] N. D. Mermin and H. Wagner, Phys. Rev. Lett. **17**, 1133 (1966).

[2] P. A. M. Dirac, Proc. Roy. Soc. (London) **133**, 60 (1931).

[3] P. A. M. Dirac, *The Principles of Quantum Mechanics*, *International Series of Monographs on Physics*, 4th ed. (Oxford University Press, Oxford, 1958), reprinted 2003.

[4] S. T. Bramwell, M. J. Harris, B. C. den Hertog, M. J. P. Gingras, J. S. Gardner, D. F. McMorrow, A. R. Wildes, A. L. Cornelius, J. D. M. Champion, R. G. Melko, and T. Fennell, Phys. Rev. Lett. **87**, 047205 (2001).

[5] W. Heitler and F. London, Z. Phys. **44**, 455 (1927).

[6] W. Heisenberg, Z. Phys. **38**, 411 (1926).

[7] P. A. M. Dirac, Proc. Roy. Soc. (London) **112A**, 662 (1926).

[8] J. H. V. Vleck, *The Theory of Electric and Magnetic Susceptibilites*, *International Series of Monographs in Physics* (Oxford University Press, Oxford, 1932), reprinted 1985.

[9] W. Heisenberg, Phys. Zeit. **49**, 619 (1928).

[10] R. M. White, *Quantum Theory of Magnetism*, *Advanced Physics Monograph Series* (McGraw-Hill, New York, 1970).

[11] K. P. Sinha and N. Kumar, *Interactions in Magnetically Ordered Solids* (Oxford University Press, Oxford, 1980).

[12] E. Ising, Z. Phys. **31**, 253 (1925).

[13] P. W. Anderson, Science **177**, 393 (1972).

[14] L. Onsager, Phys. Rev. **65**, 117 (1943).

[15] H. A. Kramers and G. H. Wannier, Phys. Rev. **60**, 252 (1941).

[16] A. P. Ramirez, Annu. Rev. Mater. Sci. **24**, 453 (1994).

[17] Z. Hiroi, H. Tsunetsugu, and H. Kawamura, J. Phys.: Condens. Matter **19**, 140301 (2007).

[18] P. Weiss, Journ. Phys. Rad **6**, 661 (1907).

[19] P. Weiss, Phys. Zeit. **9**, 358 (1908).

[20] C. Kittel, *Introduction to Solid State Physics*, 8th ed. (Wiley, New York, 2004).

[21] G. E. Uhlenbeck and S. Goudsmit, Naturwiss. **13**, 953 (1925).

[22] G. E. Uhlenbeck and S. Goudsmit, Nature **117**, 264 (1926).

[23] P. A. M. Dirac, Proc. Roy. Soc. (London) **117A**, 610 (1928).

[24] P. A. M. Dirac, Proc. Roy. Soc. (London) **118A**, 351 (1928).

[25] D. C. Mattis, *The Theory of Magnetism I. Statics and Dynamics, Springer Series in Solid-State Sciences*, 2nd ed. (Springer-Verlag, Berlin, 1988).

[26] P. Mohn, *Magnetism in the Solid State. An Introduction, Springer Series in Solid-State Sciences* (Springer, Berlin, 2003).

[27] H. E. Stanley, *Introduction to Phase Transitions and Critical Phenomena, International Series of Monographs on Physics* (Oxford University Press, Oxford, 1971).

[28] J. M. Yeomans, *Statistical Mechanics of Phase Transitions, Oxford Science Publications* (Oxford University Press, Oxford, 1992).

[29] J. J. Binney, N. J. Dowrick, A. J. Fisher, and M. E. J. Newman, *The Theory of Critical Phenomena. An Introduction to the Renormalization Group* (Oxford University Press, Oxford, 1992).

[30] N. Goldenfeld, *Lectures on Phase Transitions and the Renormalization Group, Frontiers in Physics Lecture Note Series* (Westview Press, Colorado, 1992).

[31] J. Cardy, *Scaling and Renormalization in Statistical Physics, Cambridge Lecture Notes in Physics* (Cambridge University Press, Cambridge, 1996).

[32] H. B. Callen, *Thermodynamics and an Introduction to Thermostatistics*, 2nd ed. (Wiley, New York, 1985).

[33] K. Huang, *Statistical Mechanics*, 2nd ed. (Wiley, New York, 1987).

[34] P. Ehrenfest, Acad. Sci. Amsterdam **153**, 36 (1933).

[35] L. D. Landau, Phys. Z. Sowjetunion **11**, 26 (1937), reprinted in *Collected papers of L. D. Landau*, D. ter Haar, ed. (Pergamon, London, 1965).

[36] L. D. Landau and E. M. Lifshitz, *Statistical Physics, Part 1*, Vol. 5 of *Landau and Lifshitz Course of Theoretical Physics*, 3rd ed. (Butterworth Heinemann, Oxford, 1980).

[37] M. Ley-Koo and M. S. Green, Phys. Rev. A **16**, 2483 (1977).

[38] E. A. Guggenheim, J. Chem. Phys. **13**, 253 (1945).

[39] J. Als-Nielsen, O. W. Dietrich, W. Kunnmann, and L. Passell, Phys. Rev. Lett. **27**, 741 (1971).

[40] J. P. Sethna, *Statistical Mechanics: Entropy, Order Parameters and Complexity, Oxford Master Series in Condensed Matter* (Oxford University Press, Oxford, 2006).

[41] M. Hasenbusch, K. Pinn, and S. Vinti, Phys. Rev. B **59**, 11471 (1999).

[42] M. Campostrini, M. Hasenbusch, A. Pelissetto, P. Rossi, and E. Vicari, Phys. Rev. B **65**, 144520 (2002).

[43] R. J. Baxter, *Exactly Solved Models in Statistical Mechanics* (Academic Press, London, 1982).

[44] A. Taroni, unpublished data (unpublished).

[45] T. Andrews, Phil. Trans. Royal Soc. **159**, 575 (1869).

[46] M. Plischke and B. Bergersen, *Equilibrium Statistical Physics*, 2nd ed. (World Scientific, London, 1994).

[47] L. P. Kadanoff, Physics **2**, 263 (1966).

[48] K. G. Wilson, Phys. Rev. B **4**, 3174 (1971).

[49] K. G. Wilson and J. Kogut, Phys. Rep. **12**, 75 (1974).

[50] K. G. Wilson and M. E. Fisher, Phys. Rev. Lett. **28**, 240 (1972).

[51] N. Metropolis, A. W. Rosenbluth, M. N. Rosenbluth, A. H. Teller, and E. Teller, J. Chem. Phys. **21**, 1087 (1953).

[52] M. E. J. Newman and G. T. Barkema, *Monte Carlo Methods in Statistical Physics* (Oxford University Press, Oxford, 1999).

[53] K. Binder and D. W. Heermann, *Monte Carlo Simulation in Statistical Physics, Springer Series in Solid-State Sciences*, 4th ed. (Springer, Berlin, 2002).

[54] R. H. Swendsen and J.-S. Wang, Phys. Rev. Lett. **58**, 86 (1987).

[55] J. S. Kouvel and M. E. Fisher, Phys. Rev. **136**, 1626 (1964).

[56] K. Binder, Z. Phys. B **43**, 119 (1981).

[57] K. Binder, Phys. Rev. Lett. **47**, 693 (1981).

[58] H. E. Stanley, Phys. Rev. Lett. **20**, 589 (1968).

[59] M. A. Moore, Phys. Rev. Lett. **23**, 861 (1969).

[60] S. T. Bramwell, J.-Y. Fortin, P. C. W. Holdsworth, S. Peysson, J.-F. Pinton, B. Portelli, and M. Sellitto, Phys. Rev. E **63**, 041106 (2001).

[61] J. M. Kosterlitz and D. J. Thouless, J. Phys. C **6**, 1181 (1973).

[62] J. M. Kosterlitz, J. Phys. C **7**, 1046 (1974).

[63] M. Suzuki, Prog. Theor. Phys. **51**, 1992 (1974).

[64] P. W. Anderson, *Basic Notions of Condensed Matter Physics, Frontiers in Physics Lecture Note Series* (Westview Press, Colorado, 1984).

[65] P. W. Anderson and G. Yuval, J. Phys. C **4**, 607 (1971).

[66] D. R. Nelson, in *Phase Transitions and Critical Phenomena*, edited by C. Domb and J. L. Lebowitz (Academic Press, London, 1983), Vol. 7, Chap. 1.

[67] D. R. Nelson, *Defects and Geometry in Condensed Matter Physics* (Cambridge University Press, Cambridge, 2002).

[68] J. V. José, L. P. Kadanoff, S. Kirkpatrick, and D. R. Nelson, Phys. Rev. B **16**, 1217 (1977).

[69] D. R. Nelson and J. M. Kosterlitz, Phys. Rev. Lett. **39**, 1201 (1977).

[70] V. L. Berezinskiĭ, Sov. Phys. JETP **32**, 493 (1970).

[71] V. L. Berezinskiĭ, Sov. Phys. JETP **34**, 610 (1971).

[72] J. Villain, J. Physique **36**, 581 (1975).

[73] P. M. Chaikin and T. C. Lubensky, *Principles of Condensed Matter Physics* (Cambridge University Press, Cambridge, 1995).

[74] D. J. Thouless, *Topological Quantum Mechanics in Nonrelativistic Physics* (World Scientific, London, 1998).

[75] I. Rudnick, Phys. Rev. Lett. **40**, 1454 (1978).

[76] D. J. Bishop and J. D. Reppy, Phys. Rev. Lett. **40**, 1727 (1978).

[77] S. T. Bramwell and P. C. W. Holdsworth, J. Phys.: Condens. Matter **5**, L53 (1993).

[78] S. T. Bramwell and P. C. W. Holdsworth, Phys. Rev. B **49**, 8811 (1994).

[79] R. Gupta, J. DeLapp, G. G. Batrouni, G. C. Fox, C. F. Baillie, and J. Apostolakis, Phys. Rev. Lett. **61**, 1996 (1988).

[80] R. B. Potts, Proc. Camb. Phil. Soc. **48**, 106 (1952).

[81] P. G. Maier and F. Schwabl, Phys. Rev. B **70**, 134430 (2004).

[82] P. G. Maier and F. Schwabl, Condens. Matter Phys. **8**, 103 (2005).

[83] F. Bloch, Z. Phys. **61**, 206 (1930).

[84] K. Binder and D. P. Landau, Phys. Rev. B **13**, 1140 (1976).

[85] M. Bander and D. L. Mills, Phys. Rev. B **38**, 12015 (1988).

[86] S. T. Bramwell and P. C. W. Holdsworth, J. Appl. Phys. **73**, 6096 (1993).

[87] Z. Q. Qiu, J. Pearson, and S. D. Bader, Phys. Rev. B **49**, 8797 (1994).

[88] C. N. Yang, Phys. Rev. **85**, 808 (1952).

[89] H. Ikeda and K. Hirakawa, Solid State Commun. **14**, 529 (1974).

[90] L. J. de Jongh and A. R. Miedema, Adv. Phys. **23**, 6 (1974), republished in Adv. Phys. **50**, 947 (2001).

[91] A. M. Ferrenberg and D. P. Landau, Phys. Rev. B **44**, 5081 (1991).

[92] V. L. Berezinskiĭ and A. Y. Blank, Sov. Phys. JETP **37**, 369 (1973).

[93] S. Hikami and T. Tsuneto, Prog. Theor. Phys. **63**, 387 (1980).

[94] L. P. Regnault and J. Rossat-Mignod, in *Magnetic Properties of Layered Transition Metal Compounds*, edited by L. J. de Jongh (Kluwer Academic Publishers, Dortrecht, 1990).

[95] S. T. Bramwell, P. Day, M. T. Hutchings, J. R. G. Thorne, and D. Visser, Inorg. Chem. **25**, 417 (1986).

[96] J. Als-Nielsen, S. T. Bramwell, M. T. Hutchings, G. J. McIntyre, and D. Visser, J. Phys.: Condens. Matter **5**, 7871 (1993).

[97] E. J. Samuelsen, Phys. Rev. Lett. **31**, 936 (1973).

[98] J. W. Lynn, T. W. Clinton, W.-H. Li, R. W. Erwin, J. Z. Liu, K. Vandervoort, and R. N. Shelton, Phys. Rev. Lett. **63**, 2606 (1989).

[99] K. Brennan, C. Hohenemser, and M. Eibschütz, J. Appl. Phys. **73**, 5500 (1993).

[100] R. J. Birgeneau, H. J. Guggenheim, and G. Shirane, Phys. Rev. B **1**, 2211 (1970).

[101] C. M. J. van Uijen, E. Frikkee, and H. W. de Wijn, Phys. Rev. B **19**, 509 (1979).

[102] H. Tietze-Jaensch, R. van de Kamp, and W. Schmidt, Physica B **241-243**, 566 (1998).

[103] R. van de Kamp, M. Steiner, and H. Tietze-Jaensch, Physica B **241-243**, 570 (1998).

[104] R. J. Birgeneau, H. J. Guggenheim, and G. Shirane, Phys. Rev. B **8**, 304 (1973).

[105] M. P. H. Thurlings, E. Frikkee, and H. W. de Wijn, Phys. Rev. B **25**, 4750 (1982).

[106] S. Y. Wu, W.-H. Li, K. C. Lee, J. W. Lynn, T. H. Meen, and H. D. Yang, Phys. Rev. B **54**, 10019 (1996).

[107] V. Carteaux, F. Moussa, and M. Spiesser, Europhys. Lett. **29**, 245 (1995).

[108] E. N. Khatsko, A. Zheludev, J. M. Tranquada, W. T. Clooster, A. M. Knigavko, and R. C. Srivastava, Low. Temp. Phys. **30**, 133 (2004).

[109] S. G. Carling, P. Day, and D. Visser, J. Phys.: Condens. Matter **7**, L109 (1995).

[110] M. L. Eibschütz, H. J. Guggenheim, L. Holmes, and J. L. Burnstein, Solid State Commun. **11**, 457 (1972).

[111] H. N. Bordallo, L. Chapon, J. L. Manson, J. Hernàndez-Velasco, D. Ravot, W. M. Reiff, and D. N. Arhyriou, Phys. Rev. B **69**, 224405 (2004).

[112] K. Yamada, M. Matsuda, Y. Endoh, B. Keimer, R. J. Birgeneau, S. Onodera, J. Mizusaki, T. Matsuura, and G. Shirane, Phys. Rev. B **39**, 2336 (1989).

[113] A. Rujiwatra, C. J. Kepert, J. B. Claridge, M. J. Rosseinsky, H. Kumagai, and M. Kurmoo, J. Am. Chem. Soc. **123**, 10584 (2001).

[114] S. G. Carling, P. Day, and D. Visser, Solid State Commun. **88**, 135 (1993).

[115] K. Hirakawa and K. Ikeda, J. Phys. Soc. Jpn. **35**, 1328 (1973).

[116] K. Koyama, H. Nobumasa, and M. Matsuura, J. Phys. Soc. Jpn. **56**, 1553 (1987).

[117] S. J. Blundell, A. Hausmann, T. Jestädt, F. L. Pratt, I. M. Marshall, B. W. Lovett, M. Kurmoo, T. Sugano, and W. Hayes, Physica B **289**, 115 (2000).

[118] M. Greven, R. J. Birgeneau, Y. Endoh, M. A. Kastner, M. Matsuda, and G. Shirane, Z. Phys. B **96**, 465 (1995).

[119] K. Nakajiama, K. Yamada, S. Hosoya, Y. Endoh, M. Greven, and R. J. Birgeneau, Z. Phys. B **96**, 479 (1995).

[120] S. J. Clarke, A. Harrison, T. E. Mason, G. J. McIntyre, and D. Visser, J. Phys.: Condens. Matter **4**, L71 (1992).

[121] J. Skalyo, G. Shirane, and S. A. Friedberg, Phys. Rev. **188**, 1037 (1969).

[122] T. Chattopadhyay, P. J. Brown, A. A. Stepanov, A. I. Zvyagin, S. N. Barilo, and D. I. Zhigunov, J. Magn. Magn. Mater. **104-107**, 607 (1992).

[123] C. Bellitto, P. Filaci, and S. Patrizio, Inorg. Chem. **26**, 191 (1987).

[124] A. Paduan-Filho and C. C. Becerra, J. Appl. Phys. **91**, 8294 (2002).

[125] K. W. Krämer, H. U. Güdel, P. Fischer, F. Fauth, M. T. Fernandez-Diaz, and T. Hauß, Eur. Phys. J. B **18**, 39 (2000).

[126] F. C. Coomer, V. Bondah-Jagalu, K. J. Grant, A. Harrison, G. J. McIntyre, H. M. Rønnow, R. Feyerherm, T. Wand, M. Meissner, D. Visser, and D. F. McMorrow, Phys. Rev. B **75**, 094424 (2007).

[127] R. Melzi, S. Aldrovandi, F. Tedoldi, P. Carretta, P. Millet, and F. Mila, Phys. Rev. B **64**, 024409 (2001).

[128] P. Carretta, N. Papinutto, R. Melzi, P. Millet, S. Gonthier, P. Mendels, and P. Wzietek, J. Phys.: Condens. Matter **16**, S849 (2004).

[129] A. I. Coldea, S. J. Blundell, C. A. Steer, J. F. Mitchell, and F. L. Pratt, Phys. Rev. Lett. **89**, 177601 (2002).

[130] S. Larochelle, A. Mehta, L. Lu, P. K. Mang, O. P. Vajk, N. Kaneko, L. Zhou, and M. Greven, Phys. Rev. B **71**, 024435 (2005).

[131] H. M. Rønnow, A. R. Wildes, and S. T. Bramwell, Physica B **276-278**, 676 (2000).

[132] A. R. Wildes, H. M. Rønnow, B. Roessli, M. J. Harris, and K. W. Godfrey, Phys. Rev. B **74**, 094422 (2006).

[133] M. Kurmoo, H. Kaumagai, S. M. Hughes, and C. J. Kepert, Inorg. Chem. **42**, 6709 (2003).

[134] W. Montfrooij, H. Casalta, P. Schleger, N. H. Andersen, A. A. Zhokiv, and A. N. Christiansen, Physica B **241-243**, 848 (1998).

[135] S. T. Bramwell, Ph.D. thesis, University of Oxford, 1989.

[136] M. C. Morón, F. Palacio, and J. Rodriguez-Carvajal, J. Phys.: Condens. Matter **5**, 4909 (1993).

[137] *Magnetic Properties of Layered Transition Metal Compounds*, Vol. 9 of *Physics and Chemistry of Materials with Low-Dimensional Structures*, edited by L. J. de Jongh (Kluwer Academic Publishers, Dortrecht, 1990).

[138] P. W. Anderson, Science **235**, 1196 (1987).

[139] J. Orenstein and A. J. Mills, Science **288**, 468 (2000).

[140] K. De'Bell and J. P. Whitehead, J. Phys.: Condens. Matter **3**, 2431 (1991).

[141] H. Kawamura, J. Phys. Soc. Jap. **54**, 3220 (1985).

[142] H. Kawamura, J. Phys. Soc. Jap. **55**, 2095 (1986).

[143] H. Hikeda and K. Hirakawa, J. Phys. Soc. Jpn. **33**, 393 (1972).

[144] K. Hirakawa, J. Appl. Phys. **53**, 1893 (1982).

[145] T. Thio and A. Aharony, Phys. Rev. Lett. **73**, 894 (1994).

[146] I. Dzyaloshinskii, J. Phys. Chem. Sol. **4**, 241 (1958).

[147] T. Moriya, Phys. Rev. **120**, 91 (1960).

[148] L. L. Miller, X. L. Wang, S. X. Wang, C. Stassis, D. C. Johnston, J. Faber, and C.-K. Loong, Phys. Rev. B **41**, 1921 (1990).

[149] D. Vaknin, S. K. Sinha, C. Stassis, L. L. Miller, and D. C. Johnston, Phys. Rev. B **41**, 1926 (1990).

[150] M. Greven, R. J. Birgeneau, Y. Endoh, M. A. Kastner, B. Keimer, M. Matsuda, G. Shirane, and T. R. Thurston, Phys. Rev. Lett. **72**, 1096 (1994).

[151] A. Cuccoli, T. Roscilde, V. Tognetti, R. Vaia, and P. Verrucchi, Phys. Rev. B **67**, 104414 (2003).

[152] N. Rogado, Q. Huang, J. W. Lynn, A. P. Ramirez, D. Huse, and R. J. Cava, Phys. Rev. B **65**, 144443 (2002).

[153] M. Heirich, H.-A. K. von Nidda, A. Lidl, N. Rogado, and R. J. Cava, Phys. Rev. Lett. **91**, 137601 (2003).

[154] M. Matsuura, K. Koyama, and Y. Murakami, J. Phys. Soc. Jpn. **54**, 2714 (1985).

[155] J. Mira, J. Rivas, A. Butera, L. B. Steren, J. M. García-Beneytez, and M. Vázquez, J. Appl. Phys. **87**, 5911 (2000).

[156] Y. Moritomo, A. Asamitsu, H. Kuwahara, and Y. Tokura, Nature **380**, 141 (1996).

[157] T. G. Perring, G. Aeppli, Y. Moritomo, and Y. Tokura, Phys. Rev. Lett. **78**, 3197 (1997).

[158] S. Rosenkranz, R. Osborn, L. Vasiliu-Doloc, J. W. Lynn, S. K. Sinha, and J. F. Mitchell, Physica B **312-313**, 763 (2002).

[159] S. J. Blundell and F. L. Pratt, J. Phys.: Condens. Matter **16**, R771 (2004).

[160] A. Benoit, J. Floquet, B. Gillon, and J. Schweizer, J. Magn. Magn. Mater. **31-34**, 1155 (1983).

[161] T. Sugano, S. J. Blundell, F. L. Pratt, T. Jestädt, B. W. Lovett, W. Hayes, and P. Day, Mol. Cryst. Liq. Cryst. **334**, 477 (1999).

[162] N. Giordano and W. P. Wolf, Phys. Rev. Lett. **39**, 342 (1977).

[163] H. Kawamura, J. Phys.: Condens. Matter **10**, 4707 (1998).

[164] T. E. Mason, B. D. Gaulin, and M. F. Collins, Phys. Rev. B **39**, 586 (1989).

[165] C. A. Cornelius, P. Day, P. J. Fyne, M. T. Hutchings, and P. J. Walker, J. Phys. C: Solid State **19**, 909 (1985).

[166] O. H. Seeck, D. Hupfeld, H. Krull, M. Tolan, and W. Press, Phys. Rev. B **58**, 623 (1998).

[167] H. Kawamura, J. Phys. Soc. Jap. **61**, 1299 (1992).

[168] M. L. Plumer and A. Mailhot, Phys. Rev. B **50**, 16113 (1994).

[169] D. Beckmann, J. Wosnitza, and H. von Löhneysen, Phys. Rev. Lett. **71**, 2829 (1992).

[170] H. Kawamura, J. Appl. Phys. **61**, 3590 (1987).

[171] H.-J. Elmers, Int. J. Mod. Phys. B **9**, 3115 (1995).

[172] U. Gradmann, in *Handbook of Magnetic Materials*, edited by K. H. J. Buschow (Elsevier, Amsterdam, 1993), Vol. 7.

[173] S. T. Bramwell, P. C. W. Holdsworth, and J. Rothman, Mod. Phys. Lett. B **11**, 139 (1997).

[174] E. Rastelli, S. Regina, and A. Tassi, Phys. Rev. B **69**, 174407 (2004).

[175] E. Rastelli, S. Regina, and A. Tassi, Phys. Rev. B **70**, 174447 (2004).

[176] C. Rau, P. Mahavadi, and M. Lu, J. Appl. Phys. **73**, 6757 (1993).

[177] C. Liu and S. D. Bader, J. Appl. Phys. **67**, 5758 (1990).

[178] Z. Q. Qiu, J. Pearson, and S. D. Bader, Phys. Rev. Lett. **70**, 1006 (1993).

[179] H.-J. Elmers, J. Hauschild, H. Höche, U. Gradmann, H. Bethge, D. Heuer, and U. Köhler, Phys. Rev. Lett. **73**, 898 (1994).

[180] H.-J. Elmers, J. Hauschild, and U. Gradmann, J. Magn. Magn. Mater. **140-144**, 1559 (1995).

[181] H.-J. Elmers, J. Hauschild, and U. Gradmann, Phys. Rev. B **54**, 15224 (1996).

[182] C. H. Back, C. Würsch, A. Vaterlaus, U. Ramsperger, U. Maier, and F. Pescia, Nature **378**, 597 (1995).

[183] Z. Q. Qiu, J. Pearson, and S. D. Bader, Phys. Rev. Lett. **67**, 1646 (1991).

[184] D. Li, M. Freitag, J. Pearson, Z. Q. Qiu, and S. D. Bader, Phys. Rev. Lett. **72**, 3112 (1994).

[185] J. Thomassen, F. May, B. Felfmann, M. Wuttig, and H. Ibach, Phys. Rev. Lett. **69**, 3831 (1992).

[186] D. P. Pappas, K.-P. Kämper, and H. Hopster, Phys. Rev. Lett. **64**, 3179 (1990).

[187] U. Gradmann, M. Przybylski, H.-J. Elmers, and G. Liu, Appl. Phys. A **49**, 563 (1989).

[188] M. Przybylski and U. Gradmann, Phys. Rev. Lett. **59**, 1152 (1987).

[189] H.-J. Elmers, G. Liu, and U. Gradmann, Phys. Rev. Lett. **63**, 566 (1989).

[190] W. A. A. Macedo, F. Sirotti, G. Panaccione, A. Schatz, W. Keune, W. N. Rodrigues, and G. Rossi, Phys. Rev. B **58**, 11534 (1998).

[191] H.-J. Elmers, J. Hauschild, G. H. Liu, and U. Gradmann, J. Appl. Phys. **79**, 4984 (1996).

[192] H.-J. Elmers and J. Hauschild, Surf. Sci. **320**, 134 (1994).

[193] W. Dürr, M. Taborelli, O. Paul, R. Germar, W. Gudat, D. Pescia, and M. Landolt, Phys. Rev. Lett. **62**, 206 (1989).

[194] C. Rau, Appl. Phys. A **49**, 579 (1989).

[195] M. Pärnaste, M. Marcellini, and B. Hjörvarsson, J. Phys.: Condens. Matter. **17**, L477 (2005).

[196] M. Pärnaste, M. Marcellini, E. Holmström, N. Bock, J. Fransson, O. Eriksson, and B. Hjörvarsson, J. Phys.: Condens. Matter **19**, 246213 (2007).

[197] F. Bensch, G. Garreau, R. Moosbühler, G. Bayreuther, and E. Beaurepaire, J. Appl. Phys. **89**, 7133 (2001).

[198] J. Kohlepp, H.-J. Elmers, S. Cordes, and U. Gradmann, Phys. Rev. B **45**, 12287 (1992).

[199] F. Huang, M. T. Kief, G. J. Mankey, and R. F. Willis, Phys. Rev. B **49**, 3962 (1994).

[200] C. C. Kuo, C. L. Chiu, W. C. Lin, and M.-T. Lin, Surf. Sci. **520**, 121 (2002).

[201] M. Gruyters, T. Bernhard, and H. Winter, J. Magn. Magn. Mater. **292**, 192 (2005).

[202] Y. Li and K. Baberschke, Phys. Rev. Lett. **68**, 1208 (1992).

[203] C. A. Ballantine, R. L. Fink, J. Araya-Pochet, and J. L. Erskine, Phys. Rev. B **41**, 2631 (1990).

[204] F. Huang, G. J. Mankey, M. T. Kief, and R. F. Willis, J. Appl. Phys. **73**, 6760 (1993).

[205] C. Rau, G. Xing, and M. Robert, J. Vac. Sci. Technol. A **6**, 579 (1988).

[206] M. Gajdzik, T. Trappmann, C. Sürgers, and H. v. Löhneysen, Phys. Rev. B **57**, 3525 (1998).

[207] C. Zeng, S. C. Erwin, L. C. Feldman, A. P. Li, R. Jin, Y. Song, J. R. Thompson, and H. H. Weitering, Appl. Phys. Lett. **83**, 5002 (2003).

[208] V. Rose, K. Brüggemann, R. David, and R. Franchy, Phys. Rev. Lett. **98**, 037202 (2007).

[209] R. P. Erickson and D. L. Mills, Phys. Rev. B **41**, 11825 (1991).

[210] D. L. Mills, J. Magn. Magn. Mater. **100**, 515 (1991).

[211] M. Pärnaste, personal communication (unpublished).

[212] P. Poloupoulos and K. Baberschke, J. Phys.: Condens. Matter **11**, 9495 (1999).

[213] S. D. Bader and E. R. Moog, J. Appl. Phys. **61**, 3729 (1987).

[214] C. L. Fu, A. J. Freeman, and T. Oguchi, Phys. Rev. Lett. **54**, 2700 (1985).

[215] M. Pomerantz, F. H. Dacol, and A. Segmüller, Phys. Rev. Lett. **40**, 246 (1973).

[216] H. Godfrin and R. E. Rapp, Adv. Phys. **44**, 113 (1995).

[217] M. K. Mukhopadhyay, M. K. Sanyal, M. D. Mukadam, S. M. Yusuf, and J. K. Basu, Phys. Rev. B **68**, 174427 (2003).

[218] M. K. Mukhopadhyay, M. K. Sanyal, T. Sakakibara, V. Leiner, R. M. Dalgliesh, and S. Langridge, Phys. Rev. B **74**, 014402 (2006).

[219] H. Godfrin, R. R. Ruel, and D. D. Osheroff, Phys. Rev. Lett. **60**, 305 (1988).

[220] H. M. Bozler, Y. Gu, J. Zhang, K. S. White, and C. M. Gould, Phys. Rev. Lett. **88**, 065302 (2002).

[221] J. C. Capunzano, M. S. Foster, G. Jennings, R. F. Willis, and W. Unertl, Phys. Rev. Lett. **54**, 2684 (1985).

[222] M. Sokolowski and H. Pfnür, Phys. Rev. B **49**, 7716 (1994).

[223] P. Piercy, K. De'Bell, and H. Pfnür, Phys. Rev. B **45**, 1869 (1992).

[224] I. F. Lyuksyutov and A. G. Fedorus, Sov. Phys. JETP **53**, 1317 (1981).

[225] G.-C. Wang and T.-M. Lu, Phys. Rev. B **31**, 5918 (1985).

[226] H. Pfnür and P. Piercy, Phys. Rev. B **41**, 582 (1990).

[227] H. Pfnür and P. Piercy, Phys. Rev. B **40**, 2515 (1989).

[228] K. Grzelakowski, I. Lyuksyutov, and E. Bauer, Phys. Rev. Lett. **64**, 32 (1990).

[229] D. H. Baek, J. W. Chung, and W. K. Han, Phys. Rev. B **47**, 8461 (1993).

[230] L. Floreano, D. Cvetko, G. Bavdek, M. Benes, and A. Morgante, Phys. Rev. B **64**, 075405 (2001).

[231] D. Cvetko, F. Ratto, A. Cossaro, G. Bavdek, A. Morgante, and L. Floreano, Phys. Rev. B **72**, 045404 (2005).

[232] M. J. Harris, American Mineralogist **84**, 1632 (1999).

[233] J. E. Lorenzo, L. P. Regnault, S. Langridge, C. Vettier, C. Sutter, G. Grübel, J. Souletie, J. G. Lussier, J. P. Schoeffel, J. P. Pouget, A. Stunault, D. Wermeille, G. Dhalenne, and A. Revcolevschi, Europhys. Lett. **45**, 45 (1999).

[234] R. J. Birgeneau, V. Kiryukhin, and Y. J. Wang, Phys. Rev. B **60**, 14816 (1999).

[235] B. D. Gaulin, M. D. Lumsden, R. K. Kremer, M. A. Lumsden, and H. Dabkowska, Phys. Rev. Lett. **84**, 3446 (2000).

[236] D. R. Nelson and B. I. Halperin, Phys. Rev. B **19**, 2457 (1979).

[237] A. P. Young, Phys. Rev. B **19**, 1855 (1979).

[238] W. J. Nuttall, D. Y. Noh, B. O. Wells, and R. J. Birgeneau, J. Phys.: Condens. Matter **7**, 4337 (1995).

[239] W. J. Nuttall, D. Y. Noh, B. O. Wells, and R. J. Birgeneau, Surf. Sci. **307-309**, 768 (1994).

[240] S. T. Bramwell, M. J. P. Gingras, and P. C. W. Holdsworth, Phys. Rev. E **48**, 625 (1993).

[241] V. Ambegaokar, B. I. Halperin, D. R. Nelson, and E. D. Siggia, Phys. Rev. Lett. **40**, 783 (1978).

[242] S. W. Pierson, Phys. Rev. Lett. **73**, 2496 (1994).

[243] D. J. Resnik, J. C. Garland, J. T. Boyd, S. Shoemaker, and R. S. Newrock, Phys. Rev. Lett. **47**, 1542 (1981).

[244] A. Trombettoni, A. Smerzi, and P. Sodano, Laser Physics **15**, 669 (2005).

[245] A. Trombettoni, A. Smerzi, and P. Sodano, New J. Phys. **7**, 57 (2005).

[246] Z. Hadzibabic, P. Krüger, M. Cheneau, B. Battelier, and J. Dalibard, Nature **441**, 1118 (2006).

[247] A. M. Polyakov, Phys. Lett. B **59**, 79 (1975).

[248] E. Brézin and J. Zinn-Justin, Phys. Rev. Lett. **36**, 691 (1976).

[249] D. R. Nelson and R. A. Pelcovits, Phys. Rev. B **16**, 2191 (1977).

[250] S. H. Shenker and J. Tobochnik, Phys. Rev. B **22**, 4462 (1980).

[251] O. Kapikranian, B. Berch, and Y. Holovatch, J. Phys. A: Math. Theor. **40**, 3741 (2007).

[252] H. E. Stanley and T. A. Kaplan, Phys. Rev. Lett. **17**, 913 (1966).

[253] M. Takahashi, Phys. Rev. B **36**, 3791 (1987).

[254] W. J. Camp and J. P. V. Dyke, J. Phys. C: Solid State Phys. **8**, 336 (1975).

[255] A. Aharony, Phys. Rev. B **8**, 4270 (1973).

[256] M. T. Hutchings, J. Als-Nielsen, P. A. Lindgard, and P. J. Walker, J. Phys. C: Solid State Phys. **14**, 5327 (1981).

[257] J. Tobochnik, Phys. Rev. B **26**, 6201 (1982).

[258] S.-K. Ma, *Modern Theory of Critical Phenomena, Frontiers in Physics Lecture Note Series* (Westview Press, Colorado, 1976).

[259] S. Elitzur, R. B. Pearson, and J. Shigemitsu, Phys. Rev. D **19**, 3698 (1979).

[260] M. S. S. Challa and D. P. Landau, Phys. Rev. B **33**, 437 (1986).

[261] A. Yamagata and I. Ono, J. Phys. A: Math. Gen. **24**, 265 (1991).

[262] Y. Tomita and Y. Okabe, Phys. Rev. Lett. **86**, 572 (2001).

[263] C. M. Lapilli, P. Pfeifer, and C. Wexler, Phys. Rev. Lett. **96**, 140603 (2006).

[264] P. Minnhagen and B. J. Kim, Phys. Rev. B **67**, 172509 (2003).

[265] D. D. Betts, Can. J. Phys. **42**, 1564 (1964).

[266] C. Won, Y. Z. Wu, A. Scholl, A. Doran, N. Kurahashi, H. W. Zhao, and Z. Q. Qiu, Phys. Rev. Lett. **91**, 147202 (2003).

[267] J. V. José, L. P. Kadanoff, S. Kirkpatrick, and D. R. Nelson, Phys. Rev. B **17**, 1477 (1978).

[268] P. C. W. Holdsworth, personal communication (unpublished).

[269] P. Calabrese and A. Celi, Phys. Rev. B **66**, 184410 (2002).

[270] S. T. Bramwell and P. C. W. Holdsworth, J. Appl. Phys. **75**, 5955 (1994).

[271] S. T. Bramwell, P. C. W. Holdsworth, and M. T. Hutchings, J. Phys. Soc. Jap. **64**, 3066 (1995).

[272] A. Cuccoli, T. Roscilde, R. Vaia, and P. Verrucchi, Phys. Rev. Lett. **90**, 167205 (2003).

[273] S. T. Bramwell, personal communication (unpublished).

[274] C. Rau and M. Robert, Mod. Phys. Lett. B **10**, 223 (1996).

[275] C. Rau and M. Robert, IEEE Trans. Magnetics **32**, 4553 (1996).

[276] S. Krinsky and D. Mukamel, Phys. Rev. B **16**, 2313 (1977).

[277] D. P. Landau and K. Binder, Phys. Rev. B **31**, 5946 (1985).

[278] K. De'Bell, A. B. MacIsaac, and J. P. Whitehead, Rev. Mod. Phys. **72**, 225 (2000).

[279] M. E. Fisher, S.-K. Ma, and B. G. Nickel, Phys. Rev. Lett. **29**, 917 (1972).

[280] E. Brézin and J. Zinn-Justin, Nucl. Phys. B **257**, 867 (1985).

[281] G. Kamieniarz and H. W. J. Blöte, J. Phys. A **26**, 201 (1993).

[282] E. Luijten and H. W. J. Blöte, Int. J. Mod. Phys. C **6**, 359 (1995).

[283] E. Luijten and H. W. J. Blöte, Phys. Rev. B **56**, 8945 (1997).

[284] E. Luijten and H. W. J. Blöte, Phys. Rev. Lett. **89**, 025703 (2002).

[285] A. B. MacIsaac, J. P. Whitehead, K. De'Bell, and K. S. Narayanan, Phys. Rev. B **46**, 6387 (1992).

[286] E. Rastelli, S. Regina, and A. Tassi, Phys. Rev. B **73**, 144418 (2006).

[287] S. Prakash and C. L. Henley, Phys. Rev. B **42**, 6574 (1990).

[288] S. V. Maleev, Sov. Phys. JETP **43**, 1240 (1976).

[289] V. L. Pokrovskiĭ and M. V. Feĭgel'man, Sov. Phys. JETP **45**, 291 (1977).

[290] K. De'Bell, A. B. MacIsaac, I. N. Booth, and J. P. Whitehead, Phys. Rev. B **55**, 15108 (1997).

[291] A. Carbognani, E. Rastelli, S. Regina, and A. Tassi, Phys. Rev. B **62**, 1015 (2000).

[292] G. A. Baker, Phys. Rev. **130**, 1406 (1963).

[293] J. F. Nagle, Phys. Rev. A **2**, 2124 (1970).

[294] E. Luijten, H. W. J. Blöte, and K. Binder, Phys. Rev. E **56**, 6540 (1997).

[295] A. B. MacIsaac, J. P. Whitehead, M. C. Robinson, and K. De'Bell, Phys. Rev. B **51**, 16033 (1995).

[296] M. Seul and R. Wolfe, Phys. Rev. Lett. **68**, 2460 (1992).

[297] R. Allenspach, M. Stampanoni, and A. Bischof, Phys. Rev. Lett. **65**, 3344 (1990).

[298] R. Allenspach and A. Bischof, Phys. Rev. Lett. **69**, 3385 (1992).

[299] Y. Yafet and E. M. Gyorgy, Phys. Rev. B **38**, 9145 (1988).

[300] I. Booth, A. B. MacIsaac, J. P. Whitehead, and K. De'Bell, Phys. Rev. Lett. **75**, 950 (1995).

[301] A. Abanov, V. Kalatsky, V. L. Pokrovsky, and W. M. Saslow, Phys. Rev. B **51**, 1023 (1995).

[302] S. A. Cannas, M. F. Michelson, D. A. Stariolo, and F. A. Tamarit, Phys. Rev. B **73**, 184425 (2006).

[303] D. Pescia and V. L. Pokrovskiĭ, Phys. Rev. Lett. **65**, 2599 (1990).

[304] P. J. Jensen and K. H. Bennemann, Phys. Rev. B **42**, 849 (1990).

[305] D. P. Pappas, C. R. Brundle, and H. Hopster, Phys. Rev. B **45**, 8169 (1992).

[306] H. C. Longuet-Higgins and M. E. Fisher, Biographical Memoirs of Fellows of the Royal Society **24**, 443 (1978).

[307] P. Archambault, S. T. Bramwell, and P. C. W. Holdsworth, J. Phys. A **30**, 8363 (1997).

[308] S. T. Banks, Ph.D. thesis, University College London, 2005.

[309] W. L. Bragg and E. J. Williams, Proc. Roy. Soc. (London) **145A**, 699 (1934).

[310] E. Luijten, Phys. Rev. E **60**, 7558 (1999).